ADAPTIVE OPTICS

OCTOBER 2–6, 1995

GARCHING, GERMANY

1995 TECHNICAL DIGEST SERIES

VOLUME 23

SPONSORED BY

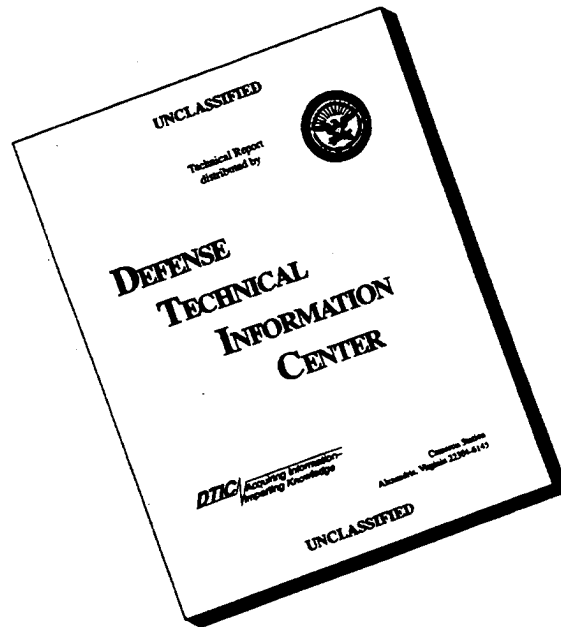OPTICAL SOCIETY OF AMERICA

EUROPEAN SOUTHERN OBSERVATORY

DISCLAIMER NOTICE

THIS DOCUMENT IS BEST QUALITY AVAILABLE. THE COPY FURNISHED TO DTIC CONTAINED A SIGNIFICANT NUMBER OF PAGES WHICH DO NOT REPRODUCE LEGIBLY.

*Summaries of the papers
presented at the topical meeting*

ADAPTIVE
OPTICS

OCTOBER 2–6, 1995
GARCHING, GERMANY

1995 TECHNICAL DIGEST SERIES
VOLUME 23

∧

Printed in the U.S.A.

Contents

LOBBY

8:00am–3:30pm
Conference Registration

AUDITORIUM

8:20am–8:30am
Opening Remarks
Fritz Merkle, *Carl Zeiss, Germany, Chair*

8:30am–10:10am
MA, Adaptive Optics Telescope Projects I
Martin Cullum, *European Southern Observatory, Germany, Presider* .

8:30am (Invited)
MA1 • ESO VLT adaptive optics program, N. Hubin, *European Southern Observatory, Germany.* We present here the high-level requirements and conceptual design of the Nasmyth Adaptive Optics System for Unit Telescope 1 of the Very Large Telescope project. Some scientific pre-studies will be presented, and an introduction of Laser Guide Star activities at ESO will be given. **(p. 2)**

8:50am (Invited)
MA2 • United Kingdom adaptive optics programs, Gerry Gilmore, *Institute of Astronomy, U.K.* The UK is building a facility for AO systems for two 4-m telescopes, pursuing system modeling, laser beacon and other R&D, and comprehensive site evaluation programs. **(p. 5)**

9:10am
MA3 • Laser guide star atmospheric compensation system for the 3.5-m Calar Alto telescope, Allan Wirth, Frank Landers, Bruce Trvalik, Joe Navetta, Terry Bruno, *Adaptive Optics Associates, Inc.* A 100-channel laser guide star atmospheric compensation system, scheduled for commissioning in spring 1996, is described. Design philosophy and current status are reviewed. **(p. 8)**

9:30am
MA4 • Adaptive optics system for the Telescopio Nazionale Galileo, Roberto Ragazzoni, *Astronomical Observatory of Padova, Italy;* Domenico Bonaccini, *European Southern Observatory, Germany.* The status of the adaptive optics system for the Italian National Telescope Galileo is reviewed, and the expected performances are discussed. **(p. 10)**

9:50am
MA5 • Low order adaptive optics at the Anglo-Australian telescope, J. W. O'Byrne, J. J. Bryant, R. A. Minard, P. W. Fekete, L. E. Cram, *Univ. Sydney, Australia.* Tip–tilt correction has been implemented as the first stage of a low order adaptive optical system based on curvature sensing and a bimorph mirror. **(p. 12)**

LOBBY

10:10am–11:00am
Coffee Break

AUDITORIUM

11:00am–12:20pm
MB, Adaptive Optics Telescope Projects II
Masanori Iye, *National Astronomical Observatory, Japan, Presider*

11:00am (Invited)
MB1 • Keck Observatory adaptive optics program, Peter L. Wizinowich, Anthony D. Gleckler, *W. M. Keck Observatory.* A 349-actuator, natural star and single sodium laser beacon, adaptive optics system is being designed for the Nasmyth platform of the Keck II telescope. **(p. 16)**

11:20am (Invited)
MB2 • The Gemini adaptive optics system, René Racine, *Univ. Montréal, Canada.* The science requirements, conceptual design and expected performance with natural guide stars of the adaptive optics system for the Gemini telescope on Mauna are described. **(p. 19)**

11:40am (Invited)
MB3 • Subaru adaptive optics program, Hideki Takami, Masanori Iye, Naruhisa Takato, Yutaka Hayano, *National Astronomical Observatory, Japan;* Masashi Otsubo, *Graduate Univ. for Advanced Studies, Japan;* Koji Nakashima, *Univ. Tokyo, Japan.* An adaptive optics program for Cassegrain focus of Subaru 8-m telescope atop Mauna Kea, which is scheduled to be completed in 1998, is presented. **(p. 22)**

12:00m
MB4 • The 6.5-m MMT infrared adaptive optics system detailed design and progress report, David G. Sandler, Michael Lloyd-Hart, Ty Martinez, Peter Gray, Roger Angel, *Univ. Arizona;* Steven Stahl, Todd Barrett, Don Bruns, *ThermoTrex Corp.* The system features adaptive secondary mirror with rapid internal feedback, 4-W sodium laser, low-noise CCD detector, and new computer architecture and algorithms. Components are under development. **(p. 25)**

12:20pm–2:00pm
Lunch on your own

AUDITORIUM

2:00pm–3:20pm
MC, Adaptive Optics Telescope Projects III
Fritz Merkle, *Carl Zeiss, Germany, Presider*

2:00pm
MC1 • ADONIS–a user-friendly adaptive optics system for the ESO 3.6-m telescope, J. L. Beuzit, N. Hubin, E. Prieto, D. Bonaccini, *European Southern Observatory, Germany;* L. Demailly, E. Gendron, P. Gigan, F. Lacombe, D. Rouan, *Observatoire de Paris, France;* F. Chazallet, D. Rabaud, P. Y. Madec, G. Rousset, *ONERA, France;* F. Eisenhauer, R. Hofmann, *MPIE, Germany.* ADONIS is an adaptive optics near infrared system offered to the European astronomical community on the ESO 3.6-m telescope. We describe here the main system characteristics and its associated instrumentation. **(p. 30)**

2:20pm
MC2 • Novel adaptive optics with the Durham University ELECTRA System, D. F. Buscher, N. Andrews, C. Dunlop, P. W. Morris, R. M. Myers, R. M. Sharples, A. J. A. Vick, A. Zadrozny, *Univ. Durham, UK;* C. A. Haniff, *MRAO Cavendish Laboratory, UK;* R. W. Wilson, *Royal Greenwich Observatory, UK.* We present the status of the Durham University ELECTRA visible-light adaptive optics system and describe novel imaging strategies to be used with this instrument. **(p. 32)**

2:40pm
MC3 • Recent results from the Martini/Whircam infrared adaptive optics system, P. Doel, D. Buscher, C. Dunlop, R. Sharples, N. Andrews, *Univ. Durham, UK.* Presented are the latest results from the Feb./June '95 Martini/Whircam low-order infrared adaptive optics system commissioning runs at the William Herschel telescope. **(p. 33)**

3:00pm
MC4 • Initial results from the Lick Observatory laser guide star adaptive optics system, Scot S. Olivier, Jong An, Kenneth Avicola, Horst D. Bissinger, James M. Brase, Herbert W. Friedman, Donald T. Gavel, Bruce Macintosh, Claire E. Max, J. Thaddeus Salmon, Kenneth E. Waltjen, *Lawrence Livermore National Laboratory.* We present initial results from the sodium-layer laser guide star adaptive optics system developed for the 3-m Shane telescope at Lick Observatory. **(p. 35)**

3:20pm
Free time

LOBBY

3:30pm–5:30pm
Informal Conference Reception

LOBBY

8:00am–12:30pm
Conference Registration

LOBBY

8:30am–12:30pm
TuA, Poster Session

TuA1 • Status of the first generation adaptive optics system for the Starfire Optical Range 3.5-m telescope, Robert Q. Fugate, *USAF Phillips Laboratory.* This is a status report on the 500-actuator adaptive optics system being assembled for the 3.5-m telescope at the Phillips Laboratory's Starfire Optical Range. **(p. 38)**

TuA2 • Advanced electro-optical system (AEOS) and Starfire Optical Range (SOR) adaptive optics, John R. Kenemuth, Janet S. Fender, Brent L. Ellerbroek, James Passaro, Tim Pennington, *USAF Phillips Laboratory;* Paul J. Berger, *MIT Lincoln Laboratory;* Conrad Neufeld, Rene Abreu, William P. Zmek, *Hughes Danbury Opt. Sys.;* Michael E. Meline, *Hughes Alfq. Eng. Lab.;* Mark A. Ealey, *Xinetics, Inc.* Advanced adaptive optics systems have been designed for the Phillips Laboratory AEOS and SOR telescopes. The 941-actuator, 200-Hz systems will be delivered in April 1997. **(p. 40)**

TuA3 • Gemini 8-m telescopes active and adaptive optics update, Jim Oschmann, Doug Simons, Dave Robertson, Matt Mountain, Dick Kurz, *Gemini 8-Meter Telescopes Project;* Charles Jenkins, *Royal Greenwich Observatory, UK;* Glenn Herriot, *Gemini Canadian Project Office, Canada.* The Gemini 8-m telescope's use of active and adaptive optics as a system is presented. The trades performed and the current concept are presented. **(p. 42)**

TuA4 • Use of the LBT to study zodiacal emission around other stars, N. Woolf, J. R. P. Angel, *Univ. Arizona.* The large binocular telescope configured as a Bracewell interferometer has uniquely powerful capability to detect 1 AU zodiacal radiation like that of the solar system. **(p. 44)**

TuA5 • Predictability of atmospherically distorted wavefronts, George J. M. Aitken, Donald McGaughey, *Queen's Univ., Canada.* Rescaled-range analysis and the estimated correlation dimension of the process attractor indicate that real, atmospherically distorted wavefronts have greater temporal predictability than was previously assumed. **(p. 47)**

TuA6 • WaveLab—Hartmann sensor data analysis software, Allan Wirth, *Adaptive Optics Associates, Inc.* A software package for the reduction and analysis of Hartmann sensor data is described. It allows for the conversion of Hartmann data to wavefronts or other types of information. **(p. 49)**

TuA7 • Linear spatio-temporal prediction for adaptive optics wavefront reconstructors, Michael Lloyd-Hart, *Univ. Arizona.* Computer simulations and telescope experiments have been performed to measure the improvement in imaging quality from an adaptive optics system through use of spatio-temporal prediction of wavefront sensor data. **(p. 50)**

TuA8 • Prediction of star wonder path with linear and nonlinear methods, D. Bonaccini, *Adaptive Optics Group, Germany;* D. Gallieni, R. Giampieretti, *Politecnico di Milano, Italy.* Linear and nonlinear autoregressive models are used to predict WFS outputs allowing closure for the adaptive optics loop even during CCD integration period. **(p. 53)**

TuA9 • Space–time wavefront analysis using a coordinate remapping Shack–Hartmann Sensor, N. J. Wooder, I. Munro, T. W. Nicholls, J. C. Dainty, *Imperial College, UK;* M. Wells, *Institute for Astronomy, UK.* We report measurements of the statistics of Zernike coefficients of wavefronts measured at a wavelength of 2.2 μm using a coordinate mapping Shack–Hartmann sensor. **(p. 56)**

TuA10 • Bispectral imaging toolbox, Pedro Negrete-Regagnon, *Imperial College, UK.* Bispectral imaging can be used in conjunction with or as an alternative to adaptive optics in order to obtain approximated diffraction-limited images. A toolbox of MATLAB functions is presented **(p. 59)**

TuA11 • Study of wavefront reconstruction methods, D. L. Ash, C. J. Solomon, *Univ. Kent at Canterbury, UK.* We present the results of a study that compares the different approaches to wavefront estimation using slope-based sensors. **(p. 62)**

TuA12 • Simulation of adaptive optical correction with deformable secondary mirrors, B. C. Bigelow, *Univ. College London, UK.* This paper documents results from closed-loop simulations of adaptive optical correction with large deformable secondary mirrors. The closed-loop simulations are based on modifications to a wavefront sensor simulation developed at the University of Durham. **(p. 63)**

TuA13 • Computationally efficient method for wavefront reconstruction, Stephen Browne, Jeff Vaughn, Glenn Tyler, *the Optical Sciences Company;* John D. Gonglewski, *USAF Phillips Laboratory.* A fast algorithm for measuring Hartmann spot positions is combined with a computationally efficient reconstructor running on a pair of i860XP processors to achieve 1000 reconstructions per second. Details of the fast reconstructor are described with particular emphasis on the creative use of computational resources. **(p. 66)**

TuA14 • Imaging by low order adaptive optics, M. L. Holohan, *Imperial College, London, UK.* A low cost, low order adaptive optical system using piezoelectric deformable elements is presented. A variety of hill climbing algorithms that drive the system are analyzed. **(p. 67)**

TuA15 • Fractional moments for investigating laser atmospheric scintillation statistics, A. Consortini, F. Rigal, *Univ. di Firenze, Italy;* F. Cochetti, *Alcatel Sietta, Italy.* Use of fractional moments to investigate probability density functions of intensity fluctuations in optical propagation measurements through atmospheric turbulence is proposed. **(p. 69)**

TuA16 • Interferogram evaluation by 4D analytic signal theory, Valeri A. Tartakowski, *Institute of Atmospheric Optics, Russia.* Conditions for the availability of the unique 4D phase function are considered. Applications to the phase restoration and the wave-front sensor design are suggested and demonstrated using a computer. **(p. 70)**

TuA17 • *Relation between conjugation error and inverted field intensity deviation,* V. A. Tartakowski, N. N. Myer, *Institute of Atmospheric Optics, Russia.* The error transfer from the input to the output is investigated in the reciprocal turbulence medium by some field modifications in the conjugation plane. **(p. 73)**

TuA18 • *The algorithms for measurement of displacement of white-light fringes,* Lev N. Butenko, Alexander G. Seregin, *S. I. Vavilov State Optical Institute, Russia;* Peter A. Fridman, *Institute for Analytical Instruments, Russia.* Abstract not available. **(p. 76)**

TuA19 • *Rapid phase retrieval using the fast Fourier transform,* T. E. Gureyev, K. A. Nugent, D. Paganin, A. Roberts, *Univ. Melbourne, Australia.* Phase retrieval from intensity data based purely on the Fourier transform is demonstrated experimentally and theoretically. Our method does not require boundary conditions. **(p. 77)**

TuA20 • *One-channel deformable mirrors for low-order adaptive optical compensation,* Andrey G. Safronov, *TURN Ltd., Russia.* One-channel deformable mirrors for use in laser adaptive systems of low-order correction were developed and investigated. Structure of the mirrors are described; the results of measurements and calculations are represented. Efficiency of the adaptive mirrors are shown for compensations of large-scale axial symmetric wavefront distortions in laser systems with the power up to 1 kW. **(p. 80)**

TuA21 • *Test and analysis of low-light characterization of the ICCD Hartmann–Shack wavefront sensor,* Qiang Zhang, Bing Xu, Li Chen, *Institute of Optics & Electronics, China.* The low-light characterization of the sensor under both continuous and pulse operations is tested and shows more light needed for the continuous operation under the same detecting accuracy. **(p. 83)**

TuA22 • *Potentialities of the methods of the posteriory processing of incoherently illuminated objects through the turbulent atmosphere,* Igor P. Lukin, *Institute of Atmospheric Optics, Russia.* Optical transfer function and integral resolution of the optical system "Turbulent Atmosphere Telescope" are treated theoretically by different methods of posteriory processing (Labeyrie, Knox–Thompson, and triple correlation of image intensity) of stellar speckle imaging. **(p. 85)**

TuA23 • *Influence of wavefront dislocations on phase-conjugation instability at thermal blooming compensation,* Boris V. Fortes, Vladimir P. Lukin, *Institute of Atmospheric Optics, Russia.* The paper presents the application of the phase conjugation method for thermal blooming compensation. Analysis of the numerical experiment data has shown that the appearance of continuous auto-oscillations in adaptive systems is connected with the occurrence of dislocations in the reference beam. **(p. 88)**

TuA24 • *Efficiency of adaptive correction of images in a telescope using an artificial guide star,* Vladimir P. Lukin, Boris V. Fortes, *Institute of Atmospheric Optics, Russia.* The paper describes the possibility of obtaining partially corrected images with resolution close to diffraction-limited for adaptation by the Rayleigh and sodium beacons. In both cases the Strehl ratio decreases as the telescope diameter increases. At the same time the angular resolution (FWHM) varies slightly and even is improved, remaining close to a diffraction one. **(p. 91)**

TuA25 • *Single-frequency Nd:YAG lasers as a light source for wavefront sensor interferometers,* Vadim A. Parfenov, Alexander G. Seregin, Sergei N. Rodin, *S. I. Vavilov State Optical Institute, Russia;* Sergei V. Kruzhalov, Vladimir A. Parfenov, *State Technical Univ., Russia.* Results are reported of the experimental study of single-frequency Nd:YAG lasers. The possibility of using Nd:YAG lasers as an internal reference light source in the adaptive telescopes wavefront sensors is discussed. **(p. 94)**

TuA26 • *Numerical simulation and test of a model thermo-adaptive mirror,* Vladimir V. Reznichenko, Victor V. Kotov, Yury V. Leonov, Vladislav N. Smirnov, Marina E. Zvezdina, *S. I. Vavilov State Optical Institute, Russia.* Experimental investigations and numerical simulation of the thermal control system performances as well as local electric heaters' control parameters are discussed. Material and parameters of reflectors for the temperature gradients compensation by heating are numerically simulated. **(p. 96)**

TuA27 • *The alternative large telescope construction,* Victor V. Sychev, Valery B. Kaspersky, *Russian Federation State Research Center, Russia.* We propose a new conception of the large astronomical telescope with a primary segmented mirror of 10 m. The telescope is supposed to be constructed using an alt-azimuthal scheme as an upper moving part having a sphere-like shape. **(p. 97)**

TuA28 • *Sodium guide star laser system for the Lick Observatory 3-m telescope,* Herbert W. Friedman, Gaylen V. Erbert, Donald T. Gavel, Thomas C. Kuklo, Jody G. Malik, J. Thaddeus Salmon, David A. Smauley, Gary R. Thompson, Jen Nan Wong, *Lawrence Livermore National Laboratory.* The design, installation, and performance data of a 20-W pulsed laser system for the 3-m Shane telescope at the Lick Observatory are presented. **(p. 98)**

TuA29 • *High accuracy capacitive displacement transducer for the position local control loops at the adaptive secondary,* Valdemaro Biliotti, Roberto Aiello, *Osservatorio Astronomico di Arcetri, Italy;* Guido Brusa, Roberto Biasi, Daniele Gallieni, Roberto Spairani, *Politecnico di Milano, Italy.* Operating principle and performance evaluation of a capacitive displacement sensor designed to measure voice coil actuator displacements for thin continuous facesheet secondary mirror adaptive control. **(p. 101)**

TuA30 • *Simulation of adaptive secondary mirror dynamic response,* R. Biasi, D. Gallieni, P. Mantegazza, *Politecnico di Milano, Italy.* 316 voice-coil actuators control a 0.64-m diameter 2-mm thick continuous facesheet adaptive secondary mirror. The control law is designed to compensate structure–actuators interaction. **(p. 104)**

TuA31 • *Wavefront generator for adaptive optics testing,* Enrico Marchetti, Roberto Ragazzoni, *Telescopio Nazionale Galileo, Italy.* The design of a wavefront simulator able to change r_0, f_G and f_0 on the produced starfield image is presented. **(p. 107)**

TuA32 • *New generation tip-tilt system,* Simone Esposito, Luca Fini, Piero Ranfagni, *Osservatorio Astrofisico di Arcetri, Italy.* The poster describes the architecture of a tip-tilt system of novel design, the laboratory optical set-up, the system behavior, and performances obtained in the image motion correction. **(p. 109)**

TuA49 • *Results from the MMT adaptive optics infrared imager FASTTRAC II,* L. M. Close, M. Lloyd-Hart, J. R. P. Angel, D. W. McCarthy Jr., G. Brusa, B. A. McLeod, T. D. Groesbeck, D. M. Wittman, P. T. Ryan, T. Martinez, P. Gray, J. M. Hughes, M. Cheselka, B. Jacobsen, *Univ. Arizona;* D. G. Bruns, D. G. Sandler, *ThermoTrex Corp.* FASTTRAC II utilizes six unique, economical, high performance tip-tilt mirrors to adaptively stack the MMT. Preliminary results show image improvement from 1.1″ to 0.6″ FWHM when the loop is closed at 60 Hz. **(p. 142)**

TuA50 • *Approaches for image processing in supporting adaptive optics,* Douglas G. Currie, Petras V. Avizonis, Daniel M. Dowling, Dianne P. O'Leary, James G. Nagy, *Univ. Maryland;* Robert Q. Fugate, *USAF Phillips Laboratory.* Image processing methods, highlighting specific hardware systems, will be demonstrated. Correcting spatial dependence and instrumental artifacts of the point-spread-function significantly improves image quality. **(p. 145)**

TuA51 • *Error reduction in centroid estimates using image intensifiers,* M. P. Cagigal, M. G. Portilla, P. M. Prieto, *Univ. Cantabria, Spain.* This paper presents a simple technique to reduce the error in the centroid estimate, due to deadtime in actual image detectors. **(p. 149)**

TuA52 • *Dynamic adaptive mirror in the algorithm of phase conjugation,* F. Yu. Kanev, V. P. Lukin, L. N. Lavrinova, *Institute of Atmospheric Optics, Russia.* The results of numerical simulation of transient processes that take place in adaptive optics systems are presented in the report. Two types of transient processes were investigated: those induced by nonlinear interaction of the laser beam and medium and those incited by oscillation of the mirror. The possibility of adaptive control was evaluated for both cases. **(p. 152)**

TuA53 • *Development of high QE, fast avalanche photodiodes for astronomical adaptive optics,* D. Bonaccini, *European Southern Observatory, Germany;* S. Cova, M. Ghioni, F. Zappa, *Politecnico di Milano, Italy;* R. Gheser, *Officine Galileo, Italy.* We show quantitatively how the read-out noise of fast read-out CCDs propagates through the correction loop and worsen its performance, both in tip-tilt sensors and in Shack-Hartmann wavefront sensors. Photon counters such as SPADs do not have read-out noise and do eliminate part of the problem. The practical cases of ESO Adonis (previously ComeOnPlus) and VLT-NAOS systems are analyzed and CCD vs. SPAD projected performance compared. **(p. 155)**

TuA54 • *Tip–Tilt correction at the Anglo-Australian Telescope,* J. J. Bryant, J. W. O'Byrne, R. A. Minard, P. W. Fekete, L. E. Cram, *Univ. Sydney, Australia.* The first stage of the AAT adaptive optics program, allowing tip–tilt correction for images and spectroscopy in the near infrared has recently been implemented. **(p. 159)**

LOBBY

8:00am–3:30pm
Conference Registration

AUDITORIUM

8:30am–10:30am
WA, Scientific Applications and Results
Peter Wizinowich, *W. M. Keck Observatory, USA, Presider*

8:30am (Invited)
WA1 • Astronomy with adaptive optics, P. Léna, *Univ. Paris VII & Observatoire de Paris.* Recent astronomical results obtained with the Adaptive Optics European system (ESO), from planets to galaxies, will be presented. **(p. 162)**

8:50am
WA2 • Post-processing of adaptive optics corrected images, Julian C. Christou, Jack D. Drummond, *USAF Phillips Laboratory.* Post-processing of adaptive optics data is presented with special attention to the problems of deconvolution given the inherent variability of the AO PSF. **(p. 163)**

9:10am
WA3 • Compensated imaging system (CIS) observations of the circumstellar envelope of P-Cygni, C. Morossi, M. Franchini, *Trieste Astronomical Observatory, Italy;* R. Ragazzoni, *Padova Astronomical Observatory, Italy;* G. Sedmak, *Univ. degli Studi Trieste, Italy;* A. Suzuki, S. Restaino, *Phillips Laboratory;* J. Albetski, *ThermoTrex Corp;* J. Africano, D. Nishimoto, *Rockwell Power Systems.* We have obtained direct CCD images with the Compensated Image System installed on the 1.6-m telescope at AMOS in Maui. To detect the emission from the nebula, we have used an occulting mask and interference filters centered on the strongest P-Cygni and nebular pure-emission lines. **(p. 166)**

9:30am
WA4 • Observational results from the University of Hawaii adaptive optics system, J. E. Graves, F. Roddier, C. Roddier, M. Northcott, *Univ. Hawaii.* Abstract not available. **(p. 169)**

9:50am
WA5 • High-resolution spectroscopy with an adaptive optics telescope, N. Woolf, J. R. P. Angel, J. Black, J. Ge, B. Jacobsen, M. Lloyd-Hart, *Univ. Arizona;* R. Fugate, *USAF Phillips Lab.* Results are shown from the mating of the SOR 1.5-m adaptive telescope with an echelle spectrograph of resolving power 700,000. **(p. 170)**

10:10am
WA6 • Imaging exoplanets with the 6.5-m MMT and Magellan telescopes, Roger Angel, David Sandler, *Univ. Arizona.* We plan to search for Jupiter-like exoplanets of nearby stars by diffraction-limited imaging, using high-resolution adaptive optics to strongly suppress the "seeing" halo. **(p. 172)**

LOBBY

10:30am–11:00am
Coffee Break

AUDITORIUM

11:00am–12:15pm
WB, Computational Methods
Glenn Tyler, *The Optical Sciences Co., USA, Presider*

11:00am
WB1 • Comparison of speckle image reconstruction techniques, David Dayton, Steve Sandven, *Applied Technology Assoc.* A number of computer post-processing algorithms have been demonstrated as being capable of producing high-resolution image reconstructions from an ensemble of short-exposure speckle images. Signal-to-noise ratio expressions have been derived for most of these techniques used. In this paper we compare the quality of different reconstruction techniques by applying them to the same sets of data, taken on 1.5-m class telescopes. These data include single and binary stars as well as extended objects. **(p. 176)**

11:15am
WB2 • Are scintillations indeed noise for wavefront sensing? Erez N. Ribak, *Technion—Israel Institute of Technology, Israel.* Stellar scintillations are the Fresnel diffraction of high-elevation turbulence. By inverting them, the contributions of low and high atmosphere can be separated. **(p. 179)**

11:30am
WB3 • Visibility signal-to-noise ratio in adaptive optics two-telescope interferometry, Jean-Marc Conan, Gérard Rousset, *Office National d'Etudes et de Recherches Aérospatiales, France.* SNRs of long and short exposure visibilities are compared. The choice of the visibility measurement technique, according to the adaptive optics correction quality, is discussed. **(p. 182)**

11:45am
WB4 • Sky coverage calculations for astronomical adaptive optics, Brent L. Ellerbroek, *USAF Phillips Laboratory;* René Racine, *Univ. Montréal, Canada;* David Tyler, *Rockwell Power Systems.* We describe computational methods and numerical results regarding the sky coverage achievable using natural and laser guide star adaptive optics on 8-m astronomical telescopes. **(p. 185)**

12:00m
WB5 • Artificial guide star tilt-anisoplanatism: its magnitude and (limited) amelioration, David L. Fried, *Consultant.* Tilt-anisoplanatism limits the quality of the image when a nearby natural guide-star is used to provide the tilt information which an artificial guide-star cannot provide. When several nearby natural guide-stars are used together, this situation is somewhat ameliorated. Analysis and quantitative results are presented. **(p. 188)**

12:15pm–2:00pm
Lunch on your own

AUDITORIUM

2:00pm-3:15pm
WC, Russian and Asian Adaptive Optics
Vladimir P. Lukin, *Institute of Atmospheric Optics, Russia,*
Presider

2:00pm (Invited)
WC1 • Computer modeling of adaptive optics and sites for tele-
scope design, Vladimir P. Lukin, *Institute of Atmospheric Optics,*
Russia. A computer code for simulation imaging in a ground-based
telescope is described. This code allows one to simulate the com-
ponents of adaptive systems, such as the wavefront sensors and vari-
ous active and adaptive mirrors, as well as different models of
turbulent atmosphere. **(p. 192)**

2:15pm
WC2 • Experimental study of compensation for laser thermal
blooming, Li Youkuan, Zhang Xinwei, *Beijing Institute of Applied*
Physics and Computational Mathematics, China; Su Yi, Zhang Kai,
Southwest Institute of Applied Electronics, China. Using 19-element
adaptive optics system, real-time correction for laser thermal bloom-
ing was realized; far field energy was 2.7 times higher without cor-
rection. **(p. 195)**

2:30pm
WC3 • Principles of development of bimorph adaptive optics,
Andrey G. Safronov, *TURN Ltd., Russia.* Current trends in the de-
velopment of deformable mirrors based on bimorph structures are
described. Also presented are results of the investigation of cooled
bimorph mirrors for laser optics of medium-powered (up to 15 kW),
industrial one-channel bimorph mirrors for low-order compensa-
tion in low-powered laser optics (up to 1 kW) as well as large aper-
ture (more than 3 m) bimorph mirrors for astronomical telescopes.
(p. 196)

2:45pm
WC4 • Adaptive astronomical telescope with two-stage wavefront
correction: current status of a project, D. N. Yeskov, B. E. Bonshtedt,
S. N. Koreshev, G. I. Lebedeva, V. A. Parfenov, V. I. Podoba, V. V.
Reznichenko, A. G. Seregin, V. I. Sidorov, V. N. Smirnov, L. G. Fedina,
N.T. Firsov, V. Kh. Khakunov, I. Sh. Etsin, *S. I. Vavilov State Optical*
Institute, Russia. Results of development of an adaptive telescope
with a primary mirror of 3.2 m diameter and field-of-view of 1° are
presented. The telescope concept is discussed in general as are prob-
lems of key components development and perspectives of the project
completion. **(p. 199)**

3:00pm
WC5 • Methods of adaptive optics to control the output radiation
of industrial lasers, A. V. Kudryashov, *Scientific Research Center for*
Technological Lasers, Russia. Efficiency of flexible mirrors applica-
tion inside the cavity of different types of technological lasers is
discussed. The results of control of the output parameters of CO_2,
excimer, copper-vapor and solid-state lasers with deformable
bimorph mirror are presented. **(p. 202)**

3:15pm
Free time

LOBBY

8:00am–3:00pm
Conference Registration

AUDITORIUM

8:30am–10:30am
ThA, Adaptive Optics Components
Robert K. Tyson, *W. J. Schaffer Associates, Inc., USA, Presider*

8:30am (Invited)
ThA1 • Adaptive optics in Western Europe, Fritz Merkle, *Carl Zeiss, Germany.* In Western Europe in the early seventies main emphasis was put on high-power laser applications. Later, compensated imaging became the main driver, leading to the first routinely operated adaptive system in astronomy. **(p. 206)**

8:50am
ThA2 • Comparison of adaptive-optics technologies for large astronomical telescopes, François Rigaut, *Canada-France-Hawaii Telescope;* Brent L. Ellerbroek, *USAF Phillips Laboratory;* Malcolm J. Northcott, *Univ. Hawaii.* We present the results of independent numerical simulations of adaptive-optics systems for 8-m astronomical telescopes using both Shack–Hartmann and curvature wavefront sensors. **(p. 207)**

9:10am
ThA3 • Performance test of the slow wavefront sensor for the large Earth-based solar telescope LEST, Mette Owner-Petersen, *Tech. Univ., Denmark;* Michael Jensen, *Roskilde Univ. Center, Denmark;* Oddjørn Engvold, *Institute of Astrophysics, Norway.* A prototype slow wavefront sensor for LEST has been constructed and tested in the laboratory under realistic conditions. The test results obtained so far indicate that the sensor will operate according to specifications. **(p. 210)**

9:30am
ThA4 • Techniques for optical fabrication of a 2-mm-thick adaptive secondary mirror, H. M. Martin, D. S. Anderson, *Univ. Arizona.* We describe techniques for the optical fabrication of a 64-cm-diameter, 2-mm-thick adaptive secondary mirror, including methods of blocking the thin shell to a rigid substrate. **(p. 213)**

9:50am
ThA5 • Spatial light modulator structures for adaptive optics, C. L. Woods, *USAF Rome Laboratory.* Spatial light modulators have substantially improved over the past few years, and several commercial devices are now available for optical signal processing. We apply our device simulations of spatial light modulators in optical correlators to analyze the performance of continuous/discrete phase-modulating SLMs and micro-optical pixel designs. **(p. 216)**

10:10am
ThA6 • Characterization of the wavefront produced by a two-dimensional spatial liquid optoelectronical light modulator, Lea V. Bourimborde, Lia M. Zerbino, Anibal P. Laquidara, Mario Garavaglia, *Univ. Nacional de La Plata, Argentina;* Eduardo Aguirre, *Univ. Technol. Nacional, Argentina.* Abstract not available. **(p. 217)**

LOBBY

10:30–11:00am
Coffee Break

AUDITORIUM

11:00am–12:30pm
ThB, Nonconventional Applications and Techniques
Willy L. Bohn, *Institute for Technology and Physics, Germany, Presider*

11:00am
ThB1 • Liquid crystal over VLSI silicon spatial light modulators for adaptive optics, J. Gourlay, A. O'Hara, D. G. Vass, *Univ. Edinburgh, UK.* Liquid crystal over silicon backplane spatial light modulators have many advantages for adaptive optics. Progress in this technology is presented, and the future potential is discussed. **(p. 220)**

11:15am
ThB2 • High-quality liquid crystal spatial light modulators for adaptive optics, Gordon D. Love, Sergio R. Restaino, Richard A. Carreras, Gary C. Loos, *USAF Phillips Laboratory;* Ray M. Sharples, *Univ. Durham, UK;* Rob V. Morrison, *Meadowlark Optics.* Results of static wavefront correction and the production of Zernike wavefront aberrations with a liquid crystal spatial light modulator are presented. **(p. 223)**

11:30am
ThB3 • Atmospheric compensation using nonlinear optical phase conjugation, A. Scott, D. C. Jones, K. D. Ridley, G. Cook, *Defence Research Agency, UK.* Abstract not available. **(p. 226)**

11:45am
ThB4 • Feedback interferometry for aberration correction, T. H. Barnes, G. T. Bold, *Univ. Auckland, New Zealand;* T. G. Haskell, *Industrial Research Ltd., New Zealand.* We describe an interferometer incorporating a spatial optical phase modulator and opto-electronic feedback, which may be used for automatic aberration correction. **(p. 229)**

12:00m
ThB5 • Adaptive telescope array for laser communications and astronomy, Klaus H. Kudielka, Walter R. Leeb, *Technische Univ., Germany.* We demonstrated that self-phased telescope arrays are useful in laser intersatellite communications. It is suggested to employ this concept to obtain images of astronomical objects. **(p. 232)**

12:15pm
ThB6 • High speed micro-machine for adaptive correction of aero-optic effects, Rod Clark, John Karpinsky, Gregg Borek, Eric Johnson, *SY Technology, Inc.;* Natalie Clark, *Phillips Laboratory.* This paper describes a complete adaptive optics system on a single integrated circuit chip. This is accomplished through a combination of micro-optics, micro-machines, and CMOS integrated circuits. **(p. 235)**

12:30pm–2:00pm
Lunch on your own

AUDITORIUM

2:00pm–3:00pm
ThC, Site Characterizations and Novel Concepts
Don Walters, *U.S. Naval Postgraduate School, USA, Presider*

2:00pm (Invited)
ThC1 • Site atmospheric characterization, Marc Sarazin, *European Southern Observatory, Germany.* As adaptive optics techniques turn into integrated self-optimized systems, a new infrastructure is proposed to answer the need of an independent routine monitoring of the spatiotemporal behavior of the optical turbulence above large ground-based telescopes. **(p. 240)**

2:15pm
ThC2 • Two decades of atmospheric site characterization, D. L. Walters, *U.S. Naval Postgraduate School.* Nearly two decades of atmospheric-optical coherence length, isoplanatic angle, thermal probe and acoustic echo-sounder data have been collected at over 15 sites from the Hawaiian islands to the Caribbean. Common site characteristics and the atmospheric conditions that produced them are discussed. **(p. 242)**

2:30pm
ThC3 • Adaptive optics requirements for a ground-to-space las communications system, Robert K. Tyson, *W. J. Schafer Assoc.* Tl interaction of adaptive optics design parameters and laser comm nication system performance is discussed. Adaptive compensatic of scintillation is examined in ground-to-space uplinks and dow links. **(p. 244)**

2:45pm
ThC4 • Mesospheric metals for guide star generation, George Papen, *Univ. Illinois.* The characteristics of several mesospher metals that may be used for guide star generation are presented. It shown that all three have roughly comparable performance. **(p. 24**

3:00pm
Free time

LOBBY

8:00am–10:30am
Conference Registration

AUDITORIUM

8:30am–10:15am
FA, Adaptive Optics Experimental Results
Marc Séchaud, *Office National d'Etudes et de Recherches Aerospatiales, France, Presider*

8:30am
FA1 • Laser and natural guide star measured turbulent wavefront correlation, Ruy Deron, Sylvain Laurent, Marc Séchaud, Gérard Rousset, *Office National d'Etudes et de Recherches Aérospatiales (ONERA), France.* A Rayleigh laser guide star experiment, implemented on the CERGA-Observatory 1.5-m telescope, is described. Laser and natural star wavefront intercorrelations are measured. **(p. 252)**

8:45am
FA2 • Short-exposure measurements of anisoplanatism using binary stars, Brent L. Ellerbroek, Julian C. Christou, James F. Riker, J. Timothy Roark, *USAF Phillips Laboratory.* Short-exposure measurements of the binary star Mizar are used to determine the effects of anisoplanatism upon the performance of closed-loop adaptive-optics. **(p. 254)**

9:00am
FA3 • Analysis and calibration of natural guide star adaptive optics data, Eric Tessier, *Royal Greenwich Observatory, UK.* From natural guide star adaptive optics data, we study the properties of the point spread function and discuss the performances of deconvolved adaptive optics images. **(p. 257)**

9:15am
FA4 • Post-detection correction of compensated imagery using phase-diverse speckle, John H. Seldin Richard G. Paxman, *Environmental Research Institute of Michigan;* Brent L. Ellerbroek, *USAF Phillips Laboratory.* Results from post-processing phase-diverse speckle images of closely-spaced binary stars collected with natural and artificial guide star adaptive-optics compensation are presented. **(p. 260)**

9:30am
FA5 • Experimental results of a low-order adaptive optics experiment on the Starfire 3.5-m telescope, John D. Gonglewski, *USAF Phillips Laboratory;* David Dayton, Steven Sandven, Darren Laughlin, *Applied Technology Associates;* Sam Rogers, Scot McDermott, *Logicon R & D Associates;* Stephen Browne, *the Optical Sciences Company;* Robert Babnick, Joe Rae, Joe Gallegos, *Rockwell Power Systems;* Ron Highland, *Kaman Sciences Corp.* An experiment with a nasmyth adaptive optics system mounted on the SOR 3.5-m telescope is described. The 183-actuator mirror allows only partial compensation in the near IR, and the imagery is enhanced by postprocessing methods. We describe the system design and evaluate the performance based on long-to-short exposure SNR ratio metrics. **(p. 263)**

9:45am
FA6 • Near-infrared imaging at the Starfire Optical Range, Paul M. Harvey, Chris D. Koresko, *Univ. Texas at Austin;* Julian C. Christou, Robert Q. Fugate, *USAF Phillips Laboratory.* We present preliminary results from one-half night of NSF-supported observing on the 1.5-m SOR telescope via a NICMOS-3 camera at 1.6 µm. **(p. 264)**

10:00am
FA7 • Optimization of closed-loop adaptive optics wavefront reconstruction algorithms using experimentally measured performance data: experimental results, Troy A. Rhoadarmer, Brent L. Ellerbroek, *USAF Phillips Laboratory.* We describe a method for optimizing wavefront reconstruction algorithms using measured closed-loop performance data and present experimental results combining laser and natural guidestar wavefront sensing. **(p. 265)**

AUDITORIUM

10:15am–10:20am
Closing Remarks

Adaptive Optics
Telescope Projects I

MA 8:30 am-10:10 am
Auditorium

Martin Cullum, *Presider*
European Southern Observatory, Germany

The ESO VLT Adaptive Optics program

N. Hubin
European Southern Observatory, Karl-Schwarzschild-Str. 2, D-85748 Garching, FRG

1. INTRODUCTION

Adaptive optics is one of the main features of the Very Large Telescope of the European Southern Observatory (ESO). Use of the large telescopes for high spatial resolution imaging, high spectral resolution spectroscopy and astronomical spatial interferometry depends substantially on the availability of adaptive optics, which allows diffraction limited imaging in the near infrared wavelength range (2.2 to 5 microns) and partial correction of atmospheric distortions towards the visible wavelength range.

A long term strategy has been followed at ESO to evaluate and demonstrate the feasibility of an adaptive optics system for 8-meter class telescopes. Prototypes such as Come-On and Come-On-Plus (COP) were developed and tested on the ESO 3.6 m telescope at La Silla Observatory[1,2,3,4,5]. The latter, from the promising technical results obtained at the telescope, was offered and is now currently used as a standard "instrument" by the European astronomical community[6]. At this stage adaptive optics is still a complex observation technique requiring specialised people to operate it: a long way from the turn-key VLT adaptive optics system. Therefore, it was decided to use the COP system as a software platform for the VLT. This allows test of observing procedures, better understanding and optimisation of the parameters and development of a user-friendly interface keeping in mind the needs of the user. This development known as ADONIS project[7,8] is being progressively implemented and will be completely available beginning 1996.

The current plans are to proceed for the construction of a "first generation" Adaptive Optics System (NAOS) for the Nasmyth focus of the Unit Telescope 1 in collaboration with European astronomical institutes and industries. NAOS will provide correction for an IR spectro-imaging instrument (CONICA) currently in construction. The first light of the complete system is expected for beginning 1999.

In parallel, ESO decided to support a system study for a second generation adaptive optics system using Laser Guide Star which could be implemented for Unit Telescope 4 of the VLT. The Laser Guide Star activities will be tackled in the final paper.

2. REQUIREMENTS FOR NAOS

The design of an Adaptive Optics system is a complex trade off that depends on the general scientific goals pursued, the physical limitations, the technology available at a given time and the budget involved.

For instance, one has to evaluate the wavelength for which the correction and the physical limitations will provide the best image quality or spectrum. For the VLT, the choice is to perform low frequency tip-tilt corrections with the secondary mirror for the long wavelengths (10 microns) in order to sharpen the image while limiting the background sources from additional mirror surfaces. At this wavelength, D/ro is in the range of 1 to 2 (ro Fried diameter) under good seeing conditions and an 8 Hz tip-tilt correction can provide image Strehl ratio of 50 to 70%.

At 5 microns where D/ro is in the range of 4 to 6 the background produced by the adaptive optics additional mirrors which is an order of magnitude lower than at 10 microns, is however a critical limitation, but a low frequency tip-tilt correction does not allow us to have a Strehl ratio better than 20% under average seeing conditions. In L band (3.8 microns); D/ro in the range of 5 to 8) the background emission is again approximately an order of magnitude lower and a Strehl of 10% is hardly achievable with a tip-tilt correction only. Between 2.5 and 1 micron (D/ro in the range of 10 to 30) both high spatial and temporal frequency corrections become essential: we are within the adaptive optics field where the technology is demonstrated and currently available. In the visible, the isoplanatism limitation and the spatial sampling of the wavefront requires brighter reference stars which lead to use of expensive artificial star techniques especially for 8 m class telescopes.

This discussion outlines the driving factors which have led ESO to go up to a near infrared adaptive optics system for the VLT allowing partial correction in the visible.

The top-level and functional requirements for NAOS are such that it should maximise as a primary scientific goal, the sky coverage for natural guide star and reach the diffraction limit (Strehl ratio=0.7) for wavelengths larger than 2.2 micron under 0.8 arcsec seeing conditions and 10.5 m/s average wind speed for a visible reference star magnitude of 13. The image motion stabilisation is required to be better than 10 milliarcsec rms on the sky. In addition, it is planned to implement an infrared wavefront sensors in order to perform a correction for object or reference stars with a visible counterpart which is too low. The infrared wavefront sensor will have a limiting magnitude of about 11-13.

3. PRELIMINARY DESIGN OF NAOS

Optimised for full correction at 2.2 μm, the sub-aperture size at the primary mirror location should be of the order of the Fried diameter at the considered wavelength. This leads to about 250 actuators for the deformable mirror. The minimum inter-actuator spacing currently achievable is 6 to 7 mm which sets the clear aperture pupil diameter to about 110 mm. Below this spacing value, local stresses and reduction of the actuator differential stroke increase drastically the wavefront high spatial frequencies and consequently degrade the image quality of the system.

The visible wavefront sensor will be based on a low noise fast readout CCD camera currently under development. The high level requirements for this camera are provided in the table below. In addition, some studies to develop high efficiency Avalanche Photodiodes for low order correction to provide a better sky coverage at low light level and for future Laser Guide Star applications are being pursued.

Parameters	Minimum	Goals	Remarks
Pixel size	25-30 µm	50-60 µm	big pixels by binning 2x2 of a 256x256
Exposure time	2-200 ms	N.A	
Frame readout time	<2 ms	<1 ms	
Number of pixels	128x128	256x256	useful pixels
Quantum efficiency	<80%	max	in average
Wavelength range	450-950 nm		
Readout noise (rms)	2-4 e-/pixel	min	@ 500 Hz frame rate
Readout noise (rms)	<2 e-/pixel	min	@ 100 Hz frame rate
Dark noise (rms)	<0.4 e-/pix/s	min	Cooling temperature <-40 C
Frame transfer	20 µs	10 µs	An optical masking for the storage area of the CCD will be provided
Photometric size	100 %	100 %	
Binning capability	2x2; 3x3; 4x4; 5x5	N.A.	
Full Well Capacity	10000	10000	
Electronic gate	no	yes	This option will be considered only if it does not reduce the other parameters

The interest in modal control has been extensively described in the literature and successfully applied to our Come-On-Plus/ADONIS prototype system[9, 10] and an astronomical AO system often implying low light levels for wavefront sensing cannot deviate from using such a powerful tool.

The computing time is widely dominated by the read-out time of the visible wavefront sensor detector. Indeed, relatively low cost DSP boards i.e. C40 based with sufficient computing power are now on the shelf products[8] and can send the deformable mirror commands as soon as the last pixel is read (a few 10s of microseconds). This type of computer has been implemented recently on our ADONIS prototype system at La Silla.

REFERENCES

1. P. Kern et al.,"Adaptive optics system for infrared astronomy: I System description", *Proc. SPIE*, 1271, 22, 1990
2. G. Rousset et al.,"First diffraction limited astronomical images with adaptive optics", *Astron. Astrophys.*, 230, L29, 1990
3. F. Rigaut et al.,"Adaptive optics on the 3.6 m telescope: results and performance", *Astron. Astrophys.*, 250, 280, 1991
4. N. Hubin et al.,"New AO prototype system for the ESO 3.6m telescope: Come-On-Plus", *Proc. SPIE* 1780, 87, 1992
5. G. Rousset et al.,"The Come-On-Plus Adaptive Optics System: Results and performance", in *ESO Conf. Workshop Proc.*, 48, F. Merkle, Ed. (European Southern Observatory, in press)
6. P. Léna, G. Monnet "Astrophysical Results with ADONIS" *in this conference*
7. N. Hubin et al., "ADONIS: A user-friendly adaptive optics system for the ESO 3.6m telescope", in *ESO Conf. Workshop Proc.*, 48, 1993
8. J.L. Beuzit et al., "ADONIS: A user-friendly adaptive optics system for the ESO 3.6m telescope", *in this conference*
9. J.Y. Wang et al., "Modal compensation of atmospheric turbulence phase distortion", *J.Opt. Soc.Am.*, 68, 1, 1978
10. E. Gendron, "Modal control optimisation in an adaptive optics system", in *ESO Conf. Workshop Proc.* 48, 1993, 1982

United Kingdom Adaptive Optics Programs

Gerry Gilmore
Institute of Astronomy,
Madingley Road,
Cambridge CB3 OHA,
United Kingdom
Tel: +44 1223 337506
Fax: +44 1223 337523

The UK has a funded, national program underway to design and construct facility (common user) natural guide star (NGS) adaptive optics systems for two telescopes:

- The 4.2m William Hershel Telescope (WHT) on La Palma, Canary Islands.

- The 3.8m United Kingdom Infrared Telesope (UKIRT) on Mauna Kea, Hawaii.

These will be locally-supported systems, capable of feeding a number of science instruments, including dedicated AO-optimised imagers and spectrographs. They will be optimised for operation in the near infrared, $\sim 2\,\mu$m.

The programme includes related work in the areas of site evaluation, instrument development, AO prototyping, system modelling and scalable-power sodium laser beacon development. These also underpin the second phase of the program, providing laser guide star, higher-order, shorter-wavelength, adaptive optics on the WHT, with near all-sky coverage.

0.1   The WHT NGS AO System

The first NGS AO instrument, for the WHT, has just passed through Conceptual Design Review, and is on schedule for use in early 1998. Its principal design features are:

- an 8×8 subaperture Shack-Hartmann wavefront sensor, coupled to a low-noise frame-transfer CCD, controlling a continuous facesheet mirror. The system may be rapidly descoped to 4×4 operation when required by observing conditions.

- optimised for 2-micron scientific operation where both high Strehl-ratio (limited sky coverage) and high sky-coverage (limited Strehl ratio) operation will be supported.

- scientific operation in the wavelength range 0.8 to 4.1 μm. An additional visible light science port is also included for partial AO at shorter wavelengths.

- an ability to use separate tip-tilt and wavefront sensing stars selected from the large ($2.9 arcmin$) field, and to offset (dither) these guide stars from the science field without losing lock and without producing pupil image shifts at the science instrument.

- a default capability to carry out sensing and correction at a conjugate image of a dominant turbulent layer, rather than just at a telescope pupil. Both vignetting and wavefront extrapolation options are being considered for dealing with the partial illumination of the wavefront sensor when conjugate correction is used.

- a flexible and scalable control system based on TI TMS320C40 digital signal processors. This will support high speed visualisation and data logging as well as the ability to optimise the system on-the-fly. The goal is to maximise the performance and availability of the system, particularly the time spent on science integration.

- a 256 × 256 InSb camera, WHIRCAM, has already been commissioned, to support $1-5\,\mu$m AO (and other) imaging on the WHT. This is a twin of the UKIRT cameras.

- support for a laser beacon (in a high sky coverage, near-IR mode) when available.

0.2   Analytic System Modelling

An end-to-end analytic model of the WHT natural guide star adaptive optics system has been developed. The model includes realistic representations of the wavefront sensor, deformable mirror, image tracker, and their control systems in closed loop operation. It produces as output the theoretical (corrected) point spread function at the science detector. The effects of photon and detector read noise in the wavefront sensor are included, as a function of reference star brightness. Angular and temporal anisoplanatism are calculated for given $C_n^2(h)$ and wind velocity distributions. Results from the UK 'JOSE' site characterisation programme are used to choose realistic parameters for the range of atmospheric models considered. The analysis is being used to investigate key problems for the WHT AO system, including:

- wavefront sensor and tracker design.

- requirements for turbulence conjugation, and the effects of wavefront extrapolation in reconjugated corrections.

- system order and bandwidth optimisation as a function of guide star(s) brightness and angular offset.

- sky coverage of the system as a function of the required properties of the corrected point spread function.

0.3   MARTINI-III - an interim AO system for the WHT

In order to provide immediate scientific access to a near-IR AO system, the 6-element segmented-mirror MARTINI system has been upgraded, with a new CCD-based wavefront sensor, and reconfigured for IR scientific operation feeding WHIRCAM. Initial trials and current (6/95) full commissioning suggest full availability for astronomy from August 1995.

0.4   JOSE - site evaluation at La Palma and Mauna Kea

Optimal real-time configuration of a common-user AO system requires algorithms which are appropriate for use under real operating conditions. Optimization of the NGS AO system design, including its conjugation capabilities, its science instrumentation and its scheduling, and development of the laser guide star system, all require knowledge of the site atmospheric properties. Very little such data exist. AO-specific site data on La Palma and Mauna Kea are therefore being obtained routinely from wavefront measurements using WHT and UKIRT, in both the near IR and the optical. The parameters currently being measured include:

- seeing coherence lengths and timescales and their temporal evolution, together with complementary meteorological and dome environment data;

- modal power spectra;

- angular decorrelation of modes;

- the vertical distribution of turbulence.

The optical data are acquired with an 8 × 8 Shack-Hartmann wavefront sensor similar in design to the final NGS AO system wavefront sensors. Thus the recorded data streams may be used directly in numerical system modelling and performance prediction work.

0.5   Sodium laser beacon development

The current emphasis of the laser beacon work is the laboratory demonstration of a fibre-fed sodium dye laser with output power scalable from a few watts to around 50 watts. It is intended to begin work on a system suitable for field use shortly.

0.6   High order AO prototyping and instrument development

High order, multi-conjugate, and laser beacon-based adaptive optics prototyping, and AO-optimised instrument development, are all under investigation. Experiments are to be supported by the second generation AO prototype system: ELECTRA. This is a segmented mirror AO system, with 76-segments and 228 degrees of freedom.

A Laser Guide Star Atmospheric Compensation System for the 3.5m Calar Alto telescope

Allan Wirth, Frank Landers, Bruce Trvalik, Joe Navetta, and Terry Bruno
Adaptive Optics Associates Inc.
54 CambridgePark Drive, Cambridge, MA 02140
(6i7) 864 0201 FAX (617) 864 1348

The Max Planck Institute for Astronomy in Heidelberg is constructing a laser guide star atmospheric compensation system for the 3.5m Calar Alto telescope. The system consists of a tilt compensation loop, a high-order adaptive optics loop, and a sodium wavelength dye laser. These subsystems are to be fully integrated into the observatory control software system. The hardware is to be installed at the telescope and testing begun in the spring of 1996. This paper deals with several aspects of the design of this system as well as reporting results from subsystem testing.

Because this system is being built on an aggressive schedule one overriding design goal was the preferential use of existing, proven components. This both reduces the technical risk and eliminates much of the development time. An analysis of the scientific goals and the available major components has produced a system design that should combine good performance with high reliability and availability. The details of some of these design choices are presented. In particular, the cameras for both the tip/tilt and the adaptive optics sensors and the higher-order control loop algorithms are thoroughly discussed.

Another part of the design philosophy was the maximization of the flexibility of the system. This stemmed, in large part, from the experiences of currently operating atmospheric compensation programs. Frequently, for unexpected (and often unexplained) reasons the performance of these systems falls below expectations. Further, the performance varies from night to night and these variations do not correlate well with measurements of traditional atmospheric parameters. To address these potential unknown effects, a system is being built that allows the operator to vary most of the critical parameters. For example, the frame rate, the spatial sampling frequency, the spatial frequency response, and the bandwidth may all be changed rapidly and

conveniently. The software approach that allows this level of flexibility is covered in detail.

Finally, the results of component testing will be presented. It is anticipated that most of the major components will have undergone characterization by the time of the conference and whatever data is available will be presented.

The Adaptive Optics system for the
Telescopio Nazionale Galileo (TNG)

R. Ragazzoni[1], D. Bonaccini[2]

[1]Astronomical Observatory of Padova, Italy
[2]European Southern Observatory, Garching, Germany

The *Telescopio Nazionale Galileo* (namely the Italian National Telescope "Galileo") is a national 3.5m facility under construction at the Roque de Los Muchachos in Canary Islands. It consists into a classical Ritchey–Chretien optical configuration with two nasmith foci available. Of the two foci one is devoted to imaging, both in the InfraRed and in the visible, the other is mainly devoted to spectroscopy.

In the imaging Nasmith side an Adaptive Optics system is under construction. Its main optical layout is shown in Fig.1 where the optical bench, rotating with the derotating system (to counter-act the field rotation, being the TNG an altazimuthal one) provides with an all–reflecting system, a magnification from the F/11 nominal focus to F/35 over a field ov view of approx one square arcmin.

Through a foldable flat mirror the optical path can be redirected toward the InfraRed or the Optical imager. The pupil is re–imaged onto the deformable mirror that, driven by the light fed from a multi–position dichroic wheel onto a wavefront sensor, will be able to produce wavefront corrections up to an 8 × 8 sub–pupils spatial coverage.

The tip–tilt correction is performed by an *ad–hoc* mirror located in the optical train.

The wavefront sensing should be able to map the wavefront with a variable sampling, in order to deal with different conditions of the atmospheric
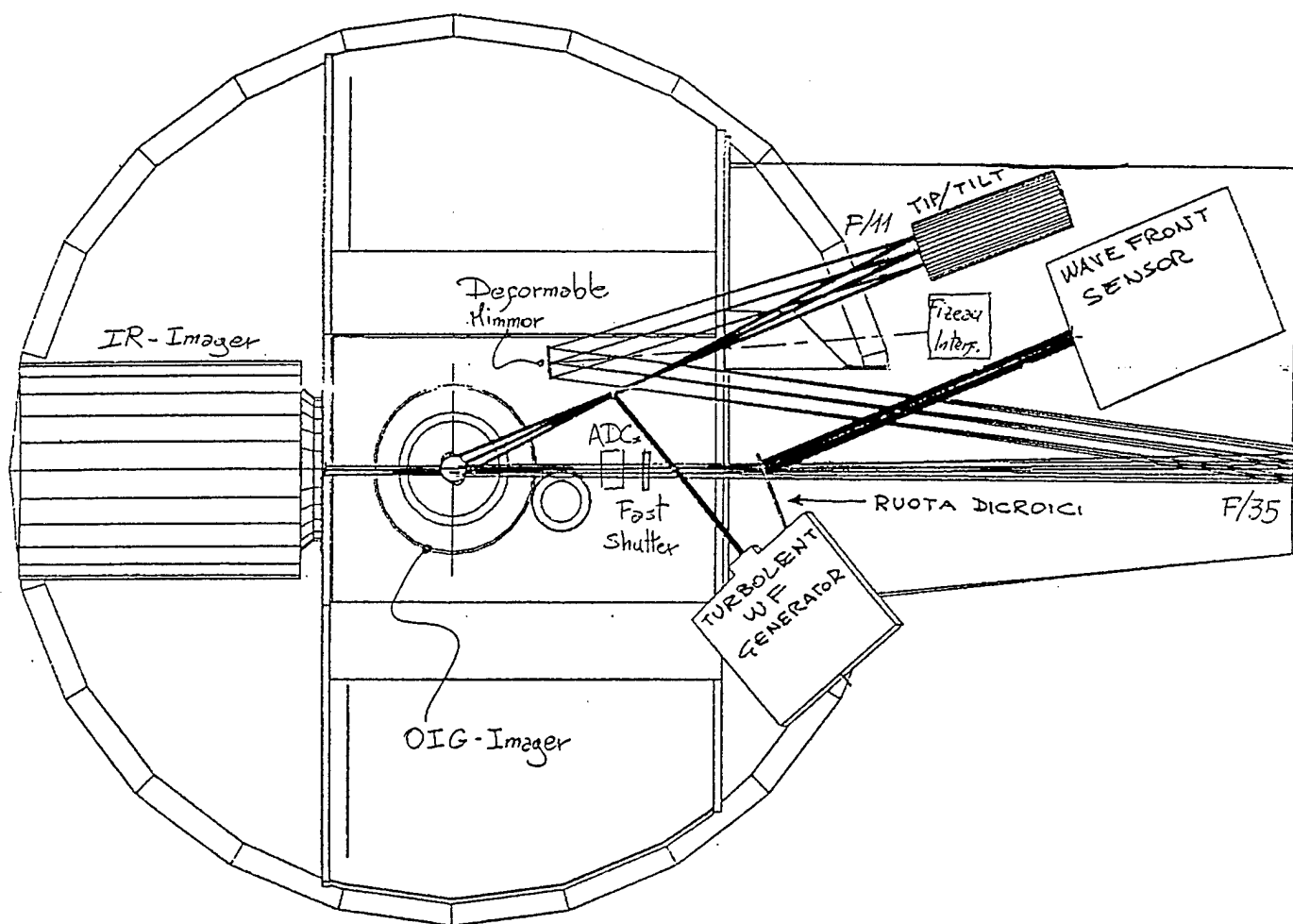
Figure 1: The optical layout for the TNG Adaptive Optics system. See the text for details.

turbulence (D/r_0) and with different brightness of the nearby natural stars used as a reference.

Addittional options, like a fast shutter to avoid broadening of the image during bad–seeing bursts and a simplified speckle facility, are also foreseen.

Low Order Adaptive Optics at the Anglo-Australian Telescope

J. W. O'Byrne*, J. J. Bryant, R. A. Minard, P. W. Fekete and L. E. Cram

School of Physics, University of Sydney, NSW Australia 2006
Ph: 61-2-351-3184, Fax: 61-2-660-2903
(* j.obyrne@physics.usyd.edu.au)

The adaptive optics (AO) project at the Anglo-Australian Telescope (AAT) is sponsored by a consortium of Australian universities and the Anglo-Australian Observatory (AAO) and funded by the Australian Research Council (ARC). The program has two objectives:

1. to prove the usefulness of adaptive optics at the AAT site, and

2. to rapidly implement an adaptive system, providing a scientifically valuable gain in the resolution and efficiency of the telescope.

The intent is to implement a system based largely on proven technology, rather than beginning a research project in adaptive optics. A relatively modest program is planned, based on correction of image motion ('tip-tilt') and low orders of aberration. A low order system using Roddier's curvature sensing scheme (Roddier 1988, Graves et al. 1994) has been chosen because it offers good performance with a minimum number of sensors. This will maximise sky coverage in the absence of any laser beacon.

The coudé focus was chosen as the best place to implement an initial AO system at the AAT since it imposes less stringent constraints on the layout and easier access during development.

Seeing at the AAT

Predicting the performance of an AO system requires a detailed knowledge of seeing parameters for the site, based on measurements over extended periods. Seeing records at the AAT primarily consist of visual estimates by various observers and FWHM measurements from a video image of a target star. These data indicate a median seeing of 1.8 arc seconds. However, improved data are now becoming available with the installation of Differential Image Motion Monitors (DIMMs) on the 20-inch finder on the side of the AAT and elsewhere on the mountain. From February 1994 to Jan 1995 the AAT DIMM measurements showed sub-arcsecond seeing a third of the time, with a median seeing of 1.26 arc seconds. This better result may reflect the difficulty of accurately measuring values below 1 arc second in the earlier records. However the initial stage of the AO system, which provides tip-tilt correction only, will provide independent r_o and τ_o data, as well as some knowledge of the atmospheric turbulence profile at Siding Spring.

Benefits of adaptive optics at the AAT

At visible wavelengths, in 0.5 arc second seeing, conventional seeing theory predicts a factor of 2 improvement in resolution with tip-tilt alone, and twice that gain with a low order system. For infrared observations, tip-tilt alone produces its maximum resolution gain (for $D/r_0 \sim 4$) and achieves Strehl ratios ~ 0.3 at K-band in the same excellent seeing. A low order system will achieve the same Strehl values and much higher resolution in median to good seeing ($\sim 50\%$ of the time). These infrared images would show an essentially diffraction limited core with FWHM of 0.14 arc seconds at K. Clearly the greatest AO gains can be made in the infrared, thus the system is designed primarily to serve IRIS, the InfraRed Imager/Spectrograph (Allen et al. 1993).

The performance of an AO system is also dictated in part by the optical quality of the telescope itself. Although a low order AO system will correct low order telescope aberrations, as well as seeing aberrations, higher order components will remain. Furthermore, a system correcting tip-tilt only must cope with the total telescope aberrations. Recent measurements at the AAT employed the 'curvature sensing' technique (Roddier & Roddier 1993) and indicated that the optical performance is very good.

The Tip-Tilt and Low Order Adaptive Systems

The first stage of the AAT AO system is the introduction of a tilting mirror into the coude optical train. The penalty in not tilting an existing mirror, such as the telescope secondary, is light loss and increased thermal background due to the extra optics. Nevertheless, this approach has been adopted in order to rapidly implement a tip-tilt system, and serve as the basis of a low order adaptive system (see Figure 1).

The tip-tilt mirror itself is a simple high quality flat mirror attached to a piezo-electrically driven mount. This mount from Physike Instrumente is designed to provide ± 5.6 arc seconds of tilt on the sky. Infrared light is directed to IRIS, while visible light is used for sensing with a photomultiplier based quadrant detector.

This sensor is a duplicate of those used in the Sydney University Stellar Interferometer (SUSI) for the same purpose. This approach has allowed early implementation of tip-tilt correction, with installation at the telescope in late April and May 1995. Basic operation of the tip-tilt servo was confirmed using internal reference targets during July and the first serious tests on stars are expected in the latter half of the year.
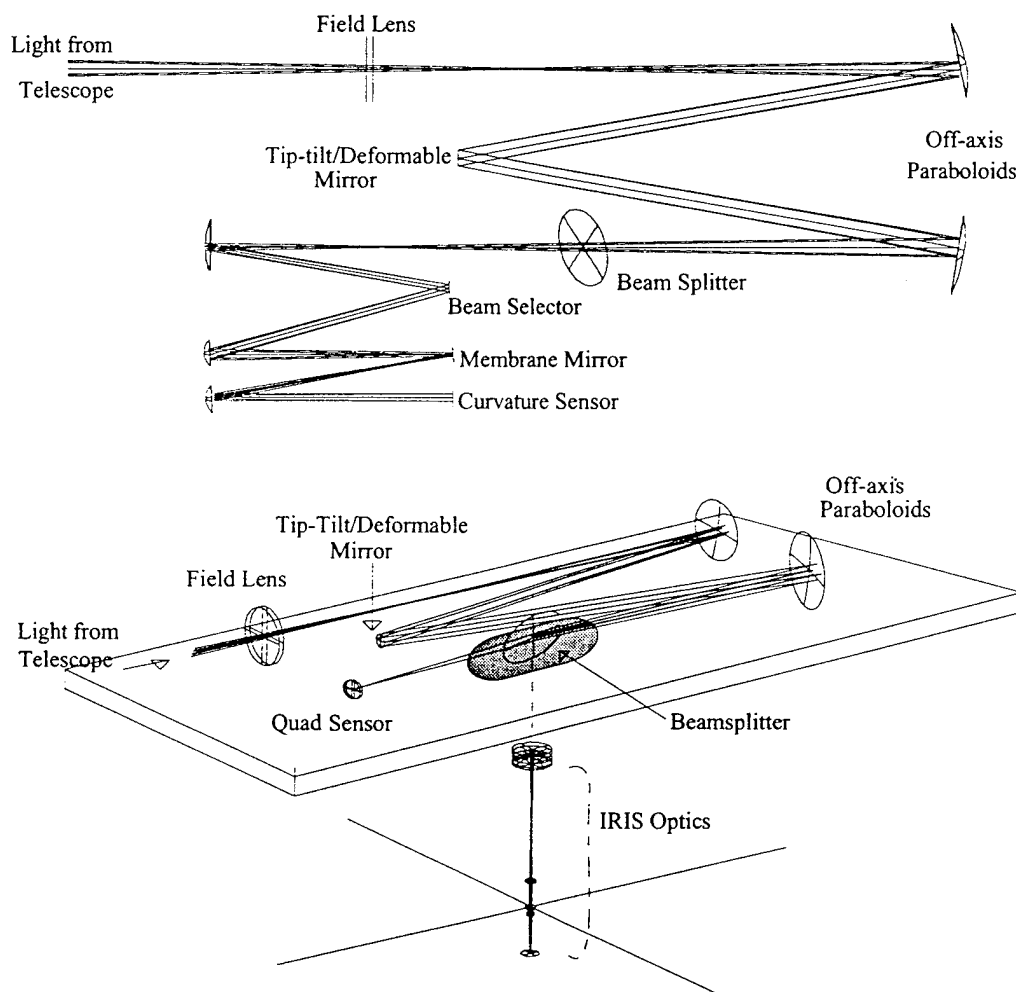
Figure 1. Optical layout of the low order AAT adaptive optics system. The sensor for tip-tilt measurement is located at the intermediate focus (in the lower view). It will be replaced by the optics associated with the curvature sensor (upper view) when the deformable mirror is incorporated to provide low order correction. Optics for target acquisition and alignment have been omitted for clarity.

Incorporation of a deformable mirror system forms the second stage of the AO project. Work at the University of Sydney has recently been directed to producing a system based on a curvature sensor, matched to a bimorph mirror. The prototype bimorph mirror has been constructed from two piezoelectric ceramic wafers, glued together with a polished mirror surface on one outside face. A pattern of 13 electrodes is placed on the inside face of one wafer, resulting in the maximum surface motion for a given applied voltage. Stroke of $\sim$ 20 μm is predicted. The 13 electrode pattern is sufficient to correct aberrations up to 9 Zernike terms, but will be increased to 19 electrodes in later versions to better correct telescope aberrations.

Upgrading the tip-tilt system to provide low order correction will involve mounting the bimorph mirror on the tip-tilt mount, thus combining the two functions in a single optical surface. The other change will be the addition of the wavefront sensor optics in place of the quadrant sensor of the tip-tilt system (see Figure 1). The wavefront sensor currently envisaged will consist of 19 avalanche photodiodes (APDs) fed by fibres coupled to an array of lenslets in a pattern similar to the electrode pattern of the bimorph mirror.

The Computing System

The AO control system consists of a SPARC workstation connected by Ethernet to a VMEbus real-time controller. The controller contains three processors: the Signal Analysis Processor (SAP), Tip-Tilt Processor (TTP), and the Wavefront Processor (WFP), all of which run the WindRiver Systems VxWorks operating system. The TTP and WFP execute real-time digital servo tasks while the SAP handles real-time communication tasks. The TTP is interfaced to the quadrant detector photomultipliers, tip-tilt mirror piezoelectric actuators and auxilliary equipment. While using the quadrant sensor the TTP is running software based on the SUSI tip-tilt system, with data analysis and logging of r_o and τ_o added.

When the low order system is implemented, the WFP will be interfaced to 19 APDs in the low order wavefront sensor, 19 electrodes in the bimorph mirror and a function generator used to drive a membrane mirror which moves the focus. The full system will be made compatible with the AATs DRAMA operating environment.

References

Allen, D. A. et al. 1993, PASA, 10, 298
Graves, J. E., Roddier, F., Northcott, M. J., & Anuskiewicz, J. 1994, in Adaptive Optics in Astronomy, ed. M. A. Ealey, & F. Merkle, Proc. SPIE, 2201, 502
Roddier, F. 1988, Appl. Opt., 27, 1223
Roddier, C. & Roddier, F. 1993, J. Opt. Soc. Am. A, 10 2277
Ryan, S.G. 1995, Report on AAT Dome-Seeing project (AAO internal memo)

Adaptive Optics
Telescope Projects II

MB 11:00 am-12:20 pm
Auditorium

Masanori Iye, *Presider*
National Astronomical Observatory, Japan

Keck Observatory Adaptive Optics Program

Peter L. Wizinowich and Anthony D. Gleckler

W. M. Keck Observatory
P.O. Box 220, Kamuela, HI 96743
Tel: 808 885-7887; Fax: 808 885-4464; email: peterw@keck.hawaii.edu

Introduction

The Keck Observatory, in collaboration with Lawrence Livermore National Laboratory (LLNL), is currently in the design phase of a natural guide star and single laser beacon adaptive optics (AO) facility for the Nasmyth platform of the Keck II telescope. Two science instruments will accompany the AO system: a near infrared camera (NIRC-2) being built at Caltech and a near infrared spectrometer (NIRSPEC) being built at UCLA. The goal is to make use of the diffraction-limited resolution (0.02 arcsec at 1 µm) and collecting aperture (10 m) of the Keck telescope, at an excellent site, to produce a new era in ground-based astronomical science.

The current status of the Keck AO program is as follows: the design requirements have been developed,[1] the overall system architecture has been specified including definition of the major subsystems,[2] subsystem design plans have been generated, and subsystem contracts have been awarded. The preliminary design reviews will occur in the Fall, 1995. The facility is scheduled to be installed on the telescope in 1997 and to be operational the following year.

Design Requirements

The AO system will be optimized for science wavelengths between 1.0 and 2.3 µm using faint natural guide stars, or a single laser beacon (~10 mag) with a natural star (> 19 mag) for tip/tilt sensing; and be operational from 0.8 to 5.0 µm. The science object can be anywhere in a 60 arcsec full field of view centered on the optic axis. The wavefront and tip/tilt sensors will be independently positionable over 60 and 120 arcsec fields, respectively. The AO system throughput should be > 70% to the science instrument and > 40% to the wavefront and tip/tilt sensors. The total emissivity of the AO system is required to be < 25%, with a goal of 10%. The detailed design requirements are found in reference 1.

System Architecture and Subsystem Designs

A block diagram of the overall single laser beacon facility is shown in Figure 1. Figure 2 shows the layout of the AO enclosure, AO optics bench and electronics, and science instruments on the Nasmyth platform. The facility is divided into four main subsystems for the purpose of fabrication: user interface and supervisory control, wavefront controller, optics bench, and the laser system.[3]

The user interface and supervisory control subsystem provides a graphical user interface with single station control and coordination of the entire AO system through an EPICS (Experimental Physics

and Industrial Control System) environment. The controllers for each subsystem are located in VME crates connected via a private ethernet link.

The optics bench consists of an image rotator to correct for the field rotation of an azimuth-elevation telescope, a fast steering mirror for global tip/tilt correction, an off-axis parabola to collimate the f/15 input beam and to reimage the telescope pupil on the deformable mirror (DM), the DM, and a second off-axis parabola to reproduce the telescope's focal ratio, pupil location and pupil size at the output of the AO system. The light to the science instrument passes through an infrared transmissive dichroic beamsplitter, and a removable atmospheric dispersion corrector. The visible light reflected by the dichroic is in turn divided into 589 nm light to the wavefront sensor and the remaining visible light to the tip/tilt sensor. Steering mirrors are used to independently locate the wavefront and tip/tilt sensors around the field. The wavefront sensor is mounted on translation stages to compensate for the variable distance to the sodium beacon. The tip/tilt sensor is also used as a simultaneous focus sensor by introducing astigmatism at 45 degrees to the quadrant detector.

The wavefront controller subsystem will consist of the wavefront sensor camera (an existing 64x64 pixel MIT/LL CCD in a Georgia Tech fabricated camera with 11 electrons noise at 2 MHz frame rate), a tip/tilt sensor (quad photon-counting APD array), a 349 actuator DM and a fast steering mirror. The reconstructor computer will be based around a Mercury board with 16 PowerPC processors. The effects of changing illumination on the wavefront sensor due to rotation of the non-circular Keck pupil is compensated by cycling through a set of reconstructor matrices.

The planned laser is a Nd:YAG pumped, 30 kHz pulsed dye laser developed by LLNL[4], with an anticipated output of 20 W. Fibers from 4 pump lasers are used to pump the dye master oscillator, a dye preamplifier and a dye amplifier. A phase modulator is used to scan the narrow dye output across the mesospheric sodium profile. The laser system includes alignment and diagnostic tools, a 50 cm projection telescope, thermal control for the laser and safety systems. The laser projection telescope, and beam transport optics, will likely be mounted on the side of the Keck telescope.

Acknowledgements

References

1. Keck Adaptive Optics Science Team, <u>Adaptive Optics for the Keck Observatory</u>, Keck Observatory Report No. 208 (November, 1994).
2. A. Gleckler and P. Wizinowich, "System architecture and subsystem definitions for the Keck AO system," CARA Document No. 163 (February, 1995).
3. A. Gleckler and P. Wizinowich, "W.M. Keck Observatory adaptive optics program," SPIE Proc. 2534, San Diego (July, 1995).
4. H. Friedman et al., "Sodium beacon laser system for the Lick Observatory," SPIE Proc. 2534, San Diego (July, 1995).
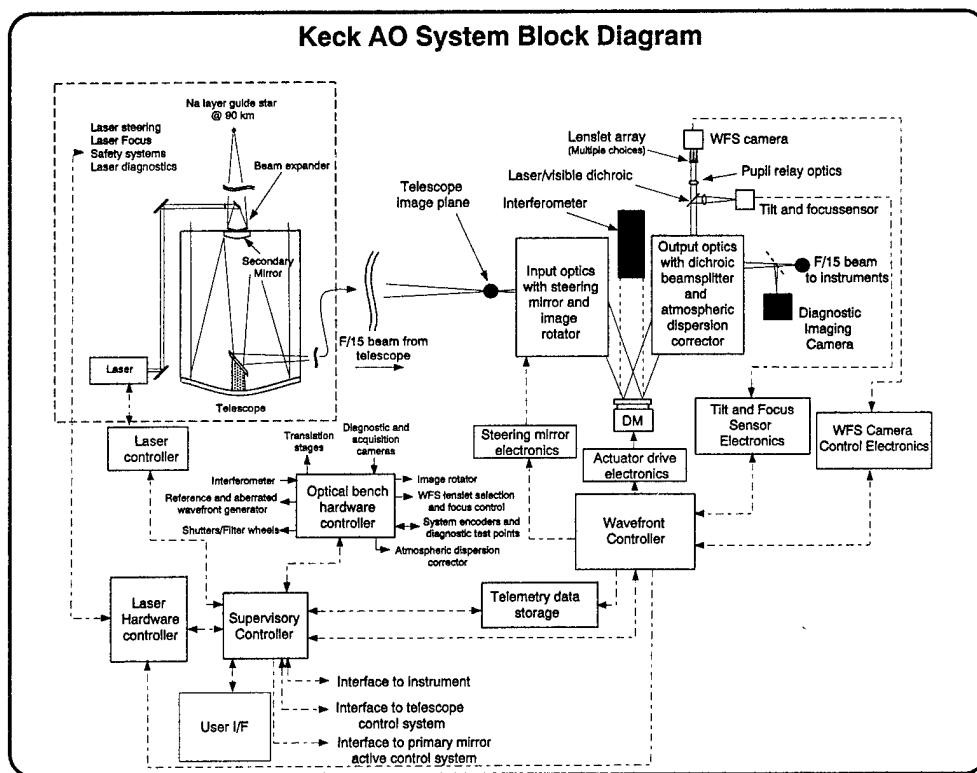
Figure 1.   AO System block diagram.
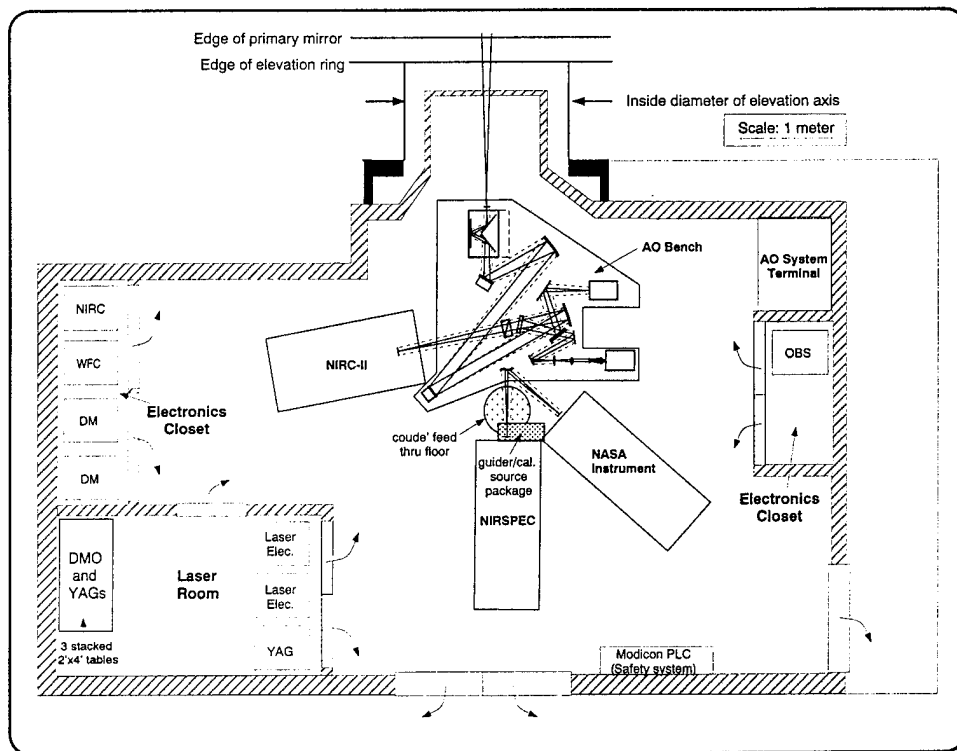
Figure 2.   Layout of AO System and science instruments on Nasmyth platform.

The GEMINI Adaptive Optics System

René Racine

Département de physique, Université de Montréal,
and Observatoire du mont Mégantic, Montréal, Canada, H3C 3J7

The GEMINI telescopes project in an international partnership between the United States of America, the United Kingdom, Canada, Chile, Brazil and Argentina to built two eight-meter astronomical telescopes, one on Mauna Kea, Hawaii and one on Cerro Pachon, Chile. The top science requirement of these instruments is superb image quality. It is intended that, in the absence of atmospheric seeing, the telescopes would deliver fully diffraction limited long exposure images in the K-band (2.2 µm). Accordingly, the telescopes and their enclosures have been designed and are being constructed with exacting attention to optical quality, thermal equilibrium and servo control accuracy. This, and the excellent natural seeing at the sites - FWHM = 0.45 arcsec (median), 0.25 arcsec (best 10th percentile) - will make the GEMINI telescopes performances well suited for further improvement by adaptive optics (AO). The Mauna Kea telescope will be highly optimized for performance in the thermal infrared, with an emissivity specification of <4% (2% goal).

An adaptive optics system (AOS) is being designed for use on the Mauna telescope. AO implementation on the Cerro Pachon instrument will await a second round of instrument construction. The following science requirements and goals have been adopted by the Gemini Science Committee for this AOS:

Requirements

- Delivered Strehl ratio >0,5 at 1.6 µm in median seeing conditions, with the intent of maximizing image concentration and sky coverage of a natural guide star system for 0.7 < $\lambda(\mu m)$ < 5.0. Such a system is expected to deliver Strehls of ~ 0.2 at 0.7 µm in the best tenth percentile seeing conditions. It is recognized that Strehls in excess of 0.1 at near-infrared and shorter wavelengths are scientifically valuable.

- The AOS should not increase the total emissivity by more than 15% for 2.2 < $\lambda(\mu m)$ < 5.0 (i.e. a total telescope emissivity requirement of < 19%).

- The throughput of the AO science path should be maximized in the 0.5 < $\lambda(\mu m)$ < 5.0 band and should not be less than 50% in this band.

- The performance of the AOS as a function of the zenith angle z should degrade no faster than $S(z) = S(0)^{\sec(z)}$.

- The stability of the AOS should be sufficient to ensure that the delivered Strehl ratios be limited only by atmospheric effects for up to a one hour integration

Goals

- The total emissivity should be less than 10% without the ADCs in the 2.2 < $\lambda(\mu m)$ < 5.0 band.

- Laser beacons: This natural guide star AOS should be designed in such a way that it can be upgraded to a laser guide star system with the priority to increase the system's sky coverage at the above performance levels.

The GEMINI telescopes are to be used at their f/16 secondary foci where the image scale is 1.6 arcsec/mm. Instruments will be mounted on the outer faces of a cubic instrument support system (ISS) attached to the back of the primary mirror cell, the telescope focus being located 600 mm outside the centers of the ISS faces. On the Mauna Kea telescope, one of these faces will be occupied by the adaptive optics system (AOS). A deployable folding flat on the optic axis above the ISS center directs the telescope beam to the AOS where the wavefront is sensed and corrected. The compensated beam is returned to the ISS where a second, central fold directs it to any one of the attached instruments. The re-imaged and AO-compensated FOV has the same scale, the same focal position and the same pupil (secondary mirror) a natural FOV would have. The AOS FOV is 3 arcmin (110 mm) in diameter. The all-reflective optics of the AOS produces spot diagrams containing 80% of the rays within a diameter of 0.03 arcsec on a flat focal surface at the edge of this field.

The primary science requirement to maximize sky coverage with a natural guide star AOS has led to a design where the deformable mirror (DM) is conjugate to the median altitude of turbulence which, on Mauna Kea, is ~6.5 km high, rather than to the telescope entrance pupil. This strategy increases the area of the isoplanatic patch, and the number of suitable guide stars, by a factor of four [1]. Performance simulations [2] show that thanks to this and to the excellent natural seeing, hence large r_o, at the site, very appreciable sky coverage with moderately high Strehls will be achieved at near infrared wavelengths. This is illustrated in Fig. 1 where, for instance, the overall-sky probability of achieving S = 0.3 in median seeing is seen to be 67% in the H (1.6 μm) and 98% in K (2.2 μm).

Final choices of the AO subsystems technology (wavefront sensor, reconstructor, deformable mirror) are still pending at this time (May 1995). It is clear that the science requirement of a ~50% Strehl in H can be achieved under median Mauna Kea seeing conditions with an AOS capable of controlling the first ~25 Zernike modes of the atmospheric wavefront. Component selections will be based on their ability to measure these modes with the faintest possible guide stars, thereby maximizing sky coverage, and of best fitting them with a limited number of degrees of freedom, thereby maximizing the system's bandwidth, modal efficiency, and reliability and minimizing its cost. At GEMINI, like at all other astronomical AOS projects presumably, we anxiously await ongoing developments in WFS detectors and DM technologies.

REFERENCES

1. R. Racine, and B.L. Ellerbroek, *Profiles of Night-Time Atmospheric Turbulence on Mauna Kea and Isoplanatism Extension in Adaptive Optics*, Pub. Astr. Soc. Pacific (submitted)

2. B.L. Ellerbroek, R. Racine, and D. Tyler, *Sky Coverage Calculations for Astronomical Adaptive Optics*, (this Conference)
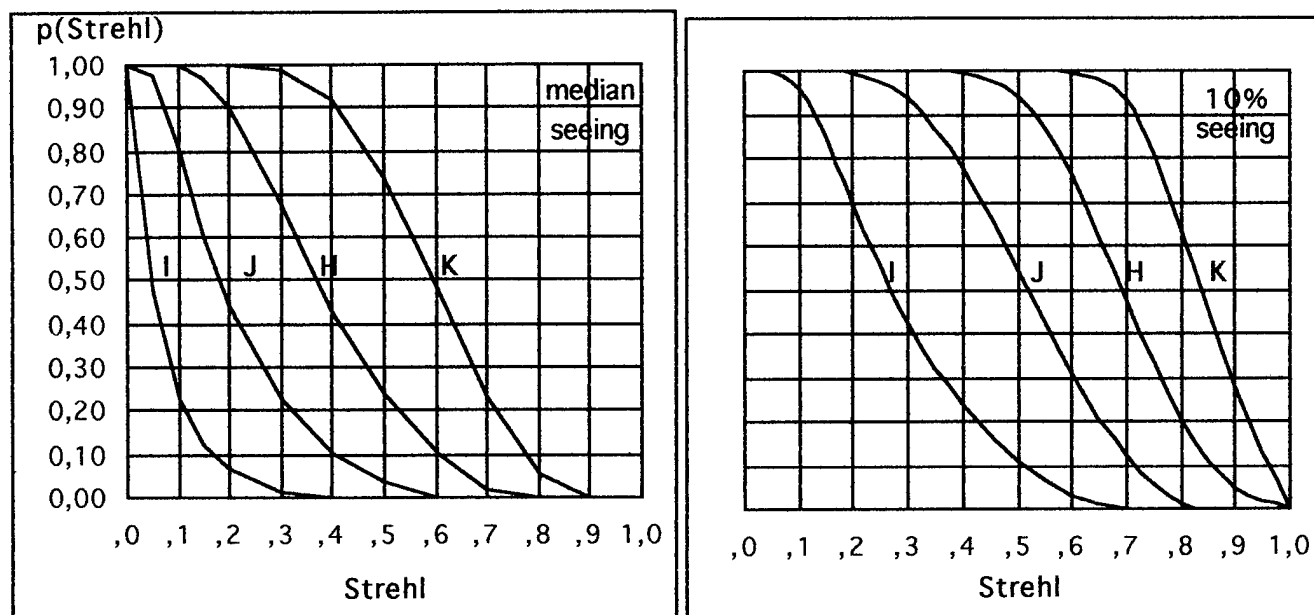
Fig.1: Probabilities of achieving a given Strehl performance with natural guide stars

The simulations in median (0.45 arcsec FWHM) and 10 percentile (0.25 arcsec FWHM) Mauna Kea seeing assume an AOS with 81 degrees of freedom (e.g. a 10x10 Shack-Hartmann WFS) AOS, an idealized zero-electron detector read noise and a DM conjugate to altitude. The curves represent the overall-sky mean performances.

SUBARU Adaptive Optics Program

Hideki Takami, Masanori Iye, Naruhisa Takato, and Yutaka Hayano
National Astronomical Observatory, 2-21-1 Osawa, Mitaka, Tokyo 181 Japan
Tel: 81-422-34-3865
Fax: 81-422-34-3864

Masashi Otsubo
The Graduate University for Advanced Studies, 2-21-1 Osawa, Mitaka, Tokyo 181, Japan
Tel: 81-422-34-3865
Fax: 81-422-34-3864

Koji Nakashima
Department of Astronomy, the University of Tokyo, 2-11-16 Yayoi, Bunkyo, Tokyo 113, Japan
Tel: 81-422-34-3865
Fax: 81-422-34-3864

1. Introduction

SUBARU telescope with 8.2 m diameter is being constructed atop Mauna Kea in the Hawaii island. It employs the thin-meniscus primary mirror that is supported by 260 actuators, providing the almost perfect surface figure for near infrared imaging. The atmospheric turbulence is now the dominant origin of image degradation. Therefore, the adaptive optics (hereafter AO) system is essential equipment for large ground telescopes.

One of the serious problems of astronomical AO system is to find guide stars bright enough to measure distorted wavefront near the astronomical objects. Several AO systems equipping laser guide star system are planned. We are building our first SUBARU AO system using natural guide stars, eventually upgrade it to LGS based system. The system is optimized for near-infrared wavelength with relatively smaller number of control elements, such as 36 elements. Considering the fairly good seeing of Mauna Kea as large as 0.5 arcsec in average, it is possible to obtain the Strehl ratio greater than 0.5 at K band, even by such a lower order compensation system.

The scheduled completion date is early 1998, to be in time for the engineering first light of SUBARU. We are building a prototype system that is nearly identical with the real system, and will test it using 1.6 m IR simulator telescope at Mitaka Japan.

2. Overview of SUBARU Cassegrain AO system

The SUBARU Cassegrain AO unit will be installed inside the peripheral optics tube with the inner diameter of 1.5 m, about 500 mm above the telescope focus. The wavefront sensor unit will be attached to the instruments to reduce the mutual mechanical flexure (Fig.1).

Tentative specifications of the system are listed in table 1. The spectral coverage of the system is 1 to 5 μm, while the optics itself covers from visible to mid-infrared wavelength.

We use wavefront curvature sensor, which will have 36 elements avalanche photo-diode photon-counting modules having 70 % photon counting efficiency. The APD based wavefront sensor system is the most sensitive detector system using currently available technologies. A micor lens array with 36 elements is located at the sensor focus. The micro lens array collects those photons to the APDs through tapered fibers.

The deformable mirror will be a bimorph type also having 36 elements control electrodes. The effective diameter of deformable mirror is 60 mm. The control closed loop matrixes can become very simple by the combination of the curvature sensor and bimorph mirror with matched geometry of the electrodes.

The optics composed of 2 offset paraboloids, a deformable mirror and 2 fold mirrors (containing 3 surfaces) covers 2 arcmin field of view, about 20 arcsec is used for higher order compensation. The maximum control bandwidth will be higher than 100 Hz, which corresponds to A/D sampling speed of about 2 kHz. The one of the paraboloid mirrors is mounted on tilt

control unit for tip/tilt correction. The secondary mirror of SUBARU also can be used for tip/tilt correction.

We have been evaluating the AO performance using natural guide stars through our system simulation works (Table 2). This shows the images are remarkably improved even by 18-th R magnitude guide stars, using optimized control algorithm.

Table 1. Specification of SUBARU Cassegrain AO system

Spectral coverage:	1 - 5 μm (Optics covers from visible to mid-infrared)
WFS:	Curvature sensor 36 photon counting APD modules Taper fiber feed micro lens array
Deformable mirror:	Bimorph mirror with 36 control elements
Beam diameter:	60 mm
Focal length:	720 mm
F ratio:	12.4
FOV:	2 arcmin. coverage of optics, tip/tilt correction 20 arcsec. higher order AO compensation
Control bandwidth:	> 100 Hz (2 k samples / sec)

Table 2. The simulated AO performance. We assumed 0.45" visible seeing, frozen flow of Kolmogorov turbulence with 20 m/s wind speed, 37 elements wavefront curvature sensor and membrane mirror, 20% throughput , 200 corrections /s

Bands	Diffraction limit image size (")	Strehl ratio for various R magnitude of guide stars						
		M_R= 10	15	16	17	18	19	no AO
J	0.032	0.365	0.248	0.157	0.089	0.047	0.022	0.007
H	0.041	0.547	0.432	0.320	0.210	0.109	0.049	0.013
K	0.057	0.705	0.613	0.512	0.389	0.237	0.117	0.025
L	0.098	0.868	0.820	0.760	0.675	0.533	0.358	0.0586

1500mm

AO Calibration Light

Visible Calibration Light
Slit Viewer Layer

Deformable Mirror

AO Optics

260 AO space

650

130

170

160

Shack-Hartman,
Auto Guider Layer

Beamsplitter

WFS unit

Telescope Focus

2000 mm to the bottom

Instrument

Effective Beam Diameter: 60mm
Maximum Field of View: 2 arcmin

1500 mm

IR ADC

Deformable Mirror
M4

M3

Parabola
f=720mm,150mm diam.

M5

M1,M6

Parabola with
Tip/Tilt Mount
f=720mm,
150mm diam.

Flat Mirror
100mm diam.
M2

200mm stroke

Fig. 1. Layout of SUBARU Cassegrain adaptive optics system

The 6.5 m MMT Infrared Adaptive Optics System: Detailed Design and Progress Report

D. G. Sandler, M. Lloyd-Hart, P. Gray, T. Martinez, R. Angel
Center for Astronomical Adaptive Optics, Steward Observatory,
University of Arizona, Tucson AZ 85721, (520)621-4409, fax (520)621-9843
T. Barrett, D. Bruns, S. Stahl
ThermoTrex Corporation, 9550 Distribution Ave., San Diego CA 92121 (619)578-5885, fax (619)578-1419

Introduction

In late 1996, the Multiple Mirror Telescope will be replaced by a 6.5 m telescope with a single borosilicate honeycomb primary mirror. Earlier we showed [1] that an adaptive optics system using a low-power sodium laser guide star could provide diffraction-limited performance for infrared imaging in H and K bands, yielding the equivalent 0.05 arcsec resolution of Hubble Space Telescope optical images over most of the sky. Our approach used a continuous-wave sodium dye laser of a few watts, projected from a flat above the secondary mirror. To yield the highest efficiency and lowest emissivity, we proposed using an adaptive secondary mirror for full correction of the wavefront. In addition, the use of an infrared field star sensor to sense the global atmospheric tilt was shown to give very good sky coverage. A schematic of the system concept for the 6.5 m MMT is shown in Fig. 1.

Since we proposed this approach, experiments using sodium and natural beacons at the current MMT array [2] have yielded valuable data on atmospheric parameters and sodium beacon properties, confirming the design concept and allowing final determination of design parameters. We have now moved on to building hardware components for system integration soon after first light. In this paper, we give the final detailed adaptive optics design for the 6.5 m MMT, pointing out key features which are necessary to achieve the limiting performance and which distinguish it from other designs for large telescopes. In addition, we give the status of hardware development for key components.
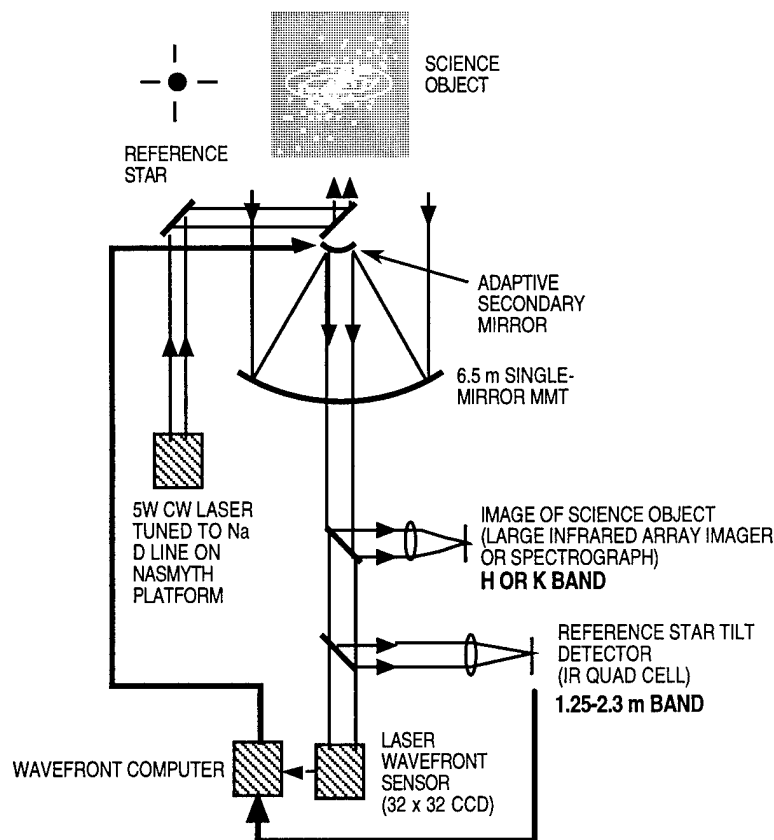
Figure 1.

System development

Optical system. An interim system (FASTTRAC II) using a sodium laser has been built for near-term science observations at the existing MMT array. FASTTRAC II is discussed in a paper by Close et al. at this conference. FASTTRAC II uses a fast adaptive beam combiner with voice coil actuators and capacitive feedback. The beam combiner controls the tip-tilts of the 6 MMT beams, directly feeding an infrared detector. The optical design for FASTTRAC II is very similar to the 6.5 m design for imaging at the f/15 Cassegrain focus, using dichroics to filter wavelengths toward shorter bands as the beam progresses from dewar, to tilt sensor, and finally to the wavefront sensor. The design similarly takes advantage of the fact that no intermediate pupil is needed to perform adaptive correction.

Adaptive secondary mirror. The adaptive secondary will consist of a thin 2 mm adaptive mirror whose shape is controlled by 300 voice-coil force actuators. Capacitive position sensors located at each actuator measure the figure of the thin adaptive mirror relative to a spherical reference surface, which is one side of a glass support structure bolted to the secondary spider hub. Small magnets are placed on the back side of the adaptive mirror, at points directly opposed to each voice coil, and provide the only interaction between thin mirror and reference surface. The actuators are inserted through holes in the support structure, which also provide contact with circulating air to remove heat from the vicinity of the adaptive mirror. Our design calls for < 100 W total power consumed by 300 actuators, and efficient removal. For compactness and ease of assembly, the drivers, controllers, and capacitor sensor boards are all fabricated using miniature electronics. The adaptive secondary design and results of tests of a prototype mirror are presented by Bruns et al. at this conference, and papers by our Italian collaborators at Arcetri Astrophysical Observatory and Politecnico di Milano describe progress in the design of the support structure and optimization of the control loop using finite-element codes.

Wavefront control. Capacitive feedback controls a fast inner loop, which maintains the shape of the mirror between wavefront updates from the digital reconstructor. The outer, atmospheric loop is controlled using Shack-Hartmann measurements of wavefront slopes over 150, d=0.5 m subapertures, corresponding to $d/r_0=0.5$ at the MMT for an imaging wavelength of 2.2 mm. The slopes are reconstructed by a wavefront processor, developed using commercial processing boards. The intensity data from the CCD wavefront detector is converted into slopes by DSP processors housed in a VME rack, along with the central controller and interface boards. A commercial processor developed for fast distributed computing performs a 300x900 matrix multiply, yielding updates for the actuator commands, including up to two past cycles of wavefront data, with negligible latency. Diagnostic and telemetry data are prepared by the central controller and sent to the user interface computer via ethernet. See the paper by Stahl and Barrett at this conference, for a detailed design of the computer hardware.

The inner capacitive feedback loop for the adaptive secondary operates at 10 kHz, fast enough to support a 1 kHz sampling rate for atmospheric aberrations. In this mode of operation, the outer loop will mimic conventional closed-loop correction of the atmosphere (with standard reconstruction algorithms), in a null-seeking mode which attempts to drive the Shack-Hartmann measurements to zero. To take full advantage of the fast inner loop, we are developing optimal reconstructors which incorporate the measured statistics of the atmospheric aberration, as provided by on-line telemetry data. With both spatial and temporal filtering of wavefront data, the full 300 actuators can be used to map the optimal expected phase profile for each update, and the atmospheric sampling rate can be lowered to increase the SNR of the wavefront sensor data. The reconstructors can be developed using analytic expressions, and parameterized by atmospheric constants. The computer hardware has been designed to allow development of reconstructors directly from measured data at the telescope, including on-line delta-rule training. The power of these methods is discussed at this conference in a talk by Lloyd-Hart.

Wavefront detector. To take maximum advantage of sodium photon return, 3 electron/pixel rms read noise is required for the CCD. At this read noise level, 4 W of sodium laser power gives better than $\lambda/10$ wavefront slope accuracy. The current state of the art is 3 electrons/pixel noise at 250 kHz pixel rate. Chips by EEV, SITE, and Lincoln Laboratory are being explored, for a 64x64, 4- port device, with binning required to reach 1 kHz frame rate.

Sodium laser. Experiments at the MMT with CW sodium lasers have shown that designs for both ring and standing wave dye lasers can give 1-2 W of power, with 1 W corresponding to a V-band magnitude 12 star. Sodium images of width 1 arcsec have been measured [2]. What remains is to develop a cost-effective, reliable laser at the 4 W level, for routine operation at the new MMT. We are developing a new ring dye laser pumped by a 24 W argon ion laser. The frequency of the ring dye laser is selected and locked to the sodium D_2 line using a sodium-vapor Faraday cell in the laser cavity. Rotation of the plane of polarization at the sodium wavelength by the cell is compensated by derotation in a quartz plate. This combination acts both to select frequency automatically, and as the optical diode requried for efficient unidirectional operation of the ring cavity. Experiments using the new laser with FASTTRAC II are planned.

Expected performance

A summary of the long-exposure Strehl ratios expected in H and K bands is shown in Table 1. The quantity S_ϕ is the Strehl ratio for high-order, sodium laser wavefront correction, which includes fitting, time delay, wavefront sensor noise errors, and focus anisoplanatism. The quantity S_θ is the image motion Strehl, which includes anisoplanatism for an off-axis field star, time delay during integration of infrared photons, and noise errors from centroiding stellar images on the infrared quad cell. The image width contribution depends on the field star angle, as the star shares laser correction with the science object due to the large isoplanatic angle in H and K bands. We have calculated the limiting stellar magnitudes which give noise contributions to S_θ of 0.8. In the Table, two cases are given for total image motion Strehl: S_θ =0.5, corresponding to off-axis tilt sensing at the field angle which gives 0.6 anisoplanatic Strehl, and S_θ =0.8, corresponding to a tilt star contained within the program object The corresponding total system Strehl ratios, S= $S_\theta S_\phi$, are given, along with the probability of finding a sufficiently bright field star.

	$\lambda = 1.6\ \mu m$		$\lambda = 2.2\ \mu m$	
S_ϕ	0.359		0.582	
S_θ	0.5	0.8	0.5	0.8
S	0.18	0.29	0.29	0.47
P_{pole}	22%		53%	
$P_{30°}$	49%		86%	

Table 1.

References
1. D.G. Sandler, S. Stahl, J.R.P. Angel,M.Lloyd-Hart, D. McCarthy, Adaptive optics for diffraction-limited infrared imaging with 8-m telescopes, JOSA A11, 925 (1994).
2. M. Lloyd-Hart et al., Adaptive optics experiments at the MMT using sodium laser guide stars, Ap J 439, 455 (1995)

Adaptive Optics Telescope Projects III

MC 2:00 pm-3:20 pm
Auditorium

Fritz Merkle, *Presider*
Carl Zeiss, Germany

ADONIS

A user-friendly adaptive optics system for the ESO 3.6 m telescope

J.L. Beuzit[1,2], N. Hubin[1], L. Demailly[2], E. Gendron[2], P. Gigan[2], F. Lacombe[2], D. Rouan[2], F. Chazallet[3], D. Rabaud[3], P.Y.Madec[3], G.Rousset[3], F. Eisenhauer[4], R. Hofmann[4], E. Prieto[1], D. Bonaccini[1]

1 ESO, Karl-Schwarzschild-Str. 2, D-85748 Garching, FRG
2 Observatoire de Paris, DESPA (URA 264/CNRS), 5 place Jules Janssen, 92195 Meudon, France
3 ONERA, B.P.72, F-92322, Chatillon, Cedex, France
4 MPIE, Karl-Schwarzschild-Str. 1, D-85748 Garching, FRG

The first astronomical results obtained at the ESO 3.6 m telescope with the Come-On adaptive optics system demonstrated the impressive potential of this technique [1,2,3]. A second generation of this system [4], called Come-On-Plus, has since been developed and tested at La Silla observatory [5]. It is now the only system of this kind offered as a standard instrument to the European astronomical community. Nevertheless, adaptive optics remains a high technology technique which uses complex technology. Although the Come-On and Come-On-Plus systems have operated very smoothly during numerous observing runs since 1990, a fairly large team of qualified personnel was required to operate the whole system. Several instrumental parameters have to be optimised according to astronomical requirements and prevailing atmospheric conditions. These include the magnitude and colour of the reference star, the wavelength of the observed object and its angular separation from the reference, and the atmospheric turbulence profile. With the previous Come-On-Plus system this optimisation was difficult to achieve and has given rise to somewhat inefficient use of telescope time. The experience gained with this system has led to the concept of ADONIS (ADaptive Optics Near Infrared System), which is intended to improve the performance, versatility and operational efficiency. A further general objective is to develop operational procedures and to test technical concepts that can be later applied to the adaptive optics system for the ESO Very Large Telescope.

The optical layout of ADONIS has not been substantially changed from that of Come-On-Plus [4]. The imaging channel has been slightly modified to bring the F/45 IR focus to a more accessible location allowing different large cameras to be installed. The beam is now bent under the optomechanical bench where visitor equipment such as coronograph, polarimeter, Fabry-Perot etalons can be mounted.

A new real time computer based on DSP C40 boards specifically developed for Adaptive Optics provides the best computing power-flexibility compromise. It provides in real time a set of Shack Hartmann images, X, Y slope information and mirror commands (figure 1) which permit the correction to be optimised during observations and provides additional information for blind PSF determination. This new RTC carries out the complete processing for 7x7 Shack Hartmann sub-apertures of 8x8 pixels in less than 1 ms after the end of the WFS integration.

The ADONIS Artificial Intelligence [6] is a synergy of interacting modules interfaced, on one side, with each element of the adaptive optics system and observatory environment and on the other side with an intelligent control panel operated by the astronomer. This panel provides an overview of the system set-up and status parameters as well as all relevant data for evaluating the current performance of the instrument. This Artificial Intelligence software is installed on a workstation, the Master Computer, which performs most of the optimisation and control tasks. Internally, a Client/Server architecture is used for interaction between the I/O or internal class clients, and the special Data Server. A Message Server records all the commands generated by the Artificial Intelligence System

(AIS) as well as all status messages sent by the clients. An important example of an advanced smart controller tool is the modal control optimisation tool which evaluates the best modal control matrix in relation to the prevailing atmospheric turbulence characteristics and the wavefront sensing noise.

Feedback via the optical system

| WFS detector | → | Centroiding Calculation | → | Command Calculation | → | Deformable & Tip-tilt mirror |

| Hartmann Picture: available for technical evaluation | X and Y slopes | Coefficients of Polynome decomposition + mirror commands |

→ off-line PSF (to be implemented)
Atmospheric data
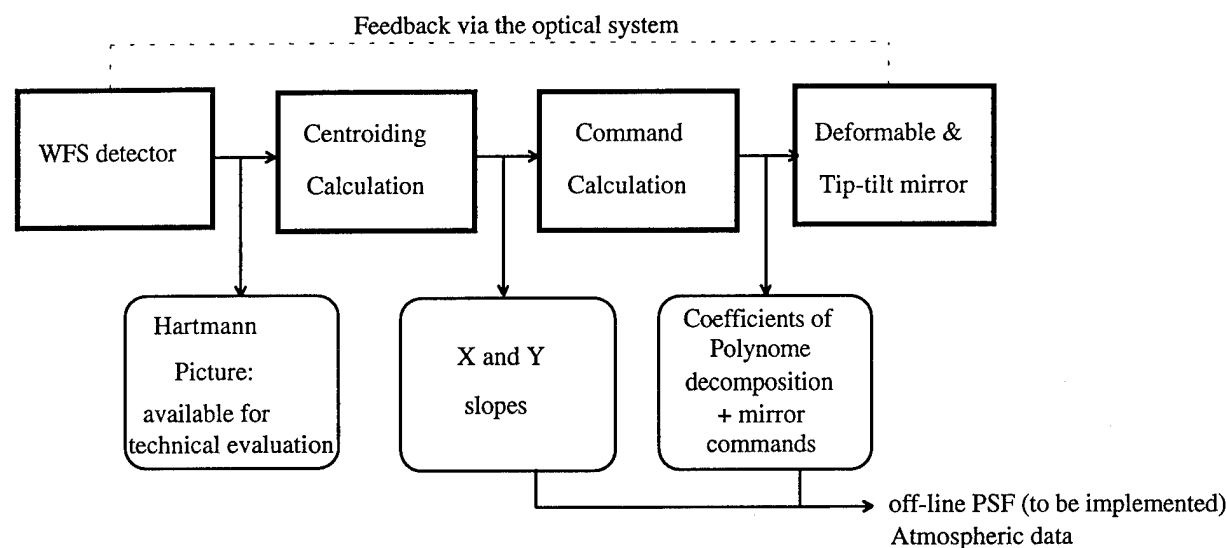
Figure 1: AO closed-loop data available for the instrument

Two infrared cameras are offered to the astronomical community with ADONIS in addition to the possibility of installing a visitor instrument as mentioned earlier.

A first camera, COMIC [7], developed to cover the 1-5 μm range is a 128x128 HgCdTe infrared camera with two image scales: 35 mas/pixel for observation in J, H and K bands, and 100 mas/pixel for observation in L and M bands. Two CVFs covering the spectral ranges 1.34-2.52 μm and 2.50-4.52 μm provide low spectral resolution imaging up to R $\approx$ 70-80. A number of narrow band filters may be used like HeI, Brγ, H_2O, PAH, H_{3+} and Brα.

The second camera, SHARP II, built by the *Max-Planck-Institut für Extraterrestrische Physik* in Garching is a 256x256 Nicmos camera working in J, H and K bands with pixel scales of 35, 50, 100 mas/pixel. It also provides a low spectral resolution imaging mode R=70 in the 1.3-2.38 μm range (CVF) and R=950 and R=2600 in the K band (Fabry Perot etalons). A polarimetric mode is also available.

References

[1]- Kern P. et al., 'Adaptive optics prototype system for infrared astronomy: I. System description', SPIE 1271-22, (1990)

[2]- Rousset G. et al., 'First diffraction limited astronomical images with adaptive optics', Astron. and Atroph.., 230, L29-L32 (1990)

[3]- Rigaut F. et al., 'Adaptive optics on the 3.6 m telescope: results and performance', A&A, 250, 280-290 (1991)

[4]- Hubin N. et al., 'New adaptive Optics on the 3.6 m telescope: Come-On-Plus', SPIE 1780-87 (1992)

[5]- Rousset G. et al., 'The Come-On-Plus adaptive Optics System: Results and performance', SPIE 2201, Kona, (1994)

[6]-Demailly L. et al., 'Artificial intelligence system and optimized modal control for the ADONIS adaptive optics instrument', SPIE 2201, Kona, (1994)

[7]-Feautrier P. et al., 'The IR COMIC imaging camera for the ADONIS adaptive optics system', SPIE San Diego (July 1995), in press

Novel Adaptive Optics with the Durham University ELECTRA System

D.F. Buscher, N. Andrews, C. Dunlop, P.W. Morris,
R.M. Myers, R.M. Sharples, A.J.A. Vick, A. Zadrozny,
University of Durham
Department of Physics
South Road, Durham DH1 3LE, United Kingdom
E-mail: david.buscher@durham.ac.uk
Phone: +44 191 374 7462

C.A. Haniff
MRAO Cavendish Laboratory
Madingley Road
Cambridge CB3 0HE, United Kingdom

R.W. Wilson
Royal Greenwich Observatory
Madingley Road, Cambridge, United Kingdom

We present the status of the Durham University ELECTRA visible-light adaptive optics system and describe novel imaging strategies to be used with this instrument.

Recent Results from the MARTINI III/WHIRCAM Infra-red Adaptive Optics System

P. Doel, D. Buscher, C. Dunlop, R.Sharples, N. Andrews
Department of Physics, University of Durham
Science Laboratories, South Road, Durham DH1 3LE, England
Telephone 44 191 374 2105, Fax 44 191 374 3749

The MARTINI-III system is an infra-red adaptive optics system designed as a semi-common user instrument for use at the Ground-based High Resolution Imaging Laboratory (GHRIL) on the William Herschel Telescope (WHT). The optical layout of the system is shown in figure 1. Light from the Nasmyth focus of the WHT is incident on a six element adaptive mirror and is reflected back onto a toroidal mirror which refocuses the light at an off-axis point. Just before this re-imaged focus the light is split by a dichroic beamsplitter and the infra-red light reflected into the infra-red camera (WHIRCAM) arm. The visible light is passed to the wavefront sensing arm where it passes through a selectable sub–aperture mask and is imaged onto the wavefront sensor (an Astromed CCD15-11 camera) by a split lens assembly. The elements of this split lens are adjustable and these are used to align the images formed by each sub-aperture in a row on a 24x4 pixel region in the corner of the wavefront sensor's CCD chip, each spot being centred on a 4x4 pixel square. On readout the 4x4 pixels are on-chip binned into a 2x2 quad–cell, the output of which is used to calculate the X and Y wavefront slopes. The system is designed to work in two modes, one an 'unco-phased' mode where the mirror segments are just controlled to remove the individual wavefront tip-tilt across each segment but no attempt is made to piston the six mirrors. The other a 'co-phased' mode where the segment slopes are used to reconstruct the piston values of each wavefront segment. The real-time reconstruction and control is performed with a Motorola 68020 microprocessor. Pixel scales on WHIRCAM of 0.05, 0.08 and 0.24 arcseconds can be selected giving fields of 12.8, 20.5 and 61.5 arcseconds respectively. A guide star of R–band magnitude 13th or brighter is required to be centred within this field.

The system has been commissioned at the WHT in February and June of 1995. Though both runs were affected by bad weather, results were obtained with the mirrors running in their unco-phased mode which showed a good image improvement even in poor seeing conditions. As an example figure 2 shows a K-band image of the binary star ξ Ursa Majoris (separation ~ 1.3 arcseconds), the uncorrected seeing was 1.5 arcseconds whilst the corrected seeing was 0.5 arcseconds.
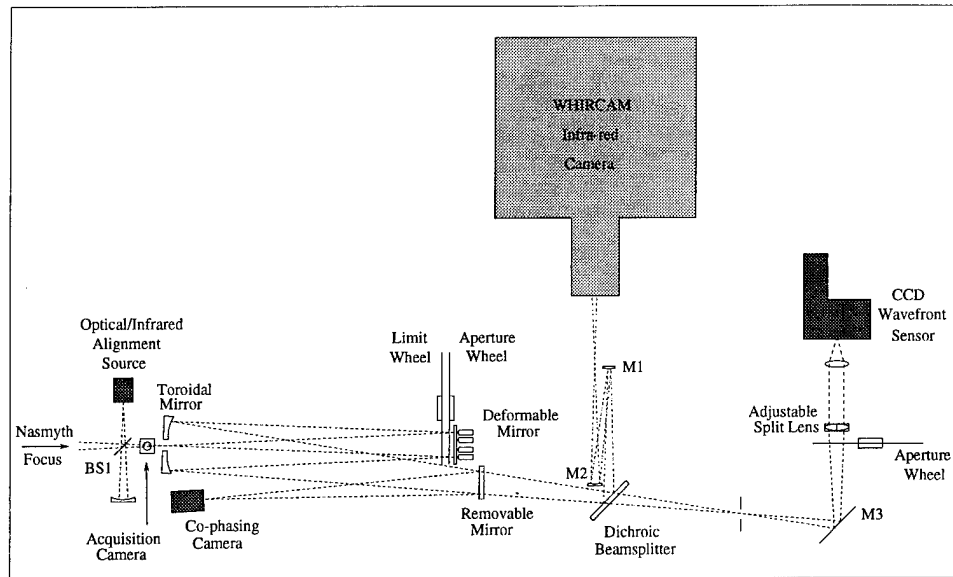
Figure 1: Schematic of the MARTINI-III optical layout
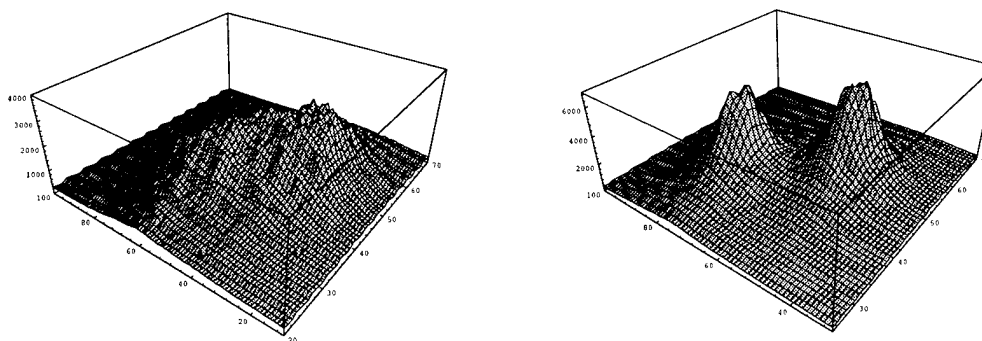
Figure 2: K-band image of the binary star system ξ Ursa Majoris in 1.5 arcsec seeing, with no correction (left) and with MARTINI-III switched on (right). The image scale is 0.05 pixels per arcsec and the star separation is ~ 1.3 arcsec.

Initial results from the Lick Observatory
laser guide star adaptive optics system

Scot S. Olivier

Imaging and Detection Program
Lawrence Livermore National Laboratory
L-495, P.O. Box 808
Livermore, CA 94551-9900
Phone: (510) 423-6483
Fax: (510) 422-3358
e-mail: olivier1@llnl.gov

Jong An, Kenneth Avicola, Horst D. Bissinger,
James M. Brase, Herbert W. Friedman, Donald T. Gavel,
Bruce Macintosh, Claire E. Max, J. Thaddeus Salmon,
Kenneth E. Waltjen

Lawrence Livermore National Laboratory

A prototype adaptive optics system has been developed at Lawrence Livermore National Laboratory (LLNL) for use on the 3-m Shane telescope at Lick Observatory. This system is currently based on a 127-actuator continuous-surface deformable mirror developed at LLNL, a high-quantum-efficiency low-noise fast CCD camera built for LLNL by Adaptive Optics Associates using a chip developed by Lincoln Laboratory, and a Mercury VME board containing four Intel i860 processors.

An earlier version of this system based on an ITEK 69-actuator continuous-surface deformable mirror, and a Kodak fast-framing intensified CCD camera was tested using natural reference stars on the 1-m Nickel telescope at Lick Observatory yielding up to a factor of 10 increase in image peak intensity and a factor of 6 reduction in image full width at half maximum (FWHM) at an observing wavelength of 0.85 μm (Olivier et al. 1994).

In order to improve performance, the intensified CCD camera was replaced by a high-quantum-efficiency low-noise fast CCD camera built for LLNL by Adaptive Optics Associates using a chip developed by Lincoln Laboratory and the system was tested was tested using natural reference stars on the 3-m Shane telescope at Lick Observatory yielding up to a factor of 13 increase in image peak intensity and a factor of 7 reduction in image FWHM at an observing wavelength of 1.0 μm (Figure 1).

This system was also tested with the Lick Observatory near-IR facility camera, LIRC II, and images were produced at 2.2 μm with a factor of 12 improvement in the peak intensity. These results are consistent with having about 30% of the light from the star in a diffraction-limited core.

The main factor limiting the performance in these tests appeared to be the limited dynamic range of the deformable mirror coupled with fairly large static aberrations in the telescope optics. The upgrade to the 127-actuator LLNL mirror is expected to alleviate this problem since it has a much larger dynamic range than the 69-actuator ITEK mirror. Tests with this mirror will be performed this Summer, and the results will be presented.

A sodium-layer laser guide star system has also been developed at LLNL to serve as a beacon for the adaptive optics system on the 3-m Shane telescope. This system is based on frequency-doubled Nd-YAG pump lasers that are fiber-optically coupled to a dye laser tuned to the D_2 Na resonance at 589 nm. This is propogated out of a 30 cm refractive launch telescope attached to the side of the 3-m Shane telescope. This sytem has been operated at the telescope and has produced a beam with up to 17 W average power.

Integrated tests with the laser guide star and adaptive optics systems will be perfromed during the Summer, and the results will be presented.

ADAPTIVE OPTICS POINT SPREAD FUNCTIONS
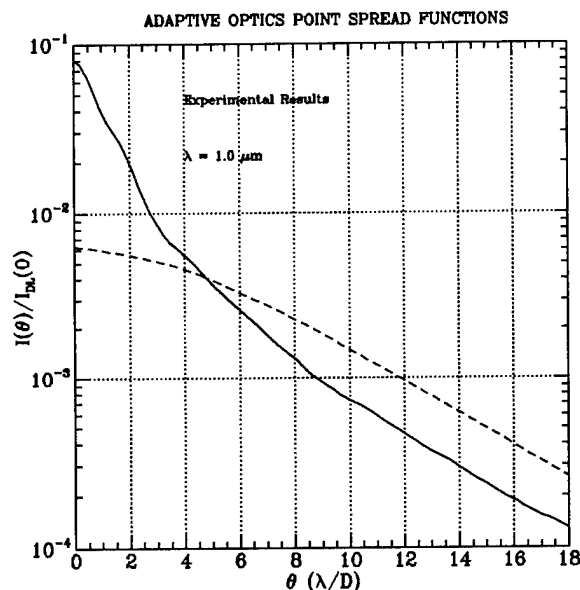
Figure 1 – Radially averaged image data from Alpha Perseus with and without adaptive optics compensation.

In addition, four astronomy programs using the laser guide star system will be begun this Summer: infrared adaptive optics imaging of active galactic nuclei and their host galaxies, a search for companions to faint Hyades main-sequence stars, a survey of nearby bright stars for faint stellar/sub-stellar companions, and a survey of stellar duplicity in the alpha Perseus cluster. A status report and some intial results from these astonomy projects will also be presented.

Work performed under the auspices of the U.S. Department of Energy by Lawrence Livermore National Laboratory under Contract W-7405-Eng-48.

References:

Olivier, S. S., J. An, K. Avicola, H. D. Bissinger, J. M. Brase, H. W. Friedman, D. T. Gavel, E. M. Johannson, C. E. Max, K. E. Waltjen, W. A. Fisher, W. Bradford, 1994, "Performance of adaptive optics at Lick Observatory", SPIE Proceedings 2201, 1110-1120.

Poster Session

TuA 8:30 am-12:30 pm
Lobby

Status of the first generation adaptive optics system for the Starfire Optical Range 3.5 m telescope

Robert Q. Fugate

Starfire Optical Range, Phillips Laboratory
3550 Aberdeen Ave, SE, Kirtland AFB, New Mexico 87117-5776, USA
Phone (505) 846-4712 ext 314, Fax (505) 846-2213, Internet: fugate@plk.af.mil

The Starfire Optical Range is currently in the process of commissioning a 3.5 m telescope for adaptive optics research. The optical configuration of the telescope allows two large and one small experimental packages to be mounted in the nasmyth area of the coude path. It is feasible to put low order adaptive optics instruments at these locations for maximum light throughput.

The main goal of this facility is to achieve the best possible performance from 0.6 to 2.2 μm wavelengths using laser beacon adaptive optics. Two generations of adaptive optics are planned. The first will employ a refurbished 577 actuator continuous facesheet deformable mirror originally manufactured by Itek and recently rebuilt by Itek using lead mangnesium niobate stacked actuators manufactured by Xinetics. Approximately 500 actuators will be inside the pupil image of the primary mirror, the rest being used as a guard band to provide a smooth transition to the edge of the mirror.

The second generation system is known as SAAO (SOR AEOS Adpative Optics). The SAAO project will provide a complete turn-key adaptive optics system for the 3.67 m Maui telescope known as Advanced Electro-Optical System (AEOS) in the 1997 time frame and subsystem level components to the SOR 3.5 m telescope. The concept is to make as many subsystems and components as possible common to both systems for economy and standardization. Hughes Danbury Optical Systems is the prime contractor for this work building most subsytems in-house but subcontracting the deformable mirrors to Xinetics. The SOR deformable mirror will be a 930 actuator continuous facesheet mirror with lead magnesium niobate stacked actuators of the same design used in the first generation 577 actuator mirror.

The first generation AO system is being set-up in the coude room of the 3.5 m facility. The relay optics have been designed by Jim Spinhirne of Rockwell Power Systems and provide for an image derotation K-mirror at the base of the telescope, pupil imaging toric mirrors, a fast steering mirror, the deformable mirror, Shack-Hartmann wavefront sensor optics and camera, tracking sensors, and science cameras. The relay optics have been designed so that laser beams can be injected into the path and propagated through the system with minimal loss, no airbreakdown, keeping focused regions well away from mirror surfaces.

The first generation laser beacon system approach is a hybrid configuration using the copper vapor laser (CVL) beacon at an altitude of ~15 km and a sodium beacon at 90 km. The CVL beacon will be sensed by ~ 400 subapertures (24 across the 3.5 m diameter) and the 10 watt sodium laser beacon by 16 subapertures. The CVL beacon will provide high spatial frequency wavefront data and the sodium frequency laser the low spatial frequency data. Data from these two sensors will be combined in the reconstructor. Two lasers are required until lower noise (~3 electrons) CCD arrays and compact, efficient sodium lasers of at least 50 watts average power are available. At such time it may be possible to mount the sodium frequency laser directly on the telescope and eliminate the copper vapor laser entirely.

This hybrid approach is very complex and requires considerable engineering both optically and in laser and wavefront sensor control. The CVL beacon will operate at a constant range independent of telescope mount position. The sodium beacon, however, is always at constant altitude so the roundtrip time is dependent on zenith angle. There is a traffic control problem when a sodium return arrives at the telescope just when a CVL pulse is leaving. This problem can be fixed by skipping pulses and adjusting slightly the pulse rate of one or both lasers.

Shack-Hartmann wavefront sensors for star and laser beacons are based on 128x128 pixel CCD arrays built by MIT/Lincoln Laboratory and integrated into a camera by Adaptive Optics Associates. The output phase vectors are passed to a digital reconstructor being built in-house by Rockwell and Air Force personnel. The reconstructor is based on digital signal processor (DSP) technology and has a DSP chip for each of the

577 channels. The system is completely parallel and completes a wavefront reconstruction in less than 25 μsec after receipt of the last piece of wavefront gradient data from the wavefront sensor. Provisions are made for many levels of diagnostics and data capture for analysis of system performance or scientific studies.

The deformable mirror is driven by a new generation of electronics built in-house at the SOR. The system features digital input, zenner diode protection, and reliable operation.

Two tracking sensors are anticipated. One is a synthetic quad cell composed of a four-sided pyramidal mirror and four avalanche photodiode photon counters (EG&G). The second is based on a 64x64 pixel MIT/LL CCD array interfaced to a high speed correlation and centroid precessor. The tracker user interface computer is able to select which sensor is used to control the fast steering mirror and to adjust the parameters used in the CCD array track algorithms.

The components for the relay optics are in fabrication and are planned for delivery in the summer of 1995. The 577 actuator deformable mirror is on site and integrated into a test set-up. The 128x128 CCD array wavefront sensor camera is on site. The DSP based wavefront reconstructor is in fabrication with integration expected to start late summer. First light for the adaptive optics on natural stars is planned for late 1995 or early 1996.

Advanced Electro-Optical System (AEOS) and Starfire Optical Range (SOR) Adaptive Optics

John R. Kenemuth
Janet S. Fender
Brent L. Ellerbroek
James R. Passaro
Tim Pennington
Phillips Laboratory
Kirtland AFB NM
87117-5776

Paul J. Berger
MIT Lincoln Lab
Lexington, MA
02173

Conrad Neufeld
Rene Abreu
William P. Zmek
Hughes Danbury Opt Sys
Danbury, CT
06810

Michael E. Meline
Hughes Albq Eng Lab
Albuquerque, NM
87106

Mark A. Ealey
Xinetics, Inc
Littleton, MA
01460

AEOS Adaptive Optical System

The purpose of the Advanced Electro-Optical System (AEOS) Adaptive Optical (A/O) System is to dynamically correct for atmospheric turbulence, so that a vastly improved image quality is achieved. The AEOS adaptive optical system is located directly beneath the new 3.6 meter telescope. Coude optics in the telescope transfer the $\pm$ 150 urad telescope FOV in the waveband from 0.5 to 5 µm to the A/O system. Operated/controlled by a single operator, the A/O system will dynamically correct the wavefront errors and deliver this corrected wavefront to a visible sensor located on the A/O optical bench or to one of the seven experiment rooms. Capability to bypass the A/O system is provided. Relay optics, a Hartmann wavefront sensor (WFS), tracker, and a deformable mirror are located on the thermally controlled, kinematically supported optical bench. Support equipment and the A/O work station are located in the adjacent access room. Observational targets will include both satellites and astronomical objects.

The full system is being developed for the AEOS facility at the Air Force Maui Optical Station (AMOS) on Mt Haleakala, Maui, Hawaii; several key subsystems will be delivered to the Starfire Optical Range (SOR) at Phillips Laboratory, Kirtland AFB, NM.

The full telescope beam is relayed first to the tilt control mirror, next to the deformable mirror, then to a dichroic which splits off the 0.5 to 0.7 μm waveband to the tracker/WFS and relays the 0.7 to 5 μm wavebands directly to the visible and IR optical sensors. Options to this sequence include (1) full bypass of the A/O system, or after the tracker/WFS split, (2) sending the light to a diagnostic camera, or (3) bypassing the on-bench visible sensor and diagnostic camera and relaying light to a sensor in one of the seven experiment rooms. Optical fibers handle the high data rates for the WFS Real-Time Reconstructor (RTR) deformable mirror operation. An optical source simulator (OSS) subsystem on the bench provides system checkout capability by inputting targets of differing size/brightness and simulating a dynamic atmosphere.

System design is driven by the requirement to operate well after sunrise, to 70° from zenith and with target crossing rates to 2.5°/ second. The WFS samples 900 subapertures over the pupil at 2,520 Hz; corrections are real time computed on the RTR; and the wavefront corrected by the deformable mirror (using 941 actuators) at up to 200 Hz. Targets to M 8 and as large as 100 urad are tracked at 20-200 Hz. Operational readiness requires ease in maintenance, built-in subsystem test capability, and high (95%) availability. Computer modeling predicts significant improvement in target identification.

The design has provided for growth to further enhance performance: provisions have been made for additional WFSs and a fast figure sensor for laser guide star compatibility, addition of a second tracker, increase to 1,500 subapertures and frame rates to 5,000 Hz.

Gemini 8-Meter Telescopes Active and Adaptive Optics Update

Jim Oschmann
Doug Simons
Dave Robertson
Matt Mountain
Dick Kurz

Gemini 8-Meter Telescopes Project, 950 N. Cherry Avenue
Tucson, Arizona 85719

Charles Jenkins

Royal Greenwich Observatory, Madingley Road
Cambridge, CB3 0EZ United Kingdom

Glen Herriot

Gemini Canadian Project Office, Herzberg Institute of Astronomy, 5071 W. Saanich Road, R.R.5,
Victoria BC V8X 4M6 Canada

The Gemini 8-Meter Telescopes are being designed to deliver near diffraction limited images at infrared wavelengths to the focal plane. This will be achieved with a combination of innovative telescope design, a fully active control system and a natural guide star adaptive optics (AO) system for the Mauna Kea Telescope. An overview of how the Gemini Adaptive Optics System works in concert with the active systems employed on the Gemini telescopes is given. Extensive trades have been made in determining the mix of sensors to support both active and adaptive operation. The current concept of how the systems will work in concert is presented here.

The Gemini Telescopes have been designed from the outset to be fully active; from control of the primary mirror surfaces and positioning of the secondary to ventilation of the enclosure by control over the ventilation gates. Descriptions of the concepts used in the various subsystems have been published previously[1]. Here, we will emphasize the system level interactions between the Gemini Adaptive Optics System and the Acquisition and Guiding System. This includes how the telescope operates with and without AO and changes between these two modes of operation.

First, the current system concept is outlined, which includes wavefront sensors/guiders in the following areas:

Acquisition and Guiding System :	Peripheral Wavefront Sensors
Scientific Instruments:	On Instrument Wavefront Sensors
Adaptive Optics System:	Facility Wavefront Sensor

The interactions of these three key sensor areas is then discussed as well as differences in how they may be used. For non-AO use, both peripheral and on instrument wavefront sensors may be used to support fast and slow guiding and active control of the telescope alignment and wavefront. For AO use, combinations of all three types of wavefront sensors may be used for adaptive atmospheric compensation in addition to the functions listed above. The system is designed to quickly change between modes of operation (AO to non-AO and back) under remote control.

This is meant as an overview to understand some of the choices made to date in the detailed implementation. Further details on the Gemini Adaptive Optics System, some of the supporting analysis, and the Acquisition and Guiding system (in terms of analyzed performance of the guiding function) are presented elsewhere at this meeting.

REFERENCES

1. Mountain C M., Kurz R., Oschmann J., "The Gemini 8-M Telescopes Project," 1994 SPIE Kona Conference on Astronomy.

Use of the LBT to study zodiacal emission around other stars

N. Woolf and J.R.P. Angel

Center for Astronomical Adaptive Optics
Astronomy Department
University of Arizona
Tucson, AZ 85721
Phone: (520)621-3234 - Fax: (520)621-9843

Introduction

Thermal emission from "planetary" discs is known in other stars such as β Pictoris. The emission, discovered by the IRAS satellite, is comparable in strength to that from the star itself at 60 μm wavelength, indicating a large quantity of material at radius $\sim$ 100 AU and temperature $\sim$ 50 K (ref 1). Such discs are uncommonly bright, far more dense and extensive than the known zodiacal dust in our solar system. Here the emission is concentrated mostly within 1 AU, where the dust temperature is $\sim$ 300K and it is optically very thin, causing an increment of only 10^{-5} in the 10 μm luminosity of the Sun as seen from afar.

It would be valuable to measure the 10 μm zodiacal emission of other sun-like stars . Our zodiacal dust is not stable, but is continuously replenished by cometary debris and the debris from the collisions of asteroids with one another and with planets and satellites. Thus dust emission around older stars would suggest that storage of material in condensed lumps (comets and asteroids) occurred, and that as in our system there is a slow destruction of these objects. Wetherill (ref 2) has suggested that the Solar System debris is less than it might be because Jupiter has "cleaned up" the system. Thus the measurements of dust level and the presence or absence of a Jupiter-like planet, also determinable from the ground, taken together should provide considerable insight into the characteristics of evolved exo-solar systems like our own.

If zodiacal emission is significantly stronger than in the Solar System, this would also be of practical interest, in assessing the viability of detecting earthlike planets from space via their thermal emission (ref 3). Since even the weak zodiacal emission in our own solar system is already 100 times brighter than the Earth, stronger zodiacal emission could pose a difficulty.

Design considerations for detection from the ground

In order to obtain a reasonable sampling of single stars like the Sun, a survey out to 10 pc is needed. At this distance a 1 AU cloud as in the solar system would have a diameter of 0.2

arcsec, unresolved at 10 μm wavelength at the diffraction limit of even the largest telescopes. Photometry at the 10^{-5} level is not a viable way of detection. There is a unique opportunity, however, to reach the resolution and sensitivity to see solar system level emission. As we show below, it should be possible with the Large Binocular Telescope (LBT), corrected with low emissivity adaptive optics and used as a Bracewell nulling interferometer.

The LBT, being built on Mt Graham, Arizona by an international partnership, consists of two mirrors of diameter d = 8.4 m co-mounted with separation s = 14 m between centers (ref 4). Both the atmospherically induced phase errors across each mirror and the path length difference between the apertures will be corrected with adaptive optics. Each telescope will then give a diffraction limited 10 μm image of width (FWHM) = λ/d = 0.25 arcsec. To suppress the starlight while allowing detection of the zodiacal emission, the binocular pair can be used as a Bracewell interferometer (ref 5). The wavefronts from the two telescopes are interfered in such a way as to produce fringes on the plane of the sky with a null centered on the star. The combined image shows the normal diffraction limited images of the single aperture, but if the telescope tracks across the sky, the stars blink in and out provided the mirror spacing is not so large as to resolve their disks. The fringe separation on the sky is given by λ/s, i.e. $10\mu/14m$ = 0.14 arcsec. When the star is overlain by the central dark fringe, there is high sensitivity to zodiacal emission outward from typically 0.03 arcsec radius, with the first maximum at 0.07 arcsec.

Suppose for the moment that the stellar nulling were perfect. Could we then detect the emission from a solar system strength zodiacal cloud at 10 pc? The signal must be detected against photon noise in the telescope's thermal emission. Typically adaptive optics systems contain many warm surfaces, and emissivities $> = 20\%$ are projected. However, we plan for the LBT adaptive correction at a silvered chopping secondary mirror (ref 6), so no more surfaces are involved than for the optimized chopping secondary systems used to obtain emissivities of a few percent. Recent experience with the MIRAC camera at the IRTF gave a limiting flux of 2 mJy in a 1 arcsec pixel in 8 minute integration (ref 7). Scaling to a 1 hour observation with the LBT, we project a limiting magnitude of N=14.5. Thus all nearby stars brighter than N=2 could be examined to the solar system level (10^{-5} or 12.5 magnitudes fainter than the star), allowing a good sampling of nearby star types A - K.

Efficiency of interferometric star rejection
In practice the interferometric null will not be perfect, and some starlight will be detected. Ideally we would like it to be weaker than the zodiacal component, but in fact as long as the leak is not a lot stronger and can be calibrated, it could be subtracted. Two components need to be considered: fundamental leakage because the stellar disc has finite angular size, and leakage because of imperfections in the wavefront correction, which prevent perfect destructive interference. Because of the angular diameter of the star, we find by integration across the $\sin^2$ response at the fringe minimum that a 500 μarcsec radius star will leak about 2.5×10^{-5} of its light into the central image. If the star has twice this angular radius, the leakage light is increased to 2×10^{-4}. These ranges correspond to a Sun-like star at 5 to 10 pc distance. In a sample of stars within 10 pc, 87% of the stars will lie in this range. Note that a larger baseline would let through more starlight, and a significantly smaller baseline would

require cutting down the size of the mirrors and not permit the sensitivity to detect the radiation. Pathlength control to around 10 nm will be needed to hold the null correctly pointed, but this will be possible from optical interferometry.

Leakage due to wavefront aberration is estimated as follows (refs 8&9): From the atmospheric aberration measured at the site, and assuming correction with 0.5 m subapertures, residual errors of < 80 nm should be obtained routinely. The rms phase error sigma = $80 \text{ nm}/2\pi\lambda$ = 0.05 radians, thus we expect a Strehl ratio $S = \exp(-\sigma^2) = 99.75\%$. The residual wavefront error will thus result in a ten μm halo containing 1/400 of the star's energy that is not removed by the interferometric cancellation. Because the individual adaptive apertures diffract into 4 arcsec, the halo energy is spread uniformly over 4 arcsec radius, its surface brightness is about 10-5 of the stellar peak, and it should not present a problem to detection of concentrated zodiacal emission.

Conclusions

The LBT is uniquely well suited to the detection of zodiacal emission around nearby stars, because of its large apertures and binocular configuration. It should be able to detect emission at solar system levels around stars over a wide range of spectral types, such as Vega and τ Ceti. Its 14 m baseline is optimum, yielding the resolution needed to discriminate emission 1 AU discs at 10 pc, while also allowing good nulling of stellar discs as close as 5 pc. Its large individual apertures and low emissivity adaptive optics are necessary to obtain adequate sensitivity in the presence of thermal background.

The operation of such a nulling interferometer on the ground would also be a valuable scientific and technical precursor to a space mission to detect and obtain infrared spectra of terrestrial exoplanets, some 100 times fainter. The ground based telescope would identify the best targets and would test many of the design principles of such a space mission, which must also rely on a nulling configuration to suppress stellar emission.

References
1) Backman, D.E. Gillett, F.C. and Witteborn, F. 1992 Ap.J. **385**, 670.
2) Wetherill, G.W., 1994 Astrophys. And Sp. Sci., **212**, 23.
3) Angel, J.R.P. Cheng, A. and Woolf, N.J. 1986 Nature **322**, 341.
4) Hill, J.M. 1994 Proc SPIE **2199**, 64.
5) Bracewell, R.N. andMcPhie, R.H. 1979 Icarus **38**, 136.
6) Bruns, D. G. Martin, H. M. Brusa, G. Sandler, D. G. Barrett, T. K. Biasi, Roberto, Gallieni, D. Salinari, P. Angel, J. R. P. 1995 These Proceedings.
7) Hoffman, W. 1994 private communication.
8) Sandler, D.G. Stahl, S. Angel, J.R.P. Lloyd Hart, M. and McCarthy, D. 1994 JOSA **11**, 925.
9) Angel, R. and Sandler, D. 1995 These Proceedings.

Predictability of Atmospherically-distorted Stellar Wavefronts

George J. M. Aitken and Donald McGaughey

Department of Electrical and Computer Engineering, Queen's University

Kingston, Ontario, Canada K7L3N6

Tel.: 613-545-2947, FAX: 613-545-6615; I: aitkeng@qucdn.queensu.ca

The errors caused by the inherent time delays in an adaptive-optics control loop could be overcome to a large extent by short-term prediction of the incident wavefront. Conversely, the bandwidth requirements of the loop could be relaxed. Furthermore, it is of interest to efficiently use all of the information available in the wavefront when making estimates of future values. In [1,2,3] Jorgenson and Aitken have described evidence suggesting that wavefront distortions should be treated as the output of a nonlinear dynamical system, and not simply as a filtered random process. Schwartz et al [4] have made similar suggestions.

In references [2] and [3], simple, unoptimized neural-network predictors, demonstrated that real, stellar wavefront distortions were indeed predictable in the short term. Reference [4] discusses the prediction of simulated fractal wavefronts by a linear predictor. In this paper we probe deeper into the temporal properties of wavefront distortions. Two statistical tools, rescaled-range (R/S) analysis [5] and correlation-dimension (CD) estimation of the phase-space attractor [6], have been applied to time series of sampled wavefront slopes obtained from the COME-ON wavefront sensor [7], operating open loop on the ESO 4m telescope at La Silla. As well, conventional power spectra and amplitude distributions have been calculated. Sequences of up to 8000 sampled slopes from each of the 20 sub-apertures of the Shack-Hartmann wavefront sensor were used. R/S analysis measures persistence, sometimes called the Hurst effect, that

occurs in fractional Brownian motion and chaotic processes. CD analysis estimates the number of independent variables needed to describe the driving process. This dimensional information is useful for designing optimum predictor networks.

Results obtained to date confirms that there is a useful degree of predictability in the wavefront time series. R/S analysis of the slopes and of the slope differences shows a high degree of persistence in both cases. The analysis of slope differences eliminates long-term dependence and non-stationarities that might bias the R/S results. We have found that slope differences exhibits a clear change in behaviour at 100 samples taken at 116 Hz. This suggests the possibility of structure extending up to about 800 ms in this data. Each set of 20 slope sequences, taken at the same time through the same atmosphere, but at different locations in the aperture, has shown excellent consistency with less than 2% variation from one sub-aperture to another in the R/S, CD, average power spectrum and amplitude distribution estimates.

References

1. M. B. Jorgenson and G. J. M. Aitken, Opt. Lett., **16**, 64-66 (1991)

2. M. B. Jorgenson and G. J. M. Aitken, Opt. Lett.,**17**, 466-468 (1992)

3. M. B. Jorgenson and G. J. M. Aitken, *Active and Adaptive Optics,* F. Merkle, Ed. (European Southern Observatory, Garching bei Munchen, Germany, 1994) 143-148

4. C. Schwartz, G. Baum and E. N. Ribak, J. Opt. Soc. Am. A, **11**, 444-451 (1994)

5. B. B. Mandelbrot, *The Fractal Geometry of Nature* (Freeman, New York, 1983)

6. J.Theiler, J.Opt. Soc. Am. A, **7**, 1065-1073 (1990)

7. G. Rousset, J. C. Fontanella, P. Kern, P. Lena, P. Gigan, F. Rigaut, J. P. Gaffard, C. Boyer, and F. Merkle, Proc. S.P.I.E.1237, 336 (1990)

WaveLab - Hartmann Sensor Data Analysis Software

Allan Wirth
Adaptive Optics Associates Inc.
54 CambridgePark Drive, Cambridge, MA 02140
(6i7) 864 0201 FAX (617) 864 1348

WaveLab is a Hartmann wavefront sensor data analysis system that permits virtually any Hartmann test data to be quickly converted to wavefronts and all derivative types of information such as point spread functions, OTFs, and encircled energies. It uses a graphical interface that makes standard data reduction straightforward and also provides a command line interface for customized data handling. It is user customizable in two ways: WaveLab is an extension to the tcl scripting language and all of the high level reduction routines are in the form of tcl scripts. The user may add their own scripts to handle data in specialized ways. Secondly, the user may add c language functions to the WaveLab / tcl system. This allows the inclusion of more esoteric or complex routines than maybe easily coded at the tcl script level.

All the data files used or generated by WaveLab are in an extension of the FITS format.

Examples will be given of input and output data for a variety of cases.

Linear Spatio-Temporal Prediction for Adaptive Optics Wavefront Reconstructors

Michael Lloyd-Hart

Steward Observatory, Center for Astronomical Adaptive Optics,

Tucson, AZ 85721, USA

Telephone: +1 520 621 8353 Fax: +1 520 621 9843 email: mhart@as.arizona.edu

1. INTRODUCTION

Detailed computer simulations have been performed to evaluate the potential for spatio-temporal prediction of wavefront slope data from a Shack-Hartmann sensor to improve the imaging quality of an astronomical adaptive optics system by overcoming the effect of the inherent delay between sensing and correcting the wavefront phase error. Results of the simulations show that an improvement of a factor of at least 2 in the residual mean-square phase error can be achieved by extrapolating into the future on the basis of past wavefront measurements. Experiments will be conducted very shortly with actual data gathered at a 1.6 m telescope using a Shack-Hartmann sensor with 31-cm subapertures to test the simulations. Both the simulations and the experimental arrangement have been chosen to match closely the measured operating conditions of the adaptive optics system under construction for the 6.5 m MMT (Martin & Anderson 1995).

In typical adaptive optics systems, the wavefront reconstructor attempts to match the deformable mirror to the instantaneous shape of the optical wavefront on the basis of a vector of phases or slopes measured by a sensor. Some finite time elapses while the measurement is made and the computations are performed, so by the time a correction is applied to the mirror, the wavefront has evolved to some slightly different shape. This is one of the major residual sources of error in the corrected wavefront, and leads to one of the fundamental constraints in the performance of adaptive optics systems. A balance must be struck between the need to perform the measurement-reconstruction-correction cycle as fast as possible, and the necessity of integrating light from the reference beacon to overcome photon noise. Angel (1994) has analysed this trade-off in detail.

Previous work by Jorgenson and Aitken (1992), however, has shown that the fluctuation in atmospheric phase measured at a point in a telescope pupil is predictable on timescales several times longer than the decorrelation time. It is therefore possible to reduce significantly the effect of temporal decorrelation by using a wavefront reconstructor algorithm which predicts the future shape of the aberration on the basis of several slope vectors measured in the immediate past. The trade-off between photon noise and decorrelation error then becomes more relaxed, which allows longer integration times on the wavefront sensor. Fainter sources may then be used as guide stars, which in turn increases the fraction of sky available for high-resolution imaging.

In the present work, computer simulations of a complete adaptive system have been performed in which the conventional wavefront reconstructor matrix is extended to provide full spatio-temporal prediction. The input vector to this matrix is a time series of several measurements from the wavefront sensor. The output then predicts the next element of the series. Furthermore, the matrix itself is derived from scratch using data taken entirely from the telescope. Thus, one may envision a system in which the first few minutes of each observing night are devoted to building the reconstructor matrix, which would then be ideally suited to the prevailing atmospheric conditions.

2. DESCRIPTION OF SIMULATIONS

2.1 Simulation of the atmosphere

The simulated atmosphere was chosen to match observed data from the present MMT (Lloyd-Hart et al. 1995). It consisted of three separate turbulent layers with a Kolmogorov power spectrum. Temporal evolution was generated by assuming the Taylor hypothesis, and propagating the three layers at different speeds, and in random directions. Parameters are given in Table 1.

Table 1

Layer	Inner Scale	Outer Scale	r_0	Wind Speed
1	1 mm	100 m	2.0 m	40 m/s
2	1 mm	100 m	1.8 m	20 m/s
3	1 mm	100 m	1.5 m	8 m/s

2.2 Simulation of the telescope, optics, and detectors

Results have been obtained for a 2.0 m diameter primary mirror with a Cassegrain hole of 0.2 m diameter. The deformable mirror was represented as a continuous facesheet with 5 × 5 actuators spaced at 50 cm intervals on a square grid. The central actuator, falling in the Cassegrain hole, was not used, but those falling outside the illuminated pupil were retained as a guard ring. The system thus had 24 degrees of freedom. A gaussian with FWHM equal to 1.5 times the actuator spacing was used for the influence function of all the actuators. This was not a realistic modelling of an actual deformable mirror, but was rather intended to provide a reasonable approximation in the spirit of a proof-of-principle.

The wavefront sensor was a Shack-Hartmann sensor with a 4 × 4 lenslet array, and square subapertures 50 cm on a side, providing 32 slope measurements per exposure. The beacon was a star of magnitude 1.75, and the detector was assumed to be a CCD with 3 electrons rms read noise, which is negligible compared to the photon noise. The exposure time in all cases was set at 10 ms. Testing was done by imaging the beacon at a wavelength of 2.2 µm. Five hundred 10-ms frames were averaged in each test case to determine the long-exposure Strehl ratio.

2.3 Derivation of the reconstructors

The code derives full spatio-temporal predictive linear wavefront reconstructors from Shack-Hartmann slope data. The whole operation is performed through the telescope optics on the sky, at the frame rate of normal operation of the adaptive servo loop.

Wavefront reconstructors were derived in two parts - the first active, the second passive. During the active phase, the influence function of each actuator was measured. First, the deformable mirror was flattened and an exposure taken. Then the actuator was pushed up and a second exposure taken. Finally, the mirror was flattened for a third exposure. The slope vectors obtained from the wavefront sensor for the two flat exposures were averaged and subtracted from the slope vector with the actuator pushed up, removing most of the effect of the atmosphere on the wavefront, and leaving just the effect of the actuator. The process was repeated for each actuator in turn over the whole mirror. To reduce further the atmospheric effects, the whole cycle was repeated a number of times, and the results averaged. The influence function matrix F thus derived is then inverted in the standard way to obtain the reconstructor matrix S:

$$S = (F^T F)^{-1} F^T.$$

Eq. 1

The passive part derived the spatio-temporal predictor for the wavefront slopes. A large number of slope vectors $V(t)$ were collected with a flat mirror, and arranged as column vectors in a matrix M_1, where each column contained a number of slope vectors equal to the lookback depth of the reconstructor, in this case three. A second matrix M_2 of slope vectors was also built up, where each column contained the slope vector immediately succeeding those in the corresponding column of M_1. Thus, if column N of M_1 contained $V(0)$, $V(1)$, and $V(2)$, then column N of M_2 would contain $V(3)$. The least-squares best fit predictor matrix P is then given by:

$$P = M_2 M_1^T \left(M_1 M_1^T \right)^{-1}.$$

Eq. 2

Finally, the desired reconstructor R is given by:

$$R = SP.$$

Eq. 3

3. RESULTS

For the present case, the standard reconstructor S was derived by cycling through all 24 actuators 1000 times, requiring a total of 48001 frames from the wavefront sensor. The predictor P was derived from 1000 slope vector measurements, which required a further 1003 frames. The derived reconstructor R was then tested under two sets of conditions. Firstly, the reconstructor was asked to predict and correct 500 wavefronts in a continuous series, drawn from the same atmosphere used in the derivation, but which had themselves not been used. As a second test, the atmosphere was rerandomised, using the same parameters as in Table 1, but with different initial conditions. The resulting Strehl ratios are presented in Table 2. For comparison, the first test was run again, this time using a reconstructor derived from Eq. 1, and similar to S, except that the influence function to be inverted was derived not by measurement on the sky, but from the influence function defined in the simulation code. This emulates the conventional procedure of measuring an influence function explicitly in the lab.

Table 2: Strehl ratios for simulated wavefront compensation

Conditions	Uncorrected	Shack-Hartmann best fit	Actuator best fit	Reconstructed
Same atmosphere	0.157	0.946	0.932	0.788
Standard reconstructor	0.157	0.946	0.932	0.640
Randomised atmosphere	0.183	0.946	0.934	0.282

For each set of conditions, four Strehl ratios are shown. The first is for the completely uncorrected case; following that is the Strehl ratio to be expected if the deformable mirror were replaced by a segmented one whose segments exactly matched the lenslet array, and the segments were explicitly fitted to the wavefront. This is very similar to the third value, which represents the result of an explicit best fit of the 24 actuators of the actual deformable mirror to the wavefront. The similarity is an indication that the deformable mirror and lenslet array are reasonably well-matched. Finally, the last column shows the result of the reconstructors' efforts. The value of 0.640 obtained by the "standard" reconstructor shows that even without prediction, the system would be expected to function very well. Nevertheless, the predictor improves the performance to a Strehl ratio of 0.788 under the same conditions, corresponding to a factor of 2 improvement in the mean square residual wavefront error. However, under atmospheric conditions very different from those the reconstructor was derived from, it fails significantly, producing a Strehl ratio of only 0.282, barely improving the performance of the telescope at all.

4. CONCLUSIONS

The work presented here extends the conventional approach to wavefront reconstruction by postmultiplying the usual reconstructor matrix by a second matrix which attempts to predict the shape of the wavefront at the time when the correction will actually be applied to the deformable mirror. The reconstruction is thus applied to up-to-date data, and much of the wavefront error introduced by the delay between sensing and correction can be eliminated. These results suggest that a factor of two reduction in mean square phase error should be readily achievable. By stretching the integration time on the wavefront sensor, the limiting magnitude of an adaptive optics system can thus be expected to improve by at least half a magnitude. A second valuable result is that it is indeed practical to build a reconstructor entirely at the telescope. At a wavefront sensor frame rate of 1 kHz, it would take less than 10 minutes to derive a matrix for an adaptive system with 300 actuators, such as the adaptive secondary mirror planned for the 6.5 m MMT. This is essential, since the predictor is not robust against dramatic changes in wind direction, and so one might expect to have to update the matrix several times a night. In fact, only the predictor P need be recomputed; the standard reconstructor S remains constant, and since deriving S takes by far the bulk of the time, it will be very quick to make the change. It may even be possible to continuously update P "on the fly".

REFERENCES

Angel, J. R. P., "Ground Based Imaging of Extrasolar Planets using Adaptive Optics," 1994, Nature, **368**, 203-207

Jorgenson, M. B. and Aitken, G. J. M., "Neural Network Prediction of Turbulence Induced Wavefront Degradations with Applications to Adaptive Optics," 1992, Proc. SPIE Conf. on Adaptive and Learning Systems, Ed. F. A. Sadjadi, **1706**, 113-121

Lloyd-Hart, M, et al., "Adaptive Optics Experiments using Sodium Laser Guide Stars," 1995, Astrophys J., **439**, 455-473

Martin, H. M. and Anderson, D. S. , "Techniques for Optical Fabrication of a 2-mm-thick Adaptive Secondary Mirror," 1995, this conference.

Prediction of Star Wonder Path
With Linear and Non-linear Methods

D. Bonaccini

ESO Instrumentation Division - Adaptive Optics Group

Karl-Schwarzschild-Str. 2 - D-85748 Garching bei Muenchen

phone +49-89-32006-567 fax +49-89-32006-358 e-mail dbonaccini@eso.org

D. Gallieni, R. Giampieretti

Dipartimento di Ingegneria Aerospaziale - Politecnico di Milano

via Golgi, 40 - 20133 Milano - Italy

phone +39-2-23994000 fax +39-2-23994034

Introduction

In adaptive optical systems using Shack-Hartmann wavefront sensors the optical wavefront is obtained measuring the star wonder or centroid of the reference object. The integration time of the wavefront sensor, especially in the case of natural guide star references, produces a phase lag of the servo-system which affects quite heavily the system performance in most cases, i.e. for faint sources.

Therefore it would be valuable to be able to conjugate the wavefront giving commands to the adaptive mirror while the CCD wavefront sensor is integrating, thus extrapolating the wavefront from previous measurements. Recent results of chaos theory have shown that the fractal nature of turbulence indeed allows that.

We present the numerical results of an attempt to predict the starlet wonder by means of linear and non-linear (neural networks) autoregressive models in order to give a preliminary evaluation of their applicability in Adaptive Optics systems.

Wave Front sensor output prediction

A sketch of an adaptive optical system model is shown figure 1. It models a segmented mirror scheme, i.e. each subaperture is supposed independent from the rest of the mirror. Each component introduces its own dynamic effect in the control loop. The most relevant one is, in most cases, the time delay due to wavefront sensor integrating period. When this is much larger than the grand total of other dynamic time constants, it represents a bottleneck for system performances.
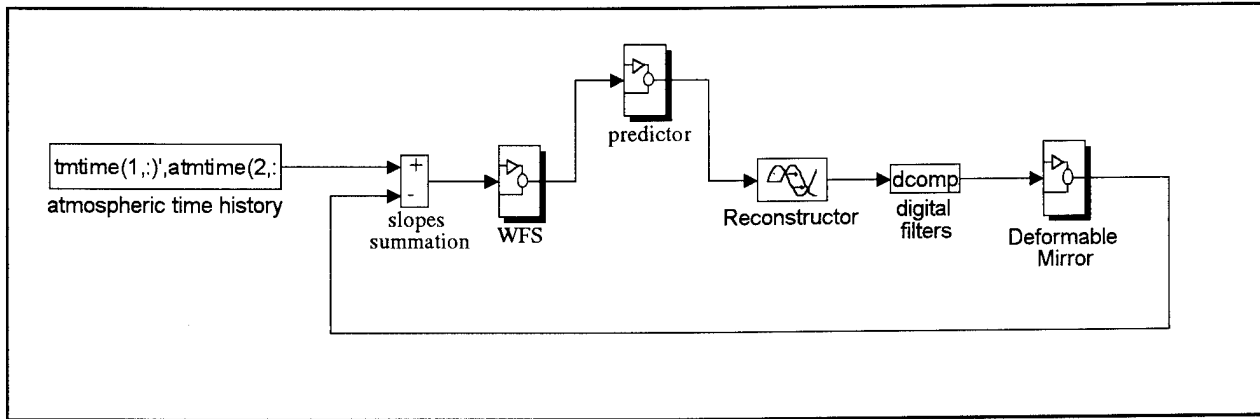
Figure 1: adaptive optics control loop

The aim of introducing a wavefront sensor output prediction into the feedback loop is to drive the deformable mirror even while the CCD is integrating, thus not providing any information to compute actuators command. In this perspective, time series derived from models of turbulence PSD are used to test different kinds of predictors.

ARMA linear predictor

The wavefront sensor output dynamics is modeled as an Auto-Regressive Moving Average time series (ARMA), whose instant (discrete-time) value is a linear function of its last past values and of both present and last past values of an unpredictable noise. The model parameters are recursively trained by an Extended Least Squares algorithm (ELS), fitted with a forgetting factor device in order to provide adaptivity. The current model is used to predict the first future value of the time series. When the sensor sampling frequency is much smaller than the mirror controller one, the predicted value stands far in the future with respect to the controller period. Then such a prediction, together with the present and past values of the sensor output, is used to provide, by means of cubic spline interpolation, the higher frequency predictions required by the controller.

Prediction results that can be achieved by using the ARMA model are shown in the example presented in figure 2. The Shack-Hartmann sensor integrating period T is 166 Hz while the adaptive optics control is commanded at a frequency four times the wavwfront sensor sampling one.

Sensor outputs within each integrating period $\tau \div \left(\tau + T \right)$ are predicted as soon as the output at $t = \tau$ is made available.
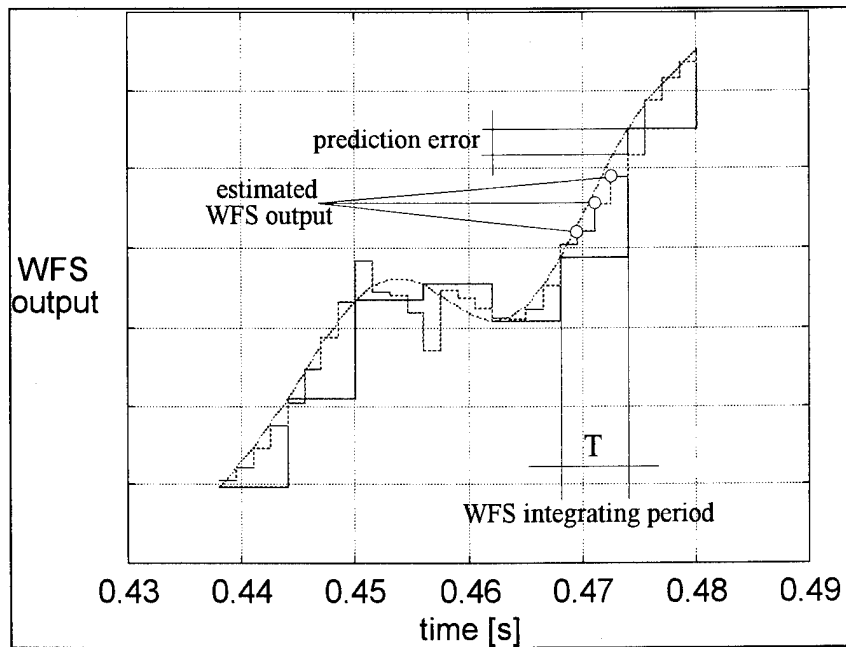
Figure 2: WFS output prediction

At the readout time $t = \tau$ the error between the actual measurement and the predicted value can be corrected, thus not affecting the next estimates.

Non Linear predictors

Other models instead of ARMA have been tried (precisely Neural Network Non-linear ARMA models, either with RBF or sigmoidal activation functions), but so far they not appear competitive, as predictors, against their linear counterparts, which are computationally cheaper.

Final remarks

The present work shows a possible way of better exploiting the adaptive optical system potentiality by extrapolating centroids positions from previous ones to compensate wavefront sensing time delays.

Further development of predictor models and their extension to continuous facesheet mirrors could provide a general form for this adaptive optical system component. Besides, the fractal nature of turbulence might be used to model more properly the WFS output dynamics, in order to unify the prediction-regularization problem. For the latter purpose it may also be thought to re-design the prediction approach in order to better exploit the Neural Network predictor-regularizer.

Space-time Wavefront Analysis Using a Coordinate Remapping Shack-Hartmann Sensor

N J Wooder, I Munro, T W Nicholls, M Wells[†] and J C Dainty

Blackett Laboratory, Imperial College, London SW7 2BZ
† Institute for Astronomy, Royal Observatory, Edinburgh, EH9 3HJ
Fax: +44 171 594 7714   nik@op.ph.ic.ac.uk

In this project, we wished to make the first measurements of the spatial-temporal characteristics of wavefronts in the infrared by taking advantage of the exisiting infrared camera (IRCAM3) and fast controller (ALICE) [1] at the 3.8m United Kingdom Infrared Telescope (UKIRT). The intention was to have a system that could eventually be used for routine measurements as part of the UK's Joint Observatories Site Evaluation (JOSE) campaign: a re-engineered version of the system described here has in fact now been constructed for the JOSE programme.

Because of the constraint of having to use the IRCAM/ALICE system, and requiring a system that could be "switched in" at any time by the telescope operator, the only real option was to place a prism-based design in one of the cold filter wheels near the Lyot stop. Using prisms (instead of lenslets) allows the array of images to be remapped on to a sub-aray of the detector to give the fastest possible frame rate. Figure 1 shows the geometry in the pupil and that in the image plane. Details of the design and construction can be found in Ref.[2] and [3]: the 24 prisms, made of water-free silica, are roughly 2×2×2mm and are optically contacted onto a 20mm diameter substrate. The mask covering the prisms has 25 apertures (one being used for a straight-through beam) equivalent to 330mm diameter in the pupil.

The original design aimed at placing all 25 images in a strip of 32 by 256 pixels, which would have allowed data recording via a custom transputer-based system of 50 frames per second, but a slight misalignment meant that 48 by 256 pixels had to be recorded at a somewhat sub-optimum 33 frames per second. The time integration per frame of ≈30ms should be considered in the interpretation of the results below.

The first step in the data analysis is to calculate the centroids of the sub-images: this was done using a slow but extremely accurate iterative procedure. Our sensor did not have a separate calibration measurement, so the average of 2000 to 4000 frames was used to find
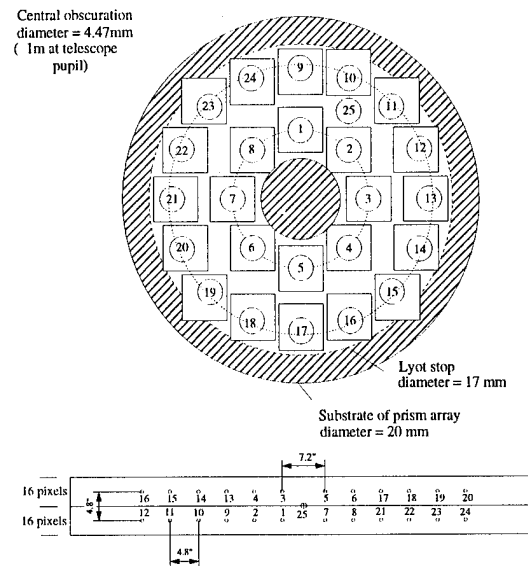
Figure 1: Distribution of prisms in pupil (upper) and of images (lower)
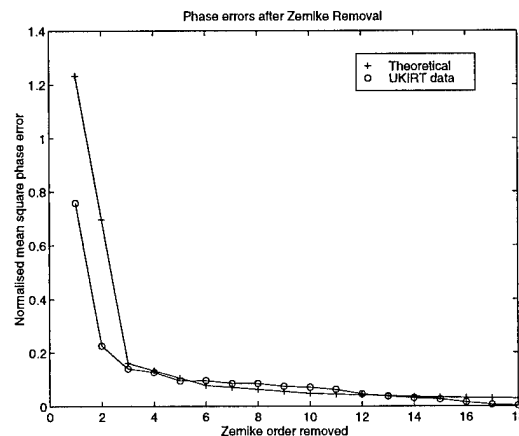
Figure 2: Plot of experimental and theoretical values of the normalised mean square phase error as a function of the Zernike order removed. The first point is for no terms removed, the second for "tip" removed, etc. The two curves are normalised to have the same integrated mean squared error for Zernike terms >3.

the mean sub-image centroids (i.e. those associated with a long exposure). Elsewhere [2] we have described results of calculations of the Fried parameter r_0 from this data using the differential variance method [4]. Here we show some calculations relating to the statistics of the Zernike coefficients for observations at K (2.2μm).

The 25 element Shack-Hartmann sensor provides 50 wavefront slopes and from these we can solve for the Zernike coefficients for each frame of data. Noll [5] has calculated the residual phase variance of the wavefront after successive Zernike terms are subtracted, on the assumption of Kolmogorov turbluence with an infinite outer scale. We have also calculated the residual variance for the experimental data, using typically 3500 frames, and in Figure 2 we plot the experimental and the theoretical values as a function of the Zernike order removed. It can be seen that apart from the "tip" term, where there was
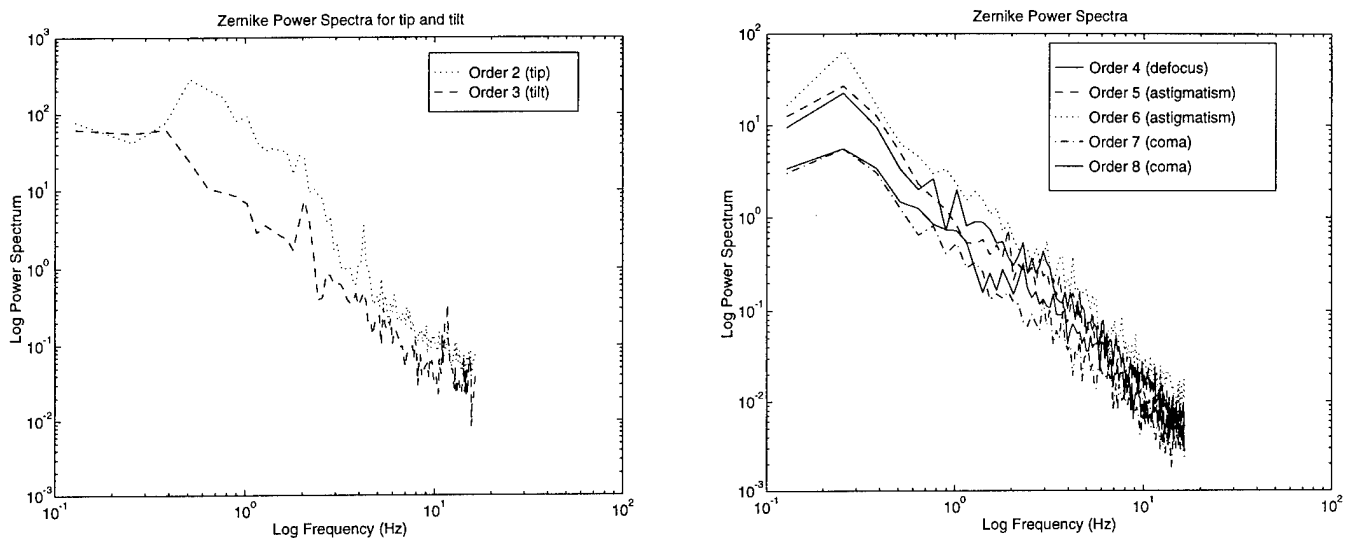
Figure 3: Power spectra for Zernike "tip" and "tilt" for two data sets.

known to be an effect due to telescope guiding (see below), there is reasonable agreement between the two curves.

The power spectra of the tip/tilt Zernike terms are plotted in Figure 3 up to the Nyquist frequency of $\approx$16.5Hz, for two data sets. The "tip" and "tilt" directions corresponded approximately to RA and DEC respectively, and the very large excess power for "tip" at low frequencies is due to telescope tracking errors: there are several other identifiable artifacts due to the telescope. Power spectra for the next five Zernike terms are shown on the right hand side of Figure 3. They show a consistent behaviour at high frequencies, with a slope of $\approx$-2.1.

References

1. P J Puxley et al, "Performance of an SBRC 256×256 array with ALICE/IRCAM3", *Proc SPIE* **2198** 350–358 (1994)

2. M Wells, I Munro, T W Nicholls, N J Wooder and J C Dainty, in preparation for *Mon Not Roy Astro Soc*

3. T W Nicholls, M Wells, N J Wooder and J C Dainty, "Infrared Wavefronts at Mauna Kea", San Diego, July 9-14, 1995 (SPIE Proc Vol 2534)

4. M Sarazin and F Roddier, "The ESO differential image motion monitor", *Astron Astrophys* **227** 294–300 (1990)

5. R J Noll, "Zernike polynomials and atmospheric turbulence", *J Opt Soc Am* **66** 207–211 (1976)

BISPECTRAL IMAGING TOOLBOX

Pedro Negrete-Regagnon

Applied Optics, Blackett Laboratory
Imperial College, London SW7 2BZ U.K.
pedro@op.ph.ic.ac.uk

Introduction

For centuries, astronomers have built larger telescopes attempting to collect more light so fainter objects could be studied, but resigned to the fact that such larger telescopes would not provide higher resolution. It was until 1970, when Antoine Labeyrie notice the significant difference between short-exposure and the long-exposure images astronomers were used to see. Labeyrie reasoned that each speckle present in the short-exposure image was actually a diffraction-limited image formed by the telescope. He concluded that a short-exposure image contains high resolution information not present in the long-exposure counterpart, and invented a method to extract such high resolution information that is termed *speckle interferometry.*

Labeyrie's technique estimates the spatial energy spectrum of an object as the ensemble average of the individual energy spectra of many short-exposure images. The technique requires simultaneous measurements on an unresolved (point-like) star in order to estimate the atmosphere-telescope point spread function (normally the reference measurements are taken from a nearby star immediately before or after the object, assuming that seeing conditions remains the same). A simple deconvolution procedure is then enough to estimate the object energy spectrum (and hence its Fourier modulus) or the object autocorrelation. The autocorrelation contains most of the desired information for simple objects, but analysis of complicated objects requires image reconstruction, which necessitates Fourier phase recovery. Complementary algorithms were proposed in 1974 (Knox-Thompson) and 1983 (speckle masking or triple correlation) to allow the object phase to be reconstructed from speckle measurements. The combination of these algorithms, aimed to obtain diffraction-limited images from speckle data, is termed *speckle imaging.*

Since then, several others techniques based on short-exposure images have been proposed. A promising technique called *wavefront deconvolution* uses simultaneous measurements of the short-exposure image and the wavefront responsible for it [1]. In a similar post-processing fashion, both measurements are deconvolved and reduced into one final image. Recently, it has been an increase of interest in the development of novel techniques, like phase-diversity speckle imaging - a blend of two concepts: speckle imaging and phase diversity. Phase diversity requires the simultaneous collection of focused and defocused speckle images. The goal is to identify an object that is consistent with both collected images, given the known defocus or phase diversity [2]. Among other new techniques, blind deconvolution (or multiframe blind deconvolution) stands out [3]. Again a deconvolution procedure is needed, but in this case both the object and the point spread function must be recovered from the blurred, noisy data. The techniques mentioned above produce satisfactory results when the incoming photon flux is high. Unfortunately, most interesting astronomical objects are too faint to produce a significant number of detected photons during the short exposure times required by such methods. At low-light level conditions, it

seems that speckle interferometry-related techniques are probably the only viable way to obtain approximated diffraction-limited images.

The need of real-time imaging, together with recent developments in technology, motivated the scientific community to built systems where the phase distortions induced by the atmosphere can be measured and corrected. In spite of the fact of that this idea has been discussed between astronomers for almost two decades, the technological requirements are enormous. The application of the so called *adaptive optics* (AO) technology to laser-beam control has been under investigation within the military community since the 1970s, but is until recently that most observatories and universities are building these systems for astronomical applications. Unfortunately, even with the impressive gain in resolution these pre-detection systems provide, at the current state of technology real-time high-resolution imaging from ground-based telescopes is still far from ideal. The current limitations of AO systems permit speckle imaging techniques to be applied in order to improve adaptively compensated speckle images, as illustrated in figure 1.

It is now commonly accepted that the algorithms used to extract the object Fourier phase from a series of speckle frames, namely the Knox-Thompson algorithm and the triple correlation or bispectrum, are from the same family of high-order statistical tools. Several authors have recognized that the Knox-Thompson algorithm is only a subset or special case from the more complete bispectrum, and that the use of the later results in slightly better results [4]. The main results with the triple correlation or bispectral technique, originally called *speckle masking*, are due to the German group lead by Lohmann and Weigelt [5]. They have reconstructed impressive images of star clusters and other difficult to image astronomical objects. Although the diffraction limit has been attained for such simple objects (resolved stars, binary stars and star cluster), bispectral imaging is still not widely used as an imaging tool. In an attempt to spread its use, the main purpose of this toolbox is to present a clear, easy to follow reference giving a "recipe" on the required methodology.

The Bispectral Imaging Toolbox

I have borrowed the concept of *toolbox* from THE MATHWORKS to name this collection of functions and programs, most of which are written in their MATLAB programming language.[1] I called it the *Bispectral Imaging Toolbox* and consists mainly of m-files (from MATLAB-files) intended to be used as a package of flexible tools or building blocks, designed to easily merge together in order to produce more complicated simulations or to reduce real astronomical data. This routines and functions were developed as part of my Ph.D. programme in High Resolution Imaging in Astronomy. A substantial part of the work is dedicated to the use of the bispectrum -hence the name of bispectral imaging- as a complement to standard speckle interferometry techniques, aimed to obtain high-resolution images from ground-based telescopes.

The main motivation for this toolbox is to present the actual working code in an ordered manner. It is intended to make the application of bispectral imaging less painful for others. Is well known to everybody familiarized with computer programming, that most of the times it is better to start a new program from scratch rather than to modify one already working. In an attempt to avoid this problem, I have tried to comment as much as possible

---

[1]Apart from the main MATLAB software, the programs and function described in this toolbox require the *Image Processing*, the *Optimization* and the *Signal Processing* toolboxes.

| Long-exposure image | AO compensated long-exposure image | Short-exposure (speckle) image | Bispectrally reconstructed image |
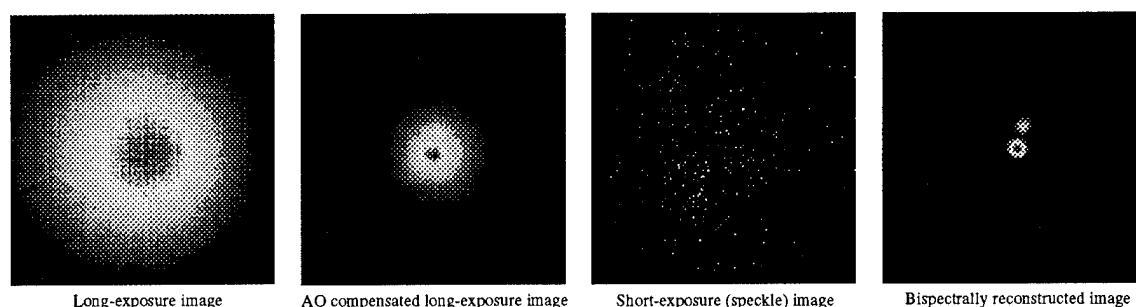
Figure 1: Bispectral imaging applied to the binary star $\beta - Del$. The field of view is 2.25 arcsec. Data courtesy of SOR (Albuquerque, NM. USA, September 1993).

the code. The programs in this toolbox are ordered in the most logical manner that I could think of, and include a brief explanation about the algorithm, its implementation and its limitations. The reliability of the algorithms and code have been assessed by processing carefully simulated data.

The toolbox material includes the simulation of the basic elements in speckle imaging: Kolmogorov phase screen, telescope image formation and low-light level imaging. The bispectral processing of speckle data (in both real and simulated data) is covered introducing the basic concepts of speckle interferometry and the bispectrum, together with the fundamental equations needed to be evaluated. Our approach to reconstruct the object Fourier phase is a least-square minimization, at difference to the recursive scheme traditionally employed in [5]. Also addressed in the toolbox is the problem of measure an atmospherically perturbed wavefront. The most common type of wavefront sensor (the Shack-Hartmann wavefront sensor) is simulated. From the resulting measurements, the incoming wavefront is reconstructed using Zernike polynomials as basis functions. This material is not directly related to the main subject in the toolbox (bispectral imaging) but can eventually be linked to the rest in a different imaging method (including for instance, wavefront deconvolution).

References

[1] J. Primot, G. Rousset, and J. C. Fontanella. "Deconvolution from wavefront sensing: a new technique for compensating turbulence-degraded images". *J. Opt. Soc. Am. A*, 7(9):1598–1608, 1990.

[2] R. G. Paxman and J. H. Seldin. "Simulation validation of phase-diverse speckle imaging". In *OSA Conference on Signal Recovery and Syntesis, Salt Lake City, USA, March 14-15 1995*, pages 85–87, 1995.

[3] G. R. Ayers and J. C. Dainty. "Iterative blind deconvolution method and its applications". *Opt. Lett.*, 13(7):547–549, 1988.

[4] J. W. Beletic. *Speckle imaging of complicated objects.* PhD thesis, Division of Applied Sciences, Harvard University, Massachusetts, 1989.

[5] G. Weigelt. Triple-correlation imaging in optical astronomy. In E. Wolf, editor, *Progress in Optics XXIX*. Elsevier Science Publishers, 1991.

A STUDY OF WAVEFRONT RECONSTRUCTION METHODS

D.L.ASH and C.J.SOLOMON
Physics Laboratory, University of Kent At Canterbury,
Canterbury, Kent, UK

The accurate estimation of atmospherically distorted wavefronts is vital to both adaptive optics systems, and statistical deconvolution methods for image enhancement, as this places an absolute limit on the achievable resolution. Thus a clear understanding of the factors affecting the accuracy of wavefront estimation is essential.

The effect of low light levels on the performance of wavefront sensors is of particular interest. We are currently comparing the standard Zernike modal reconstruction algorithm with a statistically optimal Bayesian (maximum a posteriori - MAP) solution for simulated Shack-Hartmann data produced in the low photon count regime.
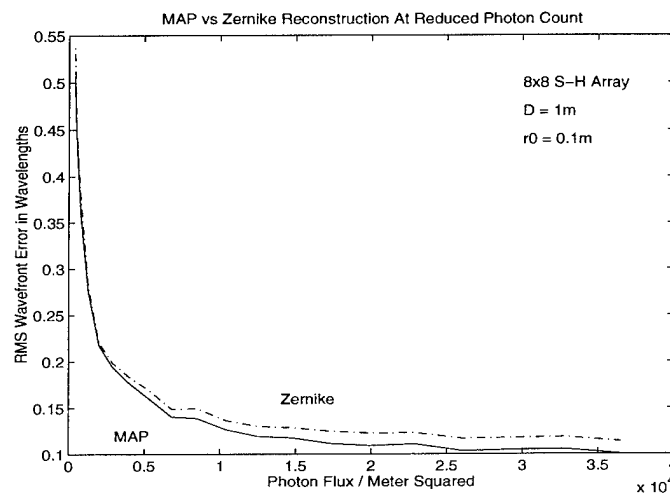
Early results suggest that the MAP solution offers a significant improvement over the use of Zernike circular polynomials in the reconstruction. We also hope to present results of other approaches on both simulated and real data.

The effect on the accuracy of the reconstruction of varying d/r_0 in the low photon flux regime will also be presented.

Simulation of Adaptive Optical Correction with
Deformable Secondary Mirrors

B. C. Bigelow
Optical Science Laboratory
University College London
Gower Street, London WC1E 6BT

tel: 44-171-419-3511
fax: 44-171-380-7153
email: bcb@star.ucl.ac.uk

1 Introduction

Adaptive secondary mirrors offer the promise of maximum throughput and minimum emissivity, when compared to traditional post-secondary adaptive optical systems. Currently, at least five telescope projects (Keck, LBT, MMT Conversion, UKIRT, VLT) are developing secondary mirrors of either the tip/tilt or deformable variety. Tip/tilt secondary mirror systems have already been demonstrated. For example, Close and McCarthy[1] have operated a tip/tilt system on a 2.3-m telescope which provides a factor of 4 improvement in Strehl ratio and nearly diffraction-limited imaging at 1.6μm. The primary objective of this work has been to examine, through detailed simulations, the wavefront correction characteristics of a deformable secondary mirror. This work is part of an on-going development program at the OSL to produce an adaptive secondary mirror system, potentially for the 3.8 m UKIRT.

2 Closed-loop Simulations

The closed-loop simulator used in this work is based on a wavefront sensor (WFS) simulator developed by A. P. Doel[2] at the University of Durham. The original simulator was used to compare Shack-Hartmann and wavefront curvature sensors with varying numbers of sub-apertures, and assumed a idealized Zernike polynomial correction to represent the adaptive mirror.

In this work, finite element modelling was used to determine the size and shape of the influence functions characteristic of a large secondary mirror with a central hole. The influence functions were orthogonalized via a singular value decomposition (SVD), in order to determine the normal modes of the mirror/actuator system. The mirror modes were then applied to the wavefront sensor to construct a mirror/sensor interaction matrix. This matrix, after inversion, was used in a matrix-multiply wavefront reconstructor to compute actuator commands for updating the mirror profile.

The aberrated atmospheric wavefronts were generated by the technique of Lane[3], with a program developed by A. Glindemann. The wavefront data files used in the previous simulations[2] were reused for comparison purposes, and correspond to $D = 8$m with r_0 values (at 500nm) of 41cm ($D/r_0 = 13$ at 0.7 microns), and 22cm ($D/r_0 = 24$ at 0.7 microns).

3 Results

The results of the simulations for the $D/r_0 = 13$ case, in terms of corrected Strehl ratios, are shown in table 1. For most combinations of photon count and pixel noise, the 36 actuator mirror provides about 15% better correction than the 20 actuator mirror, with the single exception of the lowest count and highest noise level, where the 20 actuator mirror is marginally better. For comparison, the results from the original simulations with an ideal Zernike mirror are shown along with the mirror model simulations.

A sampling of the results in terms of point spread functions are shown in figure 1. The uncorrected PSF is shown, along with the 20-Zernike corrected PSF and the corrected PSF's from the two mirror models. The cases shown represent three sets of stellar magnitude and noise conditions; high photon rate with medium readout-noise, medium photon rate with medium readout noise, and low photon count and high readout noise.

The low-order mirror modes appear to be responsible for the fact that the mirror model corrections are outperformed by the 20 Zernike term corrections. Most of the wavefront variance is in the low-order modes, and these modes are not optimally corrected by the low-order, Gaussian-based mirror shapes. A future improvement to the simulator will be to replace the low-order mirror modes with flat tip/tilt modes, which will more realistically simulate rigid-body rotations of the mirror.

M_v (K0 Star)	Photons per Frame	RMS Pixel Noise	Corrected Strehl ratio		
			36 Mirror Modes	20 Mirror Modes	20 Zernike Terms
13.9	10000	0	0.625	0.522	0.776
14.6	5000	0	0.611	0.521	0.771
16.4	1000	0	0.526	0.504	0.742
13.9	10000	3	0.622	0.522	0.775
14.6	5000	3	0.602	0.519	0.766
16.4	1000	3	0.494	0.431	0.667
13.9	10000	5	0.617	0.521	0.773
14.6	5000	5	0.597	0.514	0.756
16.4	1000	5	0.196	0.217	0.394

Table 1: Comparison of results from two mirror models and the original 20 Zernike term correction, applied to 6000 correlated atmospheric wavefronts ($D/r_0 = 13$ at 0.7 microns), at a science wavelength of 2.2 microns. The uncorrected wavefront variance at 2.2 microns was 7.09, and the uncorrected Strehl ratio was 0.095

4 Conclusions

The main objective of this work has been to simulate the characteristics and performance of adaptive optical correction with deformable secondary mirrors. The simulations have shown that an adaptive secondary with even a modest 36 actuators can closely match the performance of an idealized 20-Zernike term correction. The 36 actuator adaptive secondary model achieved as much as a seven-fold increase in Strehl ratio, and a three-fold reduction in encircled energy diameter, under $D/r_0 = 13$ conditions at 2.2 microns.

References

[1] Close, L.M., McCarthy, D.W., "High-Resolution Imaging with a Tip/Tilt Cassegrain Secondary", PASP, **106**, 77-86, January 1994

[2] Doel, A. P., "A comparison of Shack-Hartmann and Curvature Sensing for the 8m Gemini Telescope", Report to the UK Gemini Office, Sept. 1994.

[3] Lane, R.G., Glindemann, A., Dainty, J.C., "Simulation of a Kolmogorov phase screen", Waves in Random Media, **2**, No. 3, 209-224, 1992.
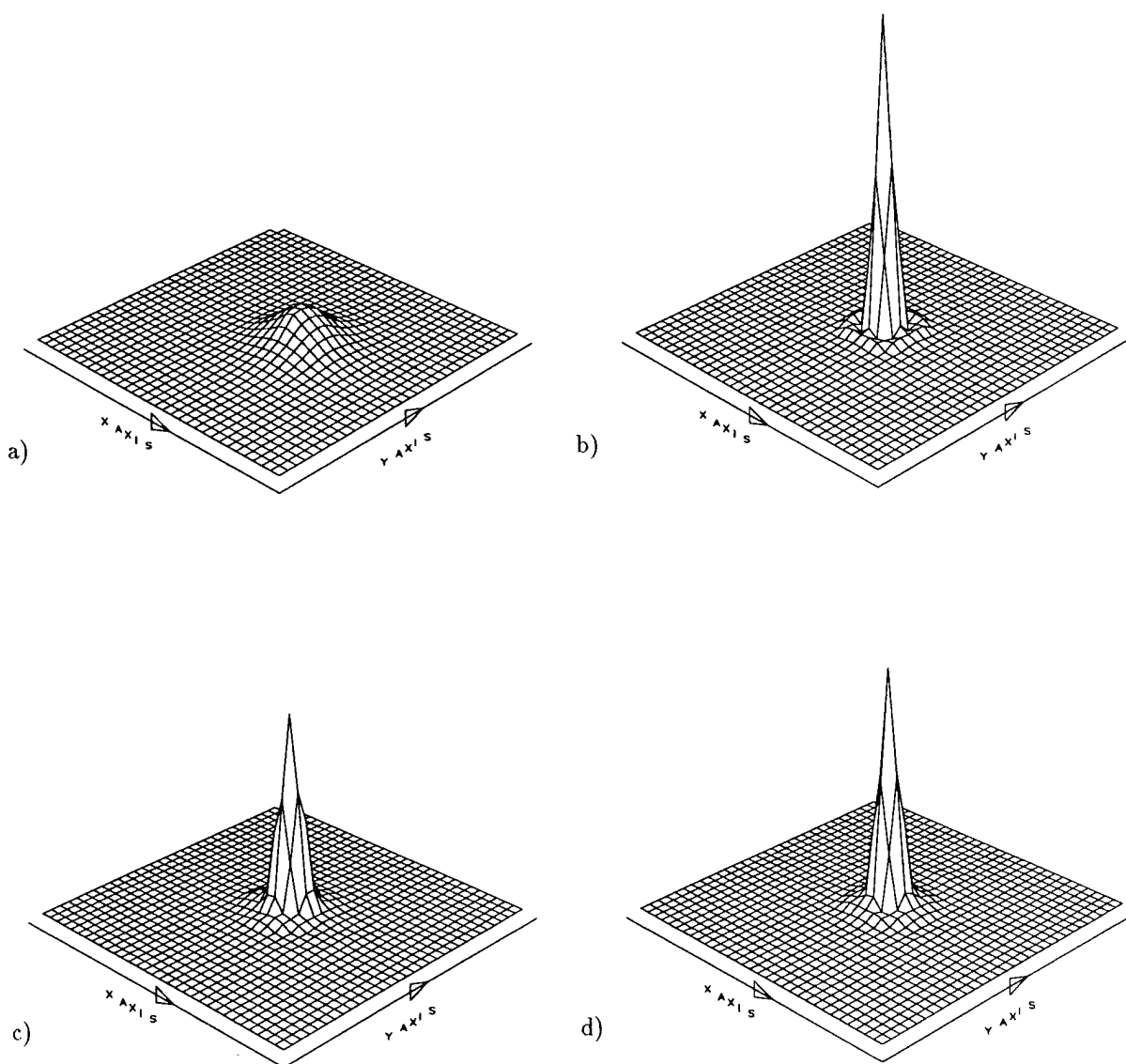
Figure 1: Point spread functions at 2.2 microns determined from 6000 correlated atmospheric wavefronts with a $D/r_0 = 13$ at 0.7 microns. The guide star magnitude was 13.9, with $3e^-$ RMS readout noise.
a) Uncorrected: SR = 0.095, FWHM = 0.174 arc-sec
b) Corrected with 20 Zernike terms: SR = 0.808, FWHM = 0.059 arc-sec
c) Corrected with 20 mirror modes: SR = 0.522, FWHM = 0.069 arc-sec
d) Corrected with 36 mirror terms: SR = 0.622, FWHM = 0.064 arc-sec

A Computationally Efficient Method for Wavefront Reconstruction

Stephen Browne, Jeff Vaughn, Glenn Tyler
the Optical Sciences Company
P.O. Box 25309
Anaheim, California, USA 92825-5309
Phone: 01-714-772-7668
FAX: 01-714-772-9870

John D. Gonglewski
USAF Phillips Laboratory
Albuquerque, New Mexico, USA 87109
Phone: 01-505-846-4405
Fax: 01-505-846-2045

A fast algorithm for measuring Hartmann spot positions is combined with a computationally efficient reconstructor running on a pair of i860XP processors to achieve 1000 reconstructions per second. The full-featured reconstructor removes unobservable modes, as well as tilt which is handed to a steering mirror with high dynamic range. Moreover, the reconstructor can perform much of its processing on the fly while the frame is being transferred from the pupil plane camera, resulting in significantly reduced servo phase lag. Details of the fast reconstructor are described with particular emphasis on the creative use of computational resources.

Imaging by Low order Adaptive Optics

M.L Holohan (M.L O' hUallacháin)

Applied optics, Blackett Laboratory,
Imperial College, London SW7 2BZ U.K.
liam@op.ph.ic.ac.uk

Introduction

As the use of optics in industrial and medical applications becomes more widespread the problems of maintaining desired optical properties during transmission through turbulent media has come to the fore. Much work has been done modelling optical transmission through such media [1, 2]. *Adaptive optics* (AO) is the name given to systems which continually monitor the incoming light and attempt to maintain the beam or image quality. The need for low cost adaptive optics will only grow as new applications develop.

The main thrust of research into AO currently lies in the area of astronomical imaging with systems being designed to work at low light levels and at high bandwidths (1kHz). The astronomical community also use the method of *post-processing* which are mathematical methods which attempt to restore an observed science object to its diffraction limit from the observed data after the fact. *Low order adaptive optics* has its emphasis on only correcting low order aberrations and then using post-processing techniques on this partially corrected data if necessary. As these systems are less expensive there are many possible applications such as underwater photography or retinoscopy.

Low order adaptive optics

Conventional AO systems as described by Hardy [3] consist of 3 parts: a wavefront sensor, a deformable optical element and a control system. A low order AO system simply has the addition of post-processing capabilities. The layout of a typical low order adaptive optical system is given in figure 1. A simple low order system was produced here at
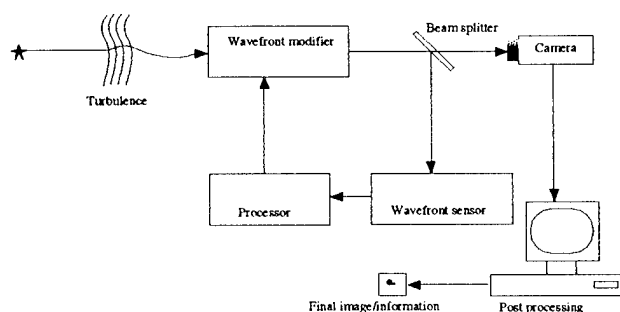
Figure 1: Typical low order AO system

Imperial college in 1994. The current system being developed has its emphasis stressed on simplicity and low cost. It is controlled by a standard personal computer with a Pentium processor. The program to control the system was written such that it could be used in the MicroSoft Windows environment. The active elements are 2 piezoelectric mirrors[4] which were produced at the International Laser Centre (ICL), Moscow State University, Moscow, Russia. The first mirror compensates for tip/tilt only while the second which is a 17 electrode mirror corrects the other aberrations is shown in figure 2. The set of
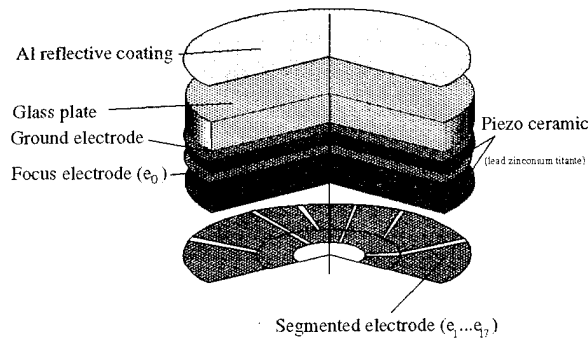
Figure 2: 17 electrode bimorph deformable mirror

bimorph mirrors had to be characterised and modelled for use in the AO system. The preliminary system set out to correct laboratory generated turbulence in the form of a heated water tank. The system did not need any form of wavefront reconstruction as a simple *hill climbing* algorithm was used with a maximum energy through a pinhole being the correction criterion. Several variations of this correction method were developed in particular one called the *Gradient method* was used and a comparative analysis of all these methods was undertaken.

Results

Results from this low order adaptive optical system as well as the characterisation of the mirrors and other control parameters will be presented at the conference.

References

[1] V.I. Tatarski. *Wave Propagation in a Turbulent Medium*. McGraw-Hill, 1961.

[2] D.L. Fried. Statistics of a geometric representation of wavefront distortion. *Journal of the Optical Society of America*, 55(11):1427–1435, November 1965.

[3] J.W. Hardy. Active optics: A new technology for the control of light. *Proceedings of the IEEE*, 66(6):651–697, June 1978.

[4] S.A. Korowski. Analysis of adaptive optical elements made from piezoelectric bimorphs. *J. Opt. Soc. Am.*, 69(1):181–187, January 1979.

Fractional moments for investigating laser atmospheric scintillation statistics

A. Consortini, F. Rigal
Università di Firenze, Dipartimento di Fisica
Via S. Marta, 50139 Florence, Italy,
tel +39-55-4796415 fax +39-55-483750,
e-mail consortini@dffs.unifi.it or consortini@fi.infn.it
and F.Cochetti
Alcatel Siette, via Provinciale Lucchese 33,
Osmannoro, Sesto Fiorentino, Italy

The problem is the determination of the probability density function of intensity fluctuations from experimental data of laser propagation through atmospheric turbulence. The proposed solution is very general and appears to be applicable to any statistical problem.

In principle any distribution can be obtained by measuring its moments and, in practice, only a few order moments (say three or four) suffice to compare experimental data with proposed theoretical distributions. In atmospheric propagation, however, it is practically impossible to obtain even a few high order experimental moments accurate enough to allow a comparison with the expected theoretical moments. The inaccuracy is due to the limited amount of data that can be collected in stationary turbulence, and therefore to the lack of data on the high side of the distribution, which have a great influence on the higher order moments. In the case of strong fluctuations for instance, the third order moment can be strongly affected by values that are as far as 30 times the mean value, and the situation gets worse for increasing values of the moments.

Our proposal of considering fractional (or even real) order moments is due to the fact that one can have the necessary number (say three or four) of moments, that is enough information, from the experimental data, by keeping the order of the moments small enough not to be affected by the lack of data on the high side of the distribution.

A description of the method and a test of its use by means of data, which have been numerically extracted from three distributions commonly used in atmospheric propagation, are presented. The results of an application to data from laser scintillation measurements through a 1200 m path are also described.

Interferogram Evaluation by 4D Analytic Signal Theory

Valeri A. Tartakowski

Institute of Atmospheric Optics, Siberian Branch of the Russian Academy of Sciences
Tomsk, 634055, Russia
E-mail: zuev@iao.tomsk.su   Fax: 3822-25-90-86

Application of the well-known principle of heterodyning was first described in Ref. 1 as the Fourier transform method for phase restoration from interferogram and in Ref. 2 as the analytic signal method for designing an interference wave-front sensor. Here we discuss a development of the latter, and go into unknown essential details of it.

The Gabor analytic signal (AS) is constructed using the Hilbert transform (H). This linear operator gives univalent determination of an envelope and phase of one-dimensional signal whose support extends from minus infinity to infinity, but the wave field has four arguments, and the interferogram is a two-dimensional function. Therefore the problem arises of introducing the AS signal in a multidimensional case. It is necessary to provide the uniqueness of the analytic signal and the AS invariance with respect to the Hilbert transform argument.

It is established that the unique four-dimensional phase function can be introduced if the wave field is quasimonochromatic and parabolic. In this case the Hilbert transform argument is the time or the wave propagation direction as well as such directions where the temporal or spatial carriers exist. Moreover, if the phase is a monotonic function on any scanning line, it can be determined by the AS as a function of parameter of this scanning line. The basic expressions are the following:

$$W(x,y,z,t) \overset{def}{=} U(x,y,z,t) + iV(x,y,z,t),$$

$$V(x,y,z,t) = \underset{t}{H}\, U(x,y,z,t) = \underset{z}{H}\, U(x,y,z,t),$$

$$V\{p(x,y,z),t\} = \underset{x}{H}\, U\{p(x,y,z),t\} = \underset{y}{H}\, U\{p(x,y,z),t\},$$

$$V\{x(\tau),y(\tau),z(\tau)\} = \left[\underset{l}{H}\, U\{\Phi^{-1}(l)\}\right]_{l=\Phi(\tau)}, \text{if } U^2(\tau) + V^2(\tau) = const$$

Here: $W(x,y,z,t)$ is the 4D analytic signal, U is the AS real part, V is the AS imaginary part, Φ is the monotonous phase of the AS, $p(x,y,z)$ is a plane with the carrier frequency, z is the direction of the wave propagation, τ is the parameter of the scanning line and a function corresponding to t.

It gives a guarantee that phase of the four-dimensional wave function, determined by the analytic signal on the scanning line, will be the corresponding cross section of the unique four-dimensional phase function determined by the analytic signal as a function of the time or the propagation direction. As a result, it is possible now to measure the two or one-dimensional sections of the four-dimensional phase separately and apart from each other.

Let us denote a filtration operator by the symbol $\mathbb{F}_{bc}$, $c>b>0$. The filter corresponding to this operator passes all the spectrum components at the frequency range $[b, c]$ without distortions and suppresses completely the components being out of this frequency range, therefore this filter makes the AS on the its output. We assume that the spectrum of the analytical signal $W(\tau)$ does not overlap other components of the interferogram $G(\tau) = |$ reference wave $+ W(\tau)|^2$. That is sufficient in order to write the relation for it direct demodulation $\Phi(\tau) = \arg \mathbb{F}_{bc} G(\tau)$. This relation is based on the principle of heterodyning, which is extended here to the case of curvilinear scanning in the 3D space.

Also it is really to obtain a few phase estimates, and to estimate the phase restoration error without any statistical procedure, using some orthogonal scanning directions, when only one interferogram is available. It turns out, the error estimates and the real errors of phase restoration have been fitted well by the first order regression line. The correlation coefficient was equal to 0.99 for the normalized rms error (Fig. 1*a*) and 0.94 for the peak-to-valley error (Fig.1*b*). The standard deviations were equal 0.01 and 0.04, respectively.
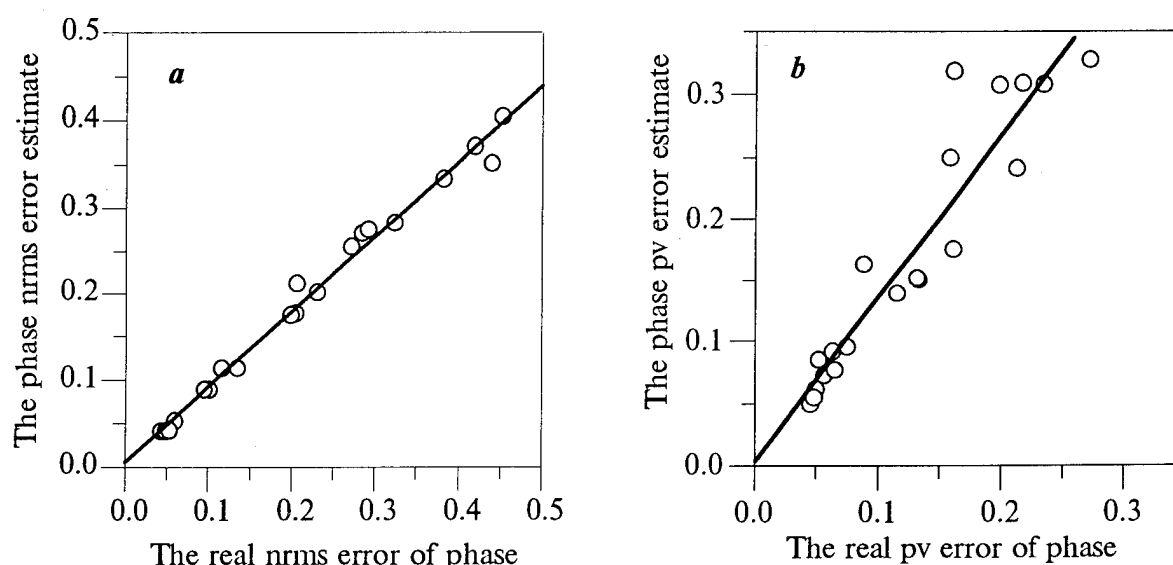
Fig. 1 *a*, *b*. The relation between the real restored-phase error and its estimate.

These graphs were given as a result of the closed numerical experiments with the following interferogram data: The interferogram matrix order was equal to 60, the interference fringe number is 12, the standard deviation of the original phase is 0.5, the normalized rms deviation of multiplicative noise was taken from {0.0, 0.1, 0.15, 0.2}, the interferogram quantization level numbers were taken from {2, 4, 5, 6, 10, 256}, the maximum of power spectrum of the original phase for the Zernike set was located in "defocusing", the original phase was apodisated.

An interferogram can be measured only in the restricted domain. There is the inconsistency between the domain of the Hilbert transform definition, which have only

one boundary at infinity and the bounded domain often being multiply connected where the interferogram is specified. This inconsistency manifests itself as a boundary large ripples in the wave function and especially in its phase when the interferogram is inverted. Consequently, the interferogram must be continued beyond its domain of definition for diminution of these ripples.

The new way of continuation of individual sections of the interferogram is proposed, according to which the continuation is constructed from the fragments of the sections themselves. In doing so some smoothness functionals are minimized at the set of readings of the cross section. The criterion of the continuation optimality is the following: In order to the Hilbert transform of the continued function will correspond most closely to the true one, it is necessary for the continuation operation to ensure the minimal width of the spectral band of the continued function when the original fragments are specified.

Our procedure results in a higher restoration accuracy and provision of its *a posteriori* estimation. Depending on the interferograms formation conditions, the rms error can be decreased down to 1/300 of wavelength.
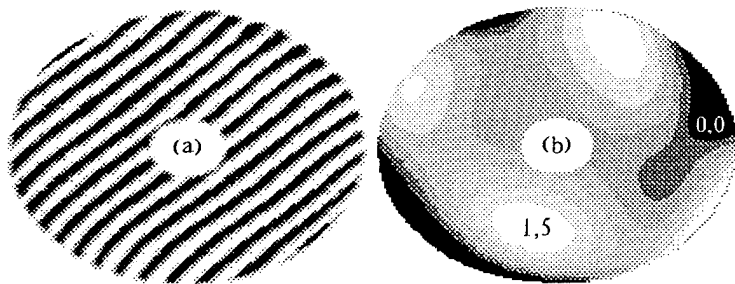
Fig. 2. The inversion of the double-connected interferogram by R10 code: (a) is the original interferogram, (b) is the restored phase in rad.

The facts are as follows, the wave-front dislocations are very probable, e.g., just for a vertical path through the turbulent atmosphere[3]. Dislocations are to disturb the results of wave-front sensors if they are based on *a priori* continuity of the phase function. These disturbances will be even due to only one dislocation.

Dislocations are some onset of the wave disintegration to separate beams that will be uncorrelated then, and there exists not so much energy in the vicinity of the dislocation appearance points. Therefore an adaptive mirror should not be bent as a singular form in these areas, but measurements of separate areas of wave front and separately fitting of these areas to adaptive mirrors are the right method of designing a wave-front sensor.

On this way the 4D analytical signal allows us to go round singular points and to connect parts of the wave front to the unique phase function.

References

1. M. Takeda, H. Ina, S. Kobayashi, J. Opt. Soc. Am. V. 72, № 1, 156–160 (1982).
2. Authors Certificate 1024746 USSR / E.A. Vitrichenko, L.A. Pushnoi, V.A. Tartakowski. Priority of 18.02.82. Published of 23.06.83. Bulletin № 23.
3. N.N. Myer, V.A. Tartakowski, Atmospheric and Oceanic Optics, V. 8, № 3, 448-454, (1995).

Relation between Conjugation Error and Inverted Field Intensity Deviation

V. A. Tartakowski, N. N. Myer

Institute of Atmospheric Optics, Siberian Branch of the Russian Academy of Sciences
Tomsk, 634055, Russia
E-mail: zuev@iao.tomsk.su   Fax: 3822-25-90-86

Adaptive optical systems use reciprocity[1] working through the turbulent atmosphere. An influence of input errors on output errors must be cleared up originally for some systems. It is interesting to elucidate relations between the conjugation error ε_c, which arises as a result of some modification of the conjugated field in the receiving plane, and the inverted field intensity deviation ε_o from the original field intensity in the source plane.
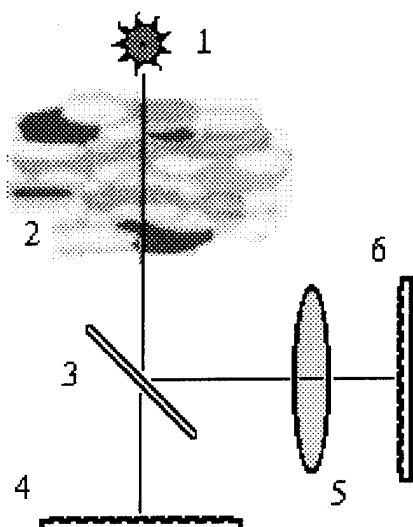
Fig. 1. The arrangement of the optical components in the experiments:
1. Light source plane, output.
2 Turbulent medium.
3. Beam splitter.
4. Field receiving and conjugation plane, input.
5. Fourier transformer.
6. Spectrum receiving and conjugation plane, input.

The Gaussian beam propagation through the turbulent medium was investigated by phase screen setting for modeling the turbulence[2] with some Fried's scale r_0. The conjugation error and the intensity deviation were calculated as normalized quadratic error for each realization of the numerical experiment.

The first modification consists in zeroing the field where its intensity was lower than the appointed threshold, which was equal to a certain part of the maximal value of this intensity. Both the field and its spatial frequency (SF) spectrum can be modified equally and be inverted either singly or together. The meaning of this modification is to cut out the singular parts, which correspond to the low intensity of the field or its spectrum, from the wave front.

It is established, both random processes ε_c and ε_o correlate with each other strongly and are fitted exactly by the first order regression line for the field inversion and by the second order regression line for inversion of its spectrum, see Fig. 2,(*a, b*).

Any amplification of error is lacking (*a*) and is small (*b*) within the framework of these experiments.
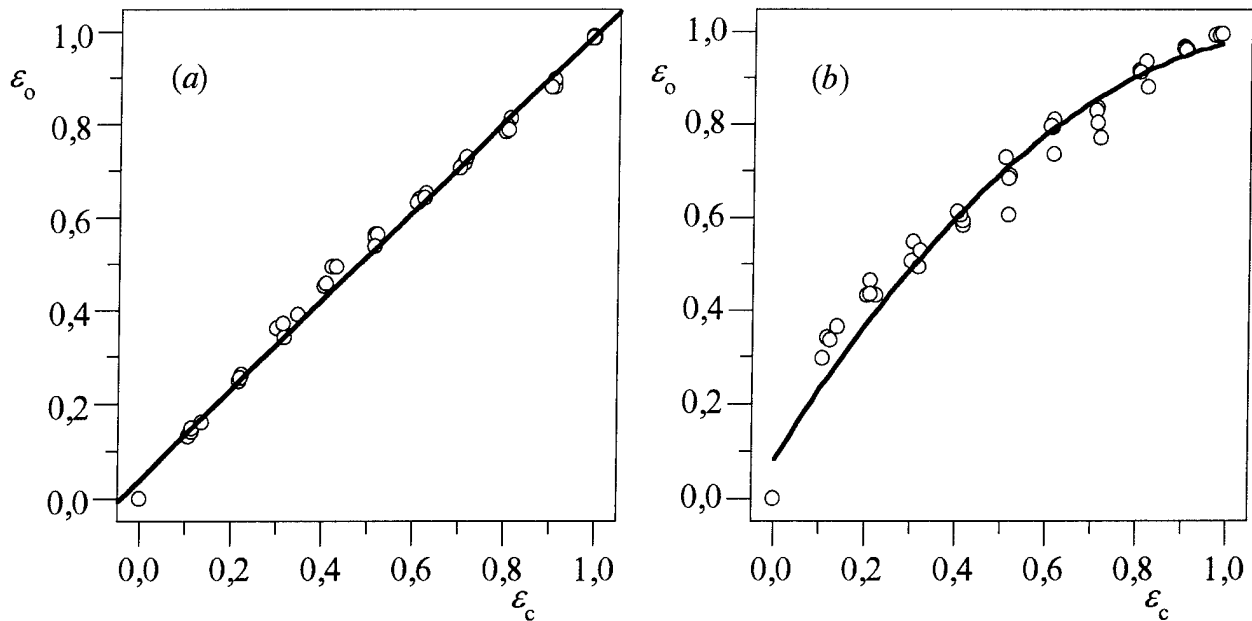
Fig. 2. $r_0 = 0.05$ cm.

(*a*) The field is inverted:

the correlation coefficient between ε_c and ε_o equals to 0.997,

the standard deviation of the points from the regression line is 0.02.

(*b*) The SF spectrum is inverted:

the correlation coefficient between ε_c and ε_c equals to 0.992,

the standard deviation of the points from the regression line is 0.05.

There is an interesting case of the combined inversion. The threshold for the field is equal to 0.1 and 0.05 for its spectrum. From Table 1 it follows that ε_o in this case is less than in the case of singly field inversion, but the threshold is the same.

Table 1

r_0 [cm]	0.03	0.1	0.3	1	3
ε_c (field)	0.40	0.16	0.12	0.10	0.10
ε_c (field + spectrum)	0.12	0.08	0.04	0.03	0.02
ε_o (field)	0.50	0.18	0.14	0.12	0.12
ε_o (field + spectrum)	0.28	0.11	0.06	0.05	0.06

The second and third modifications consist in the narrowing the SF band of the field by its inversion in the receiving plane, see Fig. 3, (a, b). In case (a) only that part of the field was inverted which had its SF in a circle with the center in the point of global maximum of the SF spectrum modulus. In case (b) only that part of the field was inverted which maximized the energy of the SF spectrum in a circle of some radius. The circle radius was changed from zero to the Nyquist frequency. It can be seen in these cases that logarithms of the random processes ε_c and ε_0 are fitted well by the first order regression line and there exist the closeness of the results (a) and (b). These experiments indicate the essential amplification of the errors with the wave field inversion.
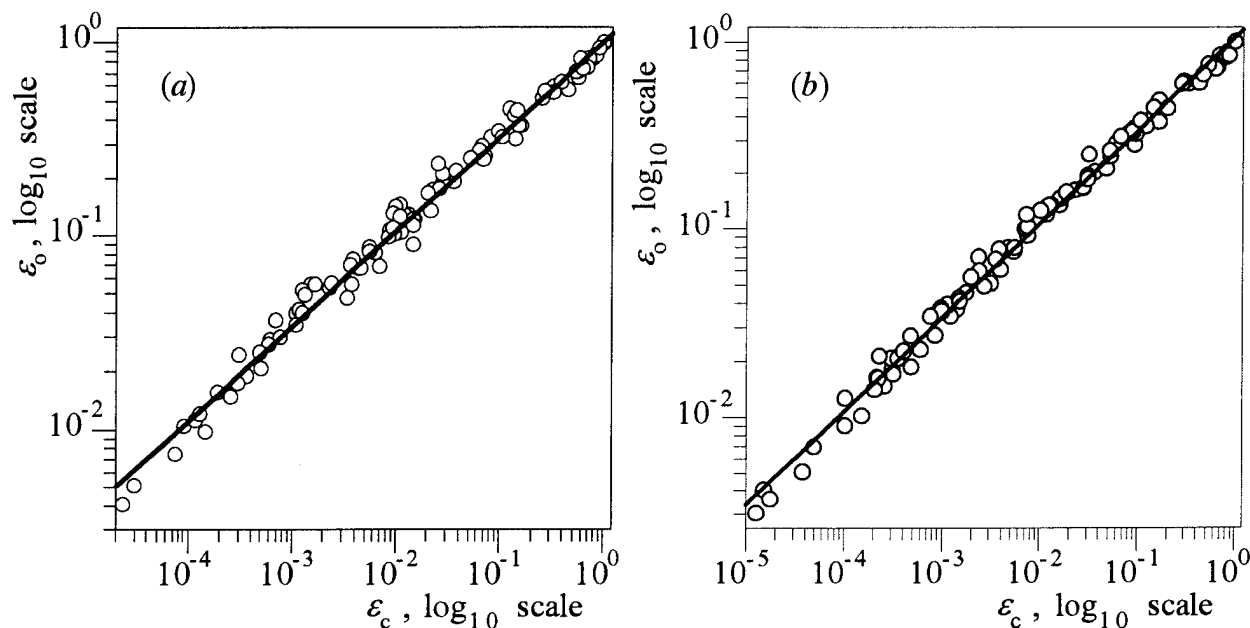
Fig. 3. $r_0 = 0.05$ cm, the field is inverted with narrowing its SF band:

(a) the correlation coefficient between $\log \varepsilon_c$ and $\log \varepsilon_0$ equals to 0.995, the standard deviation of the points from the regression line is 0.06, tangent of the line slope angle is 0.490 (0.005).

(b) the correlation coefficient between $\log \varepsilon_c$ and $\log \varepsilon_0$ equals to 0.997, the standard deviation of the points from the regression line is 0.05, tangent of the line slope angle is 0.500 (0.004).

There are the subsequent kinds of the field modifications. The results will be demonstrated.

References

1. J. H. Shapiro, J. Opt. Soc. Am. V. 61, № 4, 492-495 (1971)

2. P. A. Koniaev, V. P. Lukin, Izvestia Vuzov. Fizika. № 2, 79-89 (1983)

The algorithms for measurement of displacement of white-light fringes

Lev N. Butenko, Alexander G. Seregin
S.I. Vavilov State Optical Institute
12, Birzhevaya line, St.Petersburg, 199034, Russia
Phone: (812)218-1571, Fax: (812)218-1571 or 218-3720,
E-mail: parfenov@soi.spb.su

Peter A. Fridman
Institute for Analytical Instruments of Russian Academy
of Sciences; 26,Rizhisky Av. St.Petersburg,198103,Russia
Phone: 2516788, E-mail: fridman@iap.spb.su

A white-light source is used so that good interference occurs only when the two paths are equal, that is, when both primary mirror's segmtnts are the same distance away from the interferometer, e.g. with a double-image prism in the adaptive telescope [1,2]. When observing a small step between surfaces with comparable reference dementions, interference fringes are usually formed in white light that are perpen dicular to the boundaryline between the sufaces. An interferometer with white-light source[1,2] is based on a prism design that includes a rectangular prism with a beamspliter hypotenuse face to which an additional prism is cemented to form a double-image compound pentaprism. It makes possible to monitor the step between the elements of a compound primary mirror more simply than in an intrferometer with Kosters prism.This is because of the almost complete compensation of the optical path length in a system with couterpropogation of the interfering beams. Preliminary phasing of primary mirror segments during assembling process may be accomplished with help of a such ambiguity sensor. The experimental investigations with visual control showed a possibility to recognize displacement of 1/20 wavelength. This investigation was fulfilled at the special test bench with high resolution laser interferometer. The interferometer resolution is 1 nm.

The one part of quasi-sphere wavefront from far curvature center is formed and falls by the nomal to the small surface plot of primary mirror on the intersection of two segments. Other part falls near intersection of two segments only on one of them. The compound pentaprism performs performs the function of beamsplitting and recombination. The ambiguity of 2π n between the segments is solved by searching for singular maximum of white-light interferometer by using a tungsten arc source and CCD camera. If CCD detectors have different spectral responses the output signals are differed by 10-40 %[3,4].This fact may be used for detecting of an achromatic fringe by simple amplitude methods. But precision detection of a fringe center position may be realized with special data processing.

A CCD camera output processing in the PC equipped by a framegrabber was used to recognize the zero order interference fringe from any other order. Such a system allowed to watch achromatic fringe displacement.

The PC programme was developed to measure the moving half part of interference field displacement relatively to the fixed one.

The programme involves three methods for determines of the achromatic fringe position:
- determination of the achromatic fringe "centre of gravity";
- Fourier analysis of signals by two chosen lines and calculation of phase shifts between;
-calculation of functions convolution of signals from lines for both parts of interference field.

Reproducibility of the measurement data obtained by three mentioned methods has been experimentally shown to be less than 24 nm. The "centre of gravity" method is preferable for the achromatic fringe coarse recognizing while the Fourier transform one is advisable for the precesion detection of the achromatic fringe position.

References

1. G.N.Zvereva, A.G.Seregin, A.A.Starkov,*Soviet J.Opt.Techn.*,1992,5,p.73.

2. D.N.Eskov, V.Ph.Zakharenkov, V.I.Podoba, A.G.Seregin, *SPIE*,v.2096,p.27.

3. Yu.V.Kolomijtsov, *Optika i Spektroskopia*,v.8,No.3,1960,p363.(Russ.).

4. V.P.Koronkevich, *Optika i Spektroskopia* ,v.11,No.1,1961,p 112.(Russ.)

Rapid Phase Retrieval Using The Fast Fourier Transform

T.E. Gureyev, K.A. Nugent, D.Paganin and A.Roberts
School of Physics, The University of Melbourne, Parkville, Victoria 3052, Australia

Phone: +613 9344 5446
Fax:: +613 9347 4783
email: nugent@optics.ph.unimelb.edu.au

Phase retrieval from intensity data based purely on the Fourier transform is demonstrated experimentally and theoretically. Our method does not require boundary conditions.

In this work we consider phase retrieval based on the Transport of Intensity Equation. This approach was originally proposed by Teague[1] and later developed by Roddier[2] under the name of wavefront curvature sensing.

In a recent paper[3] we proposed a method for phase recovery with the transport of intensity equation in which all functions are expanded into series of Zernike polynomials. Such an approach reduces the transport of intensity equation to a relatively simple and well-conditioned system of algebraic equations for the Zernike coefficients of the phase and allows effective methods for its analytical and numerical solution.

In the present paper, we give a modification of our previous method. Our new approach is based on the Galerkin method of orthogonal expansions. We establish a relationship between the Fourier coefficients of the data and the Fourier coefficients of the corresponding phase distribution. Our method is suitable for arbitrary intensity distributions, but in the case of uniform intensity the relationship between phase and intensity is independent of the data. Furthermore, our method does not require independent measurements of the boundary conditions. Thus, the method described here offers the following important advantages:

- It allows the recovery of the phase in an area of a plane orthogonal to the optical axis, where the intensity distribution is not necessarily uniform.

- It does not require boundary phase data or the measurements of the wavefront boundary slopes for phase retrieval.

- The reconstruction requires only two Fourier transforms and a matrix multiplication.

We have explored the reconstruction of phase using this technique both theoretically, computationally and experimentally. We have confirmed our theoretical conclusions that the reconstruction is robust with respect to noise and that accurate phase reconstructions are obtained.

The resolution of the phase reconstructions are easily controlled via the highest order of Fourier co-efficient that is retained. This yields improved handling of noise tolerance as the resolution may be controlled dynamically; higher Fourier coefficients are less noise tolerant.

We have also developed the technique based on Zernike polynomials and investigated its performance. In the figure below we show some phase reconstructions using the Zernike polynomial formulation of our technique. In the absence of a fast Zernike transform, the reconstructions are

somewhat slower to perform, but are otherwise similar. It can be seen that the reconstruction is, to the eye, identical to the initial phase distribution. In fact, the difference between the reconstruction and the initial phase correspond to an error of less than 1/100th of a wave.
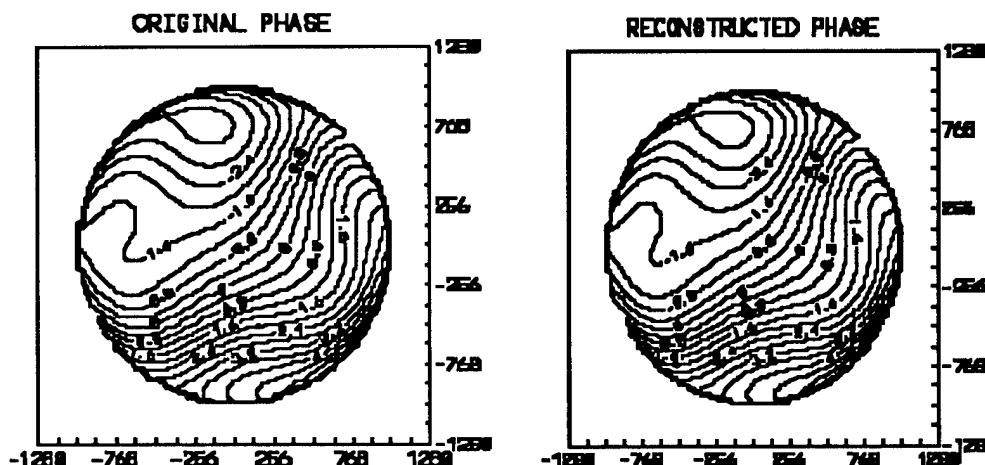
Original test phase distribution and its reconstruction using the Zernike-based approach. The reconstruction is differs from the original by less than 1/100'th of a wavelength.

The Zernike based approach may be better suited to adaptive optics given the special role that Zernike polynomials play in this field, but the speed and flexibility available using the Fourier transform technique may also offer benefits. In this paper, we will discuss both methods.

References

1. M.R.Teague, *Irradiance moments: their propagation and use for unique retrieval of phase.* J.Opt.Soc.Am. **73**, 1434-1441 (1983).

2. F.Roddier, *Curvature sensing and compensation: a new technique in adaptive optics,* Appl.Optics, **27**, 1223-1225 (1988).

3. T.E.Gureyev, A.Roberts and K.A.Nugent,*Phase retrieval with the transport of intensity equation: matrix solution using Zernike polynomials* J.Opt.Soc.Am. A , in press (1995).

One-channel deformable mirrors for low-order adaptive optical compensation

Andrei G. Safronov

TURN Ltd, P.O.Box 19, Moscow, Centre, 103104 Russia

The adaptive optics for low order correction, the so-called "small" adaptive optics, is of particular actuality and interest because of its simplicity and low cost. The present paper is dedicated to one-channel deformable mirrors designed for use in above mentioned systems including industrial ones.

The construction of the mirrors is a realization of a well-known bimorph structure [1,2]. The body is made of molybdenum, piezoceramics used is of ЦТС-19 (PZT-type). Total number of deformable mirrors of a given construction produced and tested is 5, three of the mirrors have flat initial shape, outer diameter of the body is 60 mm and inner diameter of 50 mm (mirrors No 2, 3, 4); one mirrors analogous to the previous one but having spherical concave initial optical surface, R = - 40 m (mirror No 1), and the last mirror is flat, 70 mm in outer diameter , 54 mm in inner diameter (mirror No 5).

All the mirrors of the family under consideration have copper reflecting coating and protective coating made of sapphire (Al_2O_3). Regular reflectances of all the mirrors are no less than 98.5%. Control voltage ranges from -200V to +300V. Capacitance of the control electrode is about 150 nF. Weight of a mirror about 250 g.
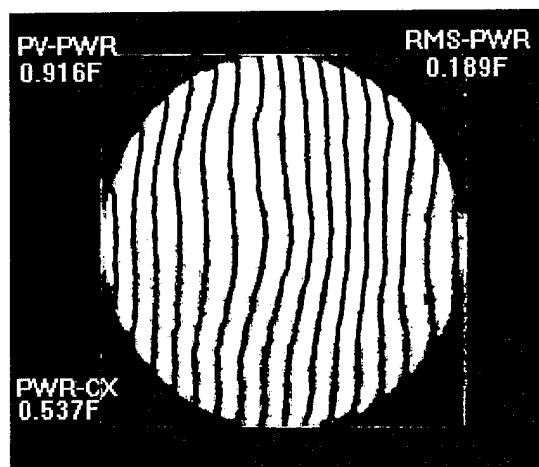
Fig.1. Interferogram of the initial shape of surface for deformable mirror N3 over the ful light diameter (42 mm). F=λ/2
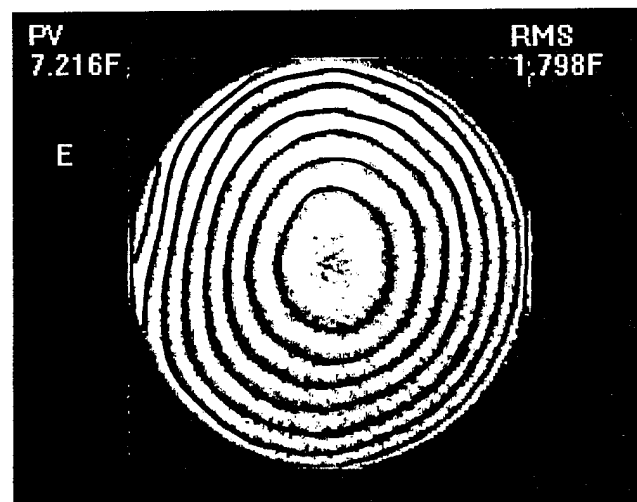
Fig.2. Interferogram of reflecting surface for deformable mirror N4 under control voltage v=20V over the ful light diameter (42 mm). F=λ/2

Measurements of the initial shapes and response functions of the mirrors were made on the automated complex based on the "MARK-3"interferometer. A typical interferogram of the initial shape of one of the mirrors is shown in fig. 1. The fig. 2 shows the interferogram of the reflecting surface for the mirror under the control voltage. The response function

PV
2.308F

RMS
0.623F

608 PTS.
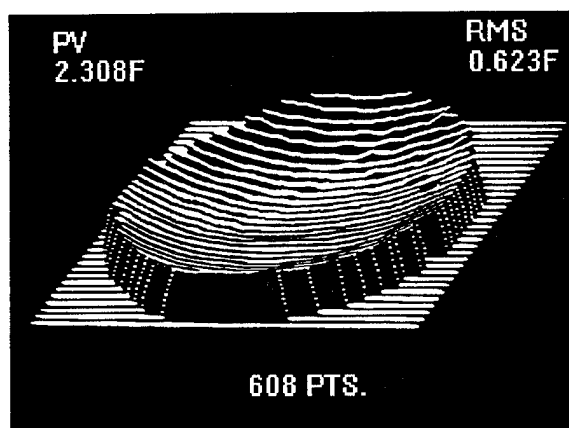
Fig.3. Responce function of the deformable mirror N4 at v=-10V. F=λ/2.

reconstructed upon the experimentally measured data for one of the deformable mirrors is shown in fig. 3. As a result of experimental measurements and further statistical data processing the sensitivity (corresponds to PV) of the adaptive mirrors were obtained: deformable mirror No 1 - 66.5 μm/kV, No 2 - 47.5 μm/kV, No 3 - 53.8 μm/kV, No 4 - 74.7 μm/kV, No 5 - 79.4 μm/kV.

Therefore the empirical formula for the response function $w(r)$ of the mirrors under control voltage v can be represented as following (without considering the effect of hysteresis):

$$w(r) = -K(r/r_1)^2 v$$

where r_1 - radius of the reflecting surface (here r_1=21 mm); K - sensitivity.

It is known that piezoelectric deformable mirrors are characterized by the presence of electromechanical hysteresis. Numerical values of hysteresis for the mirrors under investigation are: 10.3% (No1), 13.4% (No2), no more 13% (No3), 12.8% (No4), no more 14% (No5).

Because of employment of various materials in the mirror construction, its reflecting surface will be deformed at the temperature changes and therefore under the action of a laser beam. The computer simulation results of the thermal deformations are given in table, the numerical data are given for the mirror No 5 with 70 mm outer diameter. Shape of thermal deformations under the all considered conditions coincides with the obtained earlier for cooled deformable mirrors [2] and practically matches the defocusing $Z_4 = \sqrt{3}(2r^2-1)$.

Thermal deformations of adaptive mirrors

Conditions of thermal loading	Thermal deformations, μm		Increase of the mean temperature, K, of	
	PV	RMS	reflecting plate	piezoceramics
1. Change of enviromental temperature by 1°C	0.20	0.06	1	1
2. Action of laser beam of 40 mm in a diameter and integral power 1kW, Gaussian distribution. Air cooling. Air rate is 10 m/sec.	6.1	1.7	27.6	27.3
3. Action of laser beam of 40 mm in a diameter and integral power 1kW, Gaussian distribution. Water cooling. Water rate is 5 m/sec:				
a) heat removal throuth the cylindrical surface	2.2	0.6	9.7	9.3
b) heat removal throuth the rear end	2.3	0.7	10.0	9.6

So the results obtained show that at the presence of a water outer cooling thermal deformations of the described mirrors under the action of a laser beam with power 1 kW are
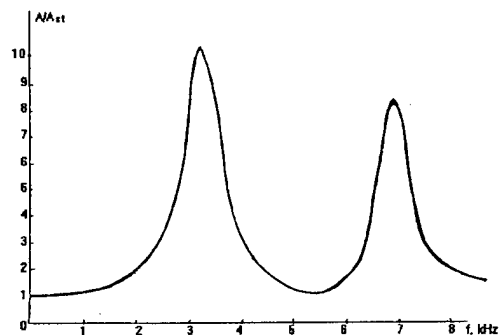
Fig.4. Amplitude of reflecting surface displacements of deformable mirror N5 (A/A$_{st}$) as a function of control voltage frequency (f). A/A$_{st}$ is static amplitude of mirror deformations (at f=0).
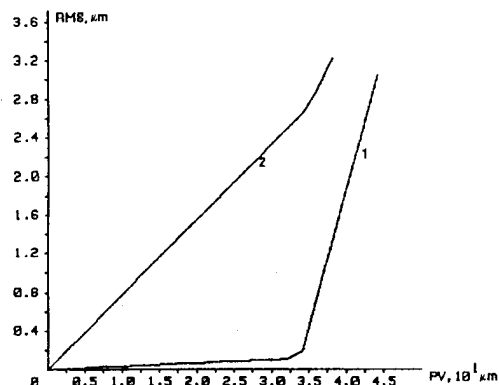
Fig.5. Minimal root-mean square compensation error (RMS) of axial symmetric Zeidel aberrations as a function of span of the aberrations for deformable mirror N5: 1 - defocusing, 2 - spherical aberration.

small compared to the intrinsic controllable displacements of the reflecting surface. Considering the above sensitivity values of the mirrors, it is easy to verify that from 6% to 10% of the range of control voltage is necessary to compensate their intrinsic thermal deformations.

Frequency-response characterestics of the mirrors were determined by means of a computer simulation. The reflecting surface displacements as a function of control voltage frequency for mirror No5 are shown in fig.4. As one can see, first resonance frequency of this mirror equals to 3.2.kHz. The shape of the amplitude-frequency response for deformable mirrors No 1-4 is similar to the shown in fig. 4, main resonance frequency for these mirrors is 3.8 kHz.

Efficiency of the described mirrors has been estimated by their ability to compensate the axial symmetric wavefront distortions. Calculational results for deformable mirror No 5 are represented in fig.5. The case of normal radiation incidence on the mirror surface was assumed. It is seen from the represented results that the described mirrors are very effective for compensation of the defocusing of wavefront. For mirror No 5 the satisfactory compensation is observed up to about 32 microns, fig.5. Because the calculated response functions of the mirrors were used at the computer simulation, the actual efficiency of the mirrors are higher, by 25% for mirror No 1 and by about 40% for mirrors No 4 and 5.

Results of the investigations have shown that the presented one-channel adaptive mirrors enable to compensate effectively large-scale axial symmetric wavefront distortions in laser optics with power level of up to 1 kW. Operational range of the mirrors is about 20 microns in amplitude of the optical surface displacements and up to 1 kHz in frequency.

References:

1. E. Steinhaus, S. G. Lipson. J. Opt. Soc. Am., 69, 478-481 (1979).

2. A.V.Ikramov, I.M.Roshchupkin, A.G.Safronov. Quantum electronics, 24, 613-617 (1994).

Test and analysis of low-light characterisation of the ICCD Hartmann-Shack wavefront sensor

Qiang Zhang, Bing Xu+, Li Chen

Institute of Optics & Electronics, Academia Sinica
PO Box 350, Shuangliu, Chengdu 610209, P.R.China

Hartmann-Shack wavefront sensors (Hartmann WFS) are widely used for optical wavefront measurement in adaptive optics.They are especially useful in the conjunction with laser guide stars that provide a quasi-point-source reference with continuous and pulse operating patterns. The principle of the sensor is that an array of lenslets is used to divide the coming wavefront into subaperatures and form images at their focal planes where the detector is placed. If the wavefront is plane, each lenslet forms an image of the source at its focus. If the wavefront is disturbed, each lenslet receives a tilted wavefront and forms an image out of axis in its focal plane. The measure of the image position gives the angle of arrival of the wave for each lenslet. The Hartmann WFS generally consists of a lenslet array, a detector which is a CCD or an intensified CCD, and an image processing system. For both natural and guide stars,a very low-light photo-counting level characterisation of the sensor is needed. And the knowledge on the low-light performance of the sensor for the both operating patterns is useful for the AO system design.

We designed and built an intensified CCD Hartmann WFS for an open-loop laser beacon experiment and test its low-light performance under the both operating patterns simulated in the laboratory. Fig.1 is a schematic of the configuration used in the test. LD is a wavelength 670 nm diode laser. M1 is a mirror which can move along a slide and reflect the light into the sensor. The photo-counting detector is Model C2761 PMT made by Hamamatsu Co. and used to measure the light into the sensor. The lenslet array of the Hartmann WFS is a 12x12 lenslet array. The ICCD system consists of a C2166-01 gated intensifier made by Hamamatsu Co., a coupling lens and 50 Hz frame frequency CCD camera. The image processing and control system is mainly used to calculate the centre-of-gravity positions of each images and control the open-time of the gated intensifier which simulated the ways of two operations of the beacon.
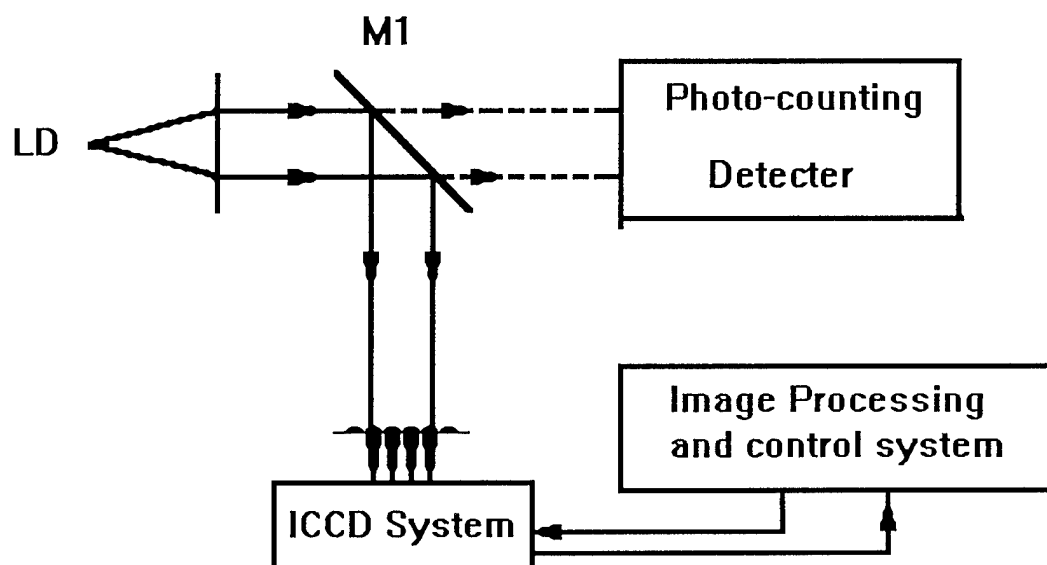
Fig.1. Schematic of the configuration in the test.

The procedure of the test is the first that ten pictures as a group are grabbed and saved in the computer for later calculatinon. For continuous operation, the gate of the intensifier is opened during the test, but for the pulse operation, the gate opened 13 μs and then closed. The second we slide the mirror away and measure the intensities of the light for the group using the photo-counting detector as the corresponding intensities into the Hartmann WFS. Finally we calculate the ten centred positions of a subimage in the one group and evaluate the variance of centring position and accuracy of the wavefront. Repeating the procedure, we can have a series of the low-light characterisations of the sensor under the different conditions of the wavefront accuracy.

Comparing the necessary light intensity/photons under the same wavefront accuracy for both operations, we found that the more light is needed for the continuous operation than the other. Later we do some theoretical analysis for this test and give the similar results. The detail results will be showed on the meeting.

+ Academic visitor at the Optics Section, the Blackett Laboratory, Imperial College of Science,Technology and Medicine, London, UK.

Atmosphere Potentialities of the Methods of the Posteriory Processing of Incoherently Illuminated Objects through the Turbulent

Igor P. Lukin

Inst. of Atmospheric Optics, SB of the Russian Acad. of Sci.,

1 Akademicheskii Ave., 634055 Tomsk, Russian Federation

Tel. (382-2) 25-96-82

Optical transfer function (OTF) and the integral resolution of the optical system ''turbulent atmosphere - telescope'' are treated theoretically by different methods of posteriory processing of incoherently illuminated objects observed through the turbulent atmosphere. The following processing methods are examined: the averaged image recording (''very long'' averaging times) and short-exposure images (''very short'' averaging times), namely, Labeyrie, Knox-Thompson, and triple correlation of image intensity methods. The influence of the finite value of the turbulent atmosphere outer and inner scales on the OTF's under consideration is also estimated.

Having assumed that $\rho_c > a_t$, or $\rho_c < a_t$ (where ρ_c is the value of the coherence radius of the plane optical wave; a_t is the receiving optical system radius) we obtain the following relation connecting the OTFs of the methods of triple correlation of the image intensity and Knox-Thompson:

$$\tau_{TC}(\mathbf{p}_1,\mathbf{p}_2) \cong \tau_{LE}(\mathbf{p}_1)\tau_{NT}(\mathbf{p}_2,\mathbf{p}_1+\mathbf{p}_2) + \tau_{LE}(\mathbf{p}_2)\tau_{NT}(\mathbf{p}_1,\mathbf{p}_1+\mathbf{p}_2) + $$
$$+ \tau_{LE}(\mathbf{p}_1+\mathbf{p}_2)\tau_{NT}(\mathbf{p}_1,-\mathbf{p}_2) - 2\tau_{LE}(\mathbf{p}_1)\tau_{LE}(\mathbf{p}_2)\tau_{LE}(\mathbf{p}_1+\mathbf{p}_2),$$

where $\tau_{LE}(p)$, $\tau_{NT}(p_1, p_2)$, $\tau_{TC}(p_1, p_2)$ are the OTF's of the turbulent atmosphere for the ''very long'' exposure, Knox-Thompson method, and triple correlation of image intensity method, respectively; p is the spatial scale. This relation shows in explicit form that potentially the

method of triple correlation of the image intensity does not make it possible to obtain more information on image than the Knox-Thompson method. The present conclusion concerns to measurements both the intensity spectrum modules of image and phase. The OTFs of the system "turbulent atmosphere - telescope" presented in the paper for the different methods of processing of the recorded short exposure images allow the following conclusion to be done. The methods of Knox-Thompson and triple correlation of the image intensity have the largest potentialities against others. Moreover, it is necessary to note especially, that these two methods practically have an equal potential accuracy of the image retrieving.

The integral resolution is one of the three standard measures of image quality, which is the bandwidth of the optical system. The integral resolution of the system ''turbulent atmosphere - telescope'' we define as the integral over spatial frequencies of the system's OTF. Knowledge of the system's integral resolution allows us to estimate the minimally resolvable distance at observations through the turbulent atmosphere.

In these cases the integral resolution of system ''turbulent atmosphere - telescope'' is defined by the following ratio:

$$R_L = 2\frac{k^2}{F_t^2}\iint d\mathbf{p}\tau_L(\mathbf{p}), \tag{1}$$

$$R_{NT} = \frac{k^2}{F_t^2}\sqrt{\iint d\mathbf{p}_1\iint d\mathbf{p}_2\tau_{NT}(\mathbf{p}_1,\mathbf{p}_2)}, \tag{2}$$

$$R_{TC} = \frac{k^2}{F_t^2}\sqrt{3\iint d\mathbf{p}_1\iint d\mathbf{p}_2\tau_{TC}(\mathbf{p}_1,\mathbf{p}_2)}, \tag{3}$$

where $\tau_L(p)$ is the OTF of Labeyrie method; F_t is the focal length of receiving lens; $k=2\pi/\lambda$, λ is the optical radiation wavelength in vacuum. The factors in formulas (1) and (3) are chosen from condition of concurrence (in absence of the atmospheric turbulence) of values R_L and R_{TC} with the integral resolution of the optical system in vacuum. The extraction of square root in formulas (2) and (3) is necessary so that the dimension of the integral resolution of the methods

of Knox-Thompson and triple correlation of the image intensity coincided with dimension of the integral resolution of the optical system ''turbulent atmosphere - telescope'' at other methods of processing of the image.

From the point of view of reception of the limiting levels of the resolution in the turbulent atmosphere for large receiver apertures ($a_t \gg \rho_c$) the advantage of methods of processing short-exposure image before the registration of the averaged image gives accordingly:

$$\lim_{a_t \to \infty} \frac{R_L}{R_{LE}} \cong 1.74$$

(method of Labeyrie);

$$\lim_{a_t \to \infty} \frac{R_{NT}}{R_{LE}} \cong \sqrt{2} = 1.4$$

(method of Knox-Thompson);

$$\lim_{a_t \to \infty} \frac{R_{TC}}{R_{LE}} \cong 2.26$$

(method of triple correlation of the image intensity).

All methods examined by that parameter are shown to give close results exceeding those obtained at recording the averaged images. Maximum resolution gives the method of triple correlation of the image intensity, minimum - the Knox-Thompson method.

THE INFLUENCE OF WAVE FRONT DISLOCATIONS ON PHASE CONJUGATION INSTABILITY AT THERMAL BLOOMING COMPENSATION

Boris V. Fortes and Vladimir P. Lukin

Institute of Atmospheric Optics,
Siberian Branch of the Russian Academy of Sciences,
av.Academicheskii 1,Tomsk, 634055, Russia

The present paper is devoted to the application of the phase conjugation method for the thermal blooming compensation. This problem was discussed previously in a series of papers of different authors[1,2,3,4,5,6,7], and the results of these papers indicate of the fact that the phase conjugation application for correction of nonlinear distortions of high–power laser beams has some specific features including the instabilities of different type. At the homogeneous horizontal paths the instability appears as parameters oscillations of corrected and reference beams, and at vertical paths the small–scale instability is developed.

In the above–mentioned papers it was assumed that the wave front of reference radiation was determined in all the points of the aperture of adaptive system and could be measured and reproduced with an arbitrary accuracy by means of some ideal sensor and corrector of wave front. At the same time, in the paper[8] it was shown that at strong distortions of optical wave the appearance of singular points was possible, where the intensity was equal to zero, and the wave front had the peculiarities (singularities) in the form of screw dislocations and represented a multisheeted surface. This hypothesis was confirmed by laboratory[9] and numerical experiments[10]. As noted in the papers, devoted to the problem of dislocations, the appearance of singular points can significantly affect the work of adaptive optical systems. However, up to now the investigations are lacking, which could allow one to understand in what way the adaptive system will work under such conditions. The purpose of our paper is the investigation of the influence of dislocations on the efficiency of phase conjugation when compensating the nonstationary thermal blooming of cw beam.

We have conducted the two types of numerical experiments on application of the phase conjugation method for correction of thermal blooming. In one case for the corrected beam we used the boundary condition of exact phase conjugation, and in the other case the phase correction was obtained as a result of simulation of the Hartmann sensor[12] and subsequent modal estimating of the reference beam phase[13,14]. In both cases we have simulated the "fast" adaptive system, focusing the Gaussian beam to the target plane, being at the distance $f = \frac{1}{\sqrt{10}} z_d$ (where $z_d = k a_0^2$ is the diffraction length, a_0 is the beam radius over the intensity level 1/e, $k = 2\pi/\lambda$ is the wave number). In the focal plane we recorded the peak intensity W_{max} and the radiation power P falling within circle with radius $a_f = a_0 \cdot f/z_d$ being equal to the radius of undistorted focal spot at the intensity level 1/e. Simultaneously we recorded the appearance and coordinates of dislocations of the reference beam wave front on the adaptive system aperture.

Let us consider the results of simulation of the exact phase conjugation. Figure 1 present the curves indicating the dependence of peak intensity W_{max} and the coordinates of dislocation x_d on the time t , normalized as follows[7]:

$$t' = \frac{t}{\tau_V}; \quad \tau_V = \frac{2a_0}{|V_\perp|}; \quad W' = W \frac{2k^2 \alpha n_T' a_0^3}{\rho C_P |V_\perp| n_0}; \quad P' = P \frac{2k^2 \alpha n_T' a_0}{\rho C_P |V_\perp| n_0}; \quad x_d' = \frac{x_d}{a_0}$$
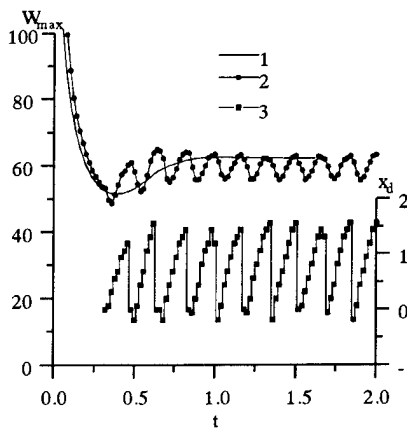
Fig. 1. Dynamics of peak intensity W_{max} of a corrected beam in focal plane: 1–at the beam initial intensity $W_0 = 16$; 2– $W_0 = 24$; 3–the coordinate of the reference beam dislocation $x_d(t)$ at $W_0 = 24$ (right Y -axis).

(later the primes of normalized values are omitted). Here $\mathbf{V}_\perp = (V_x, V_y)$ is the transverse component of wind velocity, α is the absorption coefficient; ρ is the density; C_P is the specific heat at constant pressure, n_0 is index of refraction, $n'_T = \partial n/\partial T$ where T is temperature.

The results are given for the two values of initial axial intensity of the beam: $W_0 = 16$ and $W_0 = 24$. At the beam intensity $W_0 = 16$ (curve 1) the dislocations do not appear and the beam parameters become stationary. With the increase of beam intensity up to 24 we observed the intensity oscillations (curve 2) followed by periodic appearance of dislocations in the reference beam (curve 3). Dislocations appear close to the axis of the optical system and transfer in the direction coinciding with the wind direction $\mathbf{V} = (V_x, 0), V_x > 0$, until they do not go out from the registration zone $x_d^2 + y_d^2 \leq (2a_0)^2$. The increase of intensity up to 32 resulted in the fact that a new pair of dislocations appeared before the preceding pair going out from registration zone.

Figure 2 shows the dependence of position of beam waist z_{max} and peak intensity in it on the time. At the intensity $W_0 = 16$ the beam waist is gradually shifted to the emitting aperture and its position is stabilized at the mark $z_{max} \approx 0.85 \cdot f$. At $W_0 = 24$ the waist is shifted close to the emitting aperture and its position varies near the point $z_{max} \approx 0.4 \cdot f$ with the amplitude of the order of $\Delta z_{max} \approx 0.15 \cdot f$. At the same time, the intensity in the waist much exceeds the initial intensity of the beam. The period of oscillations of waist position coincides with the period of dislocation appearance. This effect can be interpreted as the manifestation of positive feedback between the adaptive system and the thermal lens. At the initial stage of heating $t \leq \tau_V$ the main contribution to distortions is introduced by

Fig. 2. Dynamics of beam waist position of a high–power beam $z_{max}(t)$; 1 – $W_0 = 16$, 2 – $W_0 = 24$ (right Y-axis); 3 – peak intensity in the caustic for $W_0 = 24$ (left Y -axis).

defocusing. Its compensation results in an additional focusing of high–power beam and its waist shift to the source. The waist becomes narrower, and its intensity increases that leads to the medium temperature increase in the beam waist and to amplification of defocusing strength of the thermal lens. This results in subsequent shift of waist and so on.

The thermal lens shift to the emitting aperture decreases "the feedback coefficient". In the limiting case when the thermal lens intensity is concentrated close to the adaptive optical system (AOS) aperture and the additional focusing, contributed by AOS, is compensated by the defocusing thermal lens, we do not observe the subsequent increase of defocusing of reference beam and focusing of high–power beam.
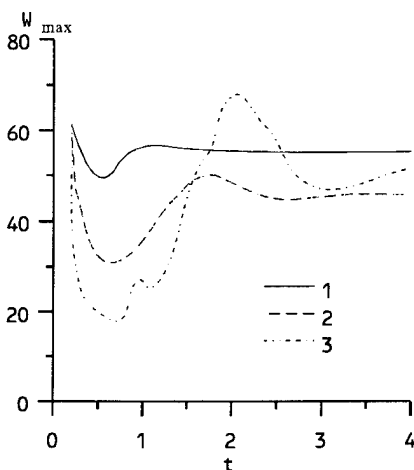

Fig. 3. Dynamics of peak intensity $W_{max}(t)$ in the AOS focus with the Hartmann sensor. $1 - W_0 = 16$; $2 - W_0 = 32$; $3 - W_0 = 64$.

If the distortions in the high–power beam waist achieve the value sufficient for appearance of dislocation in the reference beam, the information on the defocusing introduced by thermal lens, is erased without falling into adaptive system, and the high–power beam focusing decreases whereas its waist is shifted to the target. As a result, the intense thermal lens, being the reason of the occurrence of dislocations, begins to cool off and some time later the lens is cooled up to the state when dislocations disappear and the feedback is reconstructed. Then the whole cycle is repeated and the system develops into the regime of auto–oscillations typical for nonlinear systems with feedback.

At subsequent stage of work AOS was simulated with the Hartmann-Shack sensor, consisting of 16 subapertures arranged in four rows. The four angular subapertures were not taken into account, and local tilts were estimated only in 12 subapertures. The size of the sensor aperture $D = 4a_0$ corresponds to the beam diameter at the intensity level $1/e^2$. The reference beam was fed to the sensor after passing through correcting and focusing systems. The phase correction was determined as a sum of 15 of Zernike polynomials with the weight factors obtained by modal estimating the phase on the circle inscribed in the sensor aperture.

Figure 3 shows the dynamics of peak intensity at the target for three values of initial beam intensity. In all the three cases the oscillations are lacking, i. e., the application of the Hartmann sensor with modal estimate damps the oscillations or, at least, increases the threshold of their appearance. Nevertheless, the dislocations in the reference beam could appear. It turned out that in the focal plane of the sensor subaperture to which the dislocation comes, the two focal spots are observed, each having the diffraction size. In contrast to AOS with a precise phase conjugation the position of dislocations remained relatively stable.

We consider the problem of compensation of nonstationary thermal blooming by the phase conjugation method. Analysis of the numerical experiment data has shown that the appearance of continuous auto–oscillations in adaptive system is connected with the occurrence of dislocations in the reference beam. The use of the Hartmann sensor with low spatial resolution and modal estimation of the phase results in smoothing the phase estimate and damps the AOS oscillations.

REFERENCES

1. J. Herrmann, "Properties of phase conjugate adaptive optics systems", J.Opt.Soc.Am., Vol.67, No.3, pp.290-295, 1977.

2. V.E. Zuev, P.A. Konyaev, V.P. Lukin, "Minimization of atmospheric distortions of optical waves by methods of adaptive optics" Izv. Vyssh. Uchebn. Zaved., Fiz., Vol. XXVIII, No. 11, pp. 6-29, 1985.

3. V.L. Dmitriev, A.A. Mashukova, V.P. Lukin, V.V. Sychev, "Peculiarities of correction of laser radiation self-action along atmospheric paths using 'slow' phase-conjugate adaptive system", Atmospheric Optics, Vol. 3. No. 12, pp. 1269-1272, 1990.

4. B. Johnson, C. Primmerman, "Experimental observation of thermal-blooming phase-compensation instability", Opt.Lett., Vol.14, No.12, pp.639-641, 1990.

5. T.J. Karr, "Atmospheric effects on laser propagation", Proc.SPIE, Vol.1060, pp.120-128, 1989.

6. J.F. Schonfeld, "Linearized theory of thermal-blooming phase-compensation instability with realistic adaptive-optics geometry", J.Opt.Soc.Am.B, Vol.9, No.10, pp.1803-1812, 1992.

7. P.A. Konyaev, "Thermal blooming instabilties" Atmospheric and Oceanic optics, Vol. 5, No.12, pp. 1261–1268, 1992.

8. N.B. Baranova, B.Ya. Zel'dovich, "Dislocations of wave front surfaces and amplitude zeros", Zh. Eksper. Teor. Fiz., Vol. 80, pp.1789–1797, 1981.

9. N.B. Baranova, A.V. Mamaev, N.F. Pilipetsky, V.V. Shkunov, B.Ya. Zel'dovich, "Wave-front dislocations: topological limitation for adaptive systems with phase conjugation", J.Opt.Soc.Am., Vol.73, No.5, pp.525-528, 1983.

10. D.L. Fried, J.L. Vaughn "Branch cuts in the phase function", Appl.Opt., Vol.31, No.15, pp.2865-2882, 1992.

11. J.A. Fleck, J.R. Morris, M.D. Feit, "Time-dependent propagation of high-energy laser beam through the atmosphere", Appl.Phys., Vol.10, No.1, pp.129-139, 1976.

12. V.P. Lukin, N.N. Maier, B.V. Fortes, "Calculation of point spread function for an adaptive telescope with a Hartmann wave front sensor", Atmospheric Optics, Vol.5. No. 12, pp. 1241–1251, 1992.

13. R. Cubalchini, "Modal wave-front estimation from phase derivative measurements", J.Opt.Soc.Am., Vol.69, No.7, pp.972-977, 1979.

14. J. Herrmann, "Cross coupling and alliasing in modal wave-front estimation", J.Opt.Soc.Am., Vol.71, No.8, pp.989-992, 1981.

EFFICIENCY OF ADAPTIVE CORRECTION OF IMAGES IN A TELESCOPE USING AN ARTIFICIAL GUIDE STAR

Vladimir P. Lukin, Boris V. Fortes

Institute of Atmospheric Optics,
Siberian Branch of the Russian Academy of Sciences,
av.Academicheskii 1, Tomsk, 634055, Russia

It is well known that the use of a bright natural star as a reference source is limited by the angle of isoplanarity[1,2,3], which usually does not exceed 10 angular seconds, while the sufficiency bright stars are located less closely. In this connection in recent years the formation technique of artificial guide stars is gathering force, based on the effect of laser backscattering in the atmosphere[4,5].

However, phase distortions of the scattered radiation diverging wave does not coincide with the distortions of the initially plane corrected wave[6]. In this case this difference increases with the decrease of height on scattering volume and with the increase of size of the telescope entrance pupil. Formation of laser guide stars at large altitude is limited by small scattering coefficient.

The present paper describes the possibility of obtaining of partially-corrected image with resolution close to diffraction limited for adaptation by the Rayleigh and sodium beacons. For making the calculations the numerical model of the adaptive telescope[7] was supplemented by the artificial star simulator. The details of atmospheric scattering were not taken into account.

The upward propagation of a laser beam is simulated as the propagation of a convergent cone of rays intersecting in a focal plane. In this case the initial size of the cone is equal to the telescope diameter. The shift of the beacon (cone top) can be written as

$$\vec{\rho}_b = \int_0^L \vec{s}(z)dz, \tag{1}$$

where L is the path length, $\vec{s}(z)$ is the vector determining the direction of beam axis. In numerical simulation due to a discrete representation of random-inhomogeneous medium this integral is expressed as

$$\vec{\rho}_b = \sum_{K=1}^{N_z} \vec{s}(z_K) \cdot (z_{K+1} - z_K), \tag{2}$$

where Z is the K-phase screen position. The beam axis tilt is defined by its refraction at all preceding phase screens, including a running one, that is,

$$\vec{s}(z_K) = \sum_{K'=1}^{K} \vec{s}_{K'} \tag{3}$$

where $\vec{s}_K$ is the K-screens contribution to be determined as an approximation of wave front distortions $S_K(\vec{\rho})$ by the liner functions , i.e., as solution of problem:

$$\iint_{|\vec{\rho}-\vec{\rho}_K| R_K} \left[S_K(\vec{\rho}) - (\vec{\rho} - \vec{\rho}_K) \cdot \vec{s}_K - C \right]^2 d^2\rho \rightarrow \min \tag{4}$$

where

$$\vec{\rho}_K = \sum_{K'=1}^{K} \vec{s}(z_{K'}) \cdot (z_{K'-1} - z_{K'}) \text{ and } R_K = R_0 \cdot (1 - z_K/L) \tag{5}$$

is the current position of the beam center and its radius, respectively.

The subsequent part of the problem is the simulation of "downward" propagation of a scattering wave. Considering a reference source as a point one and neglecting by the ray deformation when propagating through the turbulent medium, the optical path length for the ray at the point $(\vec{\rho},0)$ can be expressed as an integral

$$l(\vec{\rho}) = \int_0^P n(p)dp = P \cdot n_0 + \int_0^L \tilde{n}\left(\vec{\rho} + (\vec{\rho}_b - \vec{\rho}) \cdot z/L, z\right) \cdot p_z' \cdot dz, \tag{6}$$

where

$$P = \sqrt{(\vec{\rho} - \vec{\rho}_b)^2 + L^2} \text{ and } p = z \cdot \sqrt{1 + \frac{(\vec{\rho}_b - \vec{\rho})^2}{L^2}} \tag{7}$$

is the beam length and the coordinate along it, real from the receiving aperture, $\tilde{n} = n - n_0$ is the refractive index fluctuations. In the paraxial approximation, i.e., at $(\vec{\rho} - \vec{\rho}_b)^2/L^2 \ll 1$ we have

$$P \approx L + \frac{\rho_b^2}{2L} + \frac{\rho^2}{2L} - \vec{\rho}\frac{\vec{\rho}_b}{L} \text{ and } p_z' = \sqrt{1 + \frac{(\vec{\rho}_b - \vec{\rho})}{L^2}} \approx 1. \tag{8}$$

Assuming $n_0 \approx 1$ for the optical path length we obtain the following expression:

$$l(\vec{\rho}) \approx L + \frac{\rho_b^2}{2L} + \frac{\rho^2}{2L} - \vec{\rho}\frac{\vec{\rho}_b}{L} + \int_0^L \tilde{n}\left(\vec{\rho} + (\vec{\rho}_b - \vec{\rho}) \cdot z/L, z\right)dz. \tag{9}$$

The first two components do not depend on ρ and are the same for all the rays. The third component corresponds to the divergent spherical wave (in paraxial approximation). If the reference wave passes through the same optics, by means of which the laser beam was focused, this component is compensated. The fourth component describes the total tilt of the reference wave occurring as a result of the fact that because of random refraction the reference wave source is shifted from the telescope axis. The last component represents the turbulent distortions of the reference wave. Random fluctuations of the optical path length are written as

$$\tilde{l}(\vec{\rho}) = -\vec{\rho}\frac{\vec{\rho}_b}{L} + \int_0^L \tilde{n}\left(\vec{\rho} + (\vec{\rho}_b - \vec{\rho}) \cdot z/L, z\right)dz. \tag{10}$$

The random-inhomogeneous field of the refractive index in accordance with the splitting technique[8,9] is represented as a sequence of thin phase screens that is equivalent to the following expression

$$\tilde{n}(\vec{\rho}, z) = \sum_{K=1}^{N_z} S_K(\vec{\rho}) \cdot \delta(z_K) \tag{11}$$

Substituting this expression to Eq. (10) we obtain:

$$\tilde{l}(\vec{\rho}) = -\vec{\rho}\frac{\vec{\rho}_b}{L} + \sum_{K=1}^{N_z} S_K\left(\vec{\rho} + (\vec{\rho}_b - \vec{\rho}) \cdot z_K/L\right) \tag{12}$$

At numerical simulation the transverse coordinates are also presented as discrete ones, i.e., the values of phase distortions are known only in the nodes of the grid

$$S_{I,J,K} = S(x_I, y_J, z_K). \tag{13}$$

Traditionally it is sufficient, however, in this case it is necessary to interpolate these values to an arbitrary point. In the software developed for this purpose we use the two-dimensional linear interpolation that is quite sufficient for the problem being studied.

For calculations we have used the following semiempirical model of the altitude profile of turbulence intensity:

$$C_n^2 \left(h[km] \right) = 5.19 \cdot 10^{-16} \cdot 10^{-0.86h} + 10^{-18.34 + 0.29h - 0.0284h^2 + 0.000743h^3} . \tag{14}$$

The calculations were performed for the visible range. The coherence radius for this altitude profile (14) is approximately equal to 18 cm at $\lambda=0.55\mu$m. **The angular position of the artificial guide star is assumed to be fixed, i.e., $\bar{\rho}_b = 0$**
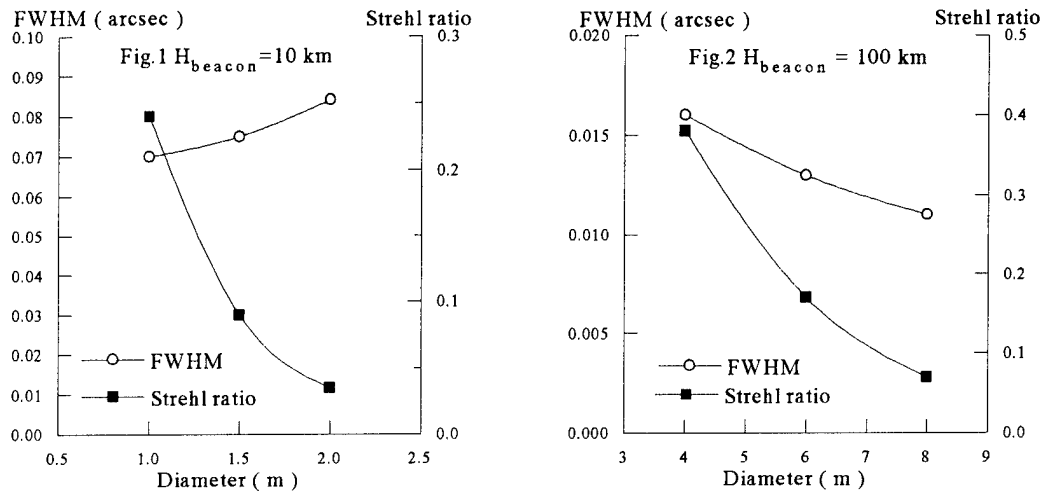

Figure 1 gives the results of calculations for the height of the reference source $H_{beacon} = L=10$ km (Rayleigh scattering), Fig.2 gives the results of calculations for the height $H_{beacon} = L=100$ km. It is assumed that the adaptive system has an infinite spatial-temporal resolution. In both cases the Strehl ratio decreases with the telescope diameter increase. At the same time the angular resolution (FWHM) varies slightly ($L=10$ km) and even is improved ($L = 100$ km) remaining close to a diffraction one.

REFERENCES

1. D. Korff, G. Dryden, R. P. Leavitt, "Isoplanicity: the translation invariance of the atmospheric Green's function", J.Opt.Soc.Am., 1975, Vol.65, No.11, P.1321-1330.
2. D. L. Fried, "Anisoplanatism in adaptive optics", J.Opt.Soc.Am., 1982, Vol.72, No.1, P.52-61.
3. R. J. Sasiela, "Strehl ratios with various types of anisoplanatism", J.Opt.Soc.Am.A, 1992, Vol.9, No.8, P.1398-1405.
4. L. A. Thompson, C. S. Gardner, "Experiments on laser guide stars at Mauna Kea observatory for adaptive imaging in astronomy", Nature (London), 1987, Vol.328, No.16 July, P.229-231.
5. L. C. Bradley, "Pulse-train excitation of sodium for use as a synthetic beacon", J.Opt.Soc.Am.B, 1992, Vol.9, No.10, P.1931-1944.
6. B. M. Welsh, C. S. Gardner, "Effects of turbulence-induced anisoplanatism on the imaging performance of adaptive-astronomical telescopes using laser guide stars", J.Opt.Soc.Am.A, 1991, Vol.8, No.1, P.69-80.
7. B. V. Fortes, V. P. Lukin., "Modeling of the image observed through the turbulent atmosphere", Proc.SPIE, 1992, Vol.1668, P.477-488.
8. J. A. Fleck, J. R. Morris, M. D. Feit, "Time-dependent propagation of high-energy laser beam through the atmosphere", Appl.Phys., 1976, Vol.10, No.1, P.129-139.
9. P. A. Konyaev, V. P. Lukin, "Thermal distortions of focused laser beams in the atmosphere", Appl.Opt., 1985, Vol.24, No.3, P.415-421.

Single-Frequency Nd:YAG Lasers as a Light Sources
for Wave front Sensors Interferometers

Vadim A. Parfenov, Alexander G. Seregin, Sergei N. Rodin

Research Centre «S.I.Vavilov State Optical Institute»
12, Birzhevaya line, St.Petersburg, 199034, Russia
Fax: (812)218-3720

Sergei V. Kruzhalov, Vladimir A. Parfenov

State Technical University
29, Polytechnicheskaya str., St.Petersburg, 191065, Russia
E-mail: mail@quel.stu.spb.su

Wave front sensors with an internal reference light source applied in the most of advanced adaptive telescopes use basically classic interferometric methods of optical surface testing and involve analyzing of the wave front reflected by the surface under test.

In last years, He-Ne lasers as well as ion ones (Ar^+, Kr^+) lasing in the visual spectral band have been widely used as light sources in interferometers. However, these lasers feature by some disadvantages that limit their practical application.

For example, He-Ne lasers are of inherently low radiation intensity and can be used effectively in those applications when an output power of ones or tens mW is sufficient for the proper measurement system functioning. On the contrary, Ar^+ and Kr^+ lasers provide extremely large output values but they features by drawbacks like large dimensions and weight, short life, water cooling systems application and high power consumption.

In contrast to the conventional approaches, we suggest to use Nd:YAG lasers as the internal reference light sources for wave front sensors interferometers.

A possibility to lase on different transitions corresponding to different wavelengths is among merits of these lasers (for example, 1.064μm, 1.32μm, 946 nm) as well as a possibility to expand their spectral band owing to nonlinear conversion of the radiation frequency. Moreover, Nd:YAG lasers active elements has unlimited operation life.

Another obvious advantage of Nd:YAG lasers is a possibility to provide single-frequency lasing mode enough easily that is of particular interest for such interferometric applications where high temporal coherence of radiation is required.

In addition, last years advances in the field of coherent pumping of solid-state lasers have resulted in appearance of compact effective Nd:YAG lasers possessing unique features. Reference [1], for instance, describes an example of this sort when the single-frequency output of 1 W has been obtained on wavelength of 0.53μm.

Papers devoted to so called chip-lasers illustrate unique possibilities of Nd:YAG lasers too. These diode-laser-pumped, single-frequency lasers with monolithic ring resonators have a lot of advantages [2]. Among them one can mark out very small dimensions, extremely narrow generation like (about 5....10 kHz) and highly stable performances [3]. Up to date, Nd:YAG chip-lasers provide the maximum

output of 1.8 W at wavelength of 1.064µm [4] that is quite enough for their application as the light sources in the interferometric wave front sensors for adaptive telescopes including ones with hologram structure on the primary mirror surface [5,6].

While working on large adaptive telescope for astronomy [5] we investigated experimentally single-frequency Nd:YAG lasers including lamp- and diode-pumped ones (including, in turn, chip-laser). The lasers generating both on the fundamental wavelength (1.064µm) and on the second harmonic wavelength were investigated.

Spatial characteristics of laser radiation were the principal purpose of the investigation. A lot of papers was known devoted to investigation of both energetic and spectral characteristics of Nd:YAG lasers while the spatial ones were studied unsatisfactorily up to the latest time. In our experiments, we investigated both spatial coherency and angular position stability of laser beams.

The experiments have shown ([6-8] for instance) that Nd:YAG lasers posses enough high performances and entirely meet the stringent requirements to internal light sources inside the adaptive telescope control channel.

Thus, a conclusion can be drawn that Nd:YAG lasers are promising light sources for interferometric wave front sensors and can be recommended for application in the adaptive telescopes.

References

1. J.Hong, C.Yelland, M.H.Dunn, W.Sibbett and B.D.Sinclair, *Journal of Modern Optics*, Vol. 41, No. 6, pp. 1227-1230, (1994).

2. T.J.Kane, A.C.Nilsson and R.L.Byer, *Optics Letters*, Vol.12, pp. 175-177, (1987).

3. N.V.Kravtsov and O.E.Nanii, *Kvantovaya elektronika*, Vol.20, No.4, pp. 322-344, (1993). (in Russian)

4. I.Freitag, A.Tunnerman and H.Welling, *Advanced Solid-state Lasers conference OSA Technical Digest (Opt. Soc. of Am., Wash.,D.C.,1995)*, Paper WC8, P. 253-255.

5. M.A.Gan, B.A.Ermakov, D.N.Yeskov, V.Ph.Zakharenkov, N.V.Ryabova, A.G.Seregin, V.I.Sidorov and S.I.Ustinov, *Trudy Gosudarstvennogo opticheskogo instituta im. S.I.Vavilova* - Vol. 74, No. 208, pp. 42-54, (1989). (in Russian)

6. V.V.Anistchenko, S.N.Koreshev, V.A.Parfenov, A.G.Seregin and V.I.Sidorov, *Optika atmosfery i okeana*, Vol. 6, No. 12, pp. 1588-1596, (1993). (in Russian)

7. V.A.Parfenov, S.N.Rodin, I.Sh.Etsin, G.F.Zaitsev, S.V.Kruzhalov and Vl.A.Parfenov, *Proceedings of SPIE*, Vol. 2375, pp. 288-293, (1995).

8. N.V.Kravtsov, V.V.Firsov, P.G.Konvisar, S.R.Rustamov and V.A.Parfenov, *Proceedings of SPIE*, Vol. 2379, pp. 325-328, (1995).

NUMERICAL SIMULATION AND TEST OF A MODEL THERMO- ADAPTIVE MIRROR

Vladimir V.Reznichenko, Victor V. Kotov, Yury V. Leonov,
Vladislav N.Smirnov, Marina E. Zvezdina,

Reseach Center "S.I.Vavilov State Optical Institute"   St.Petersburg, Russia

The majority of wavefront disturbances of space reflector and space telescopes are due to external thermal fields variations and the optical surface deformations.

This can be accomplished only by some thermal methods: either by temperature gradients elimination or by keeping some given temperature field. The latter method is carried out by a system of heaters and sensors located on mirror elements /1-3/.

A thermo-optical correction system (TOCS) consists of individual control units which contain heaters and sensors fixed to respective mirror elements as well as electronic measurement and control units (MCU) interfaced to them. The MCU are made constructively of unified printed circuit boards which can be functionally divided into various zones for interfacing of input/output, memory and supply circuits.

Experimental investigations and numerical simulation of the thermal control system performances as well as local electric heaters control parameters are discussed. Material and parameters of reflectors for the temperature gradients compensation by heating are numerical simulated.

The real thermal effect function control and control algorithms are obtained for a thin model mirror dia 180 mm. The mirror surface deformation is measured by Zygo interferometer while the mirror temperature is controlled by differential temperature sensor.

The acceptable thermal response value provides the real possibility to develop an effective mirror correction thermal modes and to consider thermal cleaning surface.

References
1. T.A.Facey, M.H.Krim, C.Ftaclas etc. "On orbit terformace of the HST optical telescope assembly". Technical Digest Series , Spase Optics. vol. 19, p.31-36, (1991).
2. V.Reznichenko, N.Yakovleva. "Mirror temperature stabilization and deformation by local heaters" SPIE vol. 2201 Adaptive Optics in Astronomy, p.1027-1034, (1994).
3. V.Reznichenko, V. Kalugina, M.Lutinskaya, Y.Leonov, "Control surface mirror with local heaters". II European Conference on Smart Structures & Materials, Glasgow, (1994).

The Alternative Large Telescope Construction

Victor V. Sychev, Valery B. Kaspersky
Russian Federation State Research Center
Scientific and Production Association "Astrophysica"
123424 Russia, Moscow, Volokolamskoye shosse, 112

We propose a new conception of the large astronomical telescope with a primary segmented mirror of 10 m. The telescope is supposed to be constructed using an alt-azimuthal scheme as an upper moving part having a sphere-like shape.

A Sodium Guide Star Laser System for the Lick Observatory 3 Meter Telescope

Herbert W. Friedman, Gaylen V. Erbert, Donald T. Gavel, Thomas C. Kuklo, Jody G. Malik, J. Thaddeus Salmon, David A. Smauley, Gary R. Thompson,

Lawrence Livermore National Laboratory, Box 808, Livermore, CA 94550

Telephone: 510-422-2257
Fax: 510-422-1413

The use of sodium-layer laser guide stars for adaptive optics systems greatly enhances the sky coverage as compared to systems using natural guide stars. In order to demonstrate the feasibility of a sodium-layer guide star, a 20 W pulsed dye laser system has been designed and installed on the 3 meter Shane telescope at the Lick Observatory, Mt. Hamilton, California. The adaptive optics system used in conjunction with the laser guide star system has been described elsewhere[1] and has already demonstrated diffraction limited images at the 2.2 micron wavelength using natural guide stars. The integration of the sodium laser guide star and the adaptive optics systems represents the first such installation on an astronomical telescope.

The 20 W power level from the laser system should correct images to a Strehl ratio of 0.5 at 2.2 microns according to models developed at LLNL and elsewhere. The pulse format of 150 ns wide pulses at 11.5 kHz results in a peak power irradiance at the sodium layer of about 4 W/cm^2 assuming a spot size in the mesosphere of 40 cm. The small spot size is achieved by a laser beam divergence of 1.5 times the diffraction limit and a laser launch telescope diameter of 30 cm. The modulation format of the laser has been designed to match the double peaked absorption profile of mesospheric sodium with the result that the saturation flux is about equal to the peak power irradiance. Higher average power lasers would require higher pulse repetition rates, longer pulse duration or both to maintain this relationship.

The laser system consists of a set of three frequency doubled YAG laser pumping a set of dye lasers to produce the output at the sodium wavelength of 0.589 microns. The YAG lasers are assembled at LLNL using commercial components and produce 65 W of green power at 0.532 microns using an intracavity KTP doubling crystal. CW flashlamps pump the Nd doped YAG laser rod and an acousto-optic Q switch produces the short pulse format. The input power for each YAG laser is approximately 8 kW. The YAG lasers pump a set of three liquid dye laser consisting of a Dye Master Oscillator (DMO), a preamplifier and a power amplifier. The DMO produces a narrow band, single (longitudinal and transverse) mode beam which is frequency stabilized using a opto-galvanic, low pressure sodium cell and then phase modulated using a pair of tuned circuit, electro-optic crystals. The laser power

from this waveform generator is then increased to the 20 W level in a set of two amplifiers which are also pumped by the YAG laser. The output beam is expanded to 20 cm and launched to the sodium layer.

A unique feature of this laser system is the use of fiber optics to separate the high power, inefficient laser components from the efficient dye laser converters to remove sources of waste heat from the dome area. An additional benefit is that the dye laser converters are sufficiently small that they can be mounted directly on the telescope eliminating the need to pass the beam through the equatorial (or azimuth) and elevation bearings. The YAG pump lasers, DMO and support equipment are located in a room below the dome floor with a separate air conditioning system. Fiber optic cables transport the low power dye light and high power pump light to the preamplifier and power amplifier units which are located in a 2' x 4' enclosure at the base of the telescope, see Figure 1.

The beam control system is located in the middle of the telescope and the laser launch telescope is located at the end as shown in Figure 1. The beam control system consists of a "dog-leg" set of optics for Pointing and Centering (P&C), a high band width tilt mirror and a Hartmann wave front sensor. The sensor for the P&C closed loop control is after the last reflective optic and maintains the laser beam position and attitude. The signal for the high band width tilt mirror is derived from the adaptive optics system and therefore removes all jitter components including those from the laser, optics and the atmosphere in the uplink propagation path. The Hartmann sensor views the wave front of the laser beam both from the output of the laser amplifier and the output of the (refractive) launch telescope as measured by a retro reflection from the primary lens. The philosophy here is to diagnose as much of the laser as possible before launching the beam to reduce the dependency of the laser guide star system on mesospheric measurements.

The laser system has been installed on the Shane telescope and over 17 W have been measured during the first light propagation series. The process of bore sighting the laser launch telescope with the Shane telescope is underway and integrated experiments with the adaptive optics system are planned for the summer. The results of these observations will be presented.

References

1. "Adaptive Optics at Lick Observatory", J. M. Brase et al., SPIE 1994 Symposium on Astronomical Telescopes & Instrumentation for the 21st Century, Kona, HI, March 1994

LLNL Laser Guide Star
installation at Lick Observatory
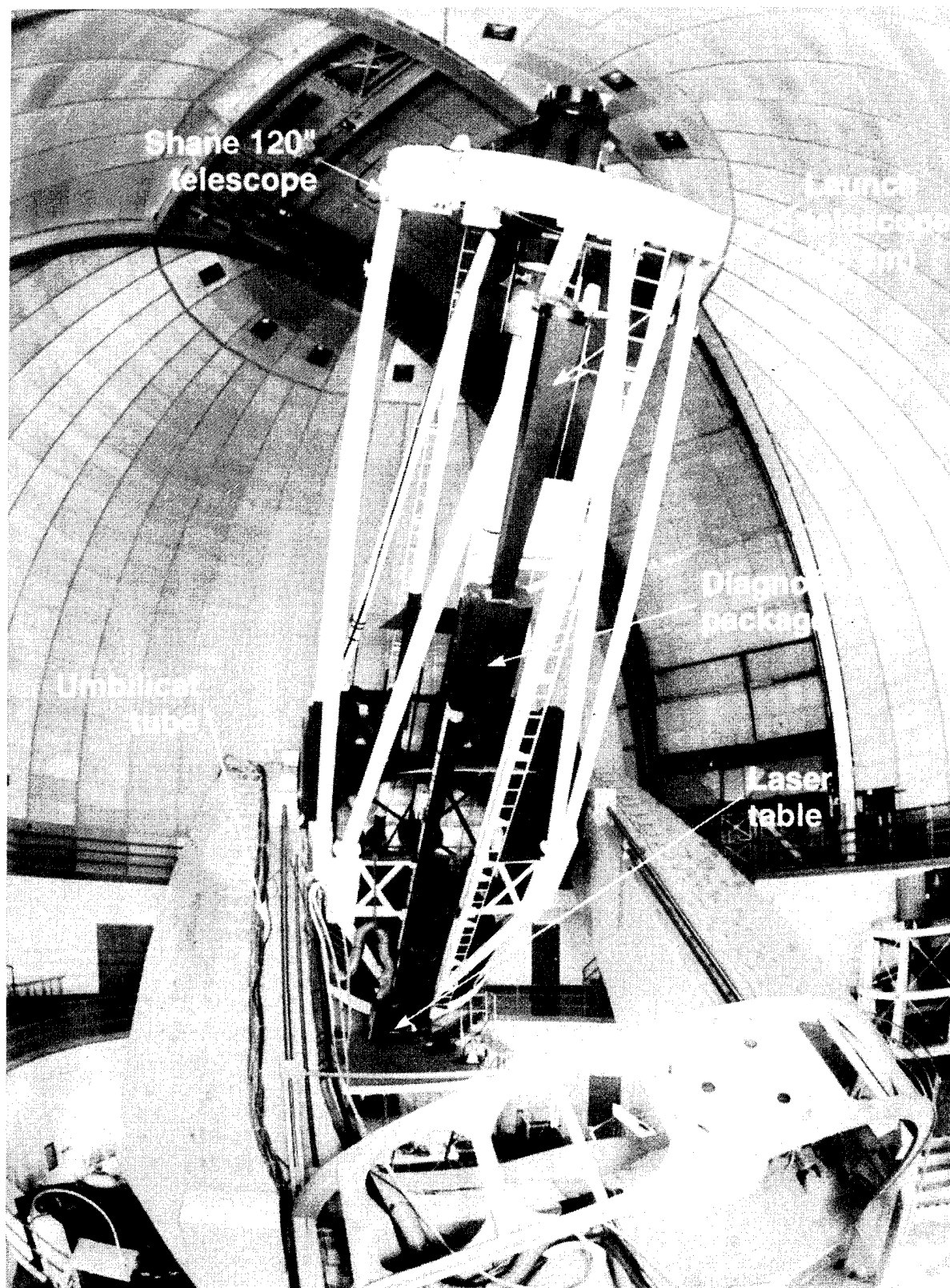
1.1.0395.0835A
12HF/geg

FIGURE 1

High Accuracy Capacitive Displacement Transducer
for the Position Local Control Loops at the Adaptive Secondary

Valdemaro Biliotti - Osservatorio Astronomico di Arcetri - Firenze (Italy)

Roberto Biasi - Dipartimento di Ingegneria Aerospaziale - Politecnico di Milano - (Italy)

Guido Brusa - Osservatorio Astronomico di Arcetri - Firenze (Italy)

Daniele Gallieni - Dipartimento di Ingegneria Aerospaziale - Politecnico di Milano - (Italy)

Roberto Spairani - Dipartimento di Ingegneria Aerospaziale - Politecnico di Milano - (Italy)

Roberto Aiello - Osservatorio Astronomico di Arcetri - Firenze (Italy)

Introduction

The thin faceplate adaptive secondary mirrors are controlled by means of electromagnetic force actuators, which seem to be a suitable choice in terms of stroke, accuracy and cost [Del Vecchio, Gallieni et al.; Biasi, Gallieni et al. in this Conference]. Those actuators need a local control loop to achieve a linear position response. The position sensor is definitely a crucial component of this control loop: both high sensitivity and high speed have to be achieved at same time.

This work presents the principle of operation and the performance evaluation of a capacitive displacement sensor.

Working principle

The sensor is based on the measurement of the capacitance variations of an air capacitor. One armature is placed on the continuos faceplate mirror, where the other one is on the backplate. Other configurations were tested, where the variable capacitance was obtained from two capacitors in series, eliminating the wires connecting the mirror to the backplate.
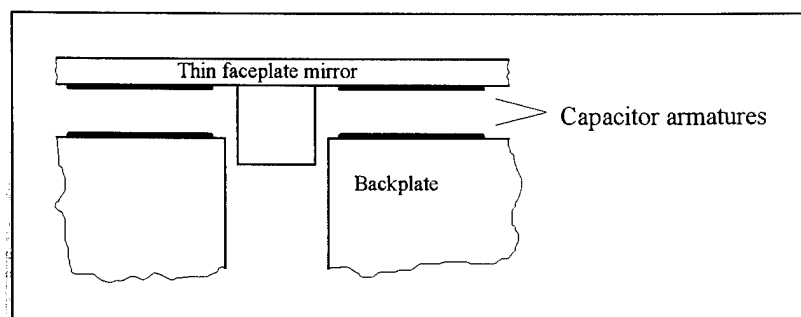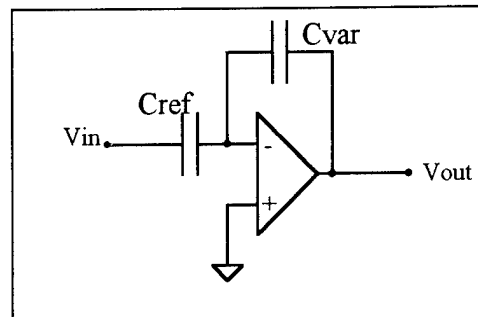

Fig. 1 - Sensing capactitor scheme

Fig. 2 - Working principle

The capacitance of a plane capacitor is related to the armatures area and to their distance:

$$C = \varepsilon \frac{A}{d}$$

With reference to the conceptual scheme above, the variable capacitance can be related to the operation amplifier output voltage V_{out} as follows:

$$V_{out} = \frac{X_{var}}{X_{ref}} V_{in} = \frac{\frac{1}{j\omega C_{var}}}{\frac{1}{j\omega C_{ref}}} V_{in} = \frac{j\omega C_{ref}}{j\omega \varepsilon_a \frac{A_{var}}{d_{var}}} V_{in} = d_{var} \frac{C_{ref}}{\varepsilon_a A_{var}} V_{in}$$

Realization aspects

The sensor electronics was designed with regard to the small capacitance variations that have to be measured. A high impedance, high speed and low noise FET input circuit is the front-end between capacitors and the actual operational amplifier. This input stage ensures reliable operation even at low capacitance values (5pF and less).
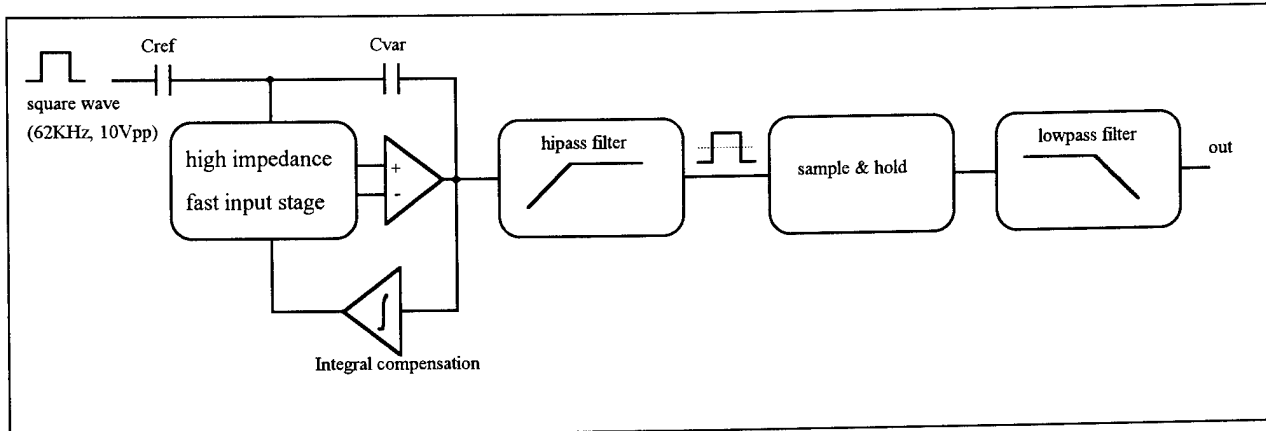
Fig. 3 - Conceptual scheme of the electronic circuit

The input signal to the circuit is a square wave at about 62 KHz, very stable over time. The amplitude-modulated output signal is filtered and sampled at constant phase of the square wave. The relatively high input frequency guarantees a flat response of the sensor over a wide frequency range.

Performance evaluation

In order to evaluate the actual performance of the sensor, a testbench based on a piezoelectric linear actuator was built. The sensitivity and the response were measured by varying the distance between the variable capacitor armatures under *quasi*-static conditions (from 0 to 20 Hz), due to the intrinsic limitations of the

testbench mechanics and of the strain-gauge reference displacement transducer. The plot besides reports the response to a 20nm peak to peak square wave input signal (6 pF sensing capacitance, 10 pF ceramic reference capacitor). It is important to notice that the sensitivity depends on the distance between the armatures. At 300 microns gap, which could be a suitable mean distance for both correction and chopping at the secondary mirror, the sensitivity is of about .01 Volt/micron. The frequency response was measured replacing the air capacitors with fixed ceramic ones, and modulating in amplitude the input signal. In this way the actual response of the sensor circuit could be investigated, avoiding unpredictable mechanical behavior. The response is flat from DC up to 10Khz.
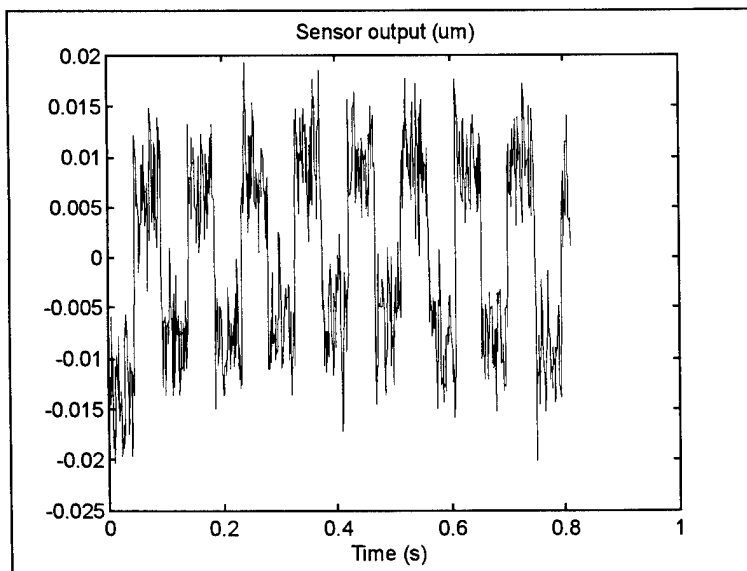
Fig. 4 - Sensor response to 20nm square wave input

The noise measurements were taken with both air (variable) and fixed capacitors, showing negligible differences between the two configurations. A noise amplitude density of $0.1nm/\sqrt{Hz}$ was obtained with two 5pF fixed capacitors. These tests revealed that the noise is significantly affected by the capacitances mismatch. Moreover, the noise power spectral density showed that the noise is higher at low frequencies. Therefore, further improvements could be achieved by optimizing the shielding and grounding of the sensor.

The sensor design has been already successfully implemented for the position control of the "Fasttrack" beam combiner for the Multiple Mirror Telescope.

Conclusions

The performances of the capacitive sensor described here seem to match the requirements for the local control loops of the secondary mirror, in terms of effectiveness, reliability, power consumption and cost.

Moreover, the circuit can be easily reduced in size to meet the maximum allowable dimensions for this device.

Some critical aspects, like noise shielding, need to be experienced directly on the first 5x5 actuators mirror prototype.

Simulation of Adaptive Secondary Mirror Dynamic Response

R. Biasi, D. Gallieni, P. Mantegazza

Dipartimento di Ingegneria Aerospaziale - Politecnico di Milano

via Golgi, 40 - 20133 Milano - Italy

phone +39-2-23994000 fax +39-2-23994034

Introduction

This work is part of a study that aims at implementing adaptive optics on a secondary mirror of an 8 m class astronomical telescope for atmospheric compensation at visible wavelength. The secondary mirror to be controlled is a continuous thin facesheet type. The goal is to fulfill operational specifications by using voice coils actuators coupled to collocated capacitive position transducers.

The task of the control system is to compensate (up to its cutoff frequency) the dynamics of the mirror. This means that within the control pass band only the static crosstalk among the actuators must be accounted for. Thus, the actuators can be controlled in position by the global adaptive optics control system, without any regard of the dynamic reaction opposed by the mirror. Another important task is to achieve the desired system behavior limiting the actuators peak forces to lessen the power dissipated by the adaptive optics control device

Model of actuators-structure interaction

The MMT 6.5 m has been chosen as a reference configuration to design the actuators and their control. The proposed adaptive secondary mirror has a diameter of 0.64 m and is 2 mm thick. To perform atmospheric compensation at visible wave lengths a high actuators density is required. The subaperture size on the secondary is 30 mm, leading to an array of 316 actuators in common subaperture configuration (figure. 1).
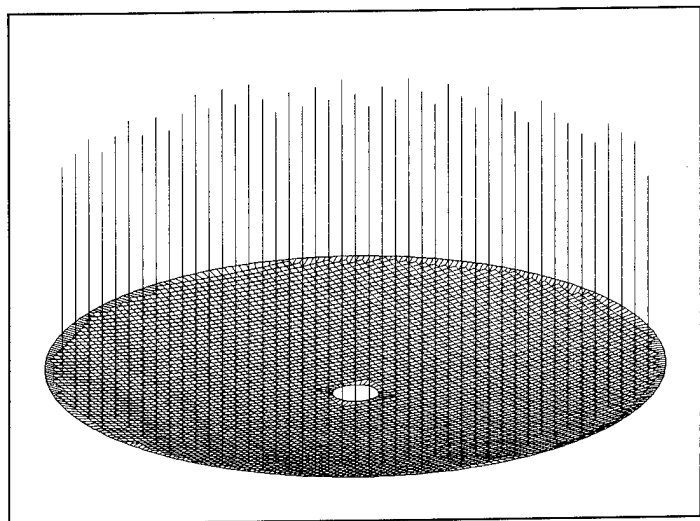

Figure 1: MMT adaptive secondary mirror

The state-space description of the structure is achieved by computing mass and stiffness matrices reduced to the active set of model dofs. It is connected to the models of the collocated control loops (one for each actuator), to form a unique state-space system (figure 2).
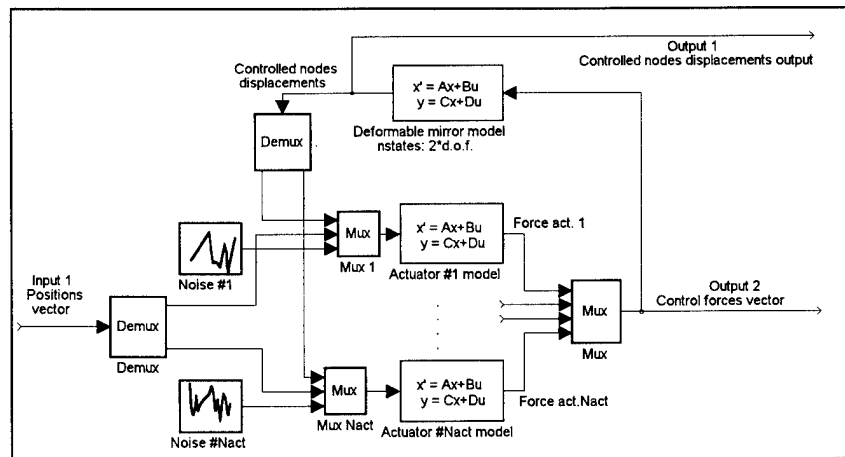
Figure 2: overall system model scheme

The input of the overall system is the vector of reference positions for the actuators, and the outputs are the vectors of the actuators displacements and of the forces produced by the actuators. For every capacitive sensor a noise source is taken into account; the r.m.s. amplitude of the noise being obtained from experimental data.

Control loop design

The goal of the control loop design is to obtain a very stiff position actuator from a voice coil motor controlled in force. The local loop has to fulfill the speed requirements related to the design of the overall adaptive optics control loop. The settling time must be kept within the range of a few milliseconds.

A simple Proportional-Integral-Derivative control law has been chosen with a further high frequency pole added to reduce loop gain at higher frequencies. In order to define the gains of the compensator, a filter-shaped control response design technique has been implemented. The nominal control was designed by a pole assignment technique, referring to an equivalent single degree of freedom mass-spring scheme, with a mass of 3.5 grams and a resonance frequency of 800 Hz; the reference response was given by a fourth order Thompson filter, with a 1300 Hz lowpass band.

Simulations

A phase screen of atmospheric turbulence (simulated according to the modified Von Karman refraction index fluctuations) has been used to model the system input. A wind speed of about 14 m/s has been assumed. A sequence of three successive wavefront corrections performed every 0.01 sec. has been simulated.

Figure 3 shows the displacement response of all the 316 actuators The peak forces needed to achieve these responses are of the same order of magnitude as those required at the steady-state, thus fulfilling one of the control loop specifications.
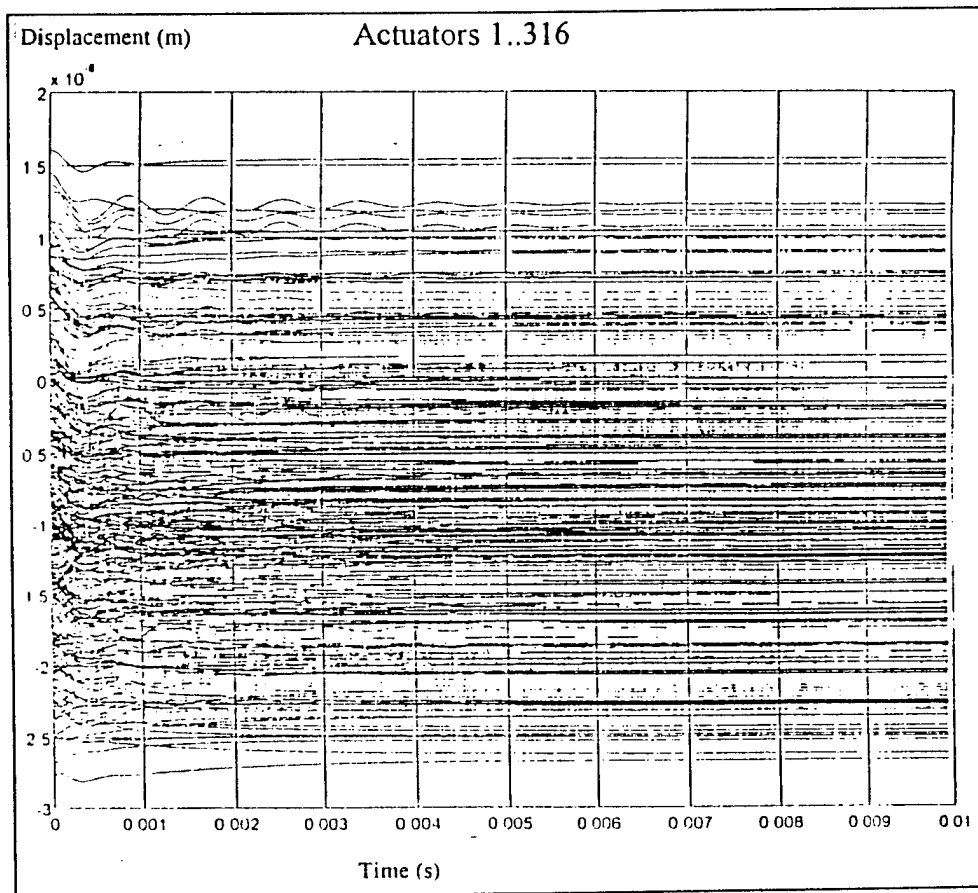
Figure 3: actuators displacements

Concluding remarks

From these simulations the following preliminary conclusions can be taken:

- some passive damping should be introduced on every actuator, to reduce spillover due to the uncontrolled modes which are close to the control cut-off frequency;

- satisfying control performances can be obtained even with simple control laws that, being independent and collocated, can be easily implemented analogically.

The analysis and design methods developed for these particular configurations are effective tools to assist the adaptive optics design. The simulation software integrates in an unique design workspace all the different branches: mechanics, control and electronics.

A Wavefront Generator for Adaptive Optics Testing

Enrico Marchetti[1] and Roberto Ragazzoni[1,2]

[1]Telescopio Nazionale Galileo (TNG) Project Office
[2]Astronomical Observatory of Padova

During day–light adaptive optics systems usually needs an artificial source in order to close the loop and provide checks for tests, upgrades and performances verifications. In this work the wavefront simulator for the Adaptive Optics system of the Telescopio Nazionale Galileo (TNG).

The starfield is generated and the related wavefront is perturbed by a first holographic wheel located at the exit pupil position of a re–imager. In this way all the beams produced by different artificial stars are modified in the same manner. After that a second wheel, located well away from the exit pupil position will deformate the wavefront further in a field–dependent manner. The distance between the two wheels can be changed and the corresponding isoplanatic patch θ_0 can be conveniently arranged.

The rotating speed of the two wheels can be easily modified, translating into different values for the Greenwood frequency parameter f_G or the corresponding wavefront correlation time f_G^{-1}. After all this process a second re–imager will collect the light beams and will fed them onto the adaptive optics system.

The two re–imagers have zooming capability and in this way the ratio D/r_0 of the wavefront simulated can be changed. Being this produced with the same F/, the resulting effect is a r_0 variation, allowing for a free choice of these three fundamental parameters of an adaptive optical system.

Holographical
Wheels

Zoom

To Ad-Opt

Zoom

High Altitude Layer
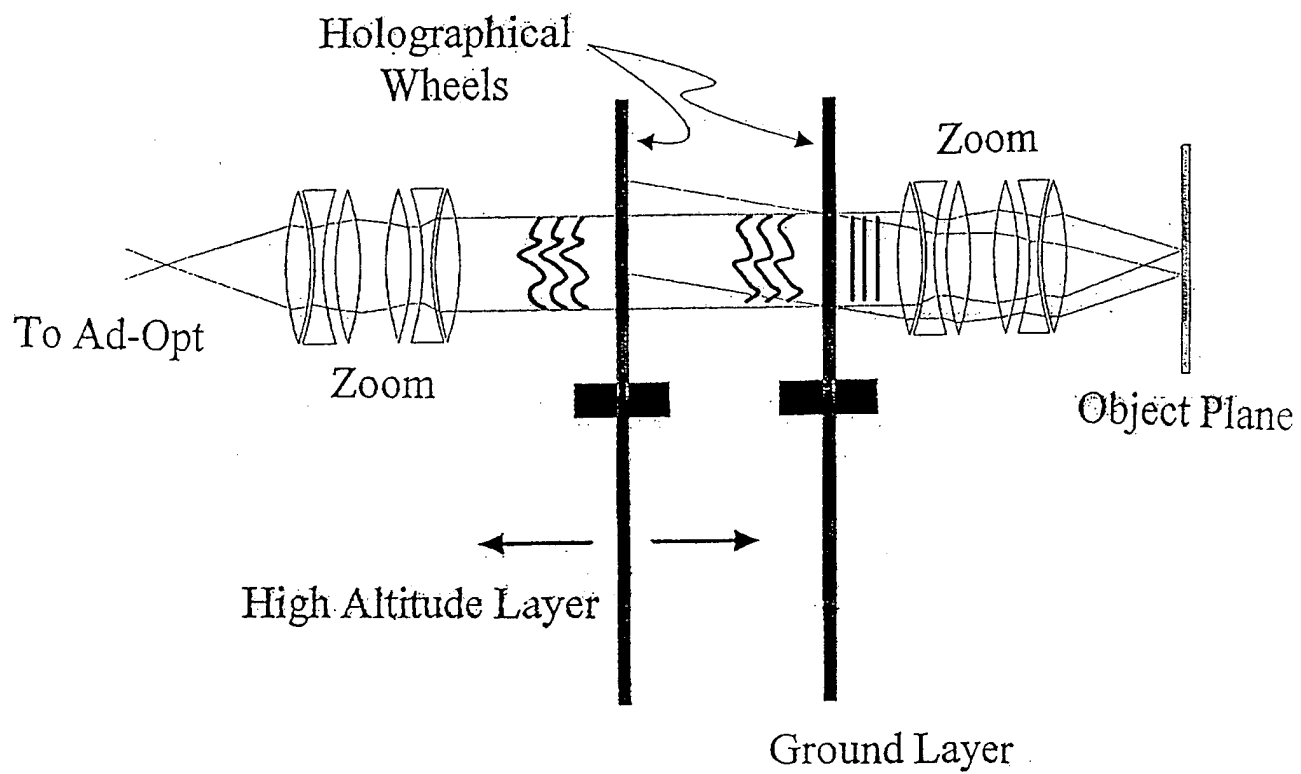
Ground Layer

Object Plane

Figure 1: The sketch of the wavefront starfield simulator.

A New Generation Tip-Tilt System

S. Esposito, L. Fini, P. Ranfagni
Osservatorio Astrofisico di Arcetri
Largo E. Fermi 5,I-50125 Firenze

The Arcetri Adaptive Optics group is in charge to design and build a closed loop control system for the reduction of astronomical *image motion* to be used in the Italian 3.6 meters "Telescopio Nazionale Galileo" (TNG) [4]. After the realization of an analog system prototype [1] the Arcetri Adaptive Optics Group has carried on the project of the final version of the control system that is scheduled to be ready for the telescope first light in middle '96. The *tip-tilt* system is the first step in the implementation of a fully developed system which will also correct higher order terms.

After some years of experience of image motion correction systems it is recognized that the overall efficiency of a *tip-tilt* system depends critically on the optimization of a complex set of parameters which are different for different sources and seeing conditions.

For this reason the main design goals in the development of the *tip-tilt* system have been the flexibility of the architecture and the ease of use. Both aspects have oriented the choice towards a completely digital design which will allow the greater flexibility in the control of loop parameters and, at the same time, naturally lends itself to the integration of the system into a software environment which, through the adoption of proper user interfaces, can help the astronomer to obtain the maximum from the system.

The poster describes: 1) the system architecture, 2) the optical setup and 3) the open and close loop system characteristics and performances.

Figure 1 shows the overall architecture of the *tip-tilt* System. The structure comprehends four major units:
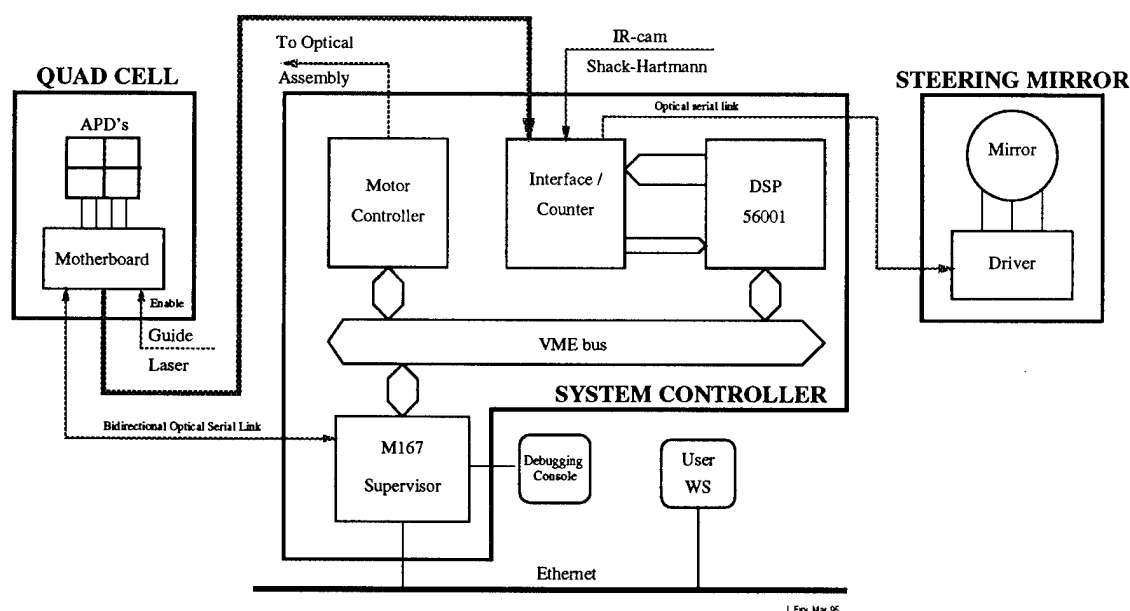

Figure 1: *tip-tilt* System Architecture

—

- the **Quad-Cell** subsystem (QC) controls and gets data from the four APD (Avalanche Photo Diodes) used for image motion sensing. It is made up of four identical boards, the APD drivers, mounted on a motherboard which provides all the required auxiliary functionalities. The QC is located close to the telescope optical path and communicates with the System Controller via dedicated optical fiber links.

- the **Steering Mirror** (SM) subsystem is the electro-mechanical assembly of the *tip-tilt* compensation mirror. It is a flat mirror operated by four voice coil magnets with square geometry in a closed loop with capacitor position sensors[1] produced by *Termotrek*. It is located in the optical path and is connected to the System Controller via a serial optical link which is used to send position data for the three mirror actuators.

- the **System Controller** (SC) is hosted in a VME crate; it contains an Interface/Counter board (IC), a DSP board and a master CPU, or supervisor. The IC is a custom made board which holds both the counters for APD pulses and the interface logic needed to send data to the Steering Mirror, together with other electronics which will be used to receive *tip-tilt* information from other devices[2]. The DSP board is a commercial board holding a Motorola DSP 56001 processor which can communicate with the supervisor via the VME bus. The Supervisor is a commercial MC 68040 based board which controls the entire system.

- the **User Workstation** (UW). While the *tip-tilt* subsystem is designed to be operable standalone, for testing and maintainance purposes, normal operation will be controlled, through a proper user interface, by a Unix Workstation connected via Ethernet.

The laboratory activity has been aimed to the realization and characterization of a closed loop control system for the astronomical "image motion". The system *tip-tilt* sensor employs four EG&G Avalanche Photodiodes (APDs) [3] in a Quad-Cell configuration. The atmospheric *tip-tilt* perturbation is simulated by using a "seeing generator" that gives a power spectral density closely resembling the $-\frac{2}{3}$ and $-\frac{11}{3}$ slopes of the theoretical results for the one turbulence layer case *tip-tilt* PSD. Here we describe the optical set-up needed to feed the sensor splitting the optical beam with a squared base reflecting pyramid. Moreover we report the experimental measurements performed to determine the system linearity range and the open and closed loop system transfer functions. These measures enable us to understand the kind of compensation needed to match the resulting system error transfer function with the *tip-tilt* PSD. Finally we show some results concerning the closed loop system performances in terms of the improvement of Strehl ratio and full width half maximum versus some critical parameters like signal to noise ratio, DC gain and photodiodes integration time.

---

[1]The design derives from a closely related project for the development of an adaptive secondary mirror [2].

[2]To increase the flexibility of the system the design allows to receive *tip-tilt* information from an IR camera or to receive *tip-tilt* correction terms from a Shack-Hartmann wavefront sensor when the *tip-tilt* system will also include the corrector for higher order terms.

References

[1] D. Bonaccini, G. Brusa, S. Esposito, P. Salinari, P. Stefanini, "Projects in Adaptive Optics". *ICO-16, ESO Conference on Active and Adaptive Optics*, 1993, 89.

[2] P. Salinari, C. Del Vecchio, V. Biliotti, "A Study of an Adaptive Secondary Mirror". *ICO-16, ESO Conference on Active and Adaptive Optics*, 1993, 89.

[3] Bonaccini, D., Cova, S., Ghioni, M., Gheser, R., Esposito, S., Brusa, G.: 1994, "Novel avalanche photo-diode for adaptive optics". *Proceedings SPIE* **2198**.

[4] F. Fusi Pecci, G. Stirpe, V. Zitelli, eds., "TNG Instrument Plan: II. A progress Report". Dec. 1994.

Preliminary mechanical design of an adaptive secondary unit for the MMT-Conversion telescope

C. Del Vecchio
(Osservatorio Astrofisico di Arcetri - Largo E.Fermi 5, 50125. Firenze, Italy
Phone +55 2752261, Fax +55 2752292)

W. Gallieni
(ADS ITALIA s.r.l.Sistemi Avanzati - C.so Promessi Sposi 23/d, 22053 Lecco, Italy
Phone +341 259231, Fax +341 250560)

P Salinari
(Osservatorio Astrofisico di Arcetri - Largo E.Fermi 5, 50125. Firenze, Italy
Phone +55 2752290, Fax +55 2752292)

P.M.Gray
(Steward Observatory, University of Arizona - Tucson, Arizona 85721
Phone (520) 6211539, Fax (520) 6219843)

Introduction

The potential advantages of using the secondary mirror of a telescope to perform adaptive correction of the wave front distorted by propagation through the atmosphere are known for long time. Among them are the drastic reduction of the number of optical surfaces, that increases the transmission and reduces the emissivity, and the possibility of providing adaptive corrections to different focal stations. The reduced emissivity makes adaptive secondary mirrors particularly attractive for work at infrared wavelengths where thermal background is of concern, provided that the design of the unit doesn't affect emissivity in other ways (e. g., with high emissivity surfaces surrounding the secondary). Another desirable feature of an adaptive secondary (AS) is the capability of providing, in addition to wave front correction with many degrees of freedom, also a large (> 0.1 mm) range of motion to perform "chopping", that is useful for sky subtraction even with modern two dimensional IR detectors. A conceptual approach to the design of an AS with the above features (+) was followed by a variety of studies and experiments that are still in progress (Bruns et al., Biasi et al., Biliotti et al., in this Conference). This paper reports the results of a preliminary study of the various problems related to the general layout, to the support of the optics and to the thermal aspects, in the specific case of the secondary mirror unit for the F/15 Cassegrain focus of the MMT Conversion telescope.

General layout and approach

The main subsystems shown schematically in Fig 1 by capital letters are briefly discussed in this paragraph. The top section of the secondary mirror unit, also visible in Fig. 1, is used for the projection optics of the laser reference star, and is not discussed here.

A: The active alignment stage supporting all the rest of the system.
We are comparing various options for this stage. The one in Fig.1 uses six position actuators mounted in a "hexapod" geometry and provides 6 degrees of freedom, five of which are used for tilt, tip, collimation and focus of the unit. The requirements are similar to the alignment stage of an "active" secondary mirror: range of adjustment of several mm, accuracy of about 1 micron.

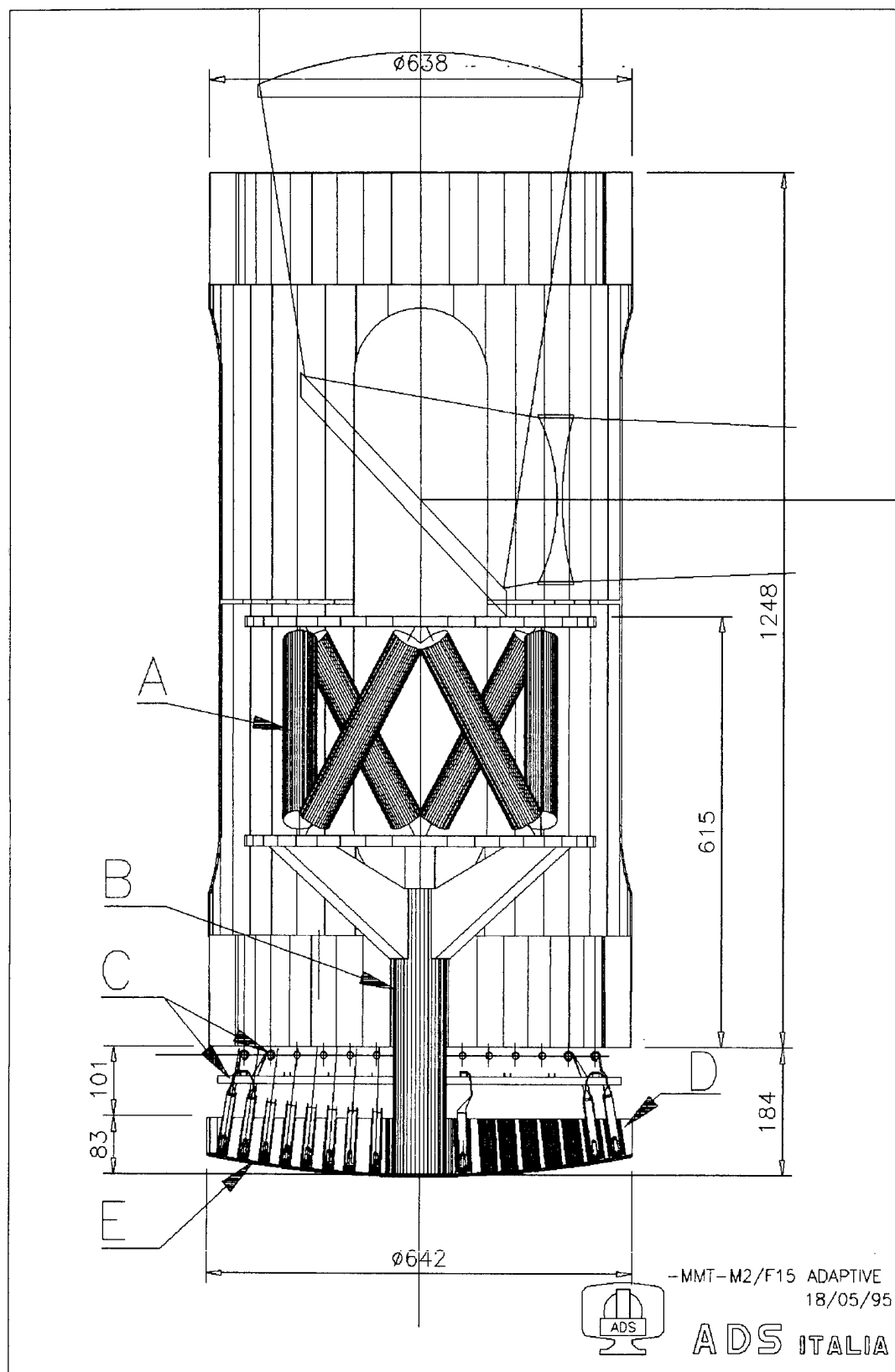B: The support system for the rigid perforated back plate.

Ø638

1248

615

A

B

C

101

83

184

D

E

Ø642

−MMT−M2/F15 ADAPTIVE
18/05/95

ADS
ADS ITALIA

Fig. 1: Scheme of the Adaptive Secondary Unit.

The back plate (which in turn supports the actuators) constitutes the reference for the measurement of the position of the thin deformable mirror (E). The requirements for the support of the back plate can be relaxed considerably, with respect to a conventional secondary mirror, due to the possibility provided by the system of actively correcting slow figure changes of the back plate. If one adopts a sufficiently thick back plate (~100 mm) and uses active correction, the back plate can be supported only in the centre, as shown in Fig. 1, . Six additional astatic supports (not shown in Fig. 1) must be added to reduce back plate deformation if it is relatively thin. Six astatic supports and a thick back plate can provide the necessary figure stability for a passive mode of operation.

C: The distribution of power and signals and the heat sink.
The design of these utilities, schematically represented by two horizontal planes in Fig.1, is made complex by the requirement of accessing, and, if necessary, replacing each individual actuator without disassembling the whole unit. An heat dissipation of less than 1W is foreseen for each actuator and for the associated electronics. This heat can be damped to a refrigerant fluid as shown in Fig. 1 by conduction. Other options are also possible. The requirement is to maintain temperature differences of a fraction of a degree C in particular between the thin mirror and ambient air. Larger temperature differences with respect to ambient air are allowed inside the unit, whose side and top are thermally insulated.

D: The back plate.
Is made of low expansion glass equal to that used for the thin mirror, is perforated to accommodate the coils, the sensors, and the local electronics, that are represented only schematically in Fig. 1 as the detailed design of the actuator is not part of this study. The separation between actuators was chosen to be 30 mm, and the diameter of the perforations 28 mm to examine a worst case and provide space for possible evolution of the actuators. The holes in the bottom plate are 8 mm in diameter. In Fig. 1 the axes of the actuators are normal to the surface of the thin mirror, but it is also possible to have them parallel to the optical axis.

E: The thin deformable mirror.
The outer edge of the 2 mm thick, 64 cm diameter mirror is free and defines the pupil of the telescope. It is supported at the centre by a membrane in tangential directions and is supported axially, in operation, only by the electromagnetic forces applied by the coils on the magnets attached to the back of the thin mirror. Of course when not in operation the mirror is supported by the central membrane and by a number of small retaining stops at its outer edge. The configuration chosen for the capacitive sensors (see Bruns et al, this Conference) does not require electrical connections between the thin mirror and the back plate. The static and dynamic analysis of the thin mirror, its influence function and the level of correction attainable for different deformed wave fronts was examined previously (+), while the numerical simulation of the behaviour of the entire system, including the local position control obtained with the force actuators, is the subject of a parallel paper (Gallieni et al., this Conference).

Conclusions

Although much work is still necessary on many details, the basic mechanical design of an adaptive secondary unit, here described for the specific case of the MMT-Conversion, seems to be well feasible along the lines we considered.

(+) P. Salinari, C. Del Vecchio, V. Biliotti (1993). Proceedings of the ICO-16 Conference on Active and Adaptive Optics, F. Merkle editor, ESO Proceedings N 48, page 247.

New Wavefront Reconstructor for the MMT Adaptive Secondary

Steven M. Stahl, ThermoTrex Corporation, 9550 Distribution Avenue, San Diego, CA
92121 (619) 536-8552, FAX (619) 536-8538.
Todd K. Barrett, ThermoTrex Corporation, 9550 Distribution Avenue, San Diego, CA
92121 (619) 536-8562, FAX (619) 536-8538.

In this paper we present a reconstructor optimized to fully utilize spatial and temporal correlations of the measured wavefront and a hardware implementation being built for the adaptive optics system for the new 6.5m single-mirror MMT. We compare the projected performance for a closed-loop system which drives the mirror to obtain a wavefront sensor null with a system designed to "optimally" utilize measurements from the source--which may be a laser guide star.

The optimal configuration of an adaptive optics system at any instant is that which conjugates the atmospheric phase seen through the pupil. Any approach taken by a real instrument will be an approximation to this. It has already been recognized that a solution which minimizes the error between the wavefront sensor slope measurements and those produced by the deformable mirror is not the same as that which minimizes the residual phase error produced after the adaptive optics.[1] A closed-loop null-seeking system which seeks to drive the measurements to zero is essentially the former. Since the MMT adaptive secondary will have capacitive internal feedback to monitor the mirror position, we may implement an alternate reconstructor which takes full advantage of spatial and temporal correlations in the phase. The advantage of this "two-loop" approach is that the bandwidth of the atmospheric sensing loop can be reduced allowing longer integration times and lower sodium laser power.

The spatial correlations in a single "frozen" instance of turbulence are well known, and may be used to estimate an optimal reconstructor using a standard prescription. If we consider the measurements to form a vector S, consisting of the gradient of the phase, while the phase in the pupil is ϕ, the optimal reconstructor M is formed according to $M = <SS^T>^{-1} <S\phi>$. The correlations might be computed online using real data or predetermined based on typical seeing conditions.[2] There will necessarily be some delay between the acquisition of data and positioning of the adaptive optics. Given past data, it should be possible to gain in performance by taking into account correlations in time as well as in space. Assumption of Taylor's "frozen turbulence" hypothesis for a single dominant layer driven by a known wind immediately prescribes a relationship between the "predicted" phase and the measurements.[3] The possible advantages of this approach have already been demonstrated.[4]

The MMT will include a sodium laser guide star. This introduces focus anisoplanatism which can be filtered using a matrix trained on data from a point source accompanied by laser observations. Given an inner mirror control loop which operates much more quickly than the Greenwood frequency presents us with the opportunity to craft a reconstructor designed to obtain the best OTF rather than to move spots on a wavefront sensor to their respective detector centers.

Our real-time-reconstructor hardware is based on board level components which conform to the VME bus standard. We have made an effort to use commercial off-the-shelf

hardware whenever possible in order to reduce costs, reduce development time, and increase reliability. We have succeeded in designing and integrating a system which is quite flexible and is able to accomplish all the computational goals described above with only two custom components required to convert digital I/O formats when passing data between components.

Figure 1 is a simplified block diagram of the reconstructor hardware. The user interface to the hardware and the development platform are accomplished with a SUN workstation running Solaris. The VME bus containing the computational boards is mastered by a single board computer (labeled Adaptive Optics Control computer or AOCC in the figure) manufactured by Motorola with a 68040 CPU. The bus master runs the VxWorks real-time operating system. Subaperture slopes are computed using 4 floating point Texas Instruments TMS320C40 DSP processors on a single VME board (labeled the subaperture slope computer SSC) manufactured by the Pentek Corp. Data is passed to a second quad C40 board (labeled the input output controller IOC) which completes preprocessing the data and orders it for the real-time reconstructor. The resconstructor input vector is transfered from the quad C40 board to the real-time resconstructor via one of the custom I/O formatting boards. The real-time rescontructor consists of a single VME board with a total of 512 integer multiply accumulators running at 10 MHz (labeled the real-time reconstructor RTR) manufactured by Adaptive Solutions Inc. The RTR reconstructs the waveform and outputs actuator commands back to the IOC controller which orders and formats the data for output to the deformable mirror drivers. Diagnostic data is provided via two components (labeled diagnostic controllers DC) which consist of a board with a single C40 processor and a second dynamic memory board. The DC store the raw wavefront sensor data, the computed subaperture slopes and the actuator commands.

Our design is both flexible and quite powerful. The C40 DSP processors allow various preprocessing algorithms to be implemented while the 5 GigaOp RTR allows the acutal wavefront reconstruction to be accomplished with almost no added latency. The RTR hardware also has the ability to implement adaptive delta-rule training on the matrix weights, so that it will be possible to implement a reconstructor which adapts to atmospheric conditions during operation.
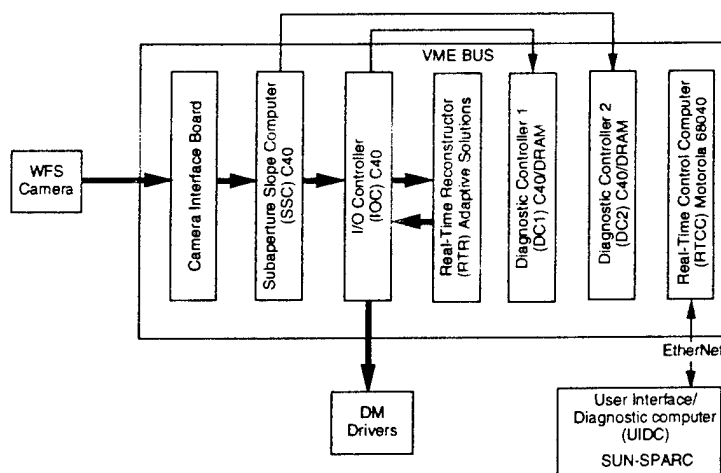
Figure 1.

[1] Michael C. Roggeman, "Optical Performance of Fully and Partially Compensated Adaptive Systems Using Least-Squares and Minimum Variance Reconstructors," Computers Elect. Engng. 18, 451-466 (1992).

[2] Michael Lloyd-Hart, et. al., this conference.

[3] C. Schwartz, G. Baum, E. N. Ribak, E. N. Lipson, S. G. Lipson, "Fractal nature of atmospherically degraded wave fronts--an aid to prediction," SPIE Proceedings 2201 (1994).

[4] S. Stahl and D. G. Sandler, "Optimization and Performance of Adaptive Optics for Imaging Extrasolar Planets", submitted to ApJ Lett.

Force-Actuated Adaptive Secondary Mirror Prototype

Donald G. Bruns, Todd K. Barrett, and David G. Sandler, ThermoTrex Corporation,
   9550 Distribution Avenue, San Diego, CA 92121, USA, Phone (619)-578-5885, FAX (619)-536-8538,
H.M. Martin, Guido Brusa, Dave Modisett, and J.R.P. Angel, Steward Observatory,
   University of Arizona, Tucson, AZ 85721, USA, Phone (520)-621-2288, FAX (520)-621-1532
Roberto Biasi and Daniele Gallieni, Dipartimento di Ingegneria Aerospaziale,
   Politecnico di Milano, via Golgi, 40 20133 Milano, Italy Phone +39 2 2399 4049, FAX +39 2 2399 4034
Piero Salinari, Osservatorio Astrofisico di Arcetri,
   Largo E. Fermi 5, 50125 Firenze, Italy Phone +55 2752290, FAX +55 2752292.

1. Introduction

The new 6.5 m single mirror Multiple Mirror Telescope (MMT) will be equipped with adaptive optics capabilities. In particular, high resolution infrared astronomy will use a new adaptive secondary on a regular basis. Before we design the adaptive secondary in detail, we fabricated a smaller prototype mirror using similar actuators and actuator geometry. The prototype's purpose is to debug the components and allow comparisons with theoretical predictions. We are studying system interactions and looking for unexpected performance characteristics. Manufacturing techniques and reliability are also being tested, to reduce risks when building the adaptive secondary.

2. Adaptive Secondary Design

Figure 1 shows a preliminary adaptive secondary design. A total of 320 electromagnetic (voice coil) force actuators, 32 mm apart on a square grid, push on a thin, 640 mm diameter glass mirror. The thin mirror's figure is referenced to a thicker, relatively stable glass surface. Fast capacitance-based position sensors located at each actuator continuously maintain the precise distances based on wavefront sensor data. The position sensor (inner control loop) is independent of the wavefront sensor (outer control loop), and serves to reduce the wavefront sensor sampling frequency requirement. This allows either weaker sensor input signals or a higher signal to noise ratio with the same signals. The end result is higher system performance.
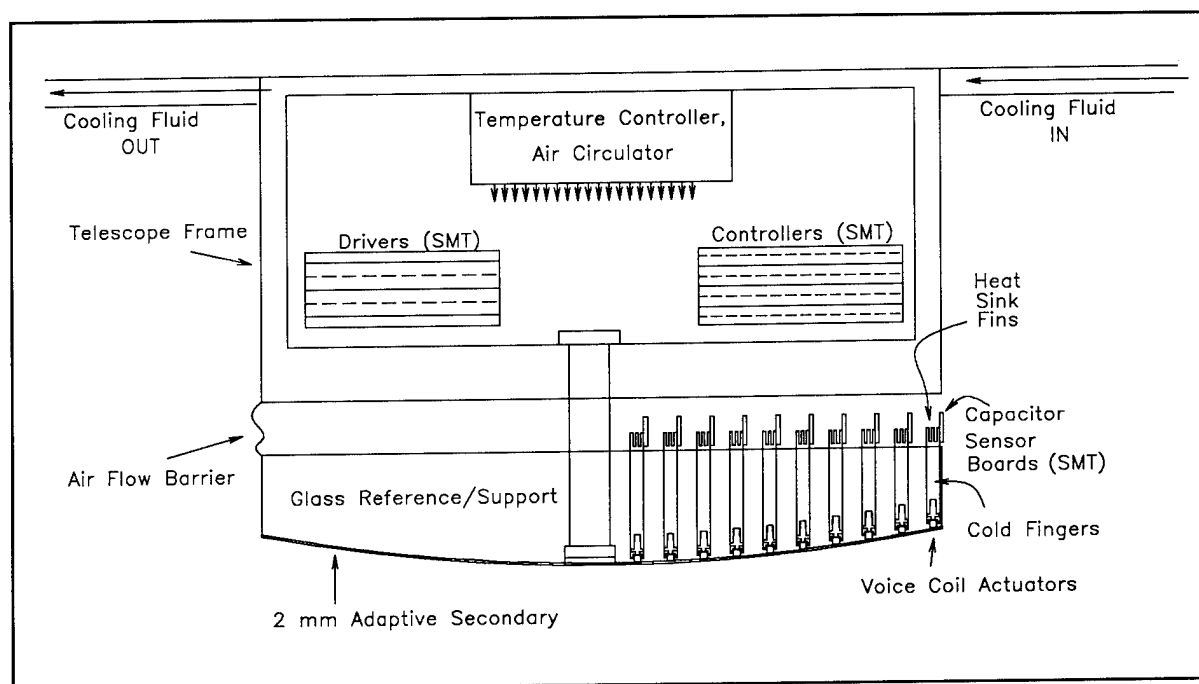

Figure 1. Adaptive Secondary Configuration

3. Actuator Design

Figure 2 shows the details of the glass and actuator design. Fifty microns separates the polished glass surfaces. A heat-conducting cold finger inserted into the reference surface contains the voice coil, a bias magnet, and connections to the capacitor sensor. The bias magnet reduces the actuator force requirement by providing a fixed force against gravity. We use a sensor arrangement which requires only one electrical connection to the secondary, simplifying assembly. The entire back surface of the adaptive secondary mirror is metallized to form one electrode, then connected to a square wave signal source through its central support. Around each actuator is a single annular capacitor electrode used to measure the gap between the reference surface and the secondary.
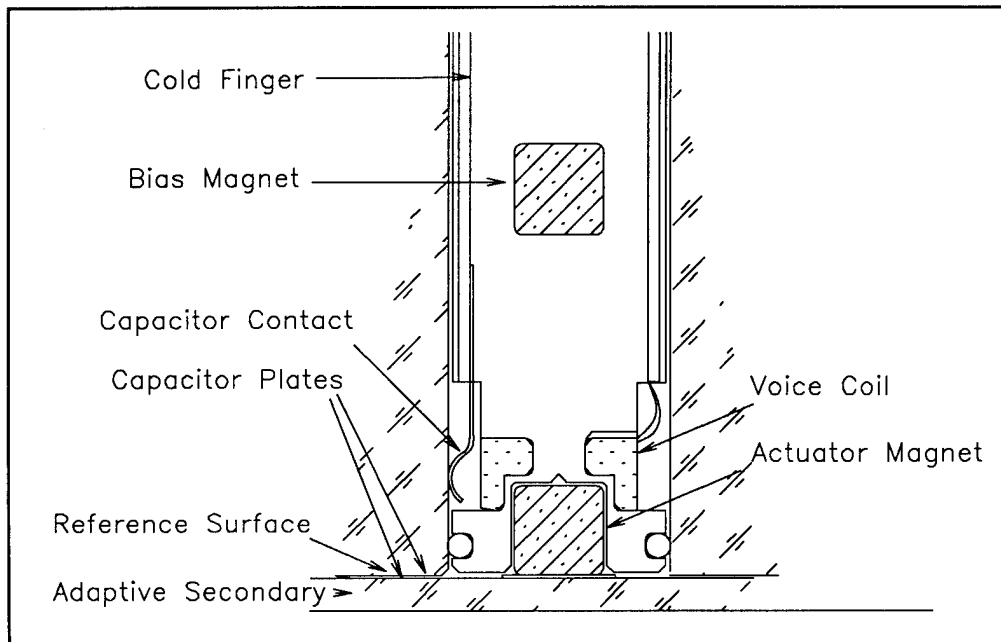

Figure 2. Actuator Assembly

Using 6.3 mm diameter rare earth magnets, the actuators required only 16 mm diameter holes bored through the reference glass. This removes only 1/4 of the total glass, leaving a stiff reference surface. In cases where the adaptive secondary is used without wavefront sensing, closing the inner feedback loop around a specified capacitor position should maintain a figure calibrated to the reference surface.

The magnet is large enough to provide an efficiency of 0.36 N/$\sqrt{W}$. We base the force necessary to deform the adaptive mirror to correct atmospheric turbulence from a previous finite element model[1]. For that study, the RMS force is only 0.05 N, requiring only 0.02 W per actuator. The estimated effects of wind (0.05 N), worse case gravity error (0.02 N), and static figure error (0.01 N) combine to make the total RMS force as large as 0.1 N. This leads to an RMS power of 0.1 W, or about 30 W for the entire adaptive secondary actuator array. At this power level, the cold finger input must be cooled only 0.2° K to maintain the ambient temperature at the secondary. The electronics in the sensors and the drivers add 100 W to the system, but these are far from the mirror. Temperature controlled, internally circulated air cools the actuators and the electronics.

A small printed circuit board, using surface mount components, contains the capacitor sensor circuit. To reduce noise, we want to place the capacitor sensor as close as possible to the capacitors on the adaptive secondary mirror. Because this circuit generates as much or more heat than the voice coil, however, it must be kept away from the adaptive secondary mirror. The best compromise placed it just off the cold finger, using a low stray-capacitance conductor down the cold finger hole. This conductor is near ground potential, so it produces a minimal effect on signal linearity or noise.

4. Twenty-five Actuator Prototype Design

To test the concept on a smaller scale, we built a twenty-five actuator prototype, shown in Figure 3, using the same actuator geometry as the planned adaptive secondary. This is large enough to explore the complicated control loops and to test the components and the assembly procedures.
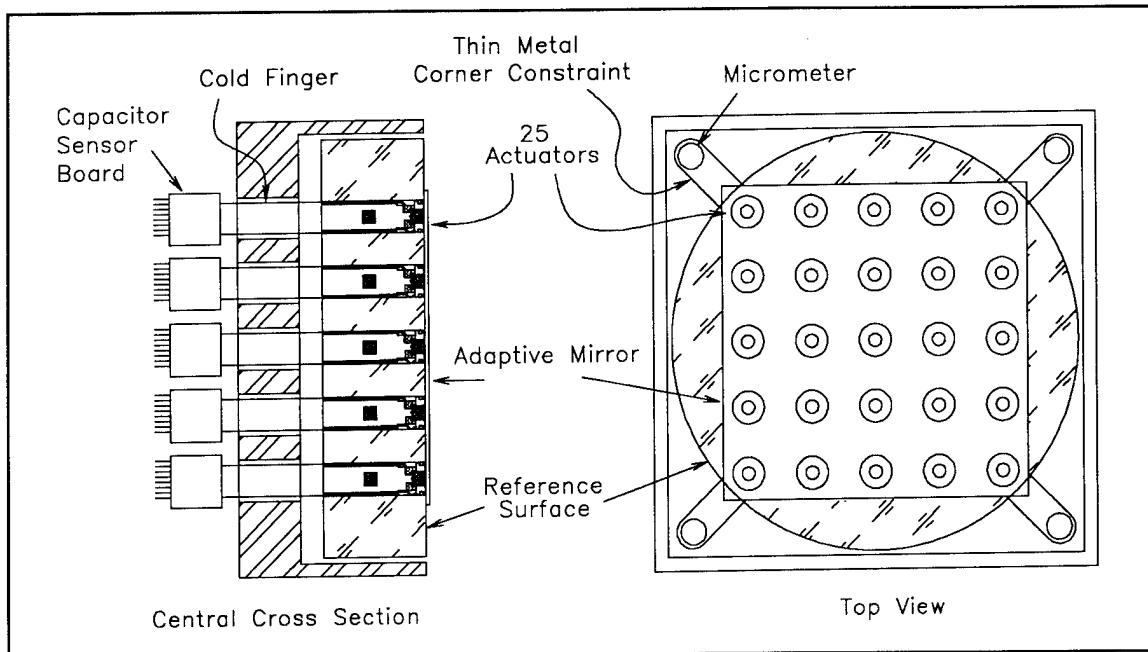

Figure 3. 25-element Prototype

This prototype uses a 200 mm diameter, 38 mm thick reference surface with 25 each, 16 mm diameter holes bored through on a 32 mm square grid. A 150 mm square, 2.2 mm thick glass mirror is suspended by flexible supports at each corner. These supports constrain motion transverse to the reference surface, but allow free motion in the vertical direction. The magnets, capacitors, and actuators are identical to the ones designed for the adaptive secondary.

5. Twenty-five Actuator Prototype Measurements

A digital feedback loop will be used to control the actuators for this prototype. The number of channels make tuning each loop difficult in an analog system. Once the digital algorithm is defined, we will design the equivalent analog circuit to be tested on the next prototype iteration.

We will implement the digital control loop with commercially available DSP hardware. These VME boards digitize the capacitor sensor output voltages, process the control loop, and output the analog control signals at a 10 kHz rate. Simple current driver electronics boost the signals from the computer to the voice coils.

The initial feedback tests will look at stability for quasi-static control. One or more actuators will be given a small force step function, and the algorithm coefficients will be adjusted to make the mirror respond correctly in a short period. We will monitor the adaptive mirror position with the capacitor sensors and with several types of laser interferometers. For static actuator influence function measurements, a Fizeau interferometer will be used. To measure transient responses, a high speed figure sensor with 31 x 31 pixel resolution will be used. Once the system works satisfactorily with a few simple actuator commands, we will apply simulated Kolmogorov turbulence corrections. The control algorithm will be optimized for the maximum bandwidth and the lowest residual errors consistent with guaranteed stability. Total and peak actuator power measurements will be recorded. Measurements of these operating conditions will be extrapolated to the full adaptive secondary.

1.) P. Salinari, C. Del Vecchio, V. Biliotti, Proceedings of the ICO-16 Conference on Active and Adaptive Optics, 1993, p. 247.

Proposed design for a scalable dye laser for use in sodium laser guide star generation

G P Hogan and C E Webb

Laser Group, Clarendon Laboratory, Parks Road, Oxford OX1 3PU UK

Tel: +44 1865 272259 Fax: +44 1865 272400 Email: g.hogan@physics.ox.ac.uk

Introduction

In designing a laser system for application as a source for a sodium laser guide star there are a number of fundamental constraints which affect the design choices to be made.

The maximum peak intensity imposed by the saturation intensity (I_{sat}), the relatively high average power required, the necessity for time gating imposed by the Rayleigh scatter for most installations, and importance of high beam quality all combine to restrict considerably the design of a system in this application.

In addition, if it is to be of use in a telescope environment, there are a number of additional demands on the system, such as input power and cooling requirements (and hence efficiency of the system as a whole), distribution of components in terms of weight and heat management, and, of course, cost (both initial and running), reliability and maintenance.

Our Approach

To generate the 590 nm of the sodium D_2 line a certain amount of tunability is required. The most obvious way to generate tunable laser light is the use of a dye laser, however, solid state alternatives using non-linear techniques do exist [Jeys, 1991].

The approach that we have chosen is one which addresses the issue of scalability. Our aim is for an architecture based on individual sub-units, each of which provides an output not exceeding the saturation intensity for the sodium. Combining the outputs from an arbitrary number of these sub-units in such a manner that is I_{sat} is never exceeded is the principle problem which must be overcome. This scalable architecture offers a number of advantages: in the initial stages of development, it allows proof of principle demonstration of, first the sub-unit design and performance, and then the multiplexing of two such sub-units; it allows a sodium laser guide star system, once installed on a telescope, to be gradually upgraded as requirements and viewing bands change, or additional funds become available; and it allows a system to be closely tailored to the requirements of any particular telescope and instrumentation without entailing unnecessary cost, power and cooling burden.

Multiplexing

To implement a scalable architecture it would be necessary to multiplex the outputs from each sub-unit. This could be done either simultaneously or sequentially. If I_{sat} is not to be exceeded then sequential combination of short duration pulses, each of intensity I_{sat}, represents one potential strategy. If a dye laser is to be employed then the use of the maximum intensity allowable assists the optimum conversion of pump power.

We have opted to use copper vapour lasers (CVLs) as the pump source for our dye laser sub-units. CVLs represent an efficient source of pulsed visible laser power at high pulse repetition frequency (prf) and with reasonable pulse parameters. They can be combined in a MOPA configuration highly efficiently, and can be readily commercially obtained in a range of output powers. Our approach, however, is not specifically tied to this pump source – solid state lasers could be used as dye laser pump units.

The most appropriate design of dye laser in this application is that of oscillator – amplifier configuration. It will be necessary for the oscillator(s) to incorporate a wavelength lock and appropriate bandwidth optimisation. If the output pulses from an arbitrary number of dye laser sub-units are to be sequentially time multiplexed then either each dye amplifier must have its own oscillator, or a single master oscillator must be used to feed all amplifiers. If the latter course is chosen then the dye master oscillator (DMO) must either run at the maximum, multiplexed output frequency (potentially hundreds of kHz) or be CW. We have chosen to use a CW DMO, which can incorporate the wavelength and bandwidth control. The output of this DMO will be fed sequentially to the dye amplifier in each sub-unit.

As the peak intensity of a CW DMO is very much lower than that of a pulsed unit of similar average power, a single amplifier stage would not give efficient conversion of pump power into the output beam. For that reason we are currently working on a retro-propagating, double pass arrangement in which a mirror behind the oscillator cell returns the beam along its own path after it has been pre-amplified on its first transit, thus ensuring saturation, and efficient conversion on the second pass.

The most difficult part of the sequential time multiplexing scalable architecture is the efficient combination of the outputs of all the dye amplifier sub-units (and simultaneously the distribution of the DMO seed beam). We propose two alternative strategies to accomplish both parts of the process.

The first is conceptually the simplest, and is the cheapest. A multi-facet, polygonal

mirror is mounted on a high speed, high precision air bearing spindle (Fig 1). The rotation scans the CW DMO seed beam, via secondary pick off mirrors, into each dye amplifier sequentially. Over the ~30 ns of the pump pulse duration however the incremental rotation is negligible. It is double pass amplified, as described above, and returned back along its outward path, being separated from it by a polarizing beam splitter cube in combination with a quarter wave plate. Accurate timing is accomplished using a secondary, low power CW laser beam, also deflected by the spinning mirror, and an array of photodetectors to provide trigger pulses to the CVL pump lasers.
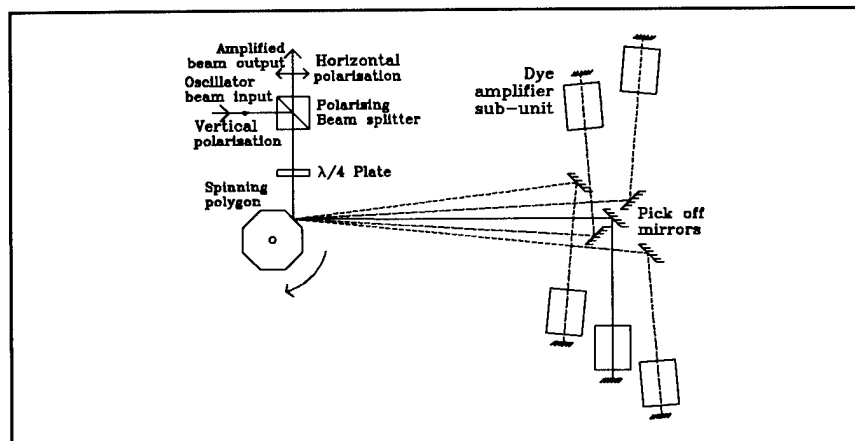
Figure 1

A more elegant, though more expensive, solid state approach employs a high speed Pockels cell, a polarizing beam splitter cube and a combination of mirrors and quarter wave plates, associated with each sub-unit (Fig 2). This has no moving parts, and allows a greater degree of multiplexing, owing to potentially closer spacing of pulses in time, although transmission losses through a large number of sub-units could impose a practical limit.
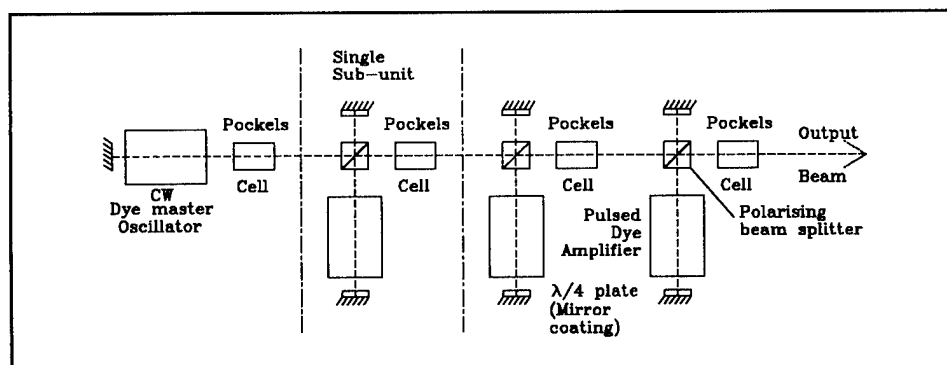
Figure 2

References

Jeys T H (1991); *The Lincoln Lab Journal* **4** (2) 133-150

Control Loop Analysis and Characterization
for an
Adaptive Optics Experiment on the Starfire 3.5m Telescope

Stephen Browne, Jeff Vaughn, Glenn Tyler
the Optical Sciences Company
P.O. Box 25309
Anaheim, California, USA 92825-5309
Phone: 01-714-772-7668
FAX: 01-714-772-9870

John D. Gonglewski
USAF Phillips Laboratory
Albuquerque, New Mexico, USA 87109
Phone: 01-505-846-4405
Fax: 01-505-846-2045

David Dayton, Steven Sandven, Darren Laughlin
Applied Technology Associates
1900 Randolf SE
Albuquerque, New Mexico, USA 87106
Phone: 505-845-6110
Fax: 505-768-1391

Ron Highland
Kaman Sciences Corporation
6400 Uptown Blvd
Abluquerque, NM   87112
Phone: 01-505-889-7027
FAX: 01-505-889-7040

An experiment with a nasmyth adaptive optics system mounted on the SOR 3.5m telescope employs an adaptive optical imager. A 148-subaperture hexagonal lenslet array provides a Hartmann wavefront sensor for the 163 actuator mirror to which it is mated. Our analysis of the control loop of the adaptive optical system is edified, and the actual implementation is explained. Performance tradeoffs between various subaperture geometries, based on reconstructor noise gain and stability considerations, are presented. A fast algorithm for measuring Hartmann spot positions is combined with a computationally efficient reconstructor running on a pair of i860XP processors to achieve 1000 reconstructions per second. Moreover, the reconstructor can perform much of its processing on the fly while the frame is being transferred from the pupil plane camera, resulting in significantly reduced servo phase lag. We describe the control loop design, with particular emphasis on the creative use of hardware data paths.

System Electronic Design for a Compact Deformable Mirror System

Sam Rogers, Scot McDermott
Logicon R & D Associates
2600 Yale SE
Albuquerque, New Mexico, USA 87106
Phone (505) 842-8911

System design for an remotely controlled adaptive optics package to be mounted on the side of a large telescope involves many components. The design goals, hardware used (wavefront sensor , deformable optics and reconstructor hardware), the final system design, and some results from an experiment performed on the SOR 3.5 meter telescope will described in this paper.

Optics Design of Compact Deformable Mirror Experiment

David Dayton, Darren Laughlin
Applied Technology Associates, 1900 Randolf SE, Albuquerque, NM 87106

John Gonglewski
Air Force Phillips Laboratory, PL/LIMI, Kirtland Air Force Base, NM 87117

1. INTRODUCTION

Optical Design of a compact adaptive optics systems, to be mounted on the side of a large telescope presents special problems. In particular the limited space requires fast optics. Signal to noise requirements for the wave-front sensor also require that the optics work over a wide optical band. In this paper we describe the design and layout of such an adaptive optics experiment performed on the SOR 3.5 meter telescope.

2. OPTICS LAYOUT

Figure 1 shows the breadboard layout of the optics for deformable mirror experiment. The experiment was required to fit on a 4 by 4.5 foot optical bench mounted vertically at the yoke tine position of the SOR 3.5 meter telescope. The full paper will go into more depth about the optical design and some of the problems encountered.
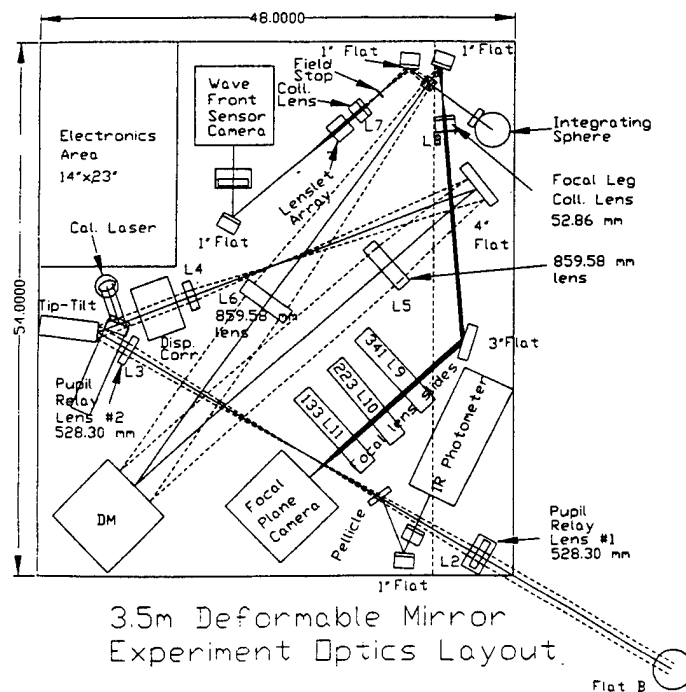

Figure 1 Low Order Adaptive Optics Experiment Layout

Gemini 8 Meter Telescopes Active Guiding System Considerations

Charles Jenkins
Nick Dillon

Royal Greenwich Observatory, Madingley Road
Cambridge, CB3 0EZ United Kingdom

Mike Burns
Rick McGonegal
Jim Oschmann
David Robertson

Gemini 8-Meter Telescopes Project, 950 North Cherry Avenue
Tucson, Arizona 85719

The GEMINI telescopes are intended to deliver very good image quality with only tip-tilt correction at the secondary mirror. Designing the guiding systems for these telescopes has made use of simple yet accurate models of the image size. These are described here, with illustrations of the complex tradeoffs that are necessary to achieve the best images. The current design of the guiders is given. These also serve as active optics wavefront sensors to provide closed loop control of the telescope alignment and figure at slow rates.

It is well-known that correction of atmospheric image motion can yield very worthwhile improvements, especially near $D/r\_0 = 4$ and for a guide star close to the object of interest. Equally it is known from experience that "fast guiding" is beneficial when $D/r\_0 >> 4$, even when the guide star is well off-axis. To make a proper assessment of the likely benefits of fast guiding, and indeed to define important parameters such as the required sampling rate, it is necessary to recognize the many factors that may affect delivered image width. It is extremely convenient if the model that represents these factors is simple enough to allow rapid exploration of the resulting large parameter space.

The importance of image quality to the GEMINI project has lead to a well-developed error budget for image quality with detailed estimates of the main sources of error. From the point of view of guiding on an offset star, the major ones are:

(i) most importantly, the raw seeing;

(ii) uncontrolled telescope shake due to wind;

(iii) photon and detector noise;

(iv) differential image motion between the guide star and the target (angular anisoplanatism);

(v) uncontrolled atmospheric image motion (temporal anisoplanatism);

(vi) rapid changes in telescope focus, due to wind loading;

(vii) non-reproducible, time-varying offsets between the science focal plane and the guider focal plane (labeled "flexure" in what follows).

Some of these factors are isoplanatic and some not; some depend on wavelength and some do not.

In this list we have not included irregularities in the telescope drive itself, because on an 8-m telescope it is easy to sample sufficiently rapidly on the guide star to control these errors.

Exhaustive calculations of wind loading on the GEMINI telescopes and domes have yielded a very detailed understanding of the power spectrum of windshake. [1] The servo performance of the control loop on the secondary mirror has of course been calculated. Theoretical atmospheric properties are well-understood, although the input parameters (especially the speed and effective height of the turbulence) are not well known. The surface density of stars has been measured and theoretical models are also available. Finally, estimates are available of the "flexure" in the mechanical systems which will support the proposed GEMINI guide probes. As described elsewhere at this meeting, these will be of two sorts; one where the guide probes patrol a large off-axis area, and another where a small field close to the target can be accessed.

From these analyses, it is apparent that the delivered image quality for GEMINI will be the result of a complex interplay of factors. Windshake tends to push the required sampling rate high (>200 Hz, in fact) and also demands lower latency in the control loop. This collides with the shortage of sufficiently bright guide stars; these can only be found well off-axis where anisoplanatism can outweigh the benefits of correcting windshake. Appreciable focus jitter poses the same benefits in a more acute form, because of the smaller isoplanatic angle for focus compared to tip-tilt. Large flexures of course tend to wash out atmospheric effects and reduce the relative penalties of guiding well off-axis. Finally we note that for CCDs used as fast guiders, increasing the frame rate inevitably results in greater readout noise.

Estimating likely performance, and making design trade-offs, requires an integrated model of the process of image formation. This model needs to be reasonably accurate, easy to use and fast in execution. We have built such a model and believe that many parts of it will be useful to other designers of guiding systems. It is, in essence, a generalisation of Fried's original model of the tip-tilt corrected PSF. Modern derivations of the adaptively-corrected PSF show easily how Fried's result may be derived as an intelligible approximation,[2] and moreover how both isoplanatic and anisoplanatic errors, and temporal effects, may be included. Anisoplanatic effects have been calculated by Chassat. [3]

Flexure and focus are special cases. Flexure is of course attitude-dependent, and we have used archival data from the La Palma telescopes to derive the flexures that would occur in practice. For any single observation, flexure will generally elongate the image. Averaged over a large number, however, its effect will be very like that of a rapid Gaussian jitter, whose effect can be modelled as described. Including focus jitter would require a considerable extension of the model, because the basic equation for the PSF is then more complex. Fortunately in our case the jitter is small enough to neglect; the errors introduced in trying to track focus are nearly equal to the original jitter.

Evidently such a model will have an inevitable stochastic character due to the random occurrence of guide stars. We have handled this in a simple and robust way by using the median; that is, performance is calculated for stars at a median off-axis distance for their brightness. This translates directly into median image size when other parameters (e.g.wind speed) are fixed. (We have not considered a full multivariate statistical case, or the distribution of image size, which is computationally much more formidable.)

Some results will be shown for the proposed GEMINI guiders. As one might expect in a situation with conflicting demands on guide star brightness and sampling rates, the median delivered image size has a minimum for a unique combination of sampling rate, latency and guide star magnitude. This is complicated by the desire to use a single wavefront sensor to provide this guiding information as well as slow signals for control of the telescope alignment and primary mirror figure (ao called active control). Our current concept of the guider is shown. This supports closed loop active control of the primary mirror (on the order of 15 Zernike terms or mirror modes) and telescope alignment at rates of about once per minute in addition to up to 200 Hz sampling for tilt and focus measurements. Investigating the sensitivity of the median value to the parameters of the design has allowed us to make informed decisions about, for example, the geometry of the CCD used in the guider and the effect on the PSF of flexure.

In operation, the user will often have a choice of several guide stars and one will be the best. It is planned that some basic atmospheric and telescope data will be available in real time so that the best choice can be made.

REFERENCES

1. Burns, M., 1994, "Tracking Performance Simulation of the Gemini 8-M Telescopes, SPIE Kona Conference on Astronomy

2. Fried, D.L., 1966, JOSA 55 1427

3. Chassat, F., 1989, J Optics (Paris) 20,13

Diffraction-Limited Wide-Field Sky Camera

Richard G. Bingham
Royal Greenwich Observatory
Madingley Road
Cambridge CB3 0EZ, England

I show the optical design for a wide-field sky camera of two meters aperture diameter. It has much better performance than existing cameras and can be diffraction limited over a field of view of two degrees diameter, and over a wide range of wavelengths. I point out the problems of implementing such a high performance optical system. I discuss how it might conceivably be exploited, for example, by using more than one adaptive optics system.

Deformable Mirrors: A Commercial Product?

Mark A. Ealey
Xinetics, Inc.
Littleton, MA 01460

Xinetics originally announced a line of cost-effective deformable mirrors in March 1994. The mirrors featured repairable construction at one quarter the cost of previous products. We report on 37, 97, and 349 channel mirrors in terms of application, customer, and performance. Application range from the use of a 37 channel DM used to better image the human retina to the 97 channel upgradeable DM built for the Max Planck Institute fur Astronomie, to the 349 channel DM built for JPL Palomar Adaptive Optics. A summary will also be given on the role of the USAF Cooperative Research Development Agreements (CRDA) in giving small business the opportunity to compete on a global scale.

Potential Application of Coherent Population Trapping to Adaptive Optics and Turbulence Metrology

P. R. Hemmer, Rome Laboratory

RL/EROP, 63 Scott Rd., Hanscom AFB, MA 01731

Tel: 617-377-5170, Fax: 617-377-5041

Coherent population trapping (CPT) in multilevel Raman resonant atomic systems is a fast, efficient process which produces large optical nonlinearities at low laser intensities. These properties are potentially useful in turbulence metrology and adaptive optics, especially for severe turbulence. To illustrate this, three experimentally demonstrated properties of CPT will be described and their possible application will be outlined.

First, in adaptive optics there is a need for high speed optical phase conjugation and/or image amplification. It has been demonstrated that CPT in sodium vapor can produce optical phase conjugation with gain greater than 10 at speeds faster than 1 μsec, using only 1 Watt/cm^2 of optical pump intensity. It has also been demonstrated that image bearing beams can be conjugated with gain. Potential applications of this Raman phase conjugator include direct compensation of small angle atmospheric distortion, or the amplification of weak guide star signals (at the sodium wavelength) to provide brighter inputs to other adaptive optics systems. Preliminary measurements have been made on the noise properties of the Raman CPT optical amplifier. It was

found that the classical noise is correlated. This suggests that a CPT optical amplifier may be useful for imaging low contrast phase objects, such as turbulent flows.

Second, in high speed turbulence metrology there is a need for a fast optical holographic cache memory to store large numbers (> 1000) of 3-d images for later playback at rates slow enough for optoelectronic storage and processing. High speed holographic storage can be accomplished using photon echo techniques, but the necessary decoupling of write and read speeds is very difficult in time domain storage. Using Raman CPT in a sodium atomic beam, it has been demonstrated that spin echoes can be used to store holographic optical information. Since spin transitions in solids have small intrinsic inhomogeneous broadening, an adjustable magnetic field gradient can be used to decouple write and read speeds by varying the inhomogeneous width of the spin transition. Spin transitions also have the advantage that spin homogeneous lifetimes up to 1 second have been observed at room temperature. Optical transitions require liquid helium to achieve such long lifetimes.

Third, an optical Raman technique analogous to NMR imaging has been demonstrated in a supersonic atomic beam for micron-scale position measurement of small volumes with high signal to noise. Here, optical pumping is used to provide the high degree of spin orientation needed to give good signal to noise at fast scan rates. Raman CPT can also establish a position dependent spin orientation without the need for optical pumping. Extension

of these techniques to metrology of seeded turbulent flow is straightforward. For example, if millimeter resolution is sufficient, larger volumes can be image. Flow imaging can be accomplished by using sheets of light to establish a plane of spin orientation perpendicular to the flow direction. Probing with sheets of light parallel to the flow can give a 3-d time domain image of the motion. Since Raman resonant systems are very efficient at scattering light, it should be possible to image high speed flows.

CRICS - Confusion Rejection Image Compensation System

Allan Wirth and Andrew Jankevics
Adaptive Optics Associates Inc.
54 CambridgePark Drive, Cambridge, MA 02140
(6i7) 864 0201 FAX (617) 864 1348

A novel concept for the compensation of aberrated images has been developed. It is based on the idea of introducing a pupil mask that blocks the most highly tilted portions of the incoming wavefront. Such a mask might consist of a spatial light modulator. The SLM would be driven by a binary Hartmann sensor. Subapertures with low tilt would turn on their corresponding SLM pixels allowing the nearly flat portions of the wavefront to propagate. Subapertures with larger tilts would act to turn off their SLM pixels, eliminating those portions of the pupil that don not contribute to the core of the image.

Across a large pupil the regions of low tilt may occur at various phases. Thus these regions will not add coherently in the image plane. In such cases the instantaneous resolution will be limited by the diffraction spot size generated by these typical low tilt patches and not by the spot size for the full aperture.

In a sense CRICS is a geometric compensation system, only allowing light whose direction of propagation is nearly parallel to the optical axis to form the image. This may be somewhat ameliorated by the use of speckle imaging techniques in combination with CRICS.

Simulations have shown that for typical atmospheric wavefronts, strehl ratio improvements of more than a factor of 10 are possible while rejecting less than 75% of the light.

CRICS is best suited to situations of relatively high light level and small coherence radii. The first is because it is not efficient with the light, rejecting the bulk of it as "too aberrated", and the second because high spatial resolution SLMs and binary Hartmann sensors are available at low cost.

Liquid Crystals for Adaptive Optics.

Sergio R. Restaino, Richard A. Carreras and Gordon D. Love.

US Air Force Phillips Laboratory, PL/LIMS, 3550 Aberdeen S.E., KAFB, NM 87117, USA.

and also Department of Physics and Astronomy. University of New Mexico, Albuquerque, NM 87131, USA.

Adaptive optics components have been used for almost twenty years without major modifications of the basic hardware. Problems connected with cost, power consumption and reliability have pushed several groups to start investigating the possibility of using different technologies. Of the many technologies under investigation two, in our opinion, demonstrate a high possibility of being an alternative to conventional adaptive mirrors. They are liquid crystal spatial light modulators and and micro-machined mirrors. The USAF Phillips Laboratory, is investigating both these technologies, however here we report on the results of the liquid crystal work, which has a slightly longer history and more maturity.

LC Type	Nematic	Ferroelectric
Equivalent Optical Device	Linear waveplate with electrically controllable retardance	Linear waveplate with electrically controllable optical axis
Achievable phase shift	Up to several visible waves. Continuously controllable.	Up to 1 Wave Bistable
Response Time	$\sim$100ms for 1 wave, typical. $\sim$10ms using optimized transient nematic effect	$< 10\mu s$
Polarization Properties	Only phase modulates linearly polarized light (see text)	In general phase modulation is coupled with polarization modulation. For half-wave phase shifters (required for AO) these effects can be decoupled to produce a polarization insensitive device.
Typical cost	$\sim$\$10K	$\sim$\$10K

Table 1: A comparison of phase switching with nematic and ferroelectric LCs.

There are many different kind of compunds that have the basic characteristics of presenting a state of aggregation that is intermediate between the crystalline solid and amorphous liquid. For the characterization of the various kind of liquid crystals the reader is referred to, for example, ref. 1. In terms of electro-optics, there are two categories of interest. The first is the so-called *nematic* LC phase and the second is referred to as the *ferroelectric* phase.
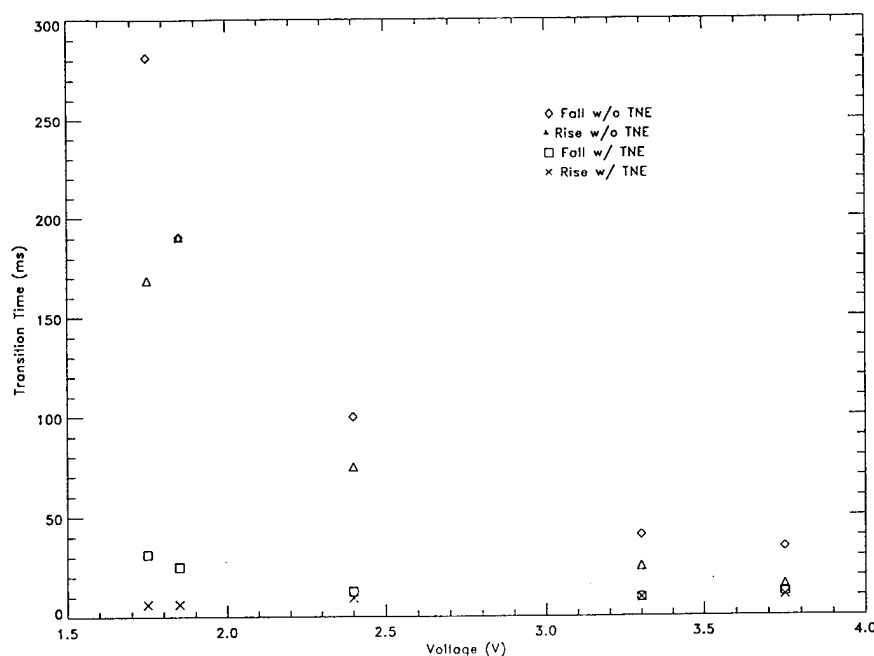
Fig. 1a. Measurement of rise and fall time in a single nematic cell, $5\mu m$ thick with and without the TNE at room temperature. Results show that the transient nematic effect can dramatically improve the LC response time.
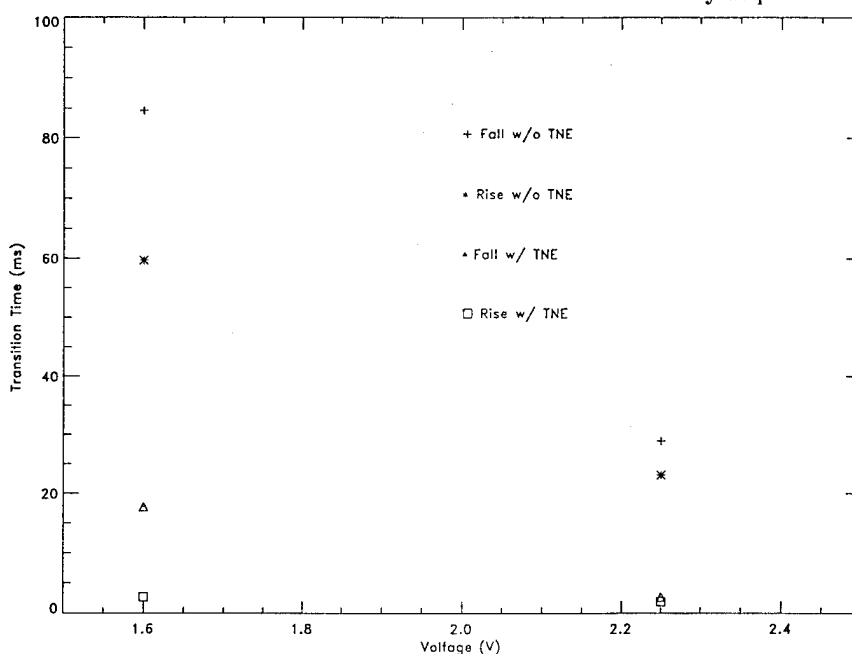

Fig. 1b. Same as Fig. 1a, except measurements taken at $41°C$.

From table. 1. it is clear that while nematic LCs offer the advantage of continuous phase switching, ferroelectric LCs offer a much faster switching time, and hence closed–loop bandwidth. In the design of an adaptive optics system a variety of requirements must be taken into account – the Greenwood frequency for the bandwidth, the atmospheric coherence diameter, r_0, etc. In light of the variety of applications that are possible we envision different types of LC devices for different needs. In this paper we report the basic work done in the field of nematic LCs by our Group, and the interested reader is referred to Ref. 2 for work on the ferroelectric LCs.

One of the first results obtained by our Group was an understanding of the use of the transient nematic effect

(TNE)[3] for reducing the refreshing time of the nematic cells. Fig. 1 shows experimental measurements taken with and without the use of the TNE, at both room temperature (Fig. 1a) and at 41°C (Fig. 1b). It is clear that thermal control plus the TNE can dramatically decrease the refreshing time of the device, allowing for a higher bandwidth. However thermal control is an extremely delicate issue, in fact we noticed degradations of the birefringence across the cell due to gradients in temperature. Our thermal control was too crude to achieve the desired speed and at the same time maintain an uniform optical quality.

Several other experiments have been carried out by our Group with different devices[4], some of which are in conjunction with the MARTINI Group at Durham University, UK[5]. Further work with high quality nematic cells is reported at this conference[6]. From the research under development at the Phillips Laboratory and elsewhere it is clear that liquid crystal devices may play an important role in adaptive optics systems in the near future.

References

(1) S. Chandrasekhar *Liquid Crystals* Cambridge University Press (1992).

(2) G D. Love, et. al. *Binary adaptive optics: atmospheric wavefront correction using a half-wave phase shifter* App. Opt. Accepted for publication (1995).

(3) S T Wu and C S Wu. *Small angled relaxation of highly deformed nematic liquid crystals.* Appl. Opt. **53**(19):1794 (1988).

(4) S. R. Restaino, E. Gates, R. A. Carreras, R. Dymale, and G. C. Loos. *On the use of electro-optical devices for OPL compensation.* Proc. SPIE **2200** 494 (1994).

(5) G D. Love, S. R. Restaino, G. C. Loos, and A. Purvis. *Wavefront control using a 64 × 64 pixel liquid crystal array.* Proc. SPIE **2201**:1068-1072 (1994).

(6) G. D. Love, S. R. Restaino, R. A. Carreras, G. C. Loos, A. Purvis, and R. Morrison. *High quality liquid crystal spatial light modulators for adaptive optics.* These proceedings.

Laser beacon compensated images of Saturn
using a high speed near infrared correlation tracker

Robert Q. Fugate, James F. Riker, J. Timothy Roark, Steve Stogsdill

Starfire Optical Range, Phillips Laboratory
3550 Aberdeen Ave, SE, Kirtland AFB, New Mexico 87117-5776, USA
Phone (505) 846-4712 ext 314, Fax (505) 846-2213, Internet: fugate@plk.af.mil

and

Burt D. O'Neil

Logicon RDA, Albuquerque, NM

The 1.5 m telescope at the Starfire Optical Range, USAF Phillips Laboratory, Albuquerque, NM, USA is equipped with laser beacon adaptive optics and a high speed full aperture tilt correction system. The laser beacon is formed by a copper vapor laser propagated out the full 1.5 m aperture and focused at 14 km range. The laser operates at 5,000 pulses per second, 50 ns per pulse, with approximately 60-70 watts average power into the atmosphere. Light backscattered from the laser beacon between the ranges of 12 and 16 km is sensed by an unintensified, Pockels-cell-gated, silicon-based CCD Shack-Hartmann wave front sensor. The optics are configured such that it is also possible to use natural stars as beacons for the higher-order adaptive optics. Wave front corrections are applied to a 241 actuator continuous facesheet deformable mirror operated at approximately 100 Hz closed loop bandwidth.

It is well known that laser beacons cannot be used to sense full aperture tilt (the best fit plane wave to the phase aberrations) induced by atmospheric turbulence. Consequently, a natural guide star or other inertial reference outside the atmosphere is needed for image stabilization. When stars are used as targets for tracking, centroid algorithms provide optimal performance, especially for low signal-to-noise environments. However, resolved objects present a more challenging problem and the optimal solution is not as evident. Furthermore, tracking and image stabilization have become the limiting factors in long exposure image quality at the 1.5 m telescope and this aspect of compensated imaging requires careful attention.

We have successfully used a germanium focal plane sensor and high speed two-dimensional correlation processor to control a fast piezoelectrically driven steering mirror to stabilize compensated images of extended objects at approximately 200 Hz closed loop bandwidth. The germanium focal plane array (48x48 pixels) is read out at 4,000 frames per second. The read noise of the array is approximately 100 electrons/pixel, which limits the usefullness of the system to 6th or 7th magniude guide stars at this sample rate. Data from the germanium sensor pass through an image track processor built by Ball Aerospace Systems Division, which produces track error signals within 85 μsec after reading the last pixel.

The track processor supports a "sieve gate" centroid algorithm and a Fitts correlation algorithm. The centroid algorithm is intensity weighted and is performed after a simple thresholding operation to select the appropriate signal pixels to use.

The correlation algorithm is based on the work of Fitts at Hughes. It incorporates a running average of incoming images to construct a correlation "map." The processor generates track error signals by comparing the instantaneous image to the map according to the formula:

$$X_{correlation}(t_k) = \frac{1}{c(t_k)} \cdot \sum_{pixels} W(t_k) \cdot [I(t_k) - MAP(t_k)],$$

where

$$W(t_k) = -\frac{MAP_{x-1}(t_k) - MAP_{x+1}(t_k)}{2},$$

$$c(t_k) = \sum_{pixels} [W(t_k)]^2,$$

and

$$MAP(t_k) = (1 - \rho) \cdot MAP(t_k - 1) + \rho I(t_k - 1).$$

In this equation, t_k is the current time and $I(t_k)$ the instantaneous image corresponding to that time. The function $W(t_k)$ is effectively a "gradient" of the image and emphasizes those portions of the image where the signal is changing rapidly. That is how the correlation algorithm recognizes that it is at an edge of a feature to be tracked. Note that the map array can change slowly or quickly depending on the value of the user-specified parameter ρ. In the implementation used here, only a 14x14 pixel window is processed.

For the Saturn observations we set-up the optics so that each pixel had a 3.5 arcsec instantaneous field of view. Even at this resoultion, which put the entire planet and rings in the 14x14 track gate, the rings were clearly visible on the Ge focal plane array and we surmised that the rings would break the symmetry of an otherwise featureless image and make it possible for the correlation algorithm to to keep the image stable on the array. In fact, simulations show that the rings are indeed responsible for for the excellent tracking performance. The germanium array was sampled at 4 kHz and the combination of high bandwidth tracking on the image of the planet and the higher-order correction using the laser beacon adaptive optics produced the excellent results shown below.

Figure 1: Saturn and Titan (barely visible in lower left) 19 July 1994. No tracking or adaptive optics

Figure 2: Tilt compensation only (by correlation tracker)

Figures 1 and 2 are one second exposure silicon CCD camera images made the morning of July 19, 1994 when Saturn was at an elevation of approximately 40 deg. Titan is also barely visible in the lower left in the original images. In Fig. 1 no compensation of any kind was used. Fig. 2 was made while tracking in the near infrared with the correlation algorithm but with the higher order adaptive optics off. The seeing was approximately 1 arcsec during these observations. Note that Figure 2 does show some improvement and in the original images one can see more clearly the Cassini division in the rings, the polar cap region and Titan.

Figure 3 is the image obtained approximately 30 miuntes after Figs. 1 and 2 with higher-order wavefront correction being done by the laser beacon adaptive optics. The tracking was the same as in Figs. 1 and 2— with the Ge array using the correlation mode algorithm. Note the improved crispness of this image compared
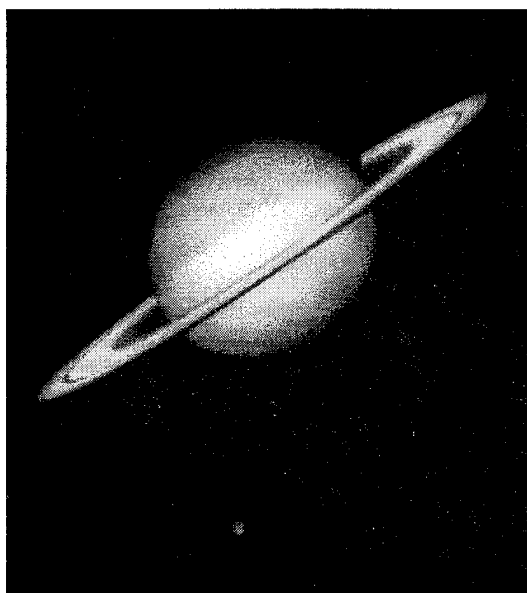
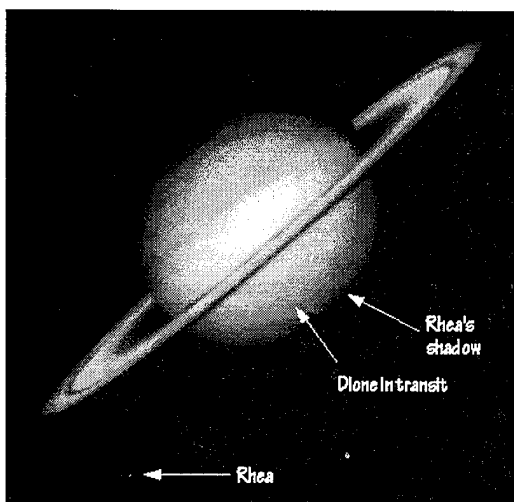Figure 3: Figure 3. Laser beacon AO and correlation tracking

Figure 4: Saturn, Rhea, and Dione, 23 July 1994, laser beacon AO and correlation tracking

with Figs. 1 and 2 and Titan's prominence. Titan subtended 0.7 arcsec during these observations. There is much finer detail in the rings, bands in the atmosphere and a clearly defined polar region. Unfortunately, we did not have narrowband spectral filters that would have allowed observation of different molecular species and perhaps highlighted storms and other atmospheric structure. All images shown here were made over the spectral band 0.6-0.9 μm. Furthermore, in order to get the entire image of the planet on the focal plane, we were unable to sample the image at the Nyquist frequency. The image scale is consequently 0.1 arcsec per pixel, roughly λ/D, and it is difficult to perform quantitative analysis of the image quality in terms of the diffraction limit. However, we can say that sharp edges (e.g. the planet's shadow on the rings) appear to show full modulation in less than two pixels.

Figure 4 is another example taken four days later on 23 July 1994. Two other moons, Rhea and Dione, were visible in this three second exposure. Rhea is seen in the lower left and its shadow on the planet is also clearly visible in the original image. Furthermore, we observed Dione in transit. We are certain that this is Dione since we watched it for a period of about two hours as it moved from left to right, starting just to the left of the lower left edge of Saturn and passing in front of Saturn, moving across the planet's disk. This image has been stretched a bit to increase the contrast of the moons. It is easy to see them in the original on-screen images but much of the detail is lost in the reproduction here.

One aspect that strikes most who have seen these images is they seem to show excellent correction over a very large field of view. Since the pixel scale is about twice the Nyquist limit, it is not easy to make a quantitative estimate of the image quality in terms of the modulation transfer function or other measure such as the Strehl ratio. The quality of the image may be such that isoplanatic effects are already less significant than the aberrations caused by effects such as focus anisoplanatism. Low image quality coupled with the coarse resolution of the camera makes it difficult to see any degradation due to anisoplanatism. In any event, we feel that these examples are among the best images of Saturn ever made from a ground based observatory.

Results from the MMT Adaptive Optics Infrared Imager FASTTRAC II

L. M. Close, M. Lloyd-Hart, J. R. P. Angel, D. W. McCarthy Jr., G. Brusa,
B. A. McLeod, T. D. Groesbeck, D. M. Wittman, P. T. Ryan, T. Martinez,
P. Gray, J. M. Hughes, M. Cheselka, and B. Jacobsen
CAAO, Steward Observatory, University of Arizona 85721, USA
Email *lclose@as.arizona.edu*, WWW http://acme.as.arizona.edu:8000
TEL 602-621-7866, FAX 602-621-9843

D. G. Bruns, and D. G. Sandler
ThermoTrex Corp. San Diego

The mission of the Center for Astronomical Adaptive Optics (CAAO) at Steward Observatory is to develop a diffraction-limited laser guide star adaptive optics system. This system is targeted for the new 6.5m mirror MMT upgrade. This single mirror will be installed in the existing Multiple Mirror Telescope (MMT) mount in late 1996 (to replace the existing six individual 1.8m primaries). Presently CAAO has focused on implementing a simpler instrument which tip-tilt corrects all six beams from the existing MMT. The major features of this instrument (called FASTTRAC II) will be used in the 6.5m system with minimal changes. In addition, FASTTRAC II fully addresses all the major optical, electrical, mechanical and computational challenges of having a common user instrument on a ALT-AZ mount utilizing a sodium laser guide star.

The MMT is a unique telescope which utilizes six individual 1.8m primaries all co-mounted to a single ALT-AZ mount. FASTTRAC combines the beams of these primaries with six independent tip-tilt mirrors which replace existing static mirrors. Therefore no extra "hot" optical surfaces are added before the infrared camera. Natural or laser guide stars can be used to eliminate relative tilt fluctuations inside the 7m baseline between the primaries. If the laser beacon is used we also utilize a faint natural off axis guide star to eliminate global tilt fluctuations over the whole telescope.

FASTTRAC II achieved first light on April 15-20, 1995 and has proved to be a promising astronomical instrument. It operates in the near infrared using a NICMOS3 256x256 1-2.5μm detector. The excellent site at Mt. Hopkins ($<r_0>\sim$90cm at 2.2 μm) allows FASTTRAC to operate in the regime of $D/r_0<3$ in the infrared (where $D=1.8$m equals the size of one of the six primaries). In this regime the removal of tilt fluctuations (to less than 0.05" rms) enables FASTTRAC to obtain diffraction-limited resolutions (0.25" FWHM at 2.2μm) and Strehl ratios of $\sim$0.5.

A cross-section of the instrument is depicted in figure 1. The major elements of system are labeled 1-4. The first element is the six sided pyramidal tip-tilt beam combiner (element #1). Two of the six mirrors are shown combining the individual f/31.6 beams into a f/8.4 common envelope. Each tip-tilt mirror includes a pair of novel high resolution ($\pm$10 nm rms) capacitive displacement sensors. The resulting positional feedback enables a simple PID analog servo control circuit to lock the mirror to the commanded tilt (via a pair of orthogonal voice coil actuators). The resulting low cost, high performance tip-tilt segments have a servo bandwidth of 120Hz at the -3dB level and are critically damped at update rates up to 150Hz. Based on the success of these mirrors a slightly modified voice coil/capacitive sensor unit is the actuator chosen for the 300 actuator adaptive secondary mirror planned for the 6.5m upgrade system (see D. Bruns's paper in this meeting).
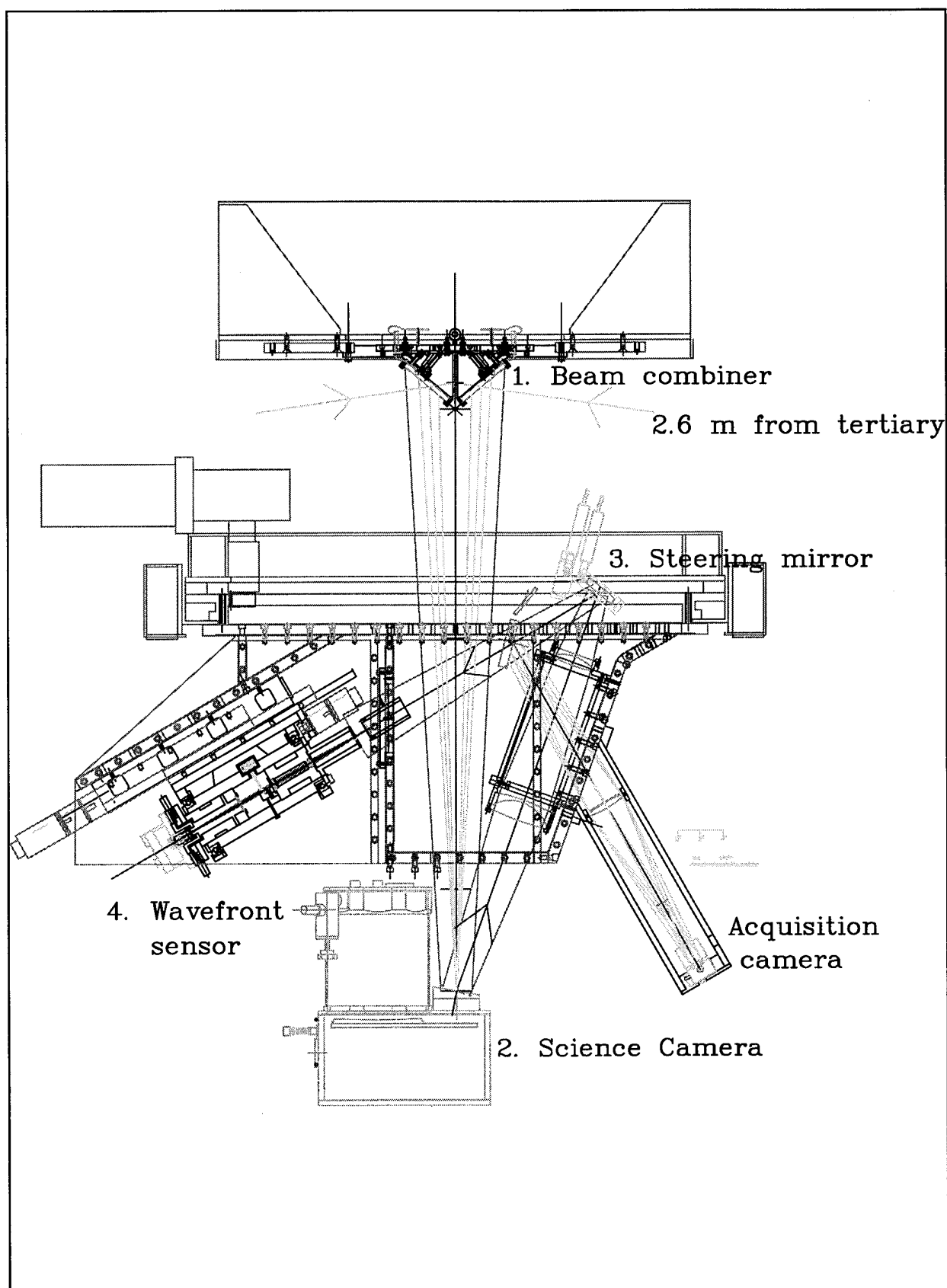
1. Beam combiner

2.6 m from tertiary

3. Steering mirror

4. Wavefront sensor

Acquisition camera

2. Science Camera

Figure 1: A cross-section and simple ray trace of the FASTTRAC II instrument on the MMT.

Following the optical path in figure 1, we find that the combined f/8.4 beam is split at the entrance window to the cryogenic science camera (element #2). The window is a dichroic flat tilted at 11° which reflects 94% of the visible light (over the 3.9' field of view (FOV)) back up to a relay lens and passes 90% of the infrared light (λ>1μm) into the camera. Inside the camera an achromatic field lens images the hexagonal unfilled pupil formed by the six primaries onto a cold pupil stop. The stop follows any rotation of the pupil due to the instrument rotator turning the instrument which is necessary to eliminate field rotation on an ALT-AZ mount. The light is then focused by a triplet on the 256x256 NICMOS3 detector generating a 0.1"/pixel platescale.

The science camera is a unique and versatile stand-alone instrument in its own right. It is capable of providing Nyquist sampled diffraction-limited imaging on any telescope with a f/45 beam at K (2.2μm), H (1.6μm), and J (1.2μm). The camera routinely produces short-exposure diffraction-limited 0.3" FWHM images with FASTTRAC II and 0.2" images at the Steward Observatory 2.3m telescope at Kitt Peak. The detector can be read out at 20Hz full frame or at much higher rates for a subarray (up to 300Hz for a 10x10 box). The camera can uniquely select a subarray (in only one quadrant of the chip) and read it out at high speed while the rest of the detector integrates. Hence, the camera can act as an infrared tilt sensor and science camera simultaneously. In addition, the camera has obtained diffraction-limited images without adaptive optics by utilizing speckle and "shift and add" post processing techniques.

The tip-tilt mirrors are controlled by tracking the reflected visible light from a guide star within the 3.9' FOV. The whole FOV passes through a 5 inch relay lens which forms an image of the pupil at a computer controlled tip-tilt flat (element #3). This flat steers all six guide star beams to a Shack-Hartmann wavefront sensor (WFS). The WFS (element #4) images the six beam pupil onto a custom built circular lenslet array which images the light, via a field and relay lens, onto a 64x64 CCD. The WFS is positioned so that all six beams come in focus at the pixel boundaries of six different quad cells (each 2.5"x2.5"). Moreover, the WFS is designed so that all six beams are also simultaneously exactly stacked and focused on the science camera when the loop is closed. The WFS also rotates under computer control to follow the rotation of the pupil.

The frame transfer CCD is binned to a 16x16 frame and can be read out at 8ms per frame with a read noise of 6e rms. The centroids from the six beams are used to retilt each of the six tip-tilt mirrors at up to 100 Hz. During the first light run in April 1995, the loop was successfully closed at 60Hz on four of the six beams on the first attempt. Individual beams improved from 1.1" to 0.6" FWHM (50s exposure) when the loop was closed. However, due to temporary optical problems with the WFS, the individual beams were not stacked well on the science camera. At this time only engineering results have been obtained with FASTTRAC II; however, we should obtain images of scientific significance in September 1995 when we return to the MMT with an improved optical alignment.

APPROACHES FOR IMAGE PROCESSING SUPPORTING ADAPTIVE OPTICS

Douglas G. Currie, Petras V. Avizonis, Daniel M. Dowling
Department of Physics
University of Maryland
College Park, MD 20742-4111

Dianne P. O'Leary, James G. Nagy,
Department of Computer Science,
University of Maryland
College Park, MD 20742-4111

Robert Q. Fugate
Starfire Optical Range,
USAF Phillips Laboratory
Kirtland AFB, NM 87117-5776

Image processing methods, highlighting specific hardware systems, will be demonstrated. Correcting spatial dependence and instrumental artifacts of the Point-Spread-Function significantly improves image quality.

Image processing techniques, focused on specific hardware attributes, can be of great use for the extraction of the maximum scientific information from imaging data. This has been especially valuable in our work with the pre-repair data from the Wide Field/Planetary Camera of the Hubble Space Telescope. However, the development of image processing techniques incorporating the attributes of adaptive optics systems has not been significantly addressed in the literature. There are two areas which apply to imaging data resulting from adaptive optics systems that will be addressed in this talk.

The first area concerns a common characteristic of all current adaptive optics systems in that they have a Point-Spread-Function (PSF) which is spatially dependant, that is, having a different functional form for the PSF at different points in the field-of-view. In principle such a problem might not exist, but in practical systems, i.e. natural source (auto-referenced) or laser guide star systems, and in those data available for the current analysis, this is a significant, if not universal, effect. The two major components of the spatially dependent PSF are (1) a less compact core of the image of an unresolved source toward the edge of the field-of-view, i.e. beyond the isoplanatic patch, and (2) a low level "skirt" which has the functional form of the uncompensated seeing disk. In general, the compensated imaging systems produce a bright core, plus a set of wings which are characteristic of the diameter of the seeing disk. This is well-handled by the Lucy-Richardson (L-R) procedure.

The second area addresses instrumental irregularities which can also be analyzed and corrected using these methods. These effects, caused by a finite number of modes, instrumental vibration and dynamical instabilities and other effects, frequently add low-level scatter and noise.
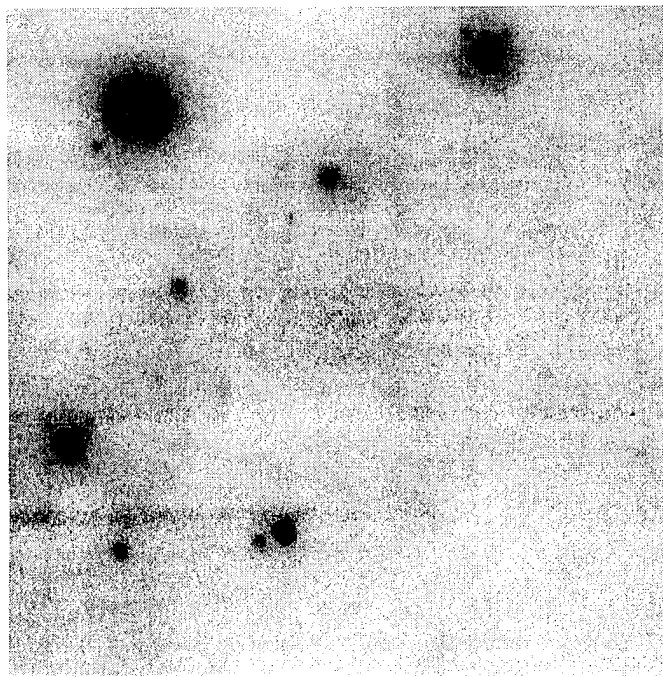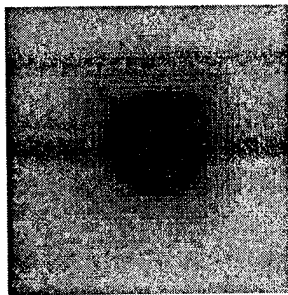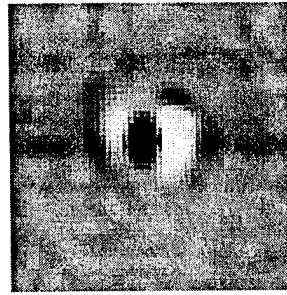

Figure 1

In order to illustrate the advantages of these processes, we first address the deconvolution with an improved L-R algorithm. Although the L-R algorithm has been developed and tested with simulated data, we demonstrate the methods on field data, using images of the Orion nebula from the Laser Guide Star System on the 1.5 meter telescope at the Starfire Optical Range. [McCullough, P. R. et. al. 1995], [Fugate et al 1995]. Figure 1 above shows a raw image frame. This representation has a large linear stretch in which the peaks of some of the stellar images are saturated.

Figure 2A below is the core of one of the brighter stars in which the structure in the wings illustrates the focal plane effect of an a diffractive "waffle" pattern in the dynamic mirror. This results in an anomalous PSF due to this instrumental problem. The processing with the L-R algorithms removes this artifact. Figure 2B is the result of processing with our conventional L-R algorithm developed for the WF/PC data processing [Lauer et. al. 1991]. This shows a definite moat or locally depressed area about the star. Figure 2C is the result of an improved version developed at the University of Maryland.
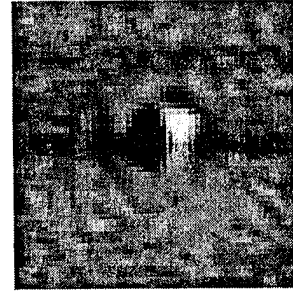
(2a)   (2b)   (2c)
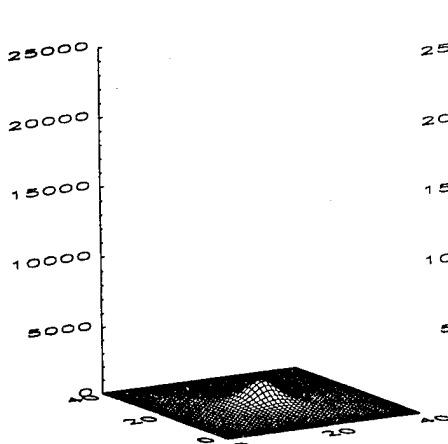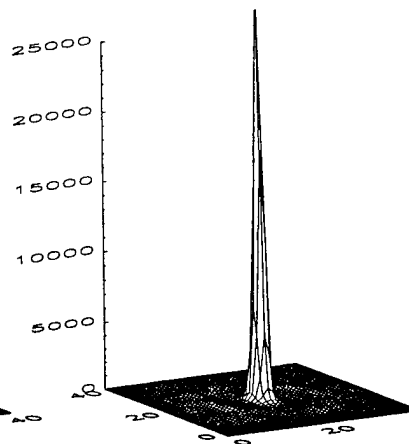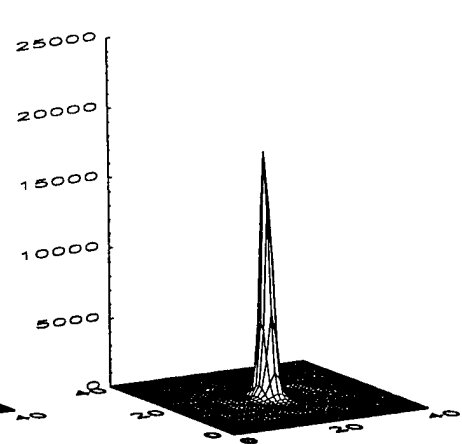
To better illustrate the structure of this diffractive "waffle" artifact and the advantage, for nearby faint features, of the removal of various elements of the wings, we present a 3D representation (Figure 3A-3C) of the image, which also includes the wider pattern due to the frequency response of the tip-tilt correction.
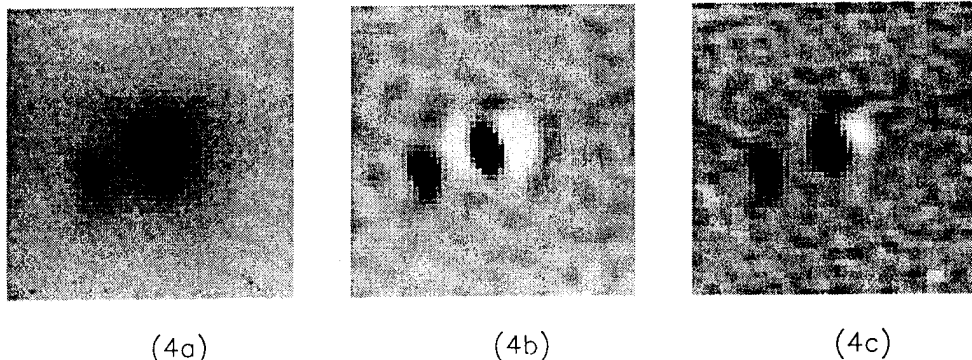

(3a)   (3b)   (3c)

Figure 4A shows the double star found in the lower central part of the original image, which has a separation of 0.97 arc-second. Figure 4B and 4C illustrate the result of L-R processing as discussed for Figure 2.

(4a)   (4b)   (4c)

We will illustrate how these methods may also be applied for a spatially dependent PSF. One of the methods which we will demonstrate uses the "conjugate gradient" technique [Nagy, J. G. and D. P. O'Leary, 1995]. The second is a special image warping technique which then uses the L-R algorithm. We will address the role of the improvements in terms of the Strehl ratio and the effects of a uniform PSF in obtaining an improved Strehl ratio. In particular, these image processing procedures improve the relative core Strehl ratio by a factor of between three and four. We will also address some other troublesome artifacts of the conventional L-R processing, i.e. ringing near a intensity step and background patterning.

Although our current analysis results will concentrate on clusters of stars, the primary interest in these methods is to process extended objects which have very fine spacial structure (e.g. the homunculus of eta Carinae). Simulations of these techniques using our Hubble data on eta Carinae will be presented, addressing both the Starfire system and the ADONIS system of ESO [Hubin et. al. 1995]. This will address both the photometric study of objects near the very bright core of eta CAR and the blurring effects far from the guide star.

REFERENCES

Lauer, T. et. al. AJ Vol 104 p. 522 1992
Nagy, J. G. and D. P. O'Leary 1995 UM Tech Rpt CSTR3426
McCullough, P. R. et. al. ApJ V. 438 p. 394 1995
Fugate,R. Q. Proc. SPIE Conf. 2201 p. 10 1994
Hubin, N.   Proc. SPIE Conf. 2201 p. 34 1994

Error reduction in centroid estimates using image intensifiers.

M. P. Cagigal, M. G. Portilla, P. M. Prieto.
Departamento de Física Aplicada. Universidad de Cantabria.
39005. SANTANDER. SPAIN.
Tel: 42-201445. Fax: 42-201402.

1.- INTRODUCTION

To estimate the centroid of a light intensity distribution is a technique widely used in different fields: motion analysis of moving objects from series of frames[1]; tracking systems for laser communication[2]; resolution improvement by recentering short-exposures images allowing motion removing[3]; and adaptive optics, when the wave-front distortion is estimated from the movement of a series of spots produced by an array of lenslet (Hartman-Shack wave-front sensor)[4].

In some cases the incoming light is so weak and the exposure time is so short that image intensifiers have to be used. The advantage of using intensifiers is the increase of the signal-to-noise ratio. However, the photocount distribution is modified due to the dead-time that appear along the different amplification stages. The result is a clipped count distribution. This fact has been checked in several experimental arrangements[5].

These kind of detectors have been used in actual experiments to remove image motion[6] and to detect spot displacement in a Hartman-Shack[7] without taken into account the possible error in the centroid evaluation introduced by the use of a modified photocount statistics. Nevertheless, theoretical analysis of errors involved in centroiding binary images appears in recent literature[1].

In this paper we quantify both the systematic and the statistical error that appear when a clipped photocount distribution is used. It can be seen that the error on the centroid estimate is a function of the intensity of the incoming light and the background noise. A simple technique is proposed to overcome the systematic error in the centroid estimate from clipped data. This technique allows an accuracy improvement under many different experimental conditions. The theoretical results have been checked using simulated data.

2.- THEORY

Let us consider an image detector sized NxN'. Two one-dimensional light intensity distributions can be obtained from the projection of the actual intensity distribution over the X and Y axis. This allows to evaluate the centroid using one-dimensional functions. We will study only the intensity obtained along the X axis. In that case, the expression to estimate the centroid of a light spot is given by

$$\widetilde{X}_c = \left[\sum_{i}^{N} n_i\, x_i \right] x \left[\sum_{i}^{N} n_i \right]^{-1} , \tag{1}$$

where

$$n_i = \frac{1}{N'} \sum_{j}^{N'} n_{ij}, \tag{2}$$

and n_{ij} is the number of counts detected in the pixel (i,j). The variance of $\widetilde{X}_c$ depends on the poissonian noise that appear in the detection. If we call n_i^b to the value of n_i obtained using Eq.(2) with clipped data, the new

expression for the centroid estimate will be

$$\tilde{X}_c^b = \left[\sum_i^N n_i^b x_i\right] \times \left[\sum_i^N n_i^b\right]^{-1}$$

(3)

The fact of using clipped data will produce systematic and statistical errors in the centroid estimate which have been described in the literature[1]. If w_{ij} is the mean intensity arriving to pixel (i,j), the ensemble average of n_i and n_i^b in low light level yields $<n_i> = w_i$ and $<n_i^b> = w_i - w_i^{(2)}/2$, where

$$w_i = \frac{1}{N'}\sum_j^{N'} w_{ij},$$

(4)

$$w_i^{(2)} = \frac{1}{N'}\sum_j^{N'} w_{ij}^2.$$

(5)

The comparison between $<n_i>$ and $<n_i^b>$ shows that the centroid evaluation using clipped data provides a biased estimate. The bias magnitude is dominated by the term $w_i^{(2)}$. It would be necessary a direct evaluation of this term in order to cancel its influence in the centroid estimate but this evaluation is not possible when binary data are used. Our proposal is to estimate approximately $w_i^{(2)}$ using a series of autocorrelation estimates as follows

$$w_i^{(2)} \approx \frac{1}{N'}\sum_j^{N'} w_{ij}\left(w_{i(j+1)}+w_{i(j-1)}\right)\Big/2.$$

(6)

This allows to define the corrected number of counts n_i^c:

$$n_i^c = \frac{1}{N'}\sum_j^{N'} n_{ij} + n_{ij}\left(n_{i(j+1)}+n_{i(j-1)}\right)\Big/4$$

(7)

3.- EXPERIMENTAL CHECKING

A series of simulated experiments were performed to check the theoretical predictions. A detector size of 20x20 pixels was chosen. The spot shape was Gaussian of width $\sigma=2.5$ pixels. In Fig.1 (upper) it has been plotted the systematic error involved in the centroid estimate for the measured binary values n_i^b and for the corrected values n_i^c. The error reduction, in %, is important for all the intensity values, specially for the lowest ones. The statistical error is slightly improved when n_i^c is used, as shown in Fig.1 (lower).

4.- CONCLUSIONS

The evaluation of a corrected photocount distribution allows an important reduction in the systematic error involved in the centroid estimate when clipped image detectors are used. The statistical error is also improved. Therefore, the evaluation of the corrected number of counts can be a useful technique applicable in all the fields where the centroid is evaluated using data provided by actual image detector.
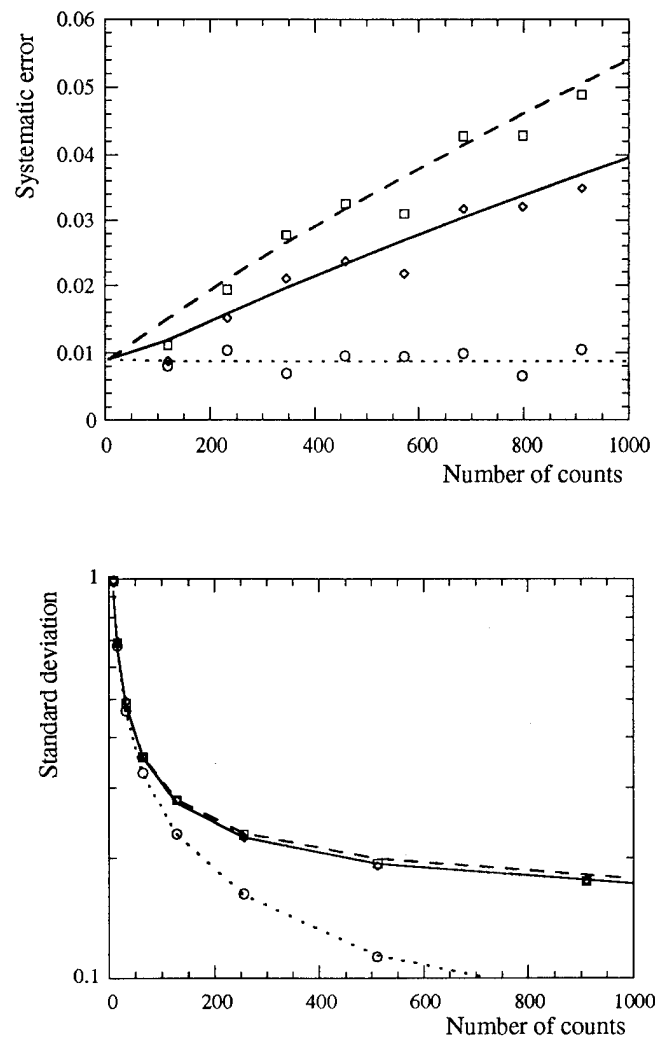
Fig.1: Systematic error and standard deviation (in pixels) of the centroid estimate, as a function of the light intensity. Theoretical predictions are represented by lines and experimental results by dots. Poissonian detection: dotted line, circles. Clipped detection: dashed line, squares. Corrected detection: solid line, rhombus.

REFERENCES

1.- Y. Bar-Shalom, X. R. Li, *Multitarget-Multisensor Tracking: Principles and Techniques*, (YBS, 1995).

2.- D. Russell, H. Ansari, "Highly accurate system for a laser communications link", Proc. Soc. Photo-Opt. Instrum. Eng. **2221**, 152-155 (1994).

3.- D. L. Fried, "Optical resolution through a randomly inhomogeneous medium for very long and very short exposures", J. Opt. Soc. Am. **56**, 1372-1379 (1966).

4.- B. M. Welsh "Imaging performance analysis of adaptive optical telescopes using laser guide stars" Appl. Opt. **30**, 5021-5030 (1991).

5.- D. J. Cho, G. M. Morris, "Local dead-time effects in microchannel-plate imaging detectors" Proc. Soc. Photo-Opt. Instrum. Eng. **976**, 172-176 (1988).

6.- J. Sebag, J. Arnaud, G. Lelievre, J. L. Nieto, E. Le Coarer, "High-resolution imaging using pupil segmentation", J. Opt. Soc. Am. A **7**, 1237-1242 (1990).

7.- G. Cao and X. Yu, "Accuracy analysis of a Hartmann-Shack wavefront sensor operated with a faint object", Opt. Eng. **33**, 2331-2335 (1994).

Dynamic Adaptive Mirror in the Algorithm of Phase Conjugation

F.Yu. Kanev, V.P. Lukin, L.N. Lavrinova

Institute of Atmospheric Optics, SB of the Russian Academy of Sciences
1 Academicheskii Ave., 634055, Tomsk, Russian Federation

Considering numerically the problem of adaptive compensation of intensive laser beam atmospheric aberrations we demonstrated the influence of transient processes that occur in adaptive systems on the effectiveness and rate of control.

Two types of transient processes were investigated. Firstly, we considered the processes induced by nonlinear interaction of the laser beam and medium. In this case the variations of parameters in the plane of observation are caused by changes of the amplitude profile of the beam, phase profile, or changes of atmospheric characteristics on the path of propagation. We showed in Ref. 1 that despite the oscillations of registered parameters the adaptive correction can be realized if the period of oscillation of parameters differs from the characteristic time of the adaptive system.

Second type of transient processes occurring at the time of adaptive control is incited by the oscillation of mirror. To study this effect we created the numerical model of dynamic mirror. The interface of the corresponding computer code is depicted in Figs.1*a* and 1*b*. The code allows a user to define the geometry of the mirror (the number and positions of actuators and points of mirror fixation to the base) and its coefficient of attenuation (Fig.1*a*). The *DEMO* panel of the interface (Fig.1*b*) illustrates the oscillation of the mirror at reproducing the low-order Zernike polynomials. Here the user can choose the polynomial whose surface will appear in the left-hand side of the panel. In the center of the panel the oscillating surface of mirror is shown. The RMS deviation of the mirror from the given surface characterizes the quality of reproduction. This code can be integrated as a separate block in a model of the whole adaptive optics system.

The results of adaptive correction of thermal blooming with the use of this model on the base of multidither algorithm were presented in Ref. 2. As was shown, the control is possible if the frequency of correction differs from the frequency of oscillation of beam's parameters. At this, the introduction of parameter filtration is essential.

Lately we have considered numerically the correction of thermal blooming on the base of phase conjugation algorithm taking into account all types of transient processes. Some peculiarities of control
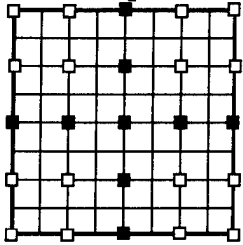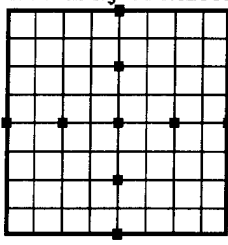
PARAMETERS

Actuator positions

Geometry of mirror

CONTROL

| Fixed Points |
| Actuators |
| Matrix |

| DEMO |
| Exit |
| Print Form |

CURRENT STATUS

Number of actuators	9
Number of fixed points	Undefined
Coefficient of attenuation	Undefined

Fig.1

DEMO

Zernike polinomial

Surface of mirror

Reproduced polinomial

| Tilt |
| Focus |
| Astigmatism |
| Coma |
| Sph. aberration |

PARAMETERS

Coordinates of fixed points	1, 9, 73, 81
Coordinates of actuators	4, 21, 35, 37, 39, 41, 43, 57, 74
Coefficient of attenuation	0.01
RMS deviation	0.16
Time	5.2

| Print Form | Exit |

Fig. 2

were detected. In particular we showed that sharp change of forces applied to the mirror causes instabilities of control. The elimination of instabilities and regular increase of intensity in the plane of observation is possible if applied forces change gradually. Of course, this results in decrease of correction speed. The optimization of mirror and mode of operation allowed us to achieve the rate of phase conjugation algorithm to be close to that of multidither algorithm.

References

1. F.Yu. Kanev and V.P. Lukin, "Algorithms of compensation for thermal blooming", Atmospheric Optics, 1991, Vol.4, No.12, pp. 856-863 [English edition].
2. F.Yu. Kanev, V.P. Lukin, L.N. Lavrinova, and S.S. Chesnokov "The dynamic model of a flexible adaptive mirror", in ESO Conf. and Workshop Proc., No. 48, 1993, pp. 229-234.

Authors: D.Bonaccini[1], S.Cova[2], M.Ghioni[2], R.Gheser[3] and F.Zappa[2]

[1] *European Southern Observatory - Karl-Schwarzschild-Str 2, D-8046 Garching b.
     Munchen, Germany*
[2] *Politecnico di Milano, Dip. di Elettronica e Informazione - piazza Leonardo da Vinci 32 -
     20133 Milano, Italy*
[3] *Officine Galileo - Via A. Einstein 35 - 50013 Campi Bisenzio - Firenze, Italy*

Title: *Development of high QE, fast Avalanche Photodiodes for Astronomical Adaptive
         Optics*

1. Development Rationale

Considering adaptive optics servosystems (AOS) in astronomical applications, a number of error sources have been identified in the wavefront sensor, which provides the reference signal of the servo-loop. These errors impair the system performance, especially with usually faint sources such as Natural Guide Stars (NGS).

A comparison is here made between CCD and single-photon counting avalanche photodiodes (Single-Photon-Avalanche Diodes, SPAD) in terms of the measured quantum detection efficiency.

We show quantitatively how the read-out noise of fast read-out CCDs propagates through the correction loop and worsen its performance, both in tip-tilt sensors and in Shack-Hartmann wavefront sensors. Photon counters such as SPADs do not have read-out noise and do eliminate part of the problem. The practical cases of ESO Adonis (previously ComeOnPlus) and VLT-NAOS systems are analysed and CCD vs. SPAD projected performance compared.

The relatively long integration time required with faint sources introduces a net delay term in the servo-loop transfer function, which dominates it and lowers the AOS performance. The advantage of SPADs is that they can be read in parallel and continuously in time, giving the possibility of eliminating the pure time delay effect on the servo-system transfer function phase component. Again for ESO's actual and planned AOS, analysis and projected performance is shown, with a comparison between CCD and SPAD for both tip-tilt and high order wavefront sensing.

2. SPAD sensor functional requirements

Currently a NGS reference is required both in AOS which use only NGS, and in systems which use laser guide stars (LGS), in the latter case for tip-tilt determination. Optimal tip-tilt determination may be done with Single-Photon Avalanche Diodes of the new Slik[TM] generation from EG&G Optoelectronics Canada. In view of the SPAD foreseen application in

AOS, a series of flexibilities have been specified for the design of new circuitry tailored for SPAD control. We have designed and implemented circuit boards including

1. active quenching and active reset circuitry working at the fastest rate; the deadtime in photon counting is reduced to 40 nsec and the SPAD measurement dynamical range is correspondingly expanded.

2. SPAD gating with nsec response, making possible fast-pulsed LGS operation;

3. flexible control of the SPAD overvoltages, which makes possible further enlargement of the dynamical range by reducing the power dissipation, and adjustment for diode-to-diode breakdown-voltage variations, due to either variations in the fabrication process or temperature variations during operation;

4. on-board 16 bit programmable counters, as well as direct access to pulses to be counted;

5. quad-cell controller with all the service circuitry for the SPAD modules, and optical fiber connection to VME hosted link;

3. SPAD Performance Characterisation

Linearity.

Experimental tests of the response linearity have been performed with the SPAD dice working above a double-stage Peltier micro-thermocooler, normally mounted in the EG&G Slik[TM] case. Full linearity is achieved up to 3 Mc/s and the dynamic range can be extended up to 6 Mc/s by employing a look-up table correction.

Thermal dissipation

A deviation from linearity is mainly caused by self-heating of the SPAD device. For a Slik device operating with 20V excess bias voltage above breakdown, the energy dissipated within the device is about 40 nJ per avalanche pulse and, therefore, at a pulse-counting rate of 1 Mc/s the mean power dissipation is about 40mW. The temperature rise in operation may be considerable, since the thermal resistance between the diode itself and the underlying thermocooler is not negligible. With the ceramic substrate currently employed for the Slik dice mounting and the Kovar metal case housing it, the total thermal resistance from the diode junction to the external heat sink is 0.1 C/mW. At a few Mc/s pulse repetition rate, the rise of the junction temperature is therefore sufficient to cause an increase of the breakdown voltage that reduces the excess bias voltage and, therefore, the detection efficiency. Significant improvement in the thermal behaviour can be obtained by employing new ceramic material, such as aluminium nitride, now available with higher thermal conductance.

Afterpulsing

In previous SPAD device generations, the dark-counting rate was considerably enhanced by phenomena of charge carrier trapping in deep levels. Carriers trapped during an avalanche pulse and then released with delay longer than the detector deadtime were able to re-trigger the avalanche, thereby causing spurious satellite pulses. The improved technology of the EG&G Slik fabrication process has almost eliminated this effect. Experimental tests performed enforcing different deadtime duration have confirmed that the dark-counting rate is almost independent from the deadtime value, and therefore practically not affected by afterpulsing.

Dark Counts

Besides eliminating the afterpulsing effect, the technological improvement has considerably reduced the concentration of centers responsible for the thermal generation of free charge carriers. The dark-counting rate has therefore been reduced to very low level: it is now possible to have less than 5 c/s dark-counting rate with SPAD operating temperature below 10 C.

Light Emission from SPAD

It is known that in the avalanche process in silicon, some light is emitted by charge carriers subject to the very high electric field values necessary for sustaining the avalanche multiplication. This emission is very weak, about one photon per 10^5 electrons crossing the junction, and distributed over a broad wavelength spectrum in the visible and infrared region. Cross-talk of adjacent detector chips of the quad-cell is avoided by providing screening barriers between them. A quantitative analysis has been made for determining also the residual crosstalk due to photons outcoming from a detector and reflected towards another one by the external optical system above the quad-cell. Taking into account the accurate data available on the intensity and spectral distribution of the emitted light and on the absorption and refraction properties of silicon, the total number and spectral distribution of outcoming photons have been evaluated, showing that the crosstalk via external reflection is at all negligible.

4. Quad-cell electronic module and controller design

A set of four modules and a controller motherboard have been designed and are being built in order to implement a focal plane system for the Telescopio Nazionale Galileo. Each electronic module is produced with SMD technology, in order to minimise the overall size of the board and optimise the high frequency path of the counting circuitry.

The four SPAD modules are physically connected to one Motherboard which is the controller of the working operating modes for the four detector devices. Modules and Motherboard are focal plane electronics. We ensure a complete interchangeability of each module as well as flexibility and programmability. Via two DAC per module the operating temperature and SPAD overvoltage are programmable via a microcontroller on the Mother Board. Significant constructional parameters of the SPADs, such as QE, breakdown voltage, temperature dependence coefficients etc. are stored on an EEPROM memory device on each SPAD module.

A Watch-dog circuit on the microcontroller supervises the operating conditions in order to prevent disruptive failures to the SPAD devices, via safely resetting the high voltage biases and the Peltier coolers. An opto-isolated hardware gating signal is allowed for pulsed laser operation, which can stop and blind the SPAD counting in a few nanosecond.

In order to program and monitor each SPAD module, as well as for the Motherboard to communicate with the VME based supervising system, an RS232 serial fiber link is used. Four high speed fiber-optic links from the focal plane SPAD Motherboard feed counter channels on the main VME-based system, where a Supervisor board as well as a DSP board are hosted. The photon-counting pulses of each SPAD module are thus read and used for computation and digital filtering of the mirror commands.

Besides direct pulse transmission, programmable integration time counting capability is also implemented on the focal plane SPAD Motherboard itself, readable as a 16-bit tri-state digital output.

Integration of the Active Quenching Circuitry and development progress

The active quenching circuit (AQC) has been first designed with discrete components and various elementary integrated circuit blocks and fabricated in compact form by surface-mounting technique. The interest of reducing the dimensions and power requirement of the AQC is quite evident. Work has therefore been started aiming at such a goal. The overall AQC has been divided in essentially two parts: i) the comparator and logic block, that senses the avalanche onset and generates the logic commands for quenching and resetting the SPAD and the output pulse, and ii) the driver block, that generates the actual voltage signals applied to the SPAD. As a first step, the design of an integrated version of the comparator and logic block has been undertaken. The design has been made for fabrication of this block in CMOS technology, providing low power consumption and very compact size. A first prototype of this block has been fabricated and tested with satisfactory results. An AQC composed by the integrated comparator and logic block and the discrete-component driver block has been tested. This AQC provides a performance equivalent to that of the previous discrete-component prototype with remarkably reduced size. Studies aiming to a complete monolithic integrated circuits are in progress: remarkable problems have to be solved, mainly concerning the technological compatibility of high-voltage components and low-voltage logic circuitry.

Tip-Tilt Correction at the Anglo-Australian Telescope

J. J. Bryant, J. W. O'Byrne, R. A. Minard, P. W. Fekete and L. E. Cram

Contact address for all authors:
School of Physics,
University of Sydney,
NSW Australia 2006
Ph: 61-2-351-5577,
Fax: 61-2-660-2903
Email: jbryant@physics.usyd.edu.au

The first stage of the AAT adaptive optics program, allowing tip-tilt correction for images and spectroscopy in the near infrared has recently been implemented.

Scientific Applications
and Results

WA   8:30 am-10:30 am
Auditorium

Peter Wizinowich, *Presider*
W.M. Keck Observatory, USA

ASTRONOMY WITH ADAPTIVE OPTICS

P.Léna
(Université Paris VII & Observatoire de Paris)

The operation of the ESO ComeOn adaptive optics system, under its successive improved versions at La Silla on the 3.6 m telescope since 1991, has produced a great number of new scientific results. In addition, it has started a learning process for an efficient use of adaptive optics in diffraction-limited imaging from the ground with large telescopes. Finally, it suggests new, original applications of adaptive optics, some of them being implemented or on the way to be implemented.

Besides the sicntific production itself, this overall activity can be considered as a preparation for the generalized use of adaptive optics on the new genration of 8-10 meters telescopes, or the retrofit of existing 4 m class instruments.

This Presentation will cover these various aspects. On the science side, a "best of" the results obtained by various groups or observers will be shown and commented : surfaces (Ceres, Vesta, Titan, Pallas) or atmospheres (Jupiter, Titan) of solar system objects, multiple stars systems resolved at the diffraction-limit, circumstellar environments with emphasis on discs, active galactic nuclei. This will demonstrate the capabilities and current limits of AO : sensitivity, dynamic range, image quality and deconvolution stability, astrometric accuracy. Comparisons with data obtained on the Hubble telescope at different wavelengths will emphasize the complementarity between space and ground observations. Some indications on this complementarity for the ISO mission will be presented. A number of new approaches will be indicated : coronographic mode, beam extraction by single mode optical fibers, spectrographic coupling, use of artificial intelligence.

A discussion of the current conclusions on the sensitivity issue versus the numerous parameters entering AO strategies will be presented : magnitude and position of the reference object, wavelength of observation of the reference and of the object, wavefront sensor performances, turbulence properties, prediction capabilities, etc.

Longer term goals towards multi-telescope interferometry will be presented in the light of the current adaptive optics performances.

Post-Processing of Adaptive Optics Corrected Images

Julian C. Christou, Jack D. Drummond
Starfire Optical Range, PL/LIG
U.S. Air Force Phillips Laboratory
3550 Aberdeen Avenue SE
Kirtland AFB, NM 87117-5776

Ground-based images of astronomical objects typically require some form of post-processing to realize their full information content. The same is true for images obtained with adaptive optics. In order to do this an unresolved source near the target of interest is required. The target image can be expressed as

$$i(\vec{r}) = o(\vec{r}) \star p(\vec{r}) + c(\vec{r}) \tag{1}$$

which is the standard expression for incoherent imaging where $i(\vec{r})$ is the measured target, $o(\vec{r})$ is the true object distribution, $p(\vec{r})$ represents the point spread function (PSF) of the optical system, $c(\vec{r})$ the noise contamination in the image and $\star$ denotes the convolution operation. When the PSF is known, inversion of (1) by various deconvolution algorithms yield the object distribution. These algorithms include linear methods such as inverse and Wiener filtering and non-linear techniques such as Richardson-Lucy and Maximum-entropy. The application of these and other algorithms to Hubble Space Telescope data has been recently published (Hanisch & White).

For Adaptive Optics (AO) imaging the compensated point spread fuction (PSF) can vary from object-to-object and also with time for the same object. There is also the spatial variation across wide field of views. In other words AO is characterized by a non-uniform PSF. The main sources of temporal variability are due to (i) variations in the instantaneous realizations of the atmospheric coherence length, r_0 and (ii) Greenwood frequency, f_g, which is inversly proportional to the atmospheric coherence time. The degree of variability is affected by the spatial sampling of the wavefront, i.e. the number of sub-apertures across the pupil, and the temporal sampling. The AO performance is also affected by the target itself. The sub-aperture tilt measurements are affected by both the extent of the target and its brightness, which affects the signal-to-noise (SNR) of the wavefront reconstruction. Observations at the Starfire Optical Range (SOR) have also shown that residual errors in the full-aperture tilt correction also affects the AO PSF. The high-order compensation of the deformable mirror compensates the speckle structure of the image for short integrations. However, longexposure integrations may be dominated by errors of the full-aperture tilt mirror. The residual rms image motion smears the compensated instantaneous PSF. These tilt errors are signal dependant and become important when using a laser beacon for the high-order compensation. A further source of PSF variability is the spatial extent of the compensation, i.e. off-axis sources have a different PSF because of anisoplanatism. Thus, PSF's measured from nearby point source references, either
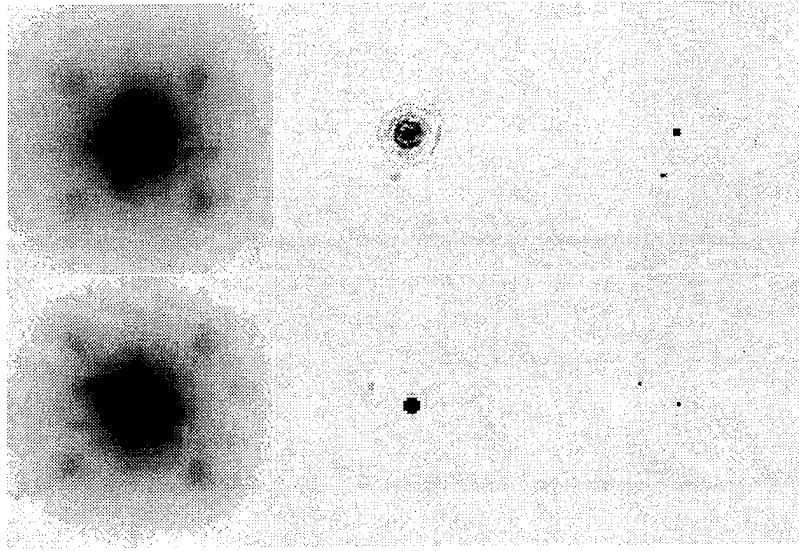
Figure 1. AO imaging of μ Cass for Aug. 18, 1994 (top) and Oct. 22, 1994 (bottom). Left to right: average AO closed-loop image, IBD result, and post-IBD Richardson-Lucy deconvolution. Post processing permits determination of astrometry and relative photometry of the two components. $\Delta m \sim 5.0$ ($\sim 100\times$).

simultaneously or sequentially, may not always be suitable for regular linear and non-linear deconvolution.

In this paper we present application of a blind deconvolution (BD) algorithm to AO data obtained at the SOR's 1.5m telescope. Blind deconvolution permits the recovery of target distributions for the cases of poorly determined or unknown PSF's. This is possible because of external contraints on both the target and PSF which satisfy the incoherent imaging equation above. These constraints are (1) that both are positive definite, (ii) that the estimates should convolve to the measurement, (iii) that the PSF is band-limited to prevent trivial solutions, and (iv) that multiple images can be used to handle the noise as well as stongly varying PSF's. The algorithm used in this paper is that developed by Jefferies & Christou.

Application of iterative blind deconvolution to long-exposure AO imaging is presented for the nearby population II binary star μ Cas. The results from two separate observations are show in figure 1. This shows an average AO image along with the corresponding BD results and the results of post-processing the BD image by a Richardson-Lucy algorithm. (see Drummond et. al., 1995).

The multiple system ADS 9731 was observed as part of an isoplanatic study. However, the two bright components separated by $\sim 14.''6$ are both binary and the compenstaed image does not permit the complete separation of the two close components. Figure 2 shows the reconstructed field mean PSF's obtained by BD for ten independant observations of ADS 9731 obtained in the I-band using Rayleigh beacon AO. Each exposure has a 30s integration time. Note the variability of these sequential PSF's illustrating the problem of using a measured AO PSF for deconvolution. The isoplanatic behaviour is discussed in more detail by Christou et al. (1995).

In addition to these long exposure data, post-processing of short exposure data, i.e. at speckle lifetimes, will also be presented. This includes measurements of aniso-
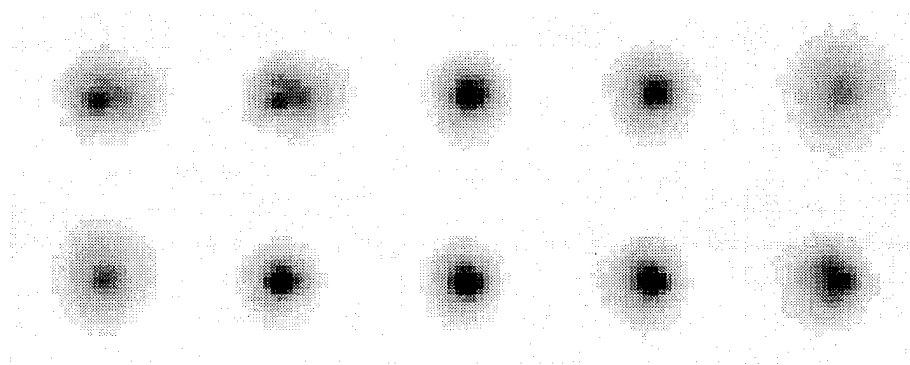
Figure 2. The ten reconstructed PSF's for the I-band iterative blind deconvolution.

planatic behaviour using a shift-and-add (SAA) algorithm (also see Ellerbroek et al.). Compensated speckle data is dominated by a single bright speckle making SAA or peak tracking very applicable. Also the application of BD to compensated speckle observations of extended objects will also be presented.

References

J.C. Christou, B.L. Ellerbroek, R.Q. Fugate, D. Bonaccini, & R. Stanga, *Astrophys. J.*, in press, 1995.

J.D. Drummond, J.C. Christou & R. Fugate, *Astrophys. J.*, in press, 1995.

B.L. Ellerbroek, J.C. Christou, J.F. Riker, & J.T. Roark, this conference.

R.J. Hanisch & R.L. White, "The Restoration of HST Images & Spectra - II", Space Telescope Science Institute, 1993.

S.M. Jefferies & J.C. Christou, *Astrophys. J.* **415**, 862–874, 1993.

Compensated Imaging System (CIS) Observations of the Circumstellar Envelope of P-Cygni

Authors: C. Morossi (1), M. Franchini (1), R. Ragazzoni (2), G. Sedmak (1,3)
A. Suzuki (4), J. Albetski (5), J. Africano (6), D. Nishimoto (6),
S. Restaino (7)

(1)   Trieste Astronomical Observatory, via G. B. Tiepolo 11, Trieste, Italy
(2)   Padova Astronomical Observatory, vicolo del'Observatorio 5, Padova, Italy
(3)   Astronomical Department, Universita' degli Studi, Trieste, Italy
(4)   Phillips Laboratory, 535 Lipoa Parkway, Suite 200, Kihei, HI 96753, USA
      Phone: 808/874-1541; 808/874-1640 FAX
(5)   ThermoTrex Corporation, 535 Lipoa Parkway, Suite 200, Kihei, HI 56753, USA
      Phone: 808/875-4500; 808/874-1630 FAX
(6)   Rockwell Power Systems, 535 Lipoa Parkway, Suite 200, Kihei, HI 96753, USA
      Phone: 808/875-4500; 808/874-1600 FAX
(7)   Phillips Laboratory/LIMI, 3550 Aberdeen Avenue SE, Albuquerque, NM 87117, USA
      Phone: 505/846-4410; 505/846-2045 FAX

Introduction

This project is a direct result from OSA and the ESO's first adaptive optics conference. The objective for the Air Force Maui Optical Station (AMOS) was to collaborate and present to the astronomical community the benefits and advantages of using an adaptive optics system for astronomical imaging research.

The star, P-Cygni, was discovered on August 18, 1600 A.D., when it brightened to about the third magnitude.

Several attempts to acquire information on size, chemical composition, and density distribution of the material around the star have already been done (i.e., Leitherer and Zickgraf, 1987). Barlow et. al, 1994 acquired [N II] narrow band images which show a nearly circular nebula with angular diameter of about 22 arcseconds and hint at the presence of nebular rings at circa 6 and 11 arcseconds. On the other hand, White and Becker (1982) obtained observations which are consistent with a homogenous, spherically symmetric, constant velocity isothermal flow.

Conclusion

Here we present the results of P-Cygni obtained in H alpha, utilizing the capabilities of adaptive optics plus coronograph as tools for analyzing circumstellar envelopes within a few arcseconds of bright stars.

The effects of the ghosts are clearly evident in the ratios of images in different filters for the same star showing that the artifacts are strongly filter-dependent.

The comparison star can be used to discriminate between ghosts and real features. Furthermore, the comparison of images in different filters for each star and in the same filter for the two stars allows us to double-check the results.

The ratio between P-Cygni and 55 Cyg in the H-alpha filter shows a radial gradient which is not observed in the ratio obtained in the filter centered in a continuum spectral window, thus indicating the presence of an extended diffuse H-alpha emission in the inner region surrounding P-Cygni.

The complete analysis based on the use of deconvolution procedure is in progress aiming to derive the morphology of H-alpha emission.

The analysis of the images obtained with the other filters, also in progress, will give hints on the physical and chemical structure of the P-Cygni nebula.

References

Barlow, M. J., Drew, J. E. Meaburn, J., Massey, R. M., 1994, Mon. Not. R. Astron. Soc., 268, L29.

IRAF 1992, *"Image Reduction and Analysis Facility,"* Version 2.10.1, NOAO, Tucson.

Leitherer, C., Zickgraf, F. J., 1987, *Astron. Astrophys.,* 174, 103.

STSDAS 1994, *"Space Telescope Science Data Analysis System,"* Version 1.3.2, STScI, Baltimore.

White, R. L., Becker, R. H., 1982, *Astrophys. J.,* 262, 657.

FIRST TIME MEASUREMENTS MADE OF THE SPECTRAL MORPHOLOGY CLOSE TO THE CORE OF P-CYGNI

Difference of P-Cygni and 55 Cygni
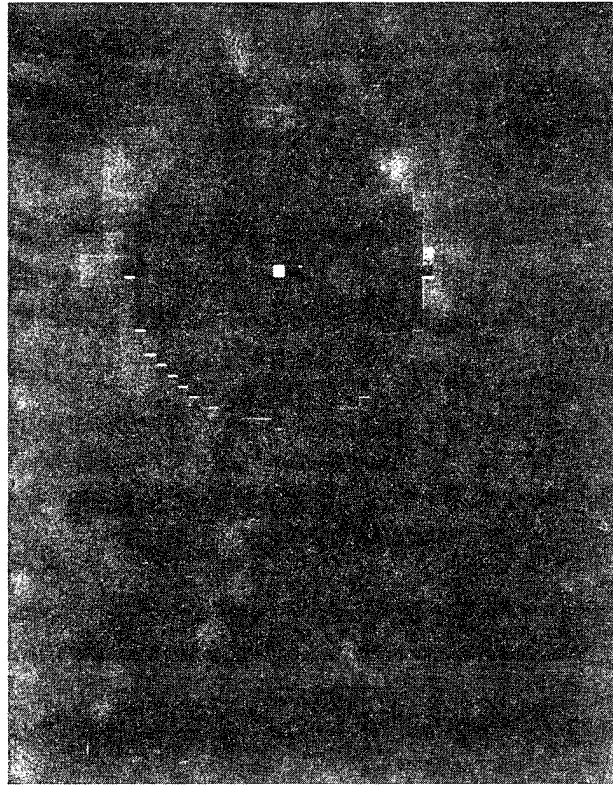
H alpha (656 nm)

Continuum (675 nm)

Observational Results from the University of Hawaii Adaptive Optics System

J.E. Graves, F. Roddier, C. Roddier, M. Northcott
University of Hawaii
2680 Woodlawn Dr., Honolulu, HI 96822

Summary not available.

High Resolution Spectroscopy
with an Adaptive Optics Telescope

N. Woolf, J.R.P. Angel, J. Black, J. Ge, B. Jacobsen, M. Lloyd-Hart
Steward Observatory, University of Arizona
Tucson, AZ 85721
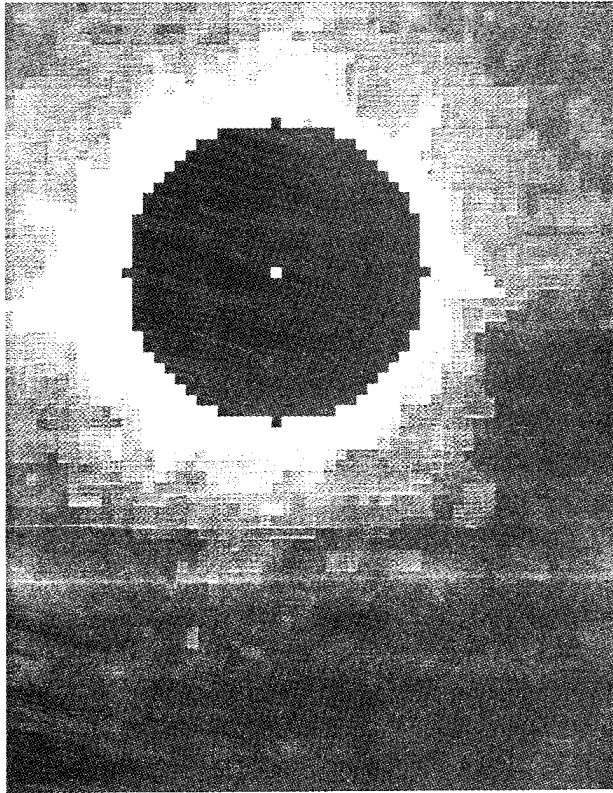Phone: (520) 621-1539 - Fax: (520)621-9843

R. Fugate
Starfire Optical Range, U.S. Air Force Phillips Lab, Kirtland AFB NM 87117
Phone: (505)846-4712 - Fax: (505)846-0439

High resolution spectroscopy of stars has been rarely used because at visible wavelengths, the atmosphere produces a star image typically 10-20 times the diffraction limit of the telescope. Either the grating must be used at a far poorer resolution than its diffraction limit, or much light must be lost at the slit.

Also, to observe as much spectrum as possible, using multi-pixel electronic detectors, which typically have a near-square format, the spectrograph needs to be a cross dispersed echelle. Even if a large echelle is used, the star image will be appreciably wider than the slit width, and the large image in the cross-dispersion direction means that relatively few orders can be observed at one time.

When an adaptive optics telescope is coupled to a spectrograph, the spectrograph accepts the diffraction limited star image and produces a narrow spectrum at near the diffraction limited resolution of the spectrograph, and many orders can be observed simultaneously.

We have mated an echelle spectrograph with a 250mm by 125mm echelle of 23 grooves/mm. to the 1.5m adaptive optics telescope at Starfire Optical Range. Our purpose is to obtain high resolution spectrograms of distant stars to study interstellar absorption lines at spectral resolution of between 500,000 and 1,000,000. The first test of the process have been made, and results are being analyzed to determine an optimum manner of use for high precision quantitative spectrometry. The goal is that by using a large format CCD, and by taking exposures at about 6 grating settings, the entire spectrum can be studied.

This paper demonstrates some of the aspects of this first test:-

The telescope divides the spectrum into two parts, from 750nm to 1μ wavelength "the red", and shortward of 750nm "the blue". In the "red" the observed spectrum of Vega was useful from 78th order at 985.2nm to the 107th order at 718.2nm, a total of 29 orders. In the "blue", some 55 orders were visible. In an ideally configured system, all these orders of the echelle could be observed at once.

The spectra show the resolution of the system, seen in the profile of a Helium-Neon laser, in which at least three modes are present, and resolved by the spectrograph. The resolving power is 700,000. Indeed, the mode-switching has been observed with the spectrograph.

Also shown are stellar spectra of Vega and Arcturus taken in the A band of the Oxygen molecule. They show the oxygen lines, and clearly show higher resolution than is seen in the atlas of the spectrum of Arcturus by Griffin. The results are encouraging that an optimum instrument can be built and the scientific study can commence.

Imaging exoplanets with the 6.5 m MMT and Magellan telescopes

Roger Angel[1] and David Sandler [1,2]

[1]Center for Astronomical Adaptive Optics
Department of Astronomy
University of Arizona
Tucson, Arizona, 85721
Phone: (520) 621-6541 - Fax: (520) 621-9843

[2]ThermoTrex
9550 Distribution Avenue
San Diego, California, 92121-2305
Phone: (619) 536-8528 - Fax: (619) 536-8538

Do stars like the sun also have similar planetary systems? No positive detection has been yet made, but observations by various ground based methods may soon produce answers. Gravitational microlensing events observed with high precision should show the presence of planets around distant normal stars[1]. Indirect searches are also currently being conducted of nearby stars, for stellar reaction motion through astrometry and doppler accelerometry . The sensitivity and length of observations should soon become adequate to sense Jupiter mass planets at a number of stars.

It should now also be possible to see exoplanets as well as detect their gravitational influence. We have proposed direct detection, by imaging with a large telescope corrected with adaptive optics[2,3]. The challenge is severe and demands unique instrumentation: seen from afar, Jupiter would be about 10^9 times fainter than the sun. Small angular separations must be reached to make a useful survey. To find a couple of dozen single stars reasonably similar to the Sun (types A - K), we need to reach out to a distance of ~ 10 pc. At this distance, the maximum elongation of Jupiter's 5 AU orbit is 0.5 arcsec.

Though the challenge is severe, conditions for applying adaptive optics are particularly favorable, in that the planets we seek are all well within the isoplanatic angle of a very bright reference object. Measurement and correction of the stellar wavefront to the diffraction limit is in principle not difficult, and will result in the recovery of a diffraction limited planet image. However, normal correction with subapertures ~ r_0 is not enough to make a detection at the 10^{-9} level. Even if quite decent Strehl ratio is recovered, the starlight halo at 1/2 arcsec radius is not

much suppressed, and its photon and speckle noise superposed on the planet would prevent detection. To address this problem, we plan to use 1) Adaptive optics on a fine scale and operating at high speed, so that the wavefront aberration is well corrected on the spatial scales that would otherwise throw energy out to 1/2 arcsec radius. 2) Large telescopes, so the diffraction limited planet image is sharply concentrated and well separated from the star.

We propose to use the twin 6.5 m telescopes the converted MMT in Arizona[4] and the Magellan telescope in Chile[5] to conduct an all sky search. These have identical optics (f/1.25 primaries), so that a single instrument developed at the MMT will serve for successive surveys in each hemisphere. Both telescopes are under construction, with operation of the MMT scheduled for 1997 and Magellan for 1998. Imaging will be in a band centered at 1.2 microns wavelength, where the diffraction limited resolution is 0.04 arcsec, and the critical spatial scale for scattering is ~ 0.5 m.

The speed and resolution of correction is limited ultimately by photon noise in the stellar flux detected by the wavefront sensor. Optimization shows that for the stars in question, which are typically 4th magnitude in the red, the sensor subaperture size should be 5 cm, and the correction cycle 0.5 millisecond. The deformable mirror thus must have some 20,000 fast actuators. Buttable prototypes with the required performance exist[6]. A wavefront sensor design based on Zernike's point diffraction interferometer has the required resolution, uses high sensitivity CCDs and has manageable computer requirements[2]. Thus the detailed correction should be realizable in practice, giving a total error in the corrected wavefront of about 25 nm rms.

After correction by such a system, the residual scattered stellar halo will contain about 2% of the stellar energy and be spread uniformly out to 5 arcsec. The halo surface brightness is thus about a million times less than the stellar peak, but still a thousand times brighter than the planet. Detection relies on long integrations to average out the speckle and photon noise in the halo background, to 2×10^{-4} for 5 σ detection. Random errors have been analysed, and are such as to allow this accuracy after a few hours of integration. Systematic halo features, such as fixed pattern from spider diffraction or ghosts, are strongly supressed by the image rotation from the alt-az telescope mount. There is also strong chromatic radial smoothing of scattered starlight. Stahl and Sandler[3] have recently completed an extensive optimization and analysis of systematic errors. They find that temporally and spatially coherent wavefront errors arising from servo lag can be strongly supressed by using forward prediction in the reconstruction algorithm. A full numerical simulation of the expected imaging has been obtained from their detailed modelling of atmospheric propagation and the correction system (figure 1).

To confirm the practicallity of such detailed wavefront correction, and of high signal/noise halo averaging, we plan to conduct experiments at the Starfire Optical Range, building on the Air Force experience and facilities for high resolution correction. The project team, including Bob Fugate, Michael Lloyd Hart, Jonathan Lunine, Don McCarthy and Steve Stahl, hopes to complete development of the full scale survey instrument at the MMT in 3 years.

References

1. Mao, S. and Paczynski, B. 1991, Ap. J. **374**, 137.
2. Angel, J.R.P., Nature, 1994, **368**, 203
3. Stahl, S. and Sandler, D., 1995, Ap.J. Lett, submitted
4. Olbert, B., Angel, R., Hill, J. and Hinman, D. 1994 Proc SPIE **2199**, 144
5. De Jonge, M.J., 1994, Proc SPIE **2199**, 22
6. Hulburd, B., and Sandler, D., 1990, Opt. Eng. **29**, 1186.
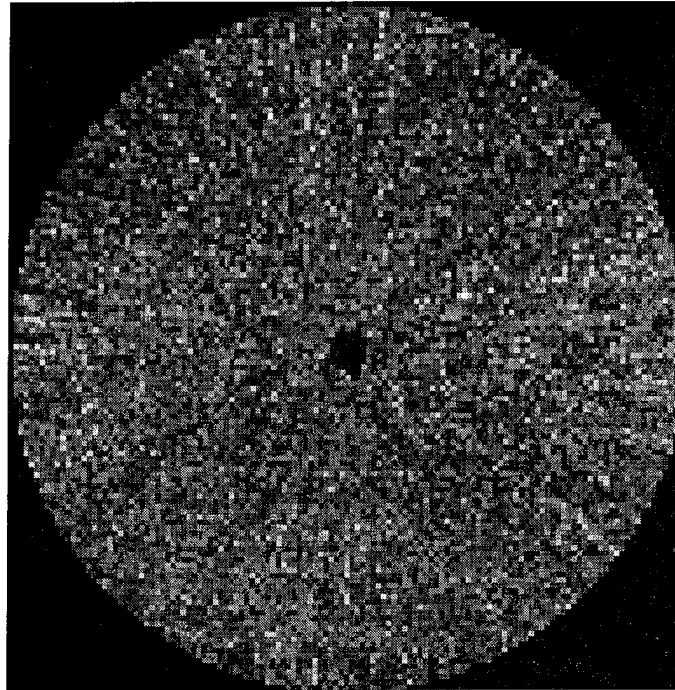
Figure 1. Simulation by Stahl and Sandler[3] of a five hour exposure with the 6.5 m MMT of a solar system twin at 8 pc. Jupiter at 0.6 arcsec radius and 2-o-clock stands out at 5 sigma above the noise. The central star is blocked by a field stop.

Computational Methods

WB   11:00 am-12:15 pm
Auditorium

Glenn Tyler, *Presider*
The Optical Sciences Company, USA

Comparison of Speckle Image Reconstruction Techniques: Experimental Measurements of Estimator Bias and Signal to Noise Ratio

David Dayton, Steve Sandven
Applied Technology Associates, 1900 Randolf SE, Albuquerque, NM 87106

John Gonglewski
Air Force Phillips Laboratory, PL/LIMI, Kirtland Air Force Base, NM 87117

1. INTRODUCTION

Deconvolution from Wave-Front Sensing (DWFS) has been investigated both through laboratory and field experiments as a method to produce high resolution images from ground based telescopes.[1,2,3] This technique has sometimes been referred to as Speckle Holography. With this technique a short exposure focal plane image is recorded simultaneously with an estimate of the atmospheric wave-front. The wave-front estimate is used to calculate an optical transfer function (OTF) for the atmosphere. This OTF estimate is then used in a deconvolution algorithm to correct the focal plane image. A synoptic sketch of a DWFS instrument is shown in figure 1.
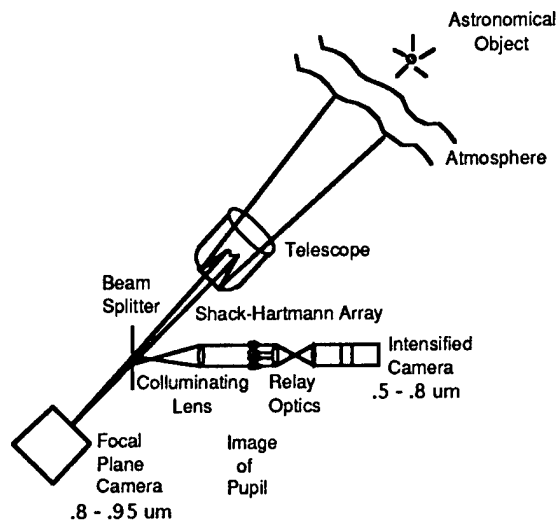
Figure 1
Synoptic Sketch of DWFS Instrument

Figure 1 shows a Shack-Hartmann wave-front sensor located at the pupil image of the telescope. This wave-front sensor produces an estimate of the integrated atmosphere induced phase error along the propagation path. If we assume the near field or thin phase screen approximation[7], the system short exposure OTF can be estimated from the wave-front measurements by calculating the auto correlation of the exponentiated phase.

$$\hat{H}(f) = e^{j\hat{\phi}} \otimes e^{-j\hat{\phi}} \tag{1}$$

Although we assume that there are no magnitude fluctuations in the pupil, (i.e. the turbulence is in the near field) the OTF estimate obtained with equation (1) will have both phase and magnitude fluctuations.

A. Primot Estimator

Primot et. al.[1] proposed an object estimator based on an ensemble of short exposure focal plane and OTF measurement pairs. For N such measurement pairs, the object estimate is given as

$$\hat{O}(f) = \frac{\sum_{i=1}^{N} \hat{H}_i^*(f)\, I_i(f)}{\sum_{i=1}^{N} \hat{H}_i^*(f)\, \hat{H}_i(f)} \qquad (2)$$

In equation (2) $I_i(f)$ refers to the Fourier transform of the ith image estimate and $\hat{O}(f)$ refers to the Fourier transform of the object estimate. The Fourier domain quantities in equation (2) are functions of two dimensional spatial frequency, however for brevity we use only one frequency variable f. As the number of ensemble members gets large the denominator of equation (2) approaches its mean value, and we get

$$\hat{O}(f) = \frac{\sum_{i=1}^{N} \hat{H}_i^*(f)\, I_i(f)}{\left\langle \hat{H}_i^*(f)\, \hat{H}_i(f) \right\rangle} \qquad (3)$$

Recently Roggeman and Welsh[4] have derived a new expression for the signal-to-noise ratio (SNR) of the estimator.

$$SNR(f) = \frac{\overline{K}\,|O(f)|\,\left|\left\langle H(f)\,\hat{H}^*(f) \right\rangle\right|}{\sqrt{\overline{K}\left\langle |\hat{H}(f)|^2 \right\rangle + \overline{K}^2 |O(f)|^2 \mathrm{var}\left[H(f)\,\hat{H}^*(f) \right]}} \qquad (6)$$

They go on to show, using computer simulations, that even for the case of high light case and very good seeing that the SNR of equation (6) is not much better than the SNR of the power spectrum estimate of simpler speckle techniques such as Knox-Thompson or bi-spectrum. In fact for the case of a point object it is shown to be often worse. In addition Roggeman[5] has shown through computer simulation that the denominator term of equation (3) is a biased estimator of the mean OTF magnitude. Previous works describing the DWFS technique[1,2,3] did not properly account for this bias effect.

2. EXPERIMENTAL MEASUREMENTS

In the full paper we present bias and SNR measurements for a series of bright stars under different seeing conditions, as well as an extended planetary object. We also compare reconstructions using the DWFS technique and the Knox-Thompson technique. A subjective comparison is made between the experimental measurements and computer simulated results presented elsewhere[4,5].

References

1. J. Primot, G. Rousset, and J.C. Fontanella, "Deconvolution from Wave-Front Sensing: a new technique for compensating turbulence-degraded images", JOSA-A **7** (1990).

2. J.D. Gonglewski, D.G. Voelz, J.S. Fender, D.C. Dayton, B.K. Spielbusch, and R.E. Pierson, "First Astronomical Application of Postdetection Turbulence Compensation", Appl. Opt. **29**, 31 (1990).

3. D.C. Dayton, S. Sandven, J.D. Gonglewski, "High Resolution Imaging of Astronomical Objects Using Deconvolution from Wave-Front Sensing", OSA Conference on Signal Recovery and Synthesis, Salt Lake City, Utah, 1995.

4. M. C. Roggeman, B. M. Welsh, "Signal-to-Noise Ratio for Astronomical Imaging by Deconvolution from Wave-Front Sensing", Appl. Opt. **33**, 23 (1994).

5. M. C. Roggeman, B. M. Welsh, J. Devey, "Biased Estimators and Object-Spectrum Estimation in the Method of Deconvolution from Wave-Front Sensing", Appl. Opt. **33**, 24 (1994).

6. J.C. Dainty, Laser Speckle and Related Phenomena Springer-Verlag (1984).

7. J.W. Goodman, Statictical Optics John Wiley and Sons (1985).

Are scintillations indeed noise for wave front sensing?

Erez N. Ribak

Department of Physics, Technion – Israel Institute of Technology,
Haifa 32000, Israel

The field of view in adaptive optics is limited by a very narrow isoplanatic angle. A number of deformable mirrors, each conjugated to a different atmospheric layer, might provide phase compensation over an extended field. For this a larger volume need be probed using a multitude of guide stars (see review in [Baharav 1994,95]). Angel [1994] noticed that the search for planets next to bright stars is limited by scintillation. Scintillation is produced by high turbulence [Tatarski 1971]. If so, why not correct it with a deformable mirror conjugate to that turbulence, whose error signal is provided by the same scintillation? [Ribak 1994,5].

Fresnel diffraction from high altitude turbulence. Turbulence tends to be concentrated in several, rather thin, layers [Coulman 1985, Ribak 1994,95], and diffraction effects within the layers are negligible. A plane wave from a star undergoes minute changes as it traverses these layers. Direct relationship between scintillation and refractive index of air can be derived either from conservation of energy and geometrical optics, or from Fermat's principle [Tatarskii 1971]. Let us expand the refractive index as $n(x,y,z) \cong 1 + \mu(x,y,z)$, where $\mu(x,y,z) \ll 1$ inside L layers and negligible between them. The logarithm of the intensity I at ground level ($z=0$) is

$$\chi(x,y) \equiv \ln\frac{I(x,y)}{\bar{I}} = -\int_0^\infty z\,\nabla^2\mu(x,y,z)\,dz \approx -\sum_{i=1}^{L} z_i\,\nabla^2\mu_i(x,y). \qquad (1)$$

Thus the effect is linear with distance, which renders the lower layers immaterial for scintillation. A similar relation between intensity and wave front phase can be shown through the irradiance transport equation [Teague 1983], derived under the assumption of Fresnel diffraction

$$\partial I(x,y,z)/\partial z = -\nabla I(x,y,z) \cdot \nabla\varphi(x,y,z) - I(x,y,z)\,\nabla^2\varphi(x,y,z). \qquad (2)$$

This is equivalent to curvature sensing [Roddier 1988,90]. Eq. (1) follows because the intensity is constant above the atmosphere, and $\nabla I = 0$.

It is possible to start with Fresnel diffraction directly, if the atmosphere is composed of two main layers, one high above the telescope and the other very close to it. Phase errors are added to the cascading beams inside these layers, and they undergo Fresnel diffraction between them. If the

scattering point is at elevation $z = H$ and we measure at a lateral (horizontal) shift of $x = \rho$, then the Fresnel approximation is valid when $H \gg k^{1/3} \rho^{4/3}/2$, where $k = 2\pi/\lambda$. For $\rho = 1\text{m}$, $\lambda = .5\mu\text{m}$, this implies [Coulman 1985] $H \gg 116\text{m}$ (see discussion in Goodman [1968] and Tatarski [1971]).

Just above the top layer the field from a star is a plane wave, $O(x,y) \equiv O(\mathbf{r}) = F$ (F real). At the layer it accumulates a phase $\varphi(\mathbf{r})$; it is this phase that we wish to estimate. Just below the layer, at altitude h, the field is $P(\mathbf{r}) = O(\mathbf{r}) \exp i\varphi(\mathbf{r}) = F \exp i\varphi(\mathbf{r})$. After propagation to the top of the boundary layer the field is convolved with a Fresnel point spread function [Goodman 1968],

$$Q(\mathbf{r}) = P(\mathbf{r}) * (2lh)^{-1} \exp[ikh(1 - r^2/2h^2)] . \tag{3}$$

The field accumulates an additional phase $\psi(\mathbf{r})$ inside the boundary layer. At the telescope it is $R(\mathbf{r}) = Q(\mathbf{r}) \exp i\psi(\mathbf{r})$. The wave front sensor phase is $\text{Arg}\{R(\mathbf{r})\} = \varphi(\mathbf{r}) + \psi(\mathbf{r})$ [Tatarski 1971]. However, the intensity (the scintillation) is *independent* of the boundary layer,

$$S(\mathbf{r}) = |R(\mathbf{r})|^2 = |Q(\mathbf{r}) \exp i\psi(\mathbf{r})|^2 = |Q(\mathbf{r})|^2 . \tag{4}$$

Application. Instead of averaging or calibrating away scintillation, it can be used as additional information about the atmosphere. Assume that the intensity is sampled densely, but is degraded by detection noise. From the measured intensity $\hat{S}(\mathbf{r})$, form $\hat{\chi}(\mathbf{r}) = \ln \hat{S}(\mathbf{r})/\bar{S}$, its (average normalized) logarithm. Assume also a turbulence altitude $\hat{h}$. It is easiest to recover the phase from Eq. (1) by integrating twice the log-intensity $\hat{\chi}(\mathbf{r})$ over the aperture. Unlike curvature sensing [Roddier 1988] we ignore piston, tip, and tilt of the top layer because of the lack of boundary conditions. The laplacian of the wave front is equivalent to a quadratic filter, $C(w) = -1/4\pi^2 w^2$, where w is the radial Fourier frequency. Inverting the laplacian amounts to deconvolution by the same filter or, better still, by a Wiener filter

$$W(w) = \frac{C^{-1}(w) F_A(w)}{C^{-2}(w) F_A(w) + F_N(w)} \cong \frac{-4\pi \bar{S} \gamma}{16\pi^2 \gamma \bar{S} w^2 + w^{5/3}} , \tag{5}$$

where $F_A(w)$ and $F_N(w)$ are the power spectra of the wave fronts of the top layer and of the noise in $\hat{\chi}(\mathbf{r})$. All these functions are real and centro-symmetric. On the right we substituted a model [Ribak 1994,95], although all functions can be measured. Here $\gamma \equiv 6.9 \cdot 2^{5/3} \Gamma^2(11/6) \pi^{-2} r_0^{-5/3}$.

Limitations. **(a)** Intensity. Additive noise (shot, read-out) can be stronger than scintillation, but use can be made of their different statistics (as in Eq. 5). **(b)** Resolution. The effect might be mitigated because scintillation is much finer than pixels in wave front sensors (the same applies for temporal resolution). **(c)** Color. The Fresnel approximation is wave length dependent (Eq. 3), but laboratory experiments and simulation do not show it. **(d)** Source size. Tatarskii [1971] calculates an angular size of objects prone to scintillation, $\gamma_0 \le \sqrt{2\lambda/\pi h} \approx 1.4"$ for $\lambda = 589$ nm and $h = 8$ km. **(e)** Isoplanatic angle. A second deformable mirror correcting the top layer widens significantly the

field of view. (e) Contributions of layers. Solving simultaneously for both wave fronts using the scintillation and total wave front should reduce their covariance. (f) Thick layers. Eqs. (1) or (2) can be solved iteratively when more than two layers are present.

Simulation. A blind test was run: Fresnel propagation was used to create scintillation, but the original phases were recovered by inversion of the laplacian. Wave fronts with $r_0 = 10$ cm were convolved with the Fresnel kernel (Eq. 3) in a square 128 or 256 array with 2.5 or 5 cm pixels. The resultant field was squared to yield the intensity at the aperture plane. Patterns were found to be independent of wave length. Poisson noise was applied to the result, and only the intensity inside a 3 or 6 m telescope with a 1/3 central obscuration was taken. On this scintillation we applied either a simple inversion of the laplacian or a Wiener filter (Eq. 5). Fig. (1) shows the results for 100 photons per pixel: in both cases the rms difference between the original and the calculated phase, global slope removed, was 0.77 waves. At 1000 photons the difference was negligible.

Acknowledgments are due to R Angel, R Dekany, K Hege, and N Woolf, and to M Cheselka and E Gershnik for aid with the simulations.

References.

J R P Angel (1994), Nature **368**, 203.

Y Baharav *et al* (1994), Opt Lett **19**, 222; (1995) Subm.

C. E. Coulman (1985), *Ann. Rev. Astron. Astrophys.* **23**, 19.

J. W. Goodman (1968), *Introduction to Fourier Optics*. Wiley.

E N Ribak (1994), SPIE **2426**, 2.2.6; E N Ribak *et al* (1995), Subm.

F. Roddier (1988), Appl. Opt. **27**, 1223; (1990), **29**, 1402.

V I Tatarskii (1971), *The effects of the turbulent atmosphere on wave propagation*. Israel Program for Scientific Translations.

M. R. Teague (1983), J. Opt. Soc. **73**, 1434.

Fig. 1. (a) A realization of high-altitude phases; also output at high flux. (b) Scintillation pattern at the aperture. (c) Direct inversion of the laplacian. (d) Wiener deconvolution. (e) Cut across the apertures. The lowest and the highest frequencies were lost.
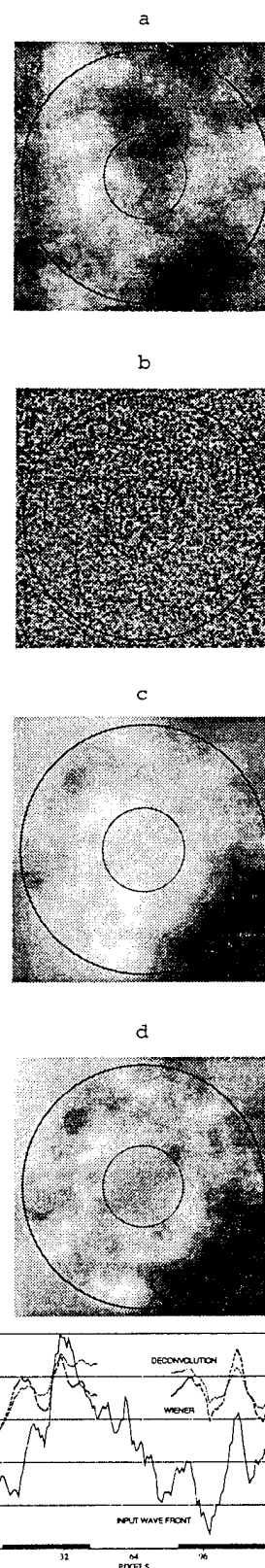
Visibility Signal to Noise Ratio in Adaptive Optics Two-Telescope Interferometry

Jean-Marc Conan and Gérard Rousset

Office National d'Etudes et de Recherches Aérospatiales, BP 72, 92322 Châtillon cedex, FRANCE
Phone:(33-1)46 73 40 40
Fax:(33-1)46 73 41 48

1. INTRODUCTION

The study of astronomical objects requires the use of very high resolution instruments. Since it is difficult to build monolithic telescopes much larger than 10 meters in diameter, one can use long baseline interferometers[1,2] that combine the optical beam of several telescopes. Each of these telescopes must be of large dimensions in order to observe very faint objects. At optical wavelengths, such instruments are therefore severely limited by the atmospheric turbulence. The telescopes must be equipped with adaptive optics (AO) systems which provide a correction of the turbulence.[3-5] The work presented here is mostly extracted from Ref. [6] and gives a comparison of the signal to noise ratio (SNR) of long and short exposure visibilities in adaptive optics partial correction. It is a complement to an earlier study by G. Rousset et al.[7]

2. LONG EXPOSURE VISIBILITY

We assume that, in addition to the AO systems, the interferometer is equipped with a real time differential piston correction system. One can therefore consider recording long exposure fringe patterns without completely blurring the fringes. When considering interferometric imaging,[8] the corresponding long exposure visibility is:[7]

$$F = \frac{OTF_{le}(\mathcal{B}/\lambda)}{OTF_{le}(0)} = \mathfrak{E}_c, \tag{1}$$

where OTF_{le} is the long exposure optical transfer function (OTF) of the interferometer. $\mathcal{B}$ is its baseline, assumed to be long enough to consider that, apart from the piston, the residual phases on each telescopes are uncorrelated. $\mathfrak{E}_c$ is the interferometric coherent energy defined by:[7,6]

$$\mathfrak{E}_c = exp\left(-\sigma_{\varphi_r}^2\right) exp(-1/2\sigma_{\Delta\mathcal{P}}^2), \tag{2}$$

where $\sigma_{\varphi_r}^2$ is the residual phase variance on one telescope and $\sigma_{\Delta\mathcal{P}}^2$ is the differential piston residual variance.

The visibility F also corresponds to the fraction of photons contributing to the fringes.[7] It is different from (and generally much smaller than) the fringe contrast V, sometimes considered in Michelson-type interferometers.[9]

Since F is simply the value of the OTF at a particular frequency, we can generalize the SNR theoretical calculations performed in the single telescope case[10-13,6] to obtain:[6]

$$SNR_F = \frac{\sqrt{2}}{2}\sqrt{\frac{n\varepsilon}{1 + n(1 - \varepsilon)}}\sqrt{M}, \tag{3}$$

where $n = \bar{N}(\tau)\,STF(\mathcal{B}/\lambda)$ is the product of the mean number of photons recorded on the imaging camera during the turbulence correlation time τ, by the interferometer speckle transfer function at the spatial frequency $\mathcal{B}/\lambda$. n is a generalization of the notion of number of photons per speckle often used in interferometry.[9] $\varepsilon = OTF_{le}^2(\mathcal{B}/\lambda)/STF(\mathcal{B}/\lambda)$ is a factor relative to the correction quality.[13,6] M is the total observing time expressed in τ units. Note that we consider here the instrumental visibility: the object is a point-like source.

3. SHORT EXPOSURE VISIBILITY

The long exposure visibility SNR is severely degraded when the AO correction is poor (faint guide star, bad turbulence conditions). In such conditions one may consider recording short exposures in order to apply speckle interferometry techniques. These techniques have the further advantage of being insensitive to the differential piston. The corresponding short exposure visibility is:[14,9,7]

$$G = 2\sqrt{\frac{STF(\mathcal{B}/\lambda)}{STF(0)}}, \tag{4}$$

which can also be expressed as follows:

$$G \approx \sqrt{E_c^2 + 4(1 - E_c^2)/N_o},$$ (5)

where $E_c = exp(-\sigma_{\varphi_r}^2)$ is the single telescope coherent energy,[5,7] and N_o is the number of speckles after correction.[5,6]

As in Section (2), the single telescope calculations can be generalized to obtain the SNR of G:[6]

$$SNR_G = \frac{n}{\sqrt{1 + 2n + \chi n^2}} \sqrt{M},$$ (6)

where χ is defined by:[6]

$$\chi = \frac{\left\langle |OTF_{se}(\boldsymbol{\mathcal{B}}/\lambda)|^4 \right\rangle - STF^2(\boldsymbol{\mathcal{B}}/\lambda)}{STF^2(\boldsymbol{\mathcal{B}}/\lambda)},$$ (7)

where OTF_{se} is the short exposure OTF of the interferometer. The factor χ was shown to be equal to 1 in the uncorrected case[15] and it slowly goes down to zero when the correction improves.[11,6]

4. SHORT OR LONG EXPOSURE VISIBILITY: A COMPARISON

The choice of the optimal procedure according to the observation conditions (wavelength, turbulence...) relies on the comparison of the respective SNRs. We give here such a comparison in the case of a VLTI-type interferometer: two 8-m telescopes, the AO system corrects the Zernike modes[16] (2 through 55) with a 50 Hz bandwidth, the differential piston is assumed to be fully corrected ($\sigma_{\Delta\mathcal{P}}^2 = 0$). The system observes at two wavelength, $0.7\mu m$ and $1.2\mu m$, in a 0.9 arcsec seeing at $0.5\mu m$ and a $16ms^{-1}$ mean wind speed. The visibilities and various quantities characterizing the correction quality are estimated using a numerical simulation.[7,6] No wave-front sensing noise is considered (bright guide star). No anisoplanatic effects are considered (on-axis correction). The results are listed in Table (1). Note a significant reduction of the number of speckles after AO correction. Notice also that χ is very close to 1 except in very good correction cases. The correction is of course much better in the infrared than in the visible.

Using Eq. (3) and Eq. (6) we then calculate SNR versus total number of photons collected. The comparison is made on an elementary observation time τ since both SNRs increase as $\sqrt{M}$. Figure (1) shows the SNR obtained at $1.2\mu m$. The coherent energy is relatively large ($E_c = 0.25$), the long exposure visibility gives the best SNR whatever the number of photons. One should however remember that we have considered the ideal case of a full correction of the differential piston. If it is not the case SNR_F will be strongly attenuated. The short exposure visibility may therefore be preferable. We show for comparison SNR_G without AO correction. This allows us to stress the gain brought by AO in speckle techniques: a large gain at low flux due to the reduction of the number of speckles and to the increase of the coherent energy, a small gain at high flux. SNR_G after correction exhibits a high flux saturation level larger than 1 due to the reduction of χ. Figure (2) shows the SNR obtained at $0.7\mu m$. Since the correction is poor, speckle techniques appear to be preferable at high flux, while long exposures are better at very low flux provided that the wave-front sensing noise remains negligible, e.g. a bright guide star. Notice that for very partial corrections, the gain brought by AO in speckle techniques is only observed at low flux: it is not large (a factor 4 here) but can still lead to a significant reduction of the observing time (by a factor 16 here).

5. CONCLUSION

We have given the expression of the SNR of both long and short exposure visibilities. This theoretical results have then been used to compare the efficiency of these two techniques depending on the correction conditions. The measurement of short exposure visibilities has been shown to be particularly interesting at short wavelengths when the correction is poor, or when the differential piston is not well corrected. Long exposures are more interesting at infrared wavelengths or at very low flux for poor corrections.

		SR	N_o	$F = E_c$	G	ε	χ
$\lambda = 0.7\mu m$	without correction	0.08 %	2300	0.0	0.21	0.0	1.0
	correction by adaptive optics	2.0 %	800	0.017	0.04	0.19	1.0
$\lambda = 1.2\mu m$	without correction	0.25 %	800	0.0	0.035	0.0	1.0
	correction by adaptive optics	25.0 %	-	0.25	0.26	0.93	0.13

Table 1: Simulation of a VLTI-type interferometer: Strehl Ratio SR and Number of Speckles N_o, Visibilities F and G, correction parameters ε and χ [see text]. N_o is not given in the last case since its evaluation is difficult for very good corrections.
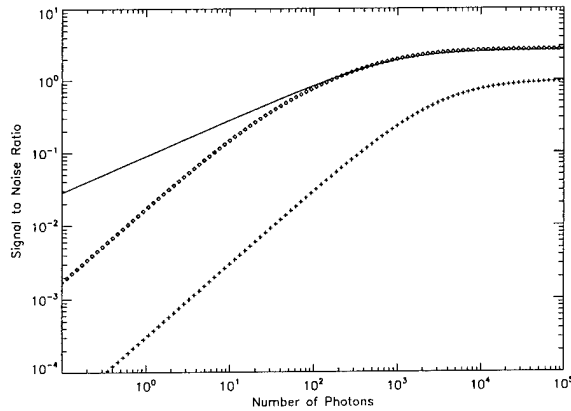

Fig. 1.   Visibility signal to noise ratios versus $\bar{N}(\tau)$ at $\lambda = 1.2\mu m$. With AO correction: SNR_F [—] and SNR_G [◇]. Without AO correction: SNR_G [+]
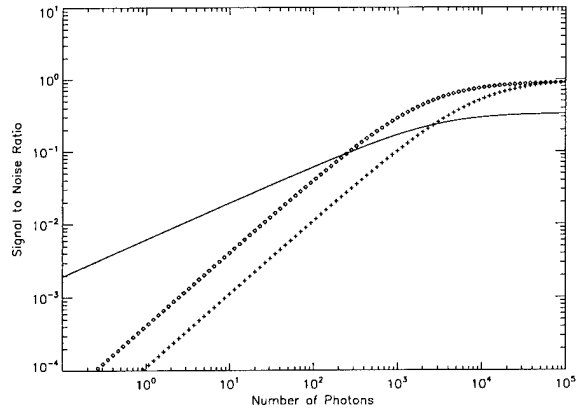

Fig. 2.   Visibility signal to noise ratios versus $\bar{N}(\tau)$ at $\lambda = 0.7\mu m$. With AO correction: SNR_F [—] and SNR_G [◇]. Without AO correction: SNR_G [+]

1. J. M. Beckers et al. In Beckers and Merkle[17], pages 775–787.
2. S. Robbe et al. In J. B. Breckinridge, editor, *Amplitude and Intensity Spatial Interferometry II*, volume 2200, pages 220–230. SPIE, 1994.
3. M. C. Roggemann. *App. Opt.*, 30(29):4227–4233, 1991.
4. F. Rigaut et al. *Astron. Astrophys.*, 250:280, 1991.
5. J.-M. Conan et al. In M. H. Ulrich, editor, *Progress in Telescope and Instrumentation Technologies*, number 42 in ESO Conference and Workshop Proceedings, pages 471–474, Garching Germany, 1992. ESO.
6. J.-M. Conan. PhD thesis, Université de PARIS XI, Orsay France, October 1994.
7. G. Rousset et al. In Beckers and Merkle[17], pages 095–1104.
8. M. Tallon and I. Tallon-Bosc. *Astron. Astrophys.*, 253:641–645, 1992.
9. F. Roddier and P. Léna. *J. Optics (Paris)*, 15(4):171–182, 1984.
10. F. Roddier. In F. Merkle, editor, *High-Resolution Imaging by Interferomy*, number 29 in ESO Conference and Workshop Proceedings, pages 565–574, Garching Germany, 1988. NOAO-ESO.
11. M. C. Roggemann and C. L. Matson. *J. Opt. Soc. Am. A*, 9(9):1525–1535, 1992.
12. M. C. Roggemann. *Computers Elect. Engng*, 18(6):451–466, 1992.
13. J.-M. Conan et al. In F. Merkle, editor, *Active and Adaptive Optics*, number 48 in ESO Conference and Workshop Proceedings, pages 181–186, Garching Germany, 1993. ICO-16 Satellite Conference.
14. W. J. Tango and R. Q. Twiss. In E. Wolf, editor, *Progress in Optics*, volume XVII, pages 239–277. North Holland, Amsterdam, 1980.
15. J. C. Dainty and A. H. Greenaway. *J. Opt. Soc. Am. A*, 69(5):786–790, 1979.
16. R. J. Noll. *J. Opt. Soc. Am.*, 66(3):207–211, 1976.
17. J. M. Beckers and F. Merkle, editors. *High-Resolution Imaging by Interferometry II*, number 39 in ESO Conference and Workshop Proceedings, Garching Germany, 1991. ESO.

Sky Coverage Calculations
for Astronomical Adaptive Optics

Brent L. Ellerbroek

U.S. Air Force Phillips Laboratory
3550 Aberdeen Blvd. SE, Kirtland Air Force Base, NM 87117

René Racine

Départment de physique, Université de Montréal,
and Observatoire du mont Mégantic, Montréal, Canada, H3C 3J7

David Tyler

Rockwell Power Systems
1650 University Blvd. NE, Albuquerque NM 87102

The fraction of the sky over which an adaptive-optics (AO) system will provide a useful level of performance is limited by anisoplanatism. One measure of sky coverage is the probabilty $P(S \geq S_*)$ that the system will provide a Strehl ratio S no smaller than a threshold value S_* when observing in a random direction selected without reference to the distribution of guide stars. This probability is a function of the atmospheric turbulence and wind velocity profiles, the telescope aperture diameter, the observing wavelength, the density of guide stars as a function of magnitude, and the characteristics of the adaptive-optics system. Some of these characteristics include the photon efficiency of the wavefront sensor (WFS), the order and efficiency of the AO correction, and bandwidth of the AO control loop. The values of these parameters which will maximize $P(S \geq S_*)$ for a natural guide star (NGS) AO system are strongly dependant upon the choice of the threshold Strehl ratio S_*, while current interest in laser guide star (LGS) adaptive-optics is of course motivated by the potential for dramatic increases in $P(S \geq S_*)$ for large values of S_* at visible and near infrared wavelengths.

This paper presents computational methods and numerical results regarding AO sky coverage for 8-meter class astromical telescopes observing under typical Mauna Kea atmospheric conditions. The fundamental approach taken is summarized by the equation

$$P(S \geq S_*) = 1 - \exp\left\{ - \int dR\, \pi \left[\theta(S_*, R)\right]^2 \rho'(R) \right\},$$

where the integration variable R is the magnitude of the guide star, $\rho(R)$ is the angular density of stars with magnitude no greater than R, and $\theta(S_*, R)$ is the allowable angular offset to a guide star of magnitude R to achieve a Strehl ratio of at least S_*. The guide star density function $\rho(R)$ depends upon the wavefront sensor spectral passband and the galactic latitude, while the remaining scenario and AO system parameters determine the allowable

guide star offset angle $\theta(S_*, R)$. This paper describes the computation of $\theta(S_*, R)$ in terms of AO modeling methods presented previously [1], and presents sample results on values of $P(S \geq S_*)$ for three basic classes of adaptive optics systems:

- A NGS AO system using a single Shack-Hartmann WFS and a common control loop bandwidth for both tip/tilt and higher-order wavefront correction,

- A NGS AO system using separate sensors and individually optimized control bandwidths for tip/tilt and higher-order wavefront control, and

- A LGS AO system requiring the use of a natural guide star for tip/tilt correction only.

The issues illustrated in these sample cases include the choice of WFS detector technology and order of correction, the effect of windshake-induced tip/tilt jitter, and the significance of the deformable mirror (DM) conjugate altitude.

Several sample results for NGS AO systems are previewed in Fig.'s 1 and 2 below. Fig. 1 plots sky coverage probabilites for Shack-Hartmann-based AO systems as a function detector technology (APD photon counters vs low-noise high-speed CCDs) and the order of correction (6 by 6 subapertures for the APDs; from 6 by 6 to 12 by 12 subapertures for the less costly but noisier CCDs). The low-order APD-based system provides the greatest values of $P(S \geq S_*)$ for Strehls less than about 0.35, but the higher-order CCD-based system has the advantage for larger Strehl ratios. Fig. 2 illustrates the effect of DM conjugate range upon sky coverage probabilities for one sample set of AO system parameters. Because the turbulence profile at Mauna Kea is frequently highly stratified, varying the DM conjugate range from the conventional value of 0 kilometers to an optimized value of 6.8 kilometers has a dramatic effect upon sky coverage.

REFERENCES

1. B.L Ellerbroek, "First-order performance evaluation of adaptive optics systems for atmospheric turbulence compensation in extended field-of-view astronomical telescopes," J. Opt. Soc. Am. A **11**, 783–805 (1994).
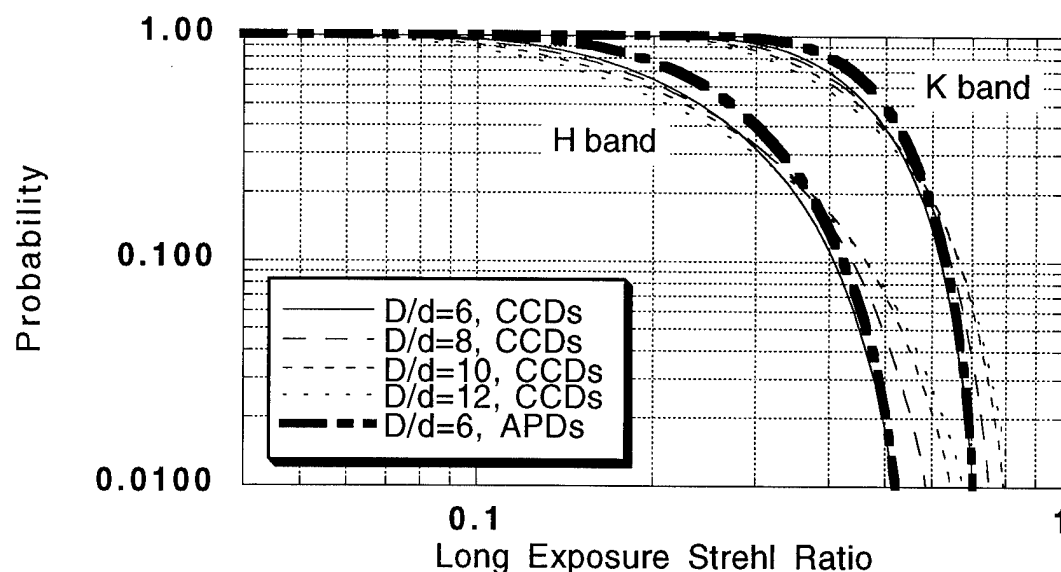
Figure 1: Sky coverage probabilities vs detector technology and order of correction (D/d)

These probabilites of achieving a specified Strehl ratio as a function of the imaging wavelength and WFS characteristics assume a 7.9-meter telescope aperture diameter, nominal Mauna Kea atmospheric conditions, a galactic latitude of 30 degrees, and a deformable mirror conjugate range which minimizes the RMS separation between the DM and atmospheric turbulence. The end-to-end photon efficiencies for the CCD- and APD-based WFSs are 0.5 and 0.35, respectively, and the CCD detector read noise is 3 noise electrons per pixel per read.
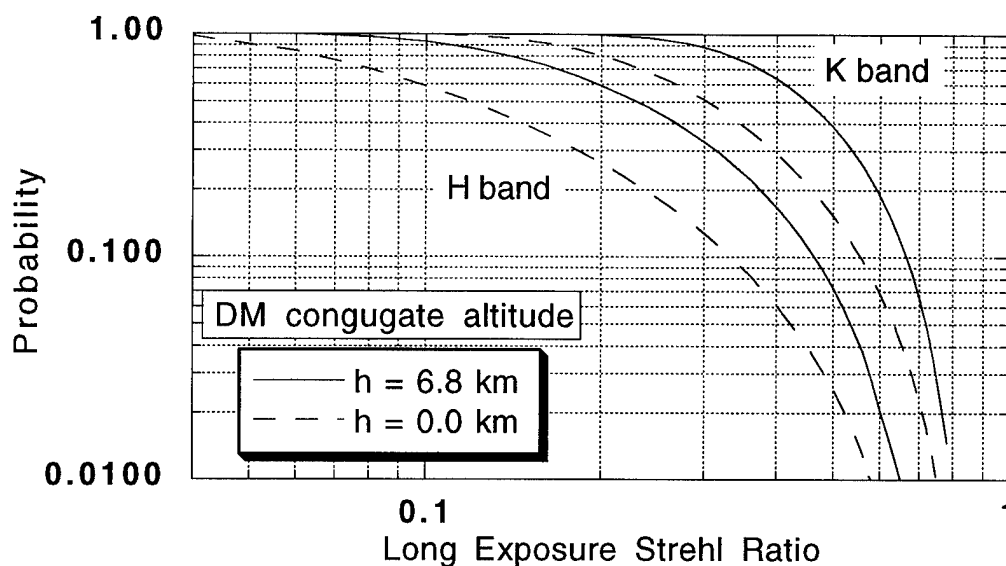

Figure 2: Effect of DM conjugate altitude upon sky coverage probabilities

This figure is similar to Fig. 1, except that the order of the Shack-Hartmann WFS is fixed at 10 by 10 subapertures, and detector read noise is fixed at 3 noise electrons/pixel/read. The DM conjugate range of 6.8 kilometers corresponds to an RMS distance of 3.8 kilometers from the DM to the turbulence, while a conjugate range of 0.0 kilometers yields an RMS distance of 6.5 kilometers.

Artificial-Guide-Star Tilt-Anisoplanatism: Its Magnitude and (Limited) Amelioration

David L. Fried

We shall be concerned here with the problem of tilt anisoplanatism in the use of an artificial-guide-star adaptive optics system in imaging some astronomical object of interest through the turbulent atmosphere. It is well known that because the position of the back scatter region is determined by the direction in which the laser beam was transmitted an artificial-guide-star can not provide any pointing information pertaining to turbulence induced tilt—at least not in any direct manner. (Indirect methods, such as those involving second harmonic generation closely coupled with the back scatter process are being considered but the feasibility of such approaches is still unclear.) If the object of interest is sufficiently bright it can serve as the guide star for correction of turbulence induced tilt—or if there is a sufficiently bright star close enough to the object of interest then it can serve as a natural-guide-star for the correction of turbulence induced tilt. The farther away that natural-guide-star is from the object of interest the greater the discrepancy between the turbulence induced tilt for the object of interest and that for the natural-guide-star, and the lower the Strehl ratio of the image of the object of interest will be—even though the artificial-guide-star may be providing a basis for perfect adaptive optics correction of the higher-order wave front distortion.

Often there is no natural-guide-star sufficiently close to the object of interest; the tilt anisoplanatism is unacceptably large and only for rather long wave lengths can high Strehl ratio imaging be accomplished. We have found, however, that by use of a *combination* of data from the *several* nearest natural-guide-stars some what better tilt information can be developed than that obtainable from the single closest natural-guide-star *alone*. We shall present results showing the effective magnitude of the tilt anisoplanatism problem when a single natural-guide-star is used to provide tilt information and when a multiplicity of natural-guide-stars is used.

We shall take as our measure of the effective magnitude of the tilt anisoplanatism problem the quantity which we shall denote by Λ_0, a quantity which has the magnitude of an optical wave length. It may be thought of as indicating the division between those shorter wave lengths for which the reduction in the Strehl ratio because of tilt anisoplanatism is substantial, and those longer wave lengths for which the Strehl ratio reduction is minor. Λ_0 has no dependence on the wave length at which the system is operating, but rather governs how short a wave length it is useful to operate an AGS system at. When a single natural guide star is used to provide tilt information Λ_0 has only a weak dependence upon the diameter of the system's aperture.

It can be shown that with no higher-order wave front distortion and a gaussian random tilt having a "one-axis one-sigma" value of σ_θ, for an aperture diameter D and imaging wave length λ the ensemble average Strehl ratio is

$$\langle S \rangle = \frac{16}{\pi D^2} \int_0^D r\, dr \left[\cos^{-1}\left(\frac{r}{D}\right) - \frac{r}{D}\sqrt{1-\left(\frac{r}{D}\right)^2} \right] \exp\left(-\frac{2\pi^2}{\lambda^2}\sigma_\theta^2 r^2\right) . \tag{1}$$

(The term "one-axis one-sigma" implies that for each of two orthogonal axes the tilts are statistically independent, and that the rms tilt for each axis has the same value, namely σ_θ.) It can be easily shown that for a fixed aperture diameter, D, as the wave length, λ, goes to very large values the dependence of the ensemble average Strehl ratio, $\langle S \rangle$, asymptotically approaches unity—and that as the wave length goes to very small values the ensemble average Strehl ratio asymptotically goes to $(2/\pi^2)\,[\lambda/(D\sigma_\theta)]^2$. These two asymptotic forms intersect at a wave length of $\Lambda_0 = (\pi/\sqrt{2})D\sigma_\theta \approx 2.22144\,D\sigma_\theta$. The curve defined by Eq. (1), showing the dependence of $\langle S \rangle$ upon λ, may be considered to have a knee at $\lambda = \Lambda_0$, at which point it can be shown that $\langle S \rangle$ has a value of 0.476222 . We shall express the effect of turbulence induced tilt anisoplanatism in terms of Λ_0, understanding that tilt anisoplanatism will (will not) be significant if we intend to operate a system at an imaging wave length much smaller (much larger) than Λ_0.

It has been shown by P. Roberts (tOSC Report. No. TR-1318) that for two point sources separated by an angle ϑ the difference between the turbulence induced tilts for the wave fronts from the two has a nominal one-axis one-sigma value, σ_θ, which we have expressed as

$$\sigma_\theta^2 = C\, D^{-1/3} \int dh\, C_N^2(h)\, g_0(h\vartheta/D) , \tag{2}$$

for vertical propagation. Here $C = 2.91(25)2^{11/3}3^{-1}\left[\Gamma\left(\frac{2}{3}\right)\right]^4$, and

$$g_0(x) = \begin{cases} c_1 - c_1 \;_4F_3\left(\frac{1}{6}, -\frac{11}{6}, -\frac{23}{6}, -\frac{11}{6}; 1, -\frac{4}{3}, -\frac{11}{6}; x^2\right) - c_2 \; x^{14/3} \;_4F_3\left(\frac{5}{2}, \frac{1}{2}, -\frac{3}{2}, \frac{1}{2}; \frac{10}{3}, \frac{1}{2}, \frac{10}{3}; x^2\right) & \text{if } x < 1 \\ c_1 - c_3 \; x^{-1/3} \;_4F_3\left(\frac{5}{2}, 3, \frac{1}{6}, \frac{1}{6}; 3, 5, 3; x^{-2}\right) & \text{if } x \geq 1 \end{cases} \quad (3)$$

where $c_1 = 2^{-14/3}\Gamma\left(\frac{14}{3}\right)\Gamma\left(\frac{1}{6}\right)\left[\Gamma\left(\frac{17}{6}\right)\Gamma\left(\frac{17}{6}\right)\Gamma\left(\frac{29}{6}\right)\right]^{-1}$, $c_2 = \Gamma\left(-\frac{7}{3}\right)\left[2\pi\Gamma\left(\frac{10}{3}\right)\right]^{-1}$, and $c_3 = \Gamma\left(\frac{1}{6}\right)\left[2^7\Gamma\left(\frac{5}{6}\right)\right]^{-1}$.

In Fig.'s 1 and 2 we show the dependence of σ_θ and of Λ_0 respectively upon the separation ϑ calculated from Eq. (2) for various aperture diameters, evaluated for the HV$_{5/7}$ strength-of-turbulence model. Anticipating the need to be able to compare these results with results obtained when using the several closest natural-guide-stars simultaneously to provide tilt information, we cast these results in terms of the density, ρ, (in stars per unit solid angle) of sufficiently bright stars. Using the fact that the probability, $P(N, \vartheta)$, that it will require a circle of angular radius ϑ to contain N stars is

$$P(N, \vartheta) = \frac{1}{(N-1)!} \int_0^{\pi\vartheta^2\rho} dx \, \exp(-x) \, x^{N-1} , \qquad (4)$$

we see that 50% of the time there will be a suitably bright star within a distance of $\vartheta_{50\%} = \sqrt{\log(2)/(\pi\rho)} = 0.469719 \, \rho^{-1/2}$. In Fig. 3 we show the value of Λ_0 that goes with $\vartheta_{50\%}$, shown as a function of the star density, ρ. One-half the time we will find a natural guide star close enough to the object of interest to yield a value of Λ_0 better than that shown in Fig. 2—and one-half the time the closest star will be farther away, so that this good a value of Λ_0 can not be achieved.

A quick check reveals that if the object of interest lies on the line between two suitably bright natural-guide-stars and is exactly half way between the two—an angular distance of ϑ from each—and if we use the average of the turbulence induced tilts of the two natural-guide-stars as our estimate of the tilt for the object of interest, then the resulting tilt anisoplanatism instead of having the one-axis one-sigma value of $(\sigma_\theta)_1$ that goes with a single natural-guide-star at a distance of ϑ (or of 0.707 of that value), will have a value of $\sqrt{(\sigma_\theta)_1 - \frac{1}{4}(\sigma_\theta)_2}$ where $(\sigma_\theta)_2$ is the one-axis one-sigma value that goes with an angular separation of 2ϑ. $\sqrt{(\sigma_\theta)_1 - \frac{1}{4}(\sigma_\theta)_2}$ is smaller than, in some cases significantly smaller than $0.707 \, (\sigma_\theta)_1$ —which is what has encouraged us to investigate the use of multiple natural-guide-stars to provide the tilt information to an artificial-guide-star adaptive optics system.

In general the array of nearest natural-guide-stars will form a complex pattern and use of simple uniformly weighted averaging of tilt information from all the stars would not be appropriate. We have approached the problem of processing the data from an array of the N closest natural-guide-stars using a least-mean-square-error method. We assume an algorithm that, at each instant, calculates the mean of the positions of all N of the natural-guide-stars and references all measurements and results for that instant to this mean position. (This mean position is of course a turbulence influenced random quantity, changing from instant to instant.) At each instant we use the least-mean-square-error method to estimate how far turbulence has shifted the position of the object of interest relative to how far it has shifted the mean position for the N natural-guide-stars. The estimation process takes as its inputs the amount that turbulence has shifted each of the natural-guide-stars, individually, relative to the current mean of the positions of all N natural-guide-stars. Formulating our problem in this way has allowed us to develop results that do not involve the turbulence induced tilt variance, involving only the mean-square difference of the turbulence induced tilt for pairs of point sources—the tilt structure function, and lets us avoid having to work with an ill-conditoned matrix.

Using the notation $\mathcal{D}_{i,j}$ to denote the ensemble average of the squares of the turbulence induced variation of the separation between the ith and the jth point sources—$i.e.$ the tilt structure function—and treating the two components of tilt together we have obtained the result that

$$\sigma_\theta^2 = \frac{1}{2}D^C + \frac{1}{4}\left(\mathbf{D}^L\right)^T \left(\mathbf{D}^Q\right)^{-1}\mathbf{D}^L , \qquad \text{where} \qquad (5)$$

$$D^C = \mathcal{D}_0^{SS} - \frac{1}{2}\mathcal{D}^{DS} \qquad D_i^L = \mathcal{D}^{DS} - \mathcal{D}_i^{SS} - \mathcal{D}_0^{SS} + \mathcal{D}_{0,i} \qquad D_{i,j}^Q = \mathcal{D}^{DS} - \mathcal{D}_i^{SS} - \mathcal{D}_j^{SS} + \mathcal{D}_{i,j} , \qquad (6)$$

D_i^L denoting the elements of $\mathbf{D}^L$ and $D_{i,j}^Q$ denoting the elements of $\mathbf{D}^Q$ —with

$$\mathcal{D}_0^{ss} = N^{-1}\sum_{i=1}^{N}\mathcal{D}_{0,i} \qquad \mathcal{D}_i^{ss} = N^{-1}\sum_{j=1}^{N}\mathcal{D}_{i,j} \qquad \mathcal{D}^{DS} = N^{-2}\sum_{i,j=1}^{N}\mathcal{D}_{i,j}\ . \tag{7}$$

But this treats the two components of turbulence induced tilt (*i.e.* the component parallel to, and the component perpendicular to the line of separation between the two point sources) as statistically equivalent. However there actually is a substantial difference between the statistics of the two components—a difference it proves worthwhile to take account of. Roberts gives a formulation equivalent to Eq. (2) for the statistics of each of the two components. Using this we have developed results equivalent to Eq.'s (5) through (7), which space considerations preclude presentation of here.

Using this formulation and randomly selected patterns of $N = 10$ stars conforming statistically to some particular star density we have run 250 realizations for various {diameter; star density}-cases. For each case we got 250 values for Λ_0. For each case we determined the 50% value for Λ_0. In Fig. 4 we show the results for Λ_0. A comparison of Fig.'s 3 and 4 shows that a significant amelioration of the tilt anisoplanatism problem is achievable through the use of multiple natural-guide-stars.

In each figure the eight curves are for $D = 1, 1.5, 2, 3, 4, 5, 7, 10$ meters. In Fig. 1 the lower the curve the larger the diameter. In Fig.'s 2, 3, and 4 the curves for the larger diameters have larger Λ_0-values where the star density, ρ, is lowest.
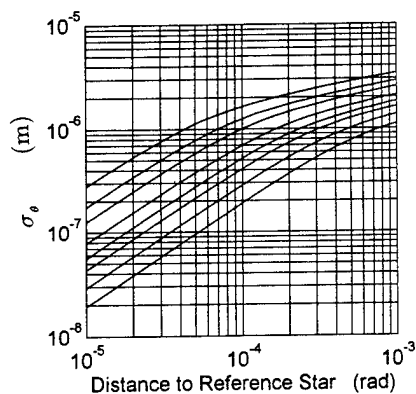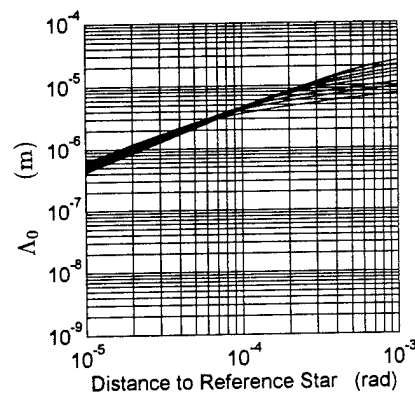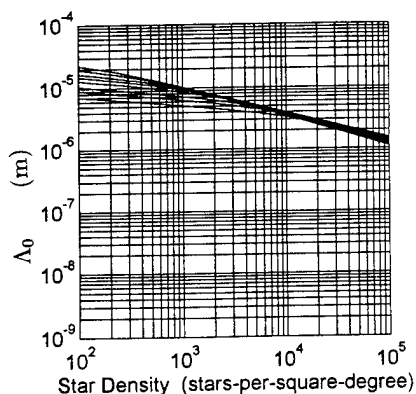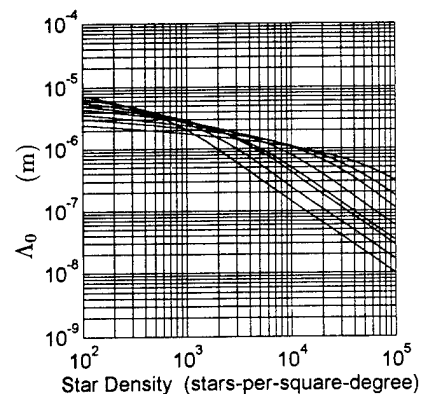

Figure 1.

Figure 2.

Figure 3.

Figure 4.

Russian and Asian Adaptive Optics

WC 2:00 pm-3:15 pm
Auditorium

Vladimir P. Lukin, *Presider*
Institute of Atmospheric Optics, Russia

Computer Modeling of Adaptive Optics & Sites for Telescope Design

Vladimir P.Lukin

Institute of Atmospheric Optics, Siberian Branch of RAS,
av.Academicheski, 1, 634055,Tomsk, Russia
tel.(382-2)25-9606, fax:25-9086, Email:ZUEV@IAO.TOMSK.SU

The scientists of the Institute of Atmospheric Optics have the experience in creation of computer codes describing different components of an adaptive system. The models of these elements have been checked solving the atmospheric problems.

1. FOUR-DIMENSIONAL COMPUTER DYNAMIC MODEL OF ATMOSPHERIC OPTICAL SYSTEMS

We are working under creation of 4D computer codes for calculations of optical waves parameters propagating in a layer-inhomogeneous and random-inhomogeneous stratified media. At present we laid the groundwork for creation of 4-dimensional computer system simulating the optical radiation propagation in the atmosphere under conditions of adaptive phase control of the optical radiation parameters. In particular, we created the numerical models of both the separate components and the whole channel of adaptive optical system. Nowadays we have the operating programs which simulate the following parameters:

a) optical radiation propagation when forming the images through the refraction and turbulent atmosphere,

b) low-frequency part of spectral density of turbulent atmosphere for ground layer (atmosphere) and for the whole atmosphere,

c) different schemes and algorithms of operation of wave front sensors of interference and diffraction types,

d) quantum fluctuations of optical radiation beam are actual under conditions of optical system operation at weak emission flux,

e) at last, different active and adaptive control elements of optical wave phase, so-called multi element segmented and deformable controlled mirrors.

We investigate the algorithms of optical wave phase restoration using the interferometers with reference wave and shift as well as some versions of Hartmann detector. Programs permit modeling of conditions of natural

optical experiment and estimate of efficiency of application of adaptive phase control for correction of distortions in optical wave including atmospheric refraction, turbulence. We are going to investigate different atmospheric paths, different regimes of adaptive control.

2. DEVELOPMENT OF MODELS OF TURBULENCE SPECTRA

This chapter deals with the theoretical and experimental studies of optical waves fluctuations for comparing different models of the atmospheric turbulence spectra. Using the experimental data we would suggested to investigate behavior of spectral density of atmospheric turbulence in the region of arge spatial scales. Special efforts will be done to detect the variability of large optical inhomogeneities as manifestation of the influence of thermodynamic instability of the atmosphere.

Our simultaneous measurements of the structure function of phase in the "saturation" region and of the turbulence intensity allow one to estimate the outer scale Lo corresponding to the horizontal transport of the optical inhomogeneities. Since the scales Lo were measured under different meteorological conditions, an attempt has been undertaken to classify the results of optical measurements of Lo depending on the degree of thermodynamic stability of the atmosphere. It was found that the values of Lo exceeding the mean value are realized under the conditions of neutral stratification.

Together with the dependence of the outer scale of turbulence on variations of meteorological parameters of the atmosphere, there exists anisotropy of the atmospheric properties, in other words, inhomogeneities with dimensions exceeding several meters possess the properties that depend on direction.

The so-called coefficient of anisoropy, being obtained immediately in the experiment, varied in the interval from 0.62 to 2.57 with the mean value 1.57 that indirectly indicated that the temperature induced optical inhomogeneities, which produce the phase fluctuations, were anisotropic in the large-scale region. The relationship is quite obvious between the coefficient of anisotropy value and the instability parameter.

3. NEW RESULTS WITH ADAPTIVE OPTICS IMAGING SYSTEMS IN THE ATMOSPHERE

The special attention will be concentrated on the investigation of efficiency of different active and adaptive algorithms for compensation of atmospheric aberrations. The simulation will be made taking into account

the finite rate of control, with the use of artificial beacons, and on the base of forecast of propagation conditions. The requests to the quality of radiated laser beams, parameters of a wave-front sensor, parameters of a ground-based telescope, etc., will be determined. The average values of temperature and wind velocity, as well as temperature and wind velocity fluctuations, are measured at fixed levels above the ground. As a result, each optical experiment is accompanied by the data on meteorological measurements, i.e., we calculate the intensity characteristics of turbulence, the parameters characterizing the atmospheric instability. The structure of wind velocity in the ground layer is studied. To analyze the atmospheric turbulence along vertical optical paths we use an optical meter of stellar image "tremor" constructed on the basis of a mirror telescope. It is well known that the atmospheric turbulence limits to a great extent the performance of the optical telescopes operating from the ground surface. We may introduce the traditional, determed by the atmosphere, parameters: spatial scale of coherence of an optical wave or the Fried's radius, dimension of isoplanatic angel of visual field for the layer of turbulent atmosphere, "life-time" of phase distortions in an optical wave. These characteristics of atmospheric turbulence determine the structure of phase distortions at the telescope aperture and technical parameters of telescope as the optical transfer function, the point spread function, the integral resolution, the Strehl parameter.

These and other atmospheric characteristics for the systems of image formation can be calculated both on the basis of atmospheric sounding at a point of location of telescope and on the basis of atmospheric models. We are developing the methods and setups for sounding of optically-active atmospheric layer as well as the models of the atmosphere. In the previous years we have developed the models for various regions of the former Soviet Union. It is of interst to compare our models with the models for "good", from the view-point of astroclimate, sites in the world. We present the data of calculations of atmospheric parameters for different models of the atmosphere.

A phenomenon of the wavefront dislocations of the optical irradiance propagating through the turbulent atmosphere. Using the numerical simulation method, the effects of the wavefront dislocations on the adaptive optical system performance have been investigated. We have found a connection between instability of the phase conjugation efficiency and the reference wavefront dislocations.

Experimental Study of Compensation for Laser Thermal Blooming

Li Youkuan, Zhang Xinwei
Beijing Institute of Applied Physics and Computational Mathematics, China

Su Yi, Zhang Kai
Southwest Institute of Applied Electronics, China

Using 19-element adaptive optics system, real-time correction for laser thermal blooming was realized; far field energy was 2.7 times higher without correction.

PRINCIPLES OF DEVELOPMENT OF ADAPTIVE BIMORPH OPTICS.

Andrey G. Safronov.
TURN Ltd., P.O. Box 19, Moscow, Center, 103104, Russia.

A low-order correction adaptive optics, the so-called "small" adaptive optics, is obviously more preferable than the ordinary adaptive optics from the standpoint of technical introduction including the industrial-scaled one. In practice controllable bimorph mirrors may be considered as ideal means for use in such a system. Analysis of up-to-date state of bimorph optics have shown that up to the present days there were no industrial samples of bimorph mirrors as well as the industrial technology of their manufacturing. Developments on large-aperture bimorph mirrors have been totally lacking. Disadvantages of the presented before bimorph mirrors have hindered their wide introducing into the industrial laser optics and astronomical telescopes.

Analysis of wavefront distortions in laser systems shows that in the most of cases large-scale distortions, corresponding to primary optical aberrations, prevail. Frequency band of such distortions may range up to about 1 kHz and amplitude may be as much as about 10 microns. From the above, the small adaptive optics on the base of bimorph mirrors seems to be appropriate for correction of such distortions.

A multi-layer mosaic technology of forming bimorph structures has been specially developed for creating the bimorph optics of high efficiency. Two versions of cooled mirrors have been realized on the basis of the bimorph optics technology developed in our company. Both versions are purposed for use in medium-power (up to 15 kW) laser optics. The first mirror is made of copper and has 18 control electrodes, another one is made of molybdenum and has 17 electrodes. Maximum sensitivity of the mirrors developed (when all the electrode are in use) equals to 37.3 μm/kV for copper mirror and to 11.8 μm/kV for molybdenum one. Main resonance frequencies amount to 2.4 kHz and 3.6 kHz correspondingly (regions of the constant sensitivity are 0 ÷ 300 kHz and 0 ÷ 1 kHz).

Computer simulation carried out for both of the mirrors under various thermal loadings has shown that about 10% of the control voltage range is needed to compensate the intrinsic thermal deformations of bimorph mirrors under the action of a laser beam with integral power of 15 kW. Thermal deformations of the mirrors under changes of temperature were verified experimentally and their qualitative and quantitative agreement with the results of calculation were obtained. At the compensation of primary optical aberration by the use of the developed bimorph mirrors it was found that effective range of correction (at residual error no more than $\lambda/14$, $\lambda = 632.8$ nm) amounts to 16.5 μm and 7.5 μm for defocusing, 0.56 μm and 1.9 μm for astigmatism, 0.38 μm and 1.4 μm for coma, 0.45 μm and 1.1 μm for

trefoil and 2.1 µm and 1.0 µm for spherical aberration using copper and molybdenum mirrors correspondingly. The obtained results demonstrate that the developed cooled bimorph mirrors remove effectively the phase distortions existing in laser systems with power up to 15 kW.

Our company has also developed one-channel deformable mirrors for use in low-power laser optics (up to 1 kW). Industrial samples of the mirrors are made of molybdenum in accordance with the developed and improved technology and incorporate multi-layer bimorph structures providing a high sensitivity (up to 79.1 µm/kV). Main resonance frequency is no less than 3.2 kHz (range of constant sensitivity is 0 ÷ 1 kHz), electromechanical hysteresis does not exceed 14 %.

Effective range of adaptive correction was found to be about 20 µm for defocusing and about 1 µm for spherical aberration (at residual error no more than $\lambda/14$, $\lambda = 632.8$ nm). No more that 7% of control voltage range therewith is enough to compensate the intrinsic thermal deformations of the mirror under the action of a laser beam of 1 kW in integral power. Three-times increase of sensitivity of controllable bimorph optics were defined for the industrial sample of one-channel molybdenum mirror due to the use of the multi-layer mosaic techniques. The results obtained show that one-channel bimorph mirrors developed by our company enable to remove effectively the axial symmetric phase distortions typical of laser systems with power up to 1 kW.

Analysis of wavefront distortions in astronomic telescope shows that in the most of cases large-scale distortions dominate which correspond to primary optical aberrations, their overall amplitude may amount up to tens of microns and typical time of change of about 1 msec.

A large-aperture active bimorph mirror 3.3-meters in a diameter based on mosaic piezoceramic structure has been investigated in order to determine a possibility to compensate the named above distortions in astronomical telescope. Response functions of control electrodes of the mirror were obtained by means of a computer simulation. Sensitivity of separate electrodes ranges from 0.95 to 4.6 µm/kV. First resonance frequency of the 3.3-meter mirror is mainly determined by pneumatic off-loading system and amounts to 2.2 Hz.

At compensation of primary optical aberrations it was obtained that the effective range of correction (at residual error no more than $\lambda/20$, $\lambda = 0.55$ µm) amounts to 69 µm for defocusing, 7.2 µm for astigmatism, 1.0 µm for coma, 4.8 µm for trefoil and 8.5 µm for spherical aberration. Amplitude of intrinsic thermal deformations of the mirror was found to be 4.0 µm/K and no more than 3% of range of control voltage is enough for their compensation. The represented results demonstrate that

the 3.3-meter active bimorph mirror removes effectively the large-scale low-frequency large amplitude distortions in up-to-date optical telescopes. The efficiency of the mirror would be expected to exceed significantly the described above if optimize a structure of the 3.3-meter bimorph mirror and use mosaic layer consisting of multi-layer piezoelectric elements.

On the basis of the obtained results it seems to be appropriate to use a large-aperture bimorph mirror for compensation of large-scale low-frequency distortions in a telescope. Using the 3.3-meter bimorph mirror as an example it was shown that the efficiency and quality of active correction of defocusing and spherical aberration is 28 times higher using the 12-electrodes bimorph mirror than with a similar mirror having 54 discrete actuators; in the case of active correction of astigmatism and coma the 54-actuator mirror is analogous in efficiency to a 36- electrode bimorph mirror. The results obtained prove that the use of large-aperture bimorph mirrors provides more efficiency and quality of active low-order correction compared to the use of large-aperture mirrors with discrete actuators.

Summarizing the represented results we may conclude that the further progress in bimorph optics is connected with the use of multi-layer piezoelectric structure which provides the increase of sensitivity as well as with the application of mosaic techniques which opens a real possibility of building up large-aperture bimorph mirrors.

Adaptive Astronomical Telescope with Two-Stage Wavefront Correction: current status of a project

D.N. Yeskov, B.E.Bonshtedt, S.N.Koreshev, G.I.Lebedeva,
V.A.Parfenov, V.I.Podoba, V.V.Reznichenko, A.G.Seregin,
V.I.Sidorov, V.N.Smirnov, L.G.Fedina, N.T.Firsov,
V.Kh.Khakunov, I.Sh.Etsin

Research Center "S.I.Vavilov State Optical Institute"
12, Birzhevaya line, St.Petersburg, 199034, Russia
Fax: (812)218-3720

At present, some large-scale programs are carried out in various countries that are aimed towards development of a new class of ground and space telescopes for both civil and military use. Being now at different stages of implementation, these programs have been initiated by both scientific and military and political causes and, to a large extent, owing to emerging technologies coupled mainly with active and adaptive optics.

In astronomy, large telescopes provide a possibility to carry out cosmological researches and studies of astrophysical and geophysical processes rather than local investigations of the Universe. Large telescopes are required for deep Space laser connection systems being developed at present for some programs of exploration of the Solar system planets.

Results of the eight years long work in Russia on development of an adaptive astronomical telescope featuring by 3.2 m primary mirror dia and 1° angular field-of-view (FOV) are presented hereinafter.

Principal features required for both ground and space-based modern telescopes are the same:
— operating spectral range from 0.2 to $1000\,\mu$;
— angular resolution of the order of 0.02 arcsec;
— angular FOV up to 1°;
— minimal dimensions and weights.

These requirements result in necessity to use entirely reflective optics and in increasing the primary dia up to 3...4 m. Fabrication of elements featuring by high optical quality is very expensive. Therefore, different ways of cost reduction are to be found. In order to provide both optimal configuration and desired performance of the telescope, some principal features are to be embedded into projects; that are mentioned below.

Two-stage optics is to be used in the telescope optical lay-out where the first stage generates the necessary angular FOV image though being of unsatisfactory optical quality while the second stage corrects field aberrations of the first one and forms a real exit pupil [1].Just here a corrector is to be installed to compensate wave distortions occurring in the primary mirror.

In addition, such a system configuration provides stray light protection precautions inside the area of the intermediate image.

To minimize the optical system total length, mirrors of enough large aperture size are to be used, i.e. mirrors featuring by f/no=1.5...2.5.

To reduce the primary unit weight, segmented mirrors are to be used.

These features have been taken as fundamentals of our telescope design. In addition, the

primary mirror unit is being developed in two versions: deformable and segmented ones. In the first case an estimated weight of the telescope is 4500...6500 kg while in the second case it can be diminished to some 3500...4500 kg.

Up to date, the telescope project proceeds the following stages of subsystems and units development.

Optical Design

— three mirror optical lay-out is calculated and the corresponding technical documentation is developed [2,3];
— four (of seven) hexagonal elements of the segmented primary mirror are fabricated of fused silica featuring by low CTE; optical surfaces of the segments is of spherical shape with the RMS error of 0.05λ ($\lambda=633$ nm);
— optical surface of the central element is aspheric;
— the deformable mirror is under initial shaping [4];
— a light-weight secondary mirror is fabricated of quartz featuring by 520 mm dia and spherical surface with the RMS error of 0.1λ ;
— fabrication technology for wave front corrector is developed in two versions: a segmented one of 68 mm dia consisting of seven elements and a liquid crystal one of 70 mm dia [5];
— an experimental prototype of the telescope wave front sensor is fabricated that is based on the heterodyne interferometer with internal reference source and hologram structure on the primary mirror surface [6];
— technology of high frequency hologram structure application on mirror surfaces is developed and a prototype of 200 mm dia is obtained [7,8];
— to control position of the primary mirror segments, local optical fiber linear movement sensors are fabricated providing a resolution of 3 nm within the movement range of 1 mm;
— to control the secondary mirror position in relation to position of the primary one, an optronic system is developed.

Mechanical Design

— main frame for both primary and secondary mirrors is fabricated as well as mechanical components of the mirror units;
— a support truss of 350 kg weight is fabricated of special light and strong alloy.

Control System Design

— a data acquisition and processing system for wave front sensors is developed;
— a control system for wave front correctors is developed;
— actuators for the primary mirror segments positioning are fabricated that function with an accuracy better than 60 nm and develop force of 70 kg.

Testing and certificating facilities

To test and certify elements, units and devices that have been developed during the telescope design process, a unique set of testing and certification test-beds and stands is used. The most part of these facilities have been designed and mounted within frames of the project, too. The set consists of the following items:
— a test-bench for high accuracy comparison of surface curvature radii of mirrors having diameters up to 1.2 m with relative error of 10^{-6};
— a test-bench for the primary mirror unit investigations;
— a mounting and adjusting stand for two-mirror telescope modulus;
— investigation test-benches for actuators and local displacement sensors;

— an investigation test-bench for the data acquisition and processing system for wave front sensors and position sensors of individual optical elements of the telescope;

— an active mirror thermostabilization and thermocorrection system based on local heaters application;

— high-precision interferometers for on-line testing of surfaces shape including a polarization common-path interferometer, a polychromatic scatter plate interferometer and white-light ones for mirrors phasing;

— compact high stability, single-frequency Nd:YAG laser.

Most of the relevant problems are considered in a special issue of the Journal of Optical Technology, 1995, No.10 (in press).

It is worth to mark out particularly that the telescope design is a module one. The telescope can be transported portion-wise to a proper site and mounted there quite easily. A built-in testing system as well as relatively small dimensions and weight of the entire instrument provide a possibility to re-target it and to adjust the optical system in an observation watch. Thus, an overall work efficiency is obviously increased. An active element-by-element thermal stabilization system used contributes to less stringent requirements to the telescope tower and reduced construction costs.

Overall expenditures for the realized part of the project are estimated $20 million plus. This figure responses to about 60 per cents of the project total cost.

For the present time, a telescope receiving-recording unit is not designed properly within the frames of the project. This provides a possibility to speculate on a form of international co-operation for the project completion while taking into consideration interests of a lot of researchers.

REFERENCES

1. A.B.Meinel, M.P.Meinel. *Opt. Eng.*, 1992, V.31, No11, pp.2271-2281.

2. D.G.Korsch. US patent No.4101195.

3. G.I.Lebedeva, A.A.Gorbul'. *Journal of Optical Technology*, 1994, No.8, (pp.57-62).

4. V.A.Gorshkov et al. *Journal of Optical Technology*, 1994, No.6, (pp.24).

5. A.P.Onokhov et al. *Proc. of SPIE*, 1994, V.2201, pp.1020-1026.

6. A.G.Seregin et al. *Journal of Optical Technology*, 1995, No.10 (in press).

7. S.N.Koreshev. *Optics and Spectroscopy*, 1994, V.76, No.1, (pp.109-115)

8. V.V.Anistchenko et al. *Proc. of SPIE*, 1994, V.2200, pp.581-592.

Methods of Adaptive Optics for Control the Output Radiation of Industrial Lasers

A.V.Kudryashov, Ph. D.

Scientific Research Center for Technological Lasers, Russian Academy of Sciences

Dm.Ulianov str. 4, bld. 2, fl. 13, Moscow, 117333, Russia

tel/fax: +7 095 1355430, e-mail: kud@lado.phys.msu.su

The application of lasers in technological processes and medicine needs the creation of special systems of control and formation of given radiation characteristics on the developed object. Such tasks could be solved by use of elements and methods of adaptive optics.

The controlled optical elements (adaptive mirrors) usually are considered to be placed outside laser cavity. But the first experiments with the intracavity control of the laser radiation showed that placing active mirror inside laser resonator increase the efficiency of the influence of adaptive corrector on the output laser beam parameters (beam quality, mode configuration, regime of laser generation). In our work we present the results of control and formation the radiation of different types of technological lasers: CO_2, excimer, copper-vapor and YAG:Nd. As an adaptive mirror we used a corrector on the semi passive bimorph piezoelement with 18 actuators. The special water-cooled flexible mirror was worked out to control the radiation of a powerful (up to 5 kW) CO_2 laser.

The use of the deformable corrector as one of the cavity

mirrors in different types of lasers allowed:

- in CO_2 CW industrial laser (output power 5 kW): to get pulse-periodic Q-switch regime of generation without any change of laser design; to control the shape of output mode structure;

- in excimer lasers: to show the possibility of control the output radiation near-field and far-field intensity distribution;

- in copper-vapor laser: to get double reduction of the output radiation divergence and focus laser beam to a line segment of different space orientation, to a number of concentric rings etc.

- in YAG:Nd lasers: to decrease the divergence of laser beam by 3 times in multymode regime, to form various mode configurations, applying different voltage to the electrodes of adaptive mirror.

Adaptive Optics Components

ThA 8:30 am-10:30 am
Auditorium

Robert K. Tyson, *Presider*
W.J. Schafer Associates, Inc., USA

Adaptive Optics in Western Europe

Fritz Merkle
Carl Zeiss
Tatzendpromenade 1A
D-85386, Jena, Germany

In Western Europe in the early seventies, main emphasis was put on high-power laser applications. Later, compensated imaging became the main driver, leading to the first routinely operated adaptive system in astronomy.

Comparison of Adaptive-Optics Technologies for Large Astronomical Telescopes

François Rigaut

Canada-France-Hawaii Telescope
P.O. Box 1597, Kamuela HI 96743

Brent L. Ellerbroek

Starfire Optical Range, U.S. Air Force Phillips Laboratory
3550 Aberdeen Blvd. SE, Kirtland Air Force Base, NM 87117

Malcolm J. Northcott

Institute for Astronomy, University of Hawaii
2680 Woodlawn Dr., Honolulu HI 96822

The emergence of new wavefront sensing techniques, such as wavefront curvature sensing, opens new pathways for astronomical adaptive optics. Even though the advantages and drawbacks of Shack-Hartmann and curvature wavefront sensing are known [1,2], no direct comparison of complete systems has yet been presented. The goal of this paper is to investigate and compare the performance of Shack-Hartmann and curvature based systems for an eight-meter telescope, evaluated at a $1.6\,\mu$m wavelength under typical Mauna Kea seeing conditions. This work was made at the request of the Gemini adaptive optics working group, who asked three independant parties to perform adaptive optics system simulations using both technologies. To make the comparison simple enough, a set of conditions was imposed on seeing, telescope size, and wavefront sensor detectors. Independant simulation codes were used. A common atmospheric turbulence generator provided consistant inputs for all packages.

The Gemini adaptive optics working group requested that we consider AO system configurations including either a curvature sensor and a bimorph deformable mirror, or a Shack-Hartmann sensor and a piezostack mirror. The goal of the simulation effort was to develop AO systems based upon near-term technology which minimized the guide star R magnitude required for an on-axis Strehl ratio of 0.5 at a wavelength of $1.6\,\mu$m. From here, the three of us were asked to design and carry out the system simulations independantly from each other, to prevent any bias in the results. The free design variables available to optimize system performance were the orders and geometries of the wavefront sensor (WFS) and deformable mirror (DM), the WFS sampling rate, the gain of the adaptive optics control loop, and the matrix coefficients of the wavefront reconstruction algorithm. In a second phase, the results were reviewed by the Gemini adaptive optics working group and additional simulations were performed to cross-check each of our results.

Fig. 1 summarizes the simulated performance of "medium-order" AO systems, in particular a curvature system with 56 subapertures and Shack-Hartmann systems with 9 by 9 and 10 by 10 subapertures. The overall agreement between the two independant simulations of each the two technologies is very satisfactory. The performance of the curvature and Shack-Hartmann systems is very close up to R=15.5, even though the curvature system has significantly fewer actuators than the Shack-Hartmann system. This results from the fact that curvature systems have better overall efficiency because they correct curvatures, which are less correlated than slopes, therefore providing more information for a given number of subapertures. The fact that the two systems presented here have exactly (within 0.1 magnitude) the same limiting magnitude for an on-axis Strehl ratio of 0.5 at a 1.6 μm wavelength is interesting. This represents an apparent crossover in the performance of the Shack-Hartmann and curvature based systems for the noise conditions adopted for this study, namely noise-free avalanche photo-diodes for the curvature system and five noise electron CCDs for the Shack-Hartmann. It is our feeling that higher order systems would have given the advantage to Shack-Hartmann based systems, whereas lower order systems would have favored curvature sensing, although this would deserve additional work.

REFERENCES

1. Roddier F., Roddier C., Roddier N., 1988, SPIE **976**, 203–209

2. Rousset G., 1994, in *Adaptive Optics for Astronomy,"* pp 115–138, D.M. Alloin and J.M. Mariotti (eds)
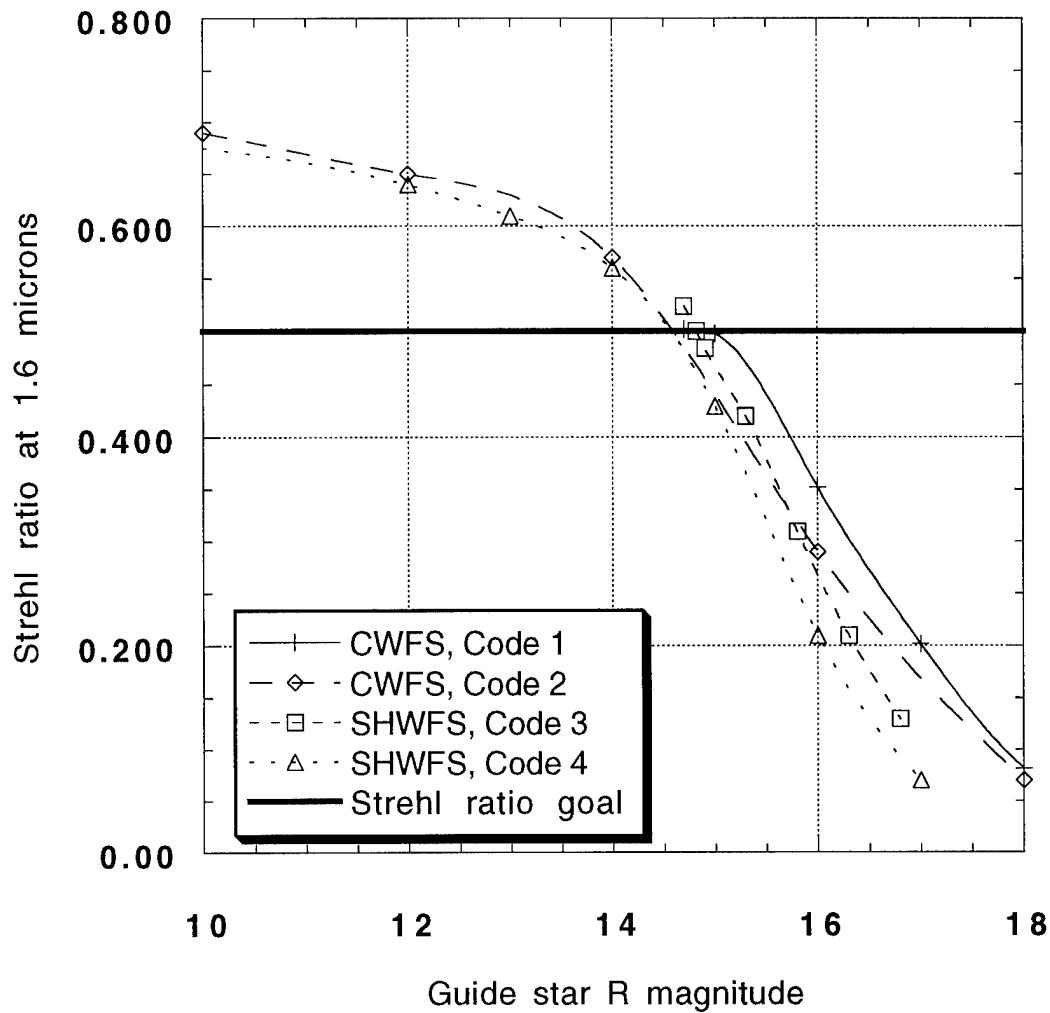
Figure 1: Summary of adaptive optics system performance versus guide star R magnitude for curvature- and Shack-Hartmann-based systems.

$D/r_0 = 23.66$ at a wavelength of $0.7\,\mu$m, wind velocity $= 20$ m/s. Codes 1 and 2 simulate a 56 subaperture curvature system, code 3 a 10 by 10 subaperture Shack-Hartmann system, and code 4 a 9 by 9 subaperture Shack-Hartmann system.

Performance Test of the slow Wavefront Sensor
for the Large Earthbased Solar Telescope LEST

Mette Owner-Petersen[1]
Michael Jensen[1]
Oddbjørn Engvold[2]

[1]:   Physics Institute. Bldg. 309
        The Technical University of Denmark.
        DK 2800 Lyngby, Denmark
        Phone: (+45)45253308   Fax: (+45)45931669

[2]:   Institute of Theoretical Astrophysics.
        University of Oslo
        P.O. Box 1029 Blindern
        N-0315 Oslo, Norway
        Phone: (47)22856521   Fax: (+47)22856505

The LEST wavefront sensor described here is intended for control of the aberrations induced by slow variations in the mechanical structure of the telescope. Hence the effects of atmospherical fluctuations must be averaged out. Active control of LEST based on the sensor signals will be performed tilting the main mirror M1 (eliminating misalignment coma), translating M3 (eliminating defocus) and adjusting the supports of the active M1 (modal compensation of other aberrations). The sensor works according to the Shack-Hartmann principle. Hartmann shifts are determined from a least squares estimate of the slope of the cross correlation spatially spectral phase. The algorithm adapts automatically to the actual spectral content of the subimages, ie to both object structure and seeing conditions.
Key parameters for the sensor are

- Subaperture diameter on M1:   150 mm
- Field of view: 15"
- Pixel resolution: 0.47" (32x32 pixels/subaperture)
- No of subapertures across M1:   15

The sensor should operate according to the following specifications:

- Hartmann shifts are calculated to a precision better than 1/10 pixel (0.05") within a dynamical range of 7 pixels (3.3").
- Aberration terms to fourth radial order included are calculated relative to a pupilcenter localized dynamically by means of the central obscuration.
- The sensor works on solar granulation with a contrast down to a few % in the subaperture images (or for Frieds parameter $r_o > 3$ cm at 500 nm wavelength).
- Exposure time is adjustable from 10 to 100 msec.
- Duty cycle for aberration update: Smaller than 2 min for $r_o > 3$ cm.

The sensor was tested in the laboratory using a solar granulation image (illuminated transparency) relayed to its LEST focus by means of an afocal imaging system. Controlled amounts of coma and third order astigmatism were induced by tilting the relay lenses, and fixed amounts of spherical aberration were induced by turning one or both of the relay lenses (standard achromats). Atmospherical distortion was simulated introducing plastic sheets between the relay lenses. Statistical analysis of the Hartmann shifts and wavefront coefficients obtained when moving the sheets documented the equivalent Frieds parameters to be in a realistic range. The sensor was absolute calibrated against defocus. It performed within specifications and the measured aberration coefficients for coma, astigmatism and spherical aberration were within 10 % of the values predicted by optical analysis (subject to an uncertainty of the same order of magnitude).

The following Figure shows the measured subimage pattern superposed with the corresponding calculated Hartmann shifts for the case of -280 nm forced spherical aberration (normalized Zernike coefficient) obtained by turning one of the imaging lenses 180 degrees around an in plane axis. No simulated atmosphere and no central obscuration were present. The Hartmann vectors have been amplified with a factor of 32, and hence vectors shorter than the subimage edge length corresponds to subpixel shifts. Using the direct image channel, the system vas visually focused to optimal performance resulting in +120 nm defocus partially compensating spherical aberration. This results in the zero shift ring clearly observed in the Hartmann pattern.
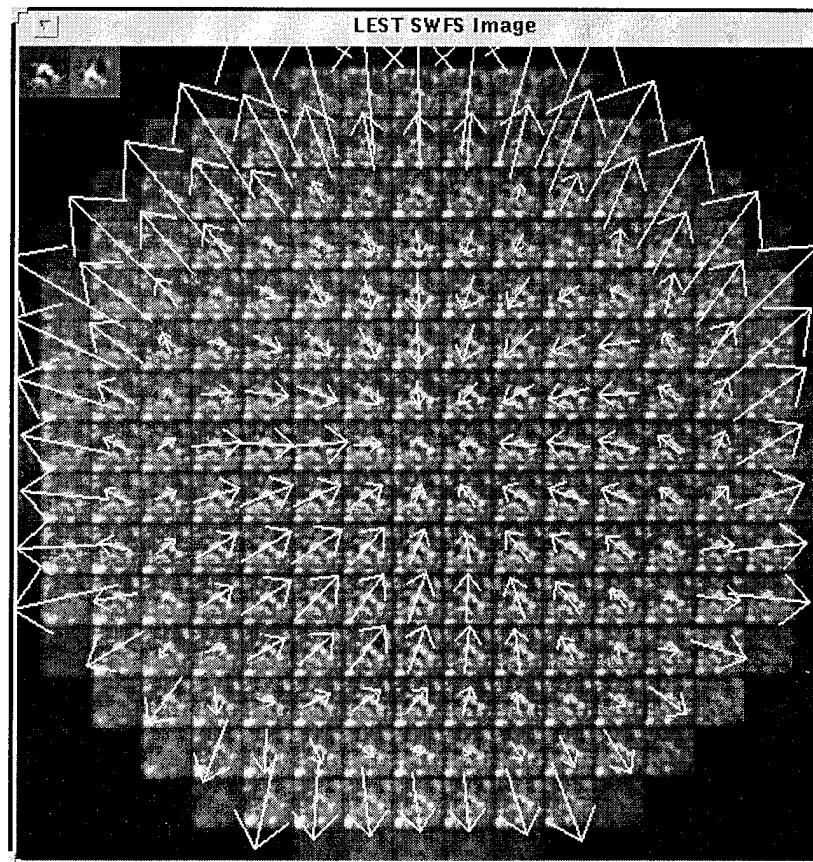
References:

M. Owner-Petersen, T.A. Darvann and O.Engvold
Design of the slow LEST wavefront sensor
Proc. of the 13 NSO/Sac Peak Summer Workshop, 63-76 (1993)

M. Owner-Petersen
An algorithm for computation of wavefront tilts in the LEST slow wavefront sensor
Proc. of the 13 NSO/Sac Peak Summer Workshop, 77-85 (1993)

J.W. Hardy and E.P. Wallner
Wavefront compensation using active lenses
SPIE Proc. 2201 (Adaptive Optics in Astronomy), 77-87 (1994)

R.J. Noll
Zernike polynomials and atmospheric turbulence
J. Opt. Soc. Am. 66, 207-211 (1976)

Techniques for Optical Fabrication of a 2-mm-thick Adaptive Secondary Mirror

H. M. Martin
Steward Observatory, University of Arizona, Tucson, AZ 85721
(520) 621-9582, fax (520) 621-1578, bmartin@as.arizona.edu

D. S. Anderson
Steward Observatory, University of Arizona, Tucson, AZ 85721
(520) 621-9595, fax (520) 621-1578, danderson@as.arizona.edu

1. MMT f/15 adaptive secondary mirror

As part of the conversion of the Multiple Mirror Telescope from six 1.8 m mirrors to one 6.5 m primary mirror, the telescope will be equipped with an adaptive f/15 secondary mirror optimized for the near infrared, $\lambda = 1 - 5$ μm. This mirror is a thin shell, 2 mm thick and 640 mm in diameter, supported on 320 voice-coil actuators which are mounted in a rigid substrate. A capacitive sensor at each actuator provides closed-loop position control with much higher bandwidth than the wavefront sensor alone allows. The geometry of the secondary is given below.

Geometry of MMT f/15 secondary

diameter	640 mm
radius of curvature (convex)	1663 mm
conic constant	-1.397
asphericity (p-v from best-fit sphere)	100 μm

2. Fabrication and measurement

The adaptive secondary requires almost the same accuracy in its polished figure (relaxed state, before adaptive correction) as that required for rigid secondaries. In both cases errors at all spatial frequencies must be much less than the wavefront error caused by the atmosphere. For the rigid secondaries this guarantees that the mirror will not appreciably degrade the wavefront delivered by the atmosphere. For the adaptive secondary it guarantees that only a small fraction of the actuator power is used to correct permanent figure errors. Some relaxation occurs because the rigid secondaries should not degrade the best seeing encountered, while the adaptive secondary's actuators are designed to handle a wide range of seeing.

Median seeing at the MMT is $r_0 \cong 40$ cm at $\lambda = 1$ μm, and the polished mirror should have no more than about 1/4 the corresponding wavefront error. This requirement is relatively loose because of the rescaling of spatial frequencies from the incoming wavefront to the secondary mirror: a high spatial frequency on the mirror corresponds to a much larger spatial frequency, with

larger allowed error, on the incoming wavefront. A tighter specification applies to errors at spatial frequencies above 15 cycles/m, which cannot be corrected by the actuators and therefore must be kept below about 10 nm rms surface error.

In most respects the adaptive secondary mirror will be fabricated using the same method being used at the Steward Observatory Mirror Lab for a number of rigid secondaries for the MMT, Large Binocular Telescope and Sloan Digital Sky Survey telescope. It will be generated and ground spherical, aspherized by loose-abrasive grinding, and polished. Aspherizing and polishing will be performed with a 1.8 m polishing machine using a stressed lap[1,2]. The stressed-lap method has been used to figure four highly aspheric primary mirrors to near the diffraction limit. The lap is bent elastically under computer control as it translates and rotates on the asphere; the bending can be programmed for convex or concave mirrors equivalently. Because the stiff lap has a strong tendency to smooth out high-frequency figure errors by removing glass, it is ideally suited to polishing mirrors that are stiff or rigidly supported and hence will not bend on small scales.

During the early stages of fabrication the ground surface will be measured with a swing-arm profilometer to an accuracy of 1μ m rms. The polished surface will then be measured interferometrically with a holographic test plate[3] to an accuracy of 5 nm rms surface error and 2×10^{-4} in conic constant. A final interferometric test will be performed after the mirror is removed from the substrate and supported optical surface down by its 320 actuators.

3. Support of the thin shell during fabrication

What sets the adaptive secondary apart from the other secondary mirrors is its flexibility, which presents a unique challenge in terms of support. During fabrication the shell must be supported uniformly and with sufficient force to resist polishing loads of 1-2 kPa, or 20-40 times the weight of the mirror. It must also remain near its relaxed state, for any strains induced by the support will be imprinted in the surface figure. The mirror cannot be supported on its actuators, since the polishing pressure would produce high-frequency bending, but must be supported more uniformly.

We plan to support the thin shell on a rigid substrate, similar if not identical to the substrate that will hold the actuators in operation. The method of attachment to the substrate is the subject of experiments on a smaller scale, described below. Regardless of the attachment method, the thin shell will be ground down from a meniscus several cm thick. The concave back of this thick meniscus and the convex front of the rigid substrate will initially be ground to matching spheres. The meniscus will be attached to the substrate and ground down to its 2 mm thickness, then aspherized and polished.

Three promising methods of attaching the shell to the substrate are being investigated through experiments on shells of 200 mm diameter. The first is optical contact (direct bonding), in which van der Waals forces hold two polished surfaces in intimate contact. The second is blocking with a thin (several hundred μ m) layer of pitch. The third is use of a soluble epoxy. All three methods are used routinely for attaching smaller optics to blocking bodies during fabrication, but we are not aware of any application to a mirror with such a large aspect ratio.

The requirements of the attachment are that it be stiff against both axial and lateral polishing forces, introduce negligible high-frequency strain, and allow safe removal of the thin shell at the

completion of fabrication. Optical contacting resists polishing forces ideally, by making the thin shell essentially a continuation of the rigid substrate. Potential challenges are avoiding contamination of the contact area--a 1 μm dust particle forms a bump 1 μm high and several mm wide-- and breaking the optical contact without breaking the shell. We must also verify that significant strains do not appear in the shell as stress is released when it is ground down to 2 mm thickness.

Pitch blocking is more forgiving of contamination and, because pitch is a viscous fluid, allows the shell to relax as stress is released. Pitch melts at modest temperature for easy removal of the shell. Pitch's fluidity has the drawback of allowing the shell to bend under the polishing force, especially near its edge where the pitch can escape. This is controlled by reducing the pitch thickness, and it remains to be seen whether we can press the pitch out to the required thickness while maintaining uniformity over the large area.

A soluble epoxy would provide nearly the stiffness of optical contacting, be somewhat more forgiving of contamination, and allow easy removal. It may, however, apply unacceptable stresses to the shell when it cures.

These issues are being addressed through the experiments with 200 mm shells. Three shells are being fabricated in the same manner planned for the secondary, attached with the three different methods. An initially thick shell is attached to the substrate, ground down to 2 mm thickness, polished to an accurate sphere (concave for ease of optical measurement), and removed from the substrate. This process identifies any difficulties in attachment, figuring and removal. The thin shell is then mounted in a nearly relaxed state and its figure is measured. Measured figure errors are compared with the requirements described above.

The most promising method(s) will be tested at roughly 400 mm diameter before the secondary is fabricated. These experiments are in progress at the time of writing and results will be presented at the meeting.

4. References

1. H. M. Martin, D. S. Anderson, J. R. P. Angel, J. H. Burge, W. B. Davison, S. T. DeRigne, B. B. Hille, D. A. Ketelsen, W. C. Kittrell, R. McMillan, R. H. Nagel, T. J. Trebisky, S. C. West and R. S. Young, "Stressed-lap polishing of 1.8-m f/1 and 3.5-m f/1.5 primary mirrors", *Proc. ESO Conference on Progress in Telescope and Instrumentation Technologies*, ed. M.-H. Ulrich, p. 169 (1992).

2. D. Anderson, H. Martin, J. Burge, D. Ketelsen and S. West, "Rapid fabrication strategies for primary and secondary mirrors at Steward Observatory Mirror Laboratory", *Advanced Technology Optical Telescopes V*, ed. L. M. Stepp, Proc. SPIE 2199, p. 199 (1994).

3. J. H. Burge and D. S. Anderson, "Full-aperture interferometric test of convex secondary mirrors using holographic test plates", *ibid*, p. 181 (1994).

SPATIAL LIGHT MODULATOR STRUCTURES FOR ADAPTIVE OPTICS

C. L. Woods

Rome Laboratory, RL/EROP, 63 Scott Rd., Hanscom AFB, MA 01731, USA

Spatial light modulators have substantially improved in the past few years. Currently, commercial 256 by 256 pixel liquid crystal binary SLMs are available with an operating speed of a millisecond and a pixel spacing of 20 microns for a price of $15,000. Additional improvements in speed by orders of magnitude should be available in the next few years, and micro-mechanical flexure and deformable membrane devices will probably become available.

In optical signal processing, ARPA funding for the TOPS (Transition of Optical Processing to Systems) program has been used to transition the patented Rome Laboratory phase-only filter (POF) technology into an automatic target recognition and tracking optical correlator. One contractor, Martin Marietta, used ferroelectric binary-phase SLMs from Boulder Nonlinear Systems to add an optical correlator accelerator to a 486-PC in a compact (total volume less than 1 cubic foot) and low power (total consumption less than 75 watts) flight rugged system capable of 1000 correlations per second.

Such liquid crystal devices and additional SLMs have the potential for adaptive optical wavefront correction. We apply our device simulations of spatial light modulators in optical correlators to analyze the performance of continuous and discrete phase-modulating SLMs. In the electrooptical phase addressed (and the piston deflector) pixel devices, a resolution of several phase levels per wavelength delay is desired. We simulate the adaptive optical correction capability of these devices, and some other possible designs based on SLMs.

CHARACTERIZATION OF THE WAVEFRONT PRODUCED BY A TWO-DIMENSIONAL SPATIAL LIQUID OPTO-ELECTRONICAL LIGHT MODULATOR *

Lea V. Bourimborde #, Lía M. Zerbino ##, Eduardo Aguirre +, Anibal P. Laquidara ++ and Mario Garavaglia ##.

Centro de Investigaciones Opticas (CIOp) **
CC 124 Correo Central, 1900 La Plata, Argentina.

The characterization of the wavefront produced by a two-dimensional spatial liquid opto-electronical light modulator was made by simple diffraction and interference experiments. The electrical video signal is injected in the thin oil film by an electron gun as in a CRT. This signal contains both the RGB carriers and their modulations. The electron activated area of the liquid opto-electronical device is illuminated by a xenon arc discharge lamp. To get an uniform illumination on that area, the light from the lamp is refracted in two lenticular plates. The thin oil film is located between the grids of a schlieren optical system. Then, the video signal injected in the active area is projected onto a screen by a projection lens. By varying the illumination of the active area and the schlieren and projection optical systems, it is possible to select appropriate experimental conditions to determine the coherence of the light emitted by the liquid opto-electronical device. Then, very interesting interferential and diffractive experiences can be performed in order to test the ability of the device to project computer synthetic wavefronts.

Nonconventional Applications and Techniques

ThB   11:00 am-12:30 pm
Auditorium

Willy L. Bohn, *Presider*
Institute for Technology and Physics, Germany

Liquid Crystal over VLSI Silicon Spatial Light Modulators for Adaptive Optics

J.Gourlay[1] , A.O'Hara, and D.G.Vass

Department of Physics and Astronomy, The University of Edinburgh,
Mayfield Road, Edinburgh EH9 3JZ
tel: (+44) 131 650 5270, fax: (+44) 131 650 5220,
e-mail: gourlay@ed.ac.uk

Liquid Crystal (LC) over Very Large Scale Integration (VLSI) electrically addressed reflective Spatial Light Modulators (SLM) have been identified as very powerful, combining the very attractive features of both the LC and VLSI technologies [1]. LC has very low power requirements for high optical modulation effects and VLSI can allow high yield and compact modulators with a high level of functionality on-chip. The device has an LC cell fabricated on top of a custom designed VLSI silicon backplane (see figure 1). The backplane contains an array of pixel memory elements, pixel mirrors and addressing circuitry. The controllable pixels in the SLM can switch the liquid crystal to achieve modulation. A number of these devices have been developed and demonstrated in a variety of optical systems such as compact displays [2], optical correlators [3] and as reconfigurable holograms [4]. A constructed SLM device in a standard chip package is shown in figure 2. In this example, the chip in the center is 1cm^2 (the package itself is $\approx 3 \times 3$ cm^2.

A variety of possible LC modulator structures can be used with silicon VLSI SLMs. If Ferroelectric Liquid Crystals (FLC) are employed, the relative phase can be quickly varied by **exactly** 0 or π due to the switchable uniaxial nature of the FLC structure, and the switching time is of the order of microseconds. Analogue phase modulation can be obtained with nematic liquid crystals, with switching times in the order of milliseconds. Both FLC and nematic phase modulation look very promising for use in adaptive optics systems [5].

Planarisation [6] is the critical technique required to make the two technologies more compatible. In the most general terms, planarisation is a post-processing technique applied to the VLSI silicon backplanes to 'isolate' the circuitry from the liquid crystal and so to avoid detrimental effects to the SLM performance due to the surface morphology [7]. The planarisation techniques were first developed on the U.K. Science and Engineering Research Council SCIOS (Scottish Collaborative Initiative in Optical Sciences) program [6]. The techniques developed on the program include: 1. deposition of a thick layer of oxide on the commercial SLM wafers, 2. chemical-mechanical polishing flat the oxide, to achieve a very flat surface, and 3. deposition and patterning of a very high quality pixel modulation mirror and via connection, hiding the addressing circuitry beneath. This results in superior device performance in comparison to non-planarised devices [7].

The main advantages of reflective VLSI silicon based SLMs are:
1. Very dense and compact modulator arrays with a high yield can be manufactured cheaply e.g. 65536 complex pixels on 1cm^2.
2. More pixel complexity and more intelligent modulator arrays can be designed e.g. SRAM, shift registers and decoders.
3. Direct voltage driving (from pixel memory) with full d.c. balance is available to switch the LC.

---

[1]Now at Durham University, Department of Physics, Durham, U.K.

4. Very high phase-flat pixel fill-factors can be obtained as all addressing circuitry can be hidden under the mirrors, particularly through planarisation techniques.

5. High quality flat substrate morphology can be achieved for improved LC alignment.

6. High quality phase-flat mirrors with custom pixel patterns optimised for system requirements can be readily achieved.
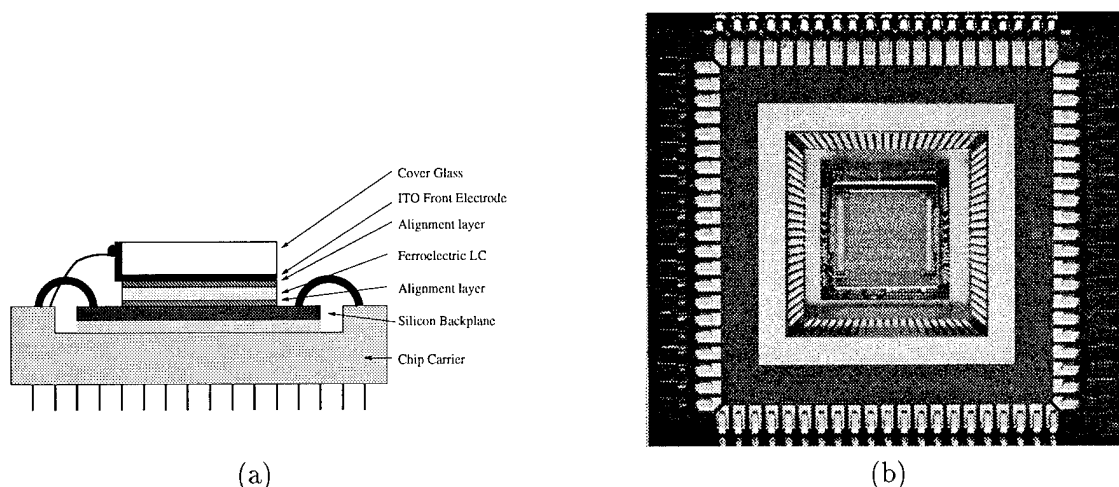

Figure 1: (a) Schematic of a liquid crystal over VLSI silicon spatial light modulator, and (b) a packaged spatial light modulator

In combination with the wide variety of LC device structures, very powerful adaptive optical components can be produced using this technology. The current state of device development is demonstrated here with reference to one particular device developed at Edinburgh. A 256×256 modulator Static Random Access Memory (SRAM) backplane was designed by D.C.Burns on the SCIOS program. The backplane was fabricated by Austria Micro Systems using their $1.2\mu m$ n-well double-metal 5.5V CMOS process. The pixels are on a $40\mu m$ pitch resulting in a $10.24 \times 10.24 mm^2$ active array. Each pixel has 10 transistors implementing an SRAM latch and XOR gate, allowing storage of data at each pixel and full d.c. balance of the LC modulator (nematic or FLC). Before planarisation, each pixel has a $19 \times 19\mu m^2$ METAL2 electrode-mirror i.e. a pixel fill-factor $< 24\%$. The fill-factor was increased to a conservative 86% through post-processing planarisation.

A $3\mu m$ cell with asymmetric medium angle deposition SiO_x alignment layer [7] was constructed on the backplane and filled with SCE13 (Merck-BDH) FLC mixture. Limited by unsatisfactory LC structures, the contrast ratio on this development device has been measured at a very low $10 : 1$ and a very low optical throughput of $< 20\%$. The SLM has been demonstrated operating at a 3kHz fully d.c. balanced frame rate, with patterns up-dated from a fast custom interface. Figure 3 shows the planarised mirrors on the SLM. Figure 4 shows a close-up of amplitude modulation with the planarised device.

A 'long range' uniformity of $0.5\mu m$ was measured across 10mm on the SLM and $< 10nm$ r.m.s. flatness at the mirror level. The low 'long range' uniformity is mechanical in origin and readily solved. Configured in a coherent optical system to investigate the SLM performing the function of an adaptive Fourier transforming element or adaptive hologram, reflected diffraction efficiency measurements are $> 60\%$. The limiting factor, again being the liquid crystal structure in this prototype device and the mechanical construction.
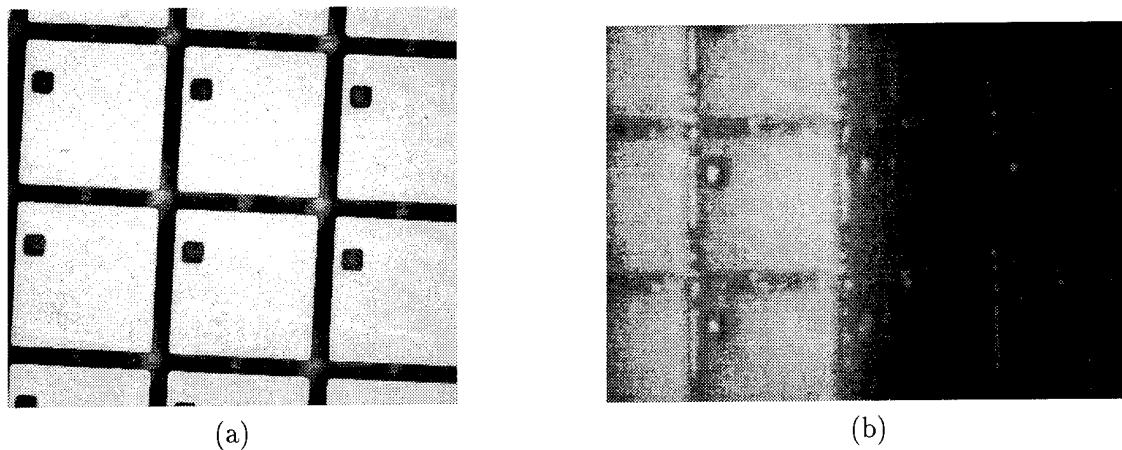
Figure 2: Photograph of (a) planarised pixel mirrors which have a $40\mu m$ pitch. The via hole connections to the underlying circuitry can clearly be seen, (b) close-up of amplitude modulation on planarised mirrors.

Investigations on the SLM described above with regard to adaptive optics are only in preliminary stages. Research and development of the planarisation techniques, device construction and liquid crystal alignment is continuing. The LC/VLSI SLMs for adaptive optics seems to be a very attractive technology with particular advantages over more traditional technologies for certain applications. A number of problems need to be overcome, particularly with regard to optical throughput efficiencies, limited by the LC alignment quality. LC/VLSI offer an attractive route to performance improvement for adaptive optics.

References

[1] K.M.Johnston, D.J.McKnight, and I.Underwood. Smart spatial light modulators using liquid crystals on silicon. *IEEE Journal of Quantum Electronics*, 29:699–713, 1993.

[2] M.R.Worboys, G.White, K.Mitchell, and A.Mosley. Miniature display technologies for integrated helmet systems. *GEC Journal of Research*, 10:111–118, 1993.

[3] R.M.Turner, D.A.Jared, G.D.Sharp, and K.M.Johnston. Optical correlator using very large scale integrated circuit ferroelctric liquid crystal electrically addressed spatial light modulator. *Appl. Opt.*, 32:3094 – 3101, 1993.

[4] J.Gourlay, S.Samus, P.McOwan, D.G.Vass, I.Underwood, and M.Worboys. Real-time binary phase holograms on a reflective ferroelectric liquid crystal spatial light modulator. *Appl. Opt.*, 35:8251 – 8254, 1994.

[5] G.D.Love, S.R.Restaino, G.C. Loos, and A.Purvis. Wavwfront control using a 64x64 pixel liquid crystal array. *Soc. Photo-Opt.Instrum.Eng.*, 2201:1068 – 1072, 1994.

[6] A.O'Hara, J.R. Hannah, I.Underwood, D.G.Vass, and R.J.Holwill. Mirror quality and efficiency improvements of reflective spatial light modulators by the use of dielectric coating chemical-mechanical polishing. *Appl. Opt.*, 32:5549 – 5556, 1993.

[7] I.Underwood, D.G.Vass, A.O'Hara, D.C.Burns, P.W.McOwan, and J.Gourlay. Impoving the performance of liquid crystal over silicon spatial light modualotors: Issues and achievements. *Appl. Opt.*, 33:2768 – 2774, 1994.

High Quality Liquid Crystal Spatial Light Modulators for Adaptive Optics.

Gordon D. Love and Sergio R. Restaino.

US Air Force Phillips Laboratory, PL/LIMI, 3550 Aberdeen S.E., KAFB, NM 87117, USA.

and also Department of Physics and Astronomy. University of New Mexico, Albuquerque, NM 87131, USA.

Richard A. Carreras and Gary C. Loos.

US Air Force Phillips Laboratory, PL/LIMI, KAFB, NM 87117, USA.

Ray M. Sharples,

Adaptive Optics Group, University of Durham, Durham DH1 3LE, U.K.

Rob V. Morrison

Meadowlark Optics, 7460 Weld County Road 1, Longmont, C0 80504-9470, USA.

Our work involves investigating adaptive wavefront correctors which may be used as alternatives to the deformable mirror in an adaptive optics system. Liquid crystal spatial light modulators (LC–SLMs) have several advantages over deformable mirrors, and also some problems of their own, as discussed in ref [1]. Much of the past work on LCs has centered around using modified LC displays which were not designed as high quality optical elements. In this paper we describe results produced using a LC–SLM which was designed specifically for wavefront correction and shaping.

Active area	14.7mm diameter or 12.5 × 12.5mm square
Pixel size	Hexagonal, max diameter = 2.08mm
Fill factor	~ 97%
Transmitted wavefront Distortion	0.038 P-V, 0.007 rms (HeNe waves).
Total stroke	1.1μm ($\pm$10V).
Transmittance	90% (HeNe).
Bandwidth	26Hz (stroke = 1 wave, 10-90%) 110Hz (stroke = 0.5 wave, 10-90%)

Table 1: Specifications of the LC–SLM.

The LC–SLM was constructed by Meadowlark Optics, and its specifications are shown in table 1. The laboratory experiments centered around using a Zygo phase shifting interferometer as the wavefront sensor in an open loop adaptive optics system.

Figure 1 shows two interferograms of the active area of the device. 1(a) shows two rings of pixels which are partially actuated producing a phase shift of approximately a quarter of a (HeNe) wave (the interferometer is a double pass device therefore one fringe shift corresponds to half a wave). 1(b) shows two rows of actuated pixels. Notice (i)

the straightness of the fringes indicating the high optical quality and (ii) the boundary between the actuated and unactuated pixels is sharp showing that the actuator impulse function is highly localized.

The next experiment involved the static correction of wavefront aberrations. A static aberrant medium was introduced by using a piece of non-optical quality glass. The phase profiles measured by the Zygo were analyzed by a PC and fedback to the LC-SLM to produce the corrected wavefront. A high-quality polarizer ensures the light is polarized along the LC's extraordinary axis. Results are shown in figure 2. The top plots show phase maps measured by the Zygo before and after the correction was applied to the LC-SLM. The rms phase aberration is reduced from 0.18 to 0.05 HeNe waves. The corresponding PSFs were calculated by Fourier transforming the phase maps, and are shown in the lower two plots of figure 2. The reduction in wavefront variance and the corresponding improvement in image quality is very clear.

(a)   (b)
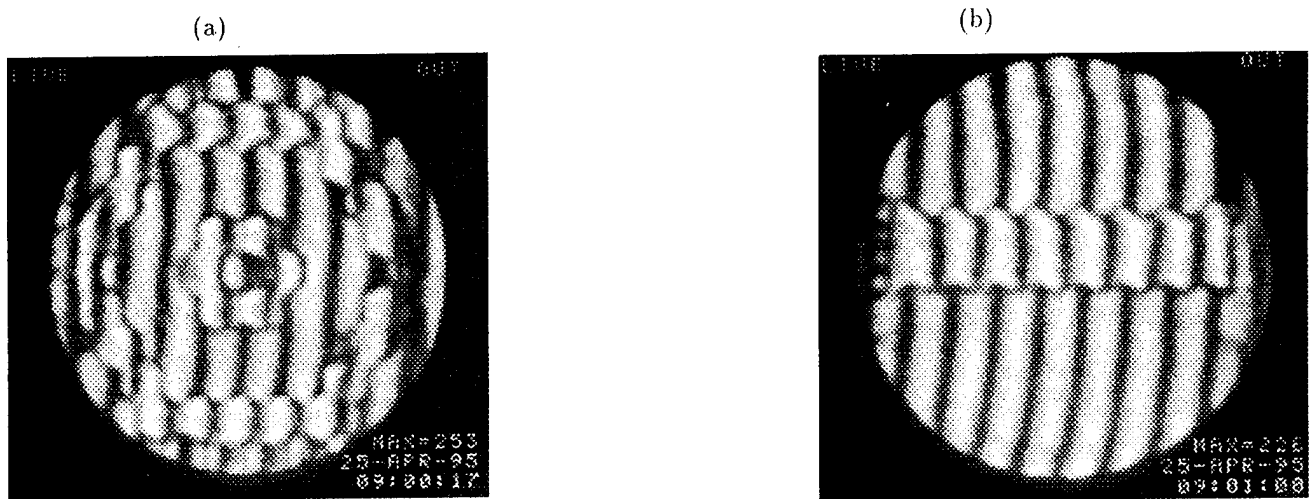
Fig. 1. Interferograms of the LC-SLM. 1(a) shows two rings of pixels which are producing a phase

shift of a quarter of a wave. 1(b) shows a similar phase shift produced by two central rows of pixels.

The second part of this study involves the production of Zernike aberrations with the LC-SLM. As well as wavefront correction, there is interest in the production of known aberrations in order to facilitate the laboratory testing of other adaptive optics components. The amplitude of each aberration (except for tip-tilt) was selected to be the mean value calculated from Kolmogorov turbulence theory. The resultant wavefronts shaped by the LC-SLM were experimentally measured using the Zygo and compared with the theoretical values. The experimentally measured phase maps are shown in figure 3. Each plot is a normalized greyscale plot also showing the Zernike mode number and the measured Zernike amplitude. The rms deviation between the theoretical and experimental values is $\lambda/31$, and the maximum deviation $\lambda/15$.

Work is in progress at the Phillips Laboratory and at Durham University to produce further experimental results with the 69 actuator device described in this paper. The first experiment will be to correct slowly varying ($\sim$ minutes) aberrations at a real observing site, which will require the construction of a wavefront sensor and control system. This will provide valuable experience for the second series of experiments which will involve the real-time

correction of atmospherically aberrant wavefronts. Work is in progress at Meadowlark Optics to circumvent some of the current problems of LC-SLMs. A device has been designed which will utilize 127 directly-driven pixels in a similar hexagonal arrangement. The results shown in this paper were recorded using linearly polarized illumination. The new device, however, will be capable of correcting errors from unpolarized sources. The electronic addressing will be modified to incorporate the transient nematic effect [2] in order to improve the temporal bandwidth of the device.
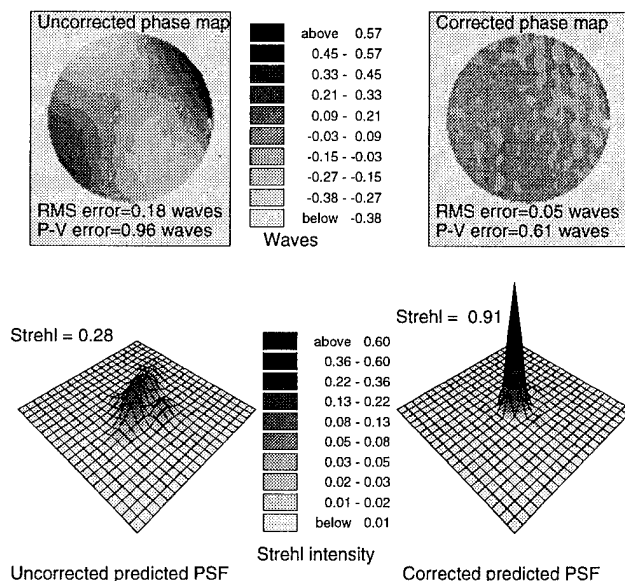
Fig. 2. Correction of static wavefront aberrations using the LC-SLM. The top two plots are un-corrected and corrected greyscale phase maps as measured by the interferometer. The bottom two plots show the expected PSFs obtained by Fourier transforming the phase maps.
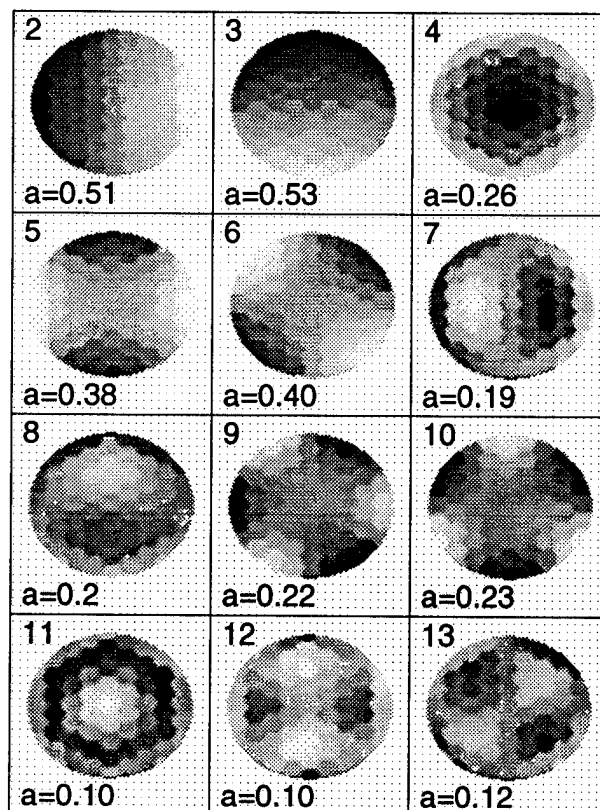
Fig. 3. The generation of Zernike aberrations using the LC-SLM. Each plot is a normalized greyscale phase map, as measured by the inter-ferometer. The number in the top left indicates the Zernike number, and a corresponds to the am-plitude of each term. Except for the tip-tilt terms, these correspond to the rms values expected from Kolmogorov turbulence for $D/r_0 = 10$.

This work clearly shows that it is possible to construct devices whose optical quality and transmission are sufficiently good to be used as high quality optical elements.

References

(1) G D Love, J V Major, and A Purvis. *Opt. Lett.* **19**(15):1170-2 (1994).

(2) S T Wu and C S Wu. *Appl. Opt.* **53**(19):1794 (1988).

Atmospheric Compensation using non-linear optical phase conjugation

G Cook, D C Jones, K D Ridley, A M Scott

Electronics Sector
DRA
St Andrews Rd, Malvern
Worcs WR14 3PS
UK
Phone +44 (0) 1684 895418
Fax +44 (0) 1684 896270
E-mail amscott@dra.hmg.gb

Introduction

Conventional adaptive optics have been developed over many years for the purpose of imaging and for directing laser beams through atmospheric turbulence. In this application light from a known point source is collected and a mirror or phase shifting array is modified until the collected light can be focused to form a point image. When this goal is achieved then a collimated laser beam can be directed back through the optical system and will retrace the path of the incident light back to the source. The limitations of conventional adaptive optics are determined by the time taken to measure the wave-front and move actuators, the number of actuators available and hence the degree of compensation which can be achieved, and the degree of computation required to get effective compensation.

An alternative approach in is to use non-linear optical phase conjugation. One of the first successful demonstrations of correcting for atmospheric turbulence was reported by Ackerman and Lebow [1] who compensated over a 600m range. In this approach light from the remote source is amplified and conjugated using a non-linear process such as four-wave mixing or stimulated Brillouin scattering, and automatically retraces its path back to the source. The incoming light must be coherent and this can be achieved by illuminating a co-operative target such as a corner cube to act as the remote coherent point source. The technique has the advantages that the conjugate beam is created instantaneously, in principle correction can be achieved for many modes (say 10,000), and no computing is required to calculate the phase correction.

Phase conjugation techniques

There are two basic phase conjugation techniques; Stimulated Brillouin scattering and four wave mixing. Stimulated Brillouin scattering occurs when a powerful (10kW or more, or 0.1mJ in 10ns) coherent laser beam is focused into a liquid such as CS_2. An acoustic wave forms in the liquid which adapts itself to match the wavefronts of the incoming beam, and perfectly retro-reflects the beam to form a phase conjugate return. The technique is characterised by a power

threshold, a reflectivity of less than 100%, and a fidelity which may also be significantly less than 100%.

The second technique of four wave mixing requires two auxiliary pump beams to be present at the same time as the signal beam. In essence the signal and one reference beam write a holographic grating and the second reference beam reads the grating to produce a conjugate beam. This is more complex but there is no threshold and the conjugate may be more intense than the input.

In the case of Brillouin-enhanced four-wave mixing, the pump and signal beams have frequency differences equal to the Brillouin shift, and acoustic waves form the holographic grating. Reflection coefficients of greater than 10^6 have been achieved and signals of as small as a 50fJ can act as an effective signal.[2]

System Requirements

For a corner cube of say 2cm diameter at a range of one km or more one requires that the amplifying phase conjugate mirror system has an overall reflection coefficient of over 10^6 simply to ensure that the illumination level of the conjugate beam exceeds the initial illumination beam.

At first sight the simplest way of achieving this is to use an SBS phase conjugate mirror and a high gain amplifier such as Nd YAG. The incoming signal passes through the amplifier, is conjugated at the SBS cell and is amplified on a second pass as it returns to the corner cube. However one of the limiting factors in such a system is that the collected signal must exceed the SBS threshold after one pass through the amplifier. This can be achieved either by using very high powers in the initial illumination beam or by using a very high gain amplifier chain. If the latter approach is used then ASE will rapidly deplete the amplifier's stored gain unless the amplifier's field of view is reduced by aperturing and spatial filtering. This makes the technique unattractive.

Amplification can instead be achieved using stimulated Raman scattering. In this case the gain is transient depending on the duration of a pump laser pulse, and ASE does not deplete stored gain. The technique results in increased complexity because two lasers are required, one to provide the illumination and one to pump the Raman amplifier, and these must be synchronised with less than 5ns jitter. In 1992 Hasselbach and Rockwell [3] demonstrated phase conjugation over a 6km range using a Raman amplifier and an SBS phase conjugate mirror.

An alternative approach is to use a phase conjugate mirror based on four wave mixing, as was used by Ackerman and Lebow. Again two synchronised lasers are required and they must be mutually coherent. However the incoming signal can be very weak (5pJ) and the synchronisation provides a degree of range gating which ensures that

returns from spurious reflections are excluded from the phase conjugation process.

High sensitivity phase conjugation

The disadvantage of Brillouin techniques is that the incoming signal must exceed the background spontaneous Brillouin scattering, arising from scattering off acoustic noise fluctuations. This limits the minimum signal to a few 10s of fJ. Pasmanik et al [4] showed that it was possible to combine a conventional laser pre-amplifier with a high reflectivity Brillouin four-wave mixing mirror. The pre-amplifier adds ASE to the amplified signal, but the Brillouin mirror has an extremely narrow spectral bandwidth and rejects the ASE noise. As a result it is possible to build a phase conjugate mirror with a sensitivity of a few photons and reflectivities in excess of 10^{12}.

We will describe a number of high sensitivity phase conjugate mirror arrangements These can respond to signal of as little as 30 photons or so. These can be based on Brillouin induced four wave mixing or Brillouin amplification and conventional SBS. We will show that they can be used to correct for atmospheric turbulence and produce good quality conjugate beams.

We will also show that in the absence of a retro-reflecting mirror it is possible for the phase conjugation system to respond to the back-scatter from atmospheric aerosols at a range of 500m, demonstrating the principle of phase conjugating the return from a synthetic guide star.

References

[1]   P. Lebow, J. Ackerman, Opt Lett 14, p236 1989

[2]   A. Scott, K. Ridley, J Quant Electron 25 p438-459 1989

[3]   H. Hasselbach, D. Rockwell, CLEO Digest 1992

[4]   O. Kulagin, G. Pasmanik, A, Shilov, Sov Phys Usp 35,6, 506-519 1992

Feedback Interferometry for Aberration Correction

T.H.Barnes, G.T.Bold, and T.G.Haskell

T.H.Barnes and G.T.Bold are with the Physics Department, University of Auckland, Private Bag 92019, Auckland, New Zealand. Tel: +64 9 373 7599 Ext 5872, Fax: +64 9 373 7445

T.G.Haskell is with Industrial Research Ltd., P.O.Box 30311, Lower Hutt, New Zealand.
Tel: +64 4 569 0000, Fax: +64 4 569 0067

Introduction

Feedback interferometers, in which the output fringe pattern is fed back to modulate the phase-difference in the interferometer via a spatial optical phase modulator, have been used for investigations of spatial structure formation[1], optical memories[2], and to achieve unambiguous fringe phase display for optical testing[3]. If these interferometers are operated in the negative feedback regime, it is possible to obtain output fringe patterns where intensity is almost linearly dependant on the physical path-difference in the system. This intensity distribution is fed back to a phase modulator in the interferometer as part of the negative feedback scheme, and so the resultant phase modulation partially cancels the interferometer path-difference - the degree of cancellation depending on the gain of the feedback loop. With an appropriate interferometer system (for example a radial shearing interferometer) it is, in principle, possible to automatically correct the aberrations of the input wavefront even at low optical powers[4]. We have built an interferometer of this type and describe its characteristics here.

Feedback Interferometry

Fig. 1 shows the system used in this work. It is a Mach Zender interferometer, with a beam expanding telescope in one arm, and the phase modulator in the other. The system is therefore a radial shearing interferometer where the shape of the input wavefront may be estimated from fringe phase in the output intensity distribution. Feedback is provided by detecting the output fringe pattern with a CCD camera and feeding the video signal to the phase modulator with a variable feedback loop gain, using a framegrabber and computer. In our work the phase modulator was a parallel aligned liquid crystal panel with 9 x 9 pixels. The modulator phase characteristic is shown in Fig. 2.
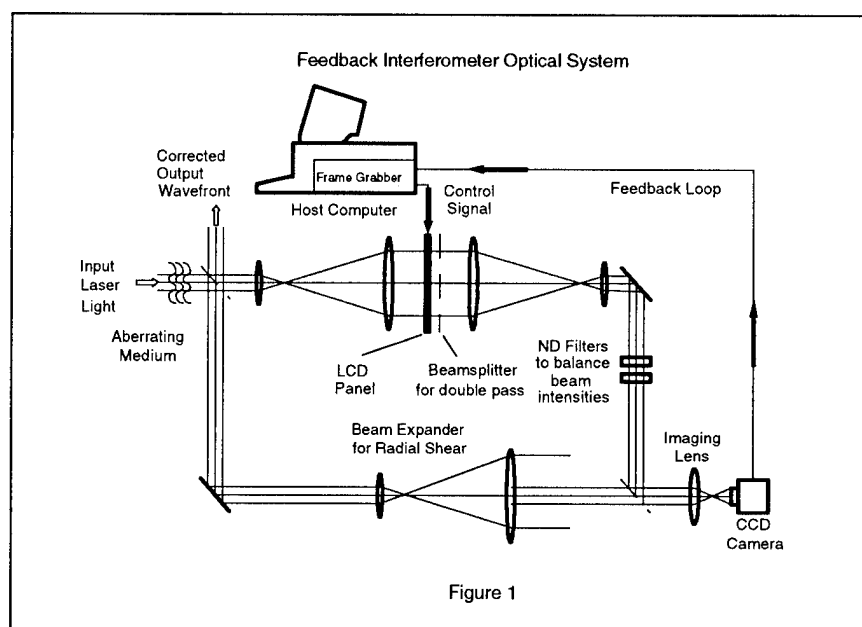

Figure 1

In order to analyse the interferometer, we make the approximation that the reference wave obtained from the beam-expanding telescope is a plane wave, and that the interferometer path difference arises only from the phase distribution of the input wave, $\phi(x, y)$, where x, y are lateral coordinates across the input wavefront. The output intensity from the interferometer is then given by:

$$I(x,y) = \varepsilon I_{in}\left[1 + VCos\left(\phi(x,y) + f\left(GI(x,y)\right)\right)\right] \tag{1}$$

Where:
- ε is a factor taking into account the interferometer efficiency
- I_{in} is the input intensity to the interferometer
- V is a factor taking into account the fringe contrast in the system
- G is the feedback loop gain
- $f()$ is the phase modulator characteristic

This equation represents a system where the feedback is alternately positive and negative depending on $\phi(x, y)$. The practical system will automatically adjust the phase modulator to find stable points where the feedback is negative. The equation may be solved numerically for $I(x, y)$ at the stable points, and the result then converted to the phase of the modulator: $\phi_m = f(GI(x, y))$. Fig. 3 shows the variation of ϕ_m (modulator phase) with ϕ (input wavefront phase) for a typical interferometer system with several different values of feedback loop gain. The modulator phase is related to the conjugate of the phase of the input wavefront, with a maximum available correction of ~0.65 wavelengths per wavelength deviation of the input wavefront. 0.5 wavelength correction per wavelength deviation of the input wave is available at a feedback loop gain of 0.33. Under these conditions it should therefore be possible to achieve full automatic correction of the input wavefront by arranging that it pass twice through the phase modulator. This is done by placing a beam splitter behind the modulator to reflect some of the input light back through it and out of the interferometer via the input beamsplitter.

Figure 2
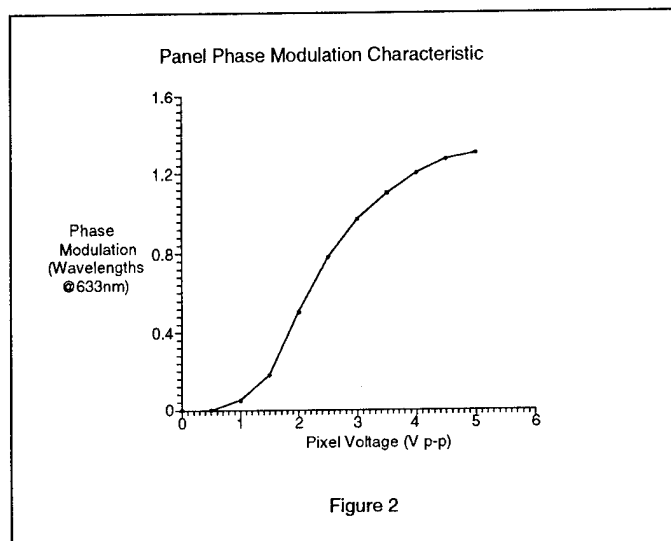
Experiment

We constructed the optical system shown in Fig. 1 to demonstrate how feedback interferometry might be applied to aberration correction. Our system is driven by a 5mW HeNe laser, has an input aperture diameter of 20mm, and a beam expansion in the reference arm of 5:1. The interferometer stable points depend on input intensity, and so considerable care was taken to expand the beam from this laser so that intensity variations over the interferometer input aperture are less than 10%.

The active area of the liquid crystal modulator is 45mm square, and so two identical afocal lens systems are used to match it to the 20mm aperture size of the rest of the optical system. The interferometer lens system is arranged so that the panel plane is imaged onto the CCD camera at the output. The panel is controlled by a dedicated microprocessor which accepts commands from a host computer (IBM PC compatible) via a serial interface. Panel response time is about 50msec.

Figure 3
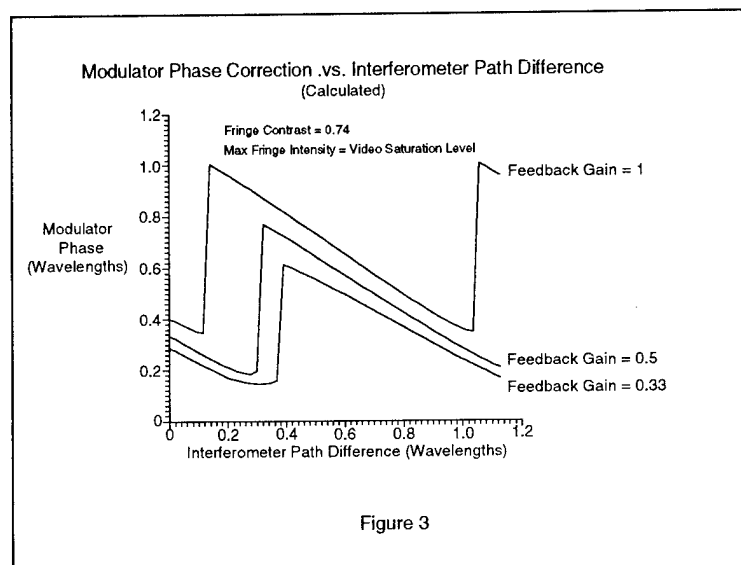
The control program in the host computer samples the output intensity of the interferometer at points corresponding to the panel pixel positions in the output field, and then feeds these intensities electronically, with variable gain, back to the panel via a lookup table which allows modification of the intensity/phase-modulation characteristic. Several different types of feedback (proportional, integral, and proportional-integral) may be implemented with varying feedback time-constants to prevent unwanted system oscillations due to the finite time response of the panel and sampling system.

Measured Phase Correction capability of Feedback Interferometer

Modulator Phase (Wavelengths @633nm)

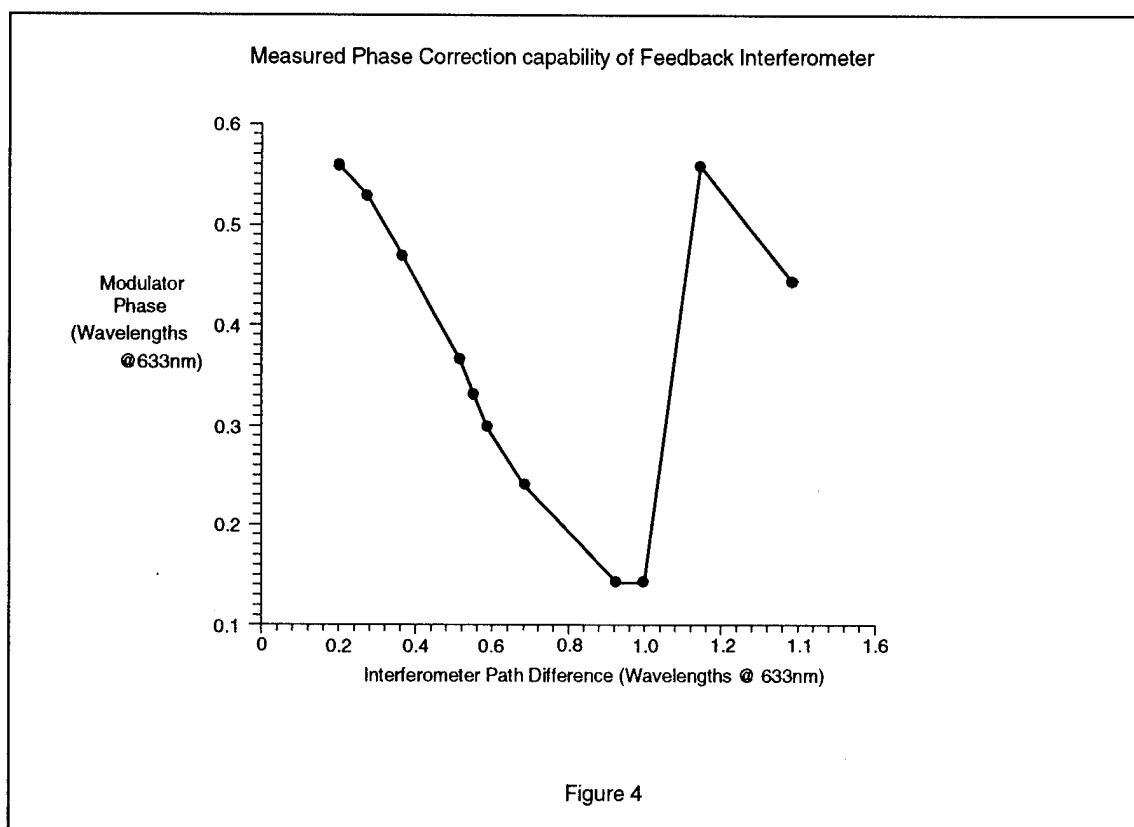Interferometer Path Difference (Wavelengths @ 633nm)

Figure 4

In initial tests, one of the mirrors of the interferometer was moved by a controlled amount using a piezo translator and the output intensity (and therefore modulator phase) measured as a function of the introduced path difference. The results are shown in Fig. 4 where it can be seen that the modulator phase varies almost in proportion to the conjugate of the path difference variation introduced in the interferometer.

Conclusion

We have described a novel feedback interferometer in which the two-dimensional phase distribution across a spatial optical phase modulator in the system is approximately proportional to the conjugate of the input wavefront to the system. This interferometer has potential for automatic aberration correction in coherent systems with uniform input intensity distribution.

Acknowledgements

We are most grateful to Professor T.Tschudi, Dr. Cornelia Denz, and Jan Lembke of the Institut fur Angewandte Physik der Technischen Hochshule, Darmstadt, Germany, for providing the liquid crystal panel we used in this work. This work is a collaborative project between the University of Auckland, and Industrial Research Ltd.

References

1) M.Kreuzer, R.Neubecker, and T.Tschudi "Formation of spatial structures in bistable elements containing nematic liquid crystals" Appl. Opt. **29** 579 - 582 (1990)

2) T.H.Barnes, T. Eiju, S.Kokaji, K.Matsuda, and N.Yoshida "Bistable optically writable image memory using phase-only spatial light modulator" Optik **96** 107 - 114 (1994)

3) T.H.Barnes, T.Eiju, and K.Matsuda "Direct unambiguous display of phase-difference using optical feedback to a phase-only spatial light mdulator" Accepted for publication in Optik, May 1995

4) E.Marom and U.Efron "Phase conjugation of low power optical beams using liquid crystal light valves" Opt. Lett. **12** 504 - 506 (1987)

Adaptive Telescope Array for Laser Communications and Astronomy

Klaus H. Kudielka and Walter R. Leeb

Institut für Nachrichtentechnik und Hochfrequenztechnik, Technische Universität Wien

Gußhausstraße 25/389, A-1040 Wien

Phone: ++43-1-58801-3530, Fax: ++43-1-5870583, E-mail: Klaus.Kudielka@tuwien.ac.at

1   Introduction

Phased telescope arrays can be used to coherently receive or transmit optical radiation [1], even in the presence of wavefront distortion due to turbulent media [2]. In addition, phased telescope arrays operating in receive mode allow to obtain images with high angular resolution [3] and to implement wide field-of-view imaging systems [4].

For coherent optical space communications, multi-aperture receive telescopes provide non-mechanical, adaptive fine steering of the main lobe direction, thus compensating sattelite attitude jitter. Further benefits of a receive telescope array (RTA) over a single, large telescope are modularity, ease of fabrication, and implicit redundancy. Since adaptive RTAs automatically compensate any distortion of the incident wavefront, they can be considered for coherent space-to-ground links.

For astronomy, adaptive RTAs offer a large collecting area and a high angular resolution, while diminishing the influence of atmospheric turbulence. By intentionally steering the RTA's main lobe close to a reference axis, the image of a stellar object can be acquired. The reference axis is determined, e.g., by a guide star. The angular resolution is only limited by the diffraction angle associated with the RTA diameter. The RTA's field of view is equal to the diffraction-limited divergence of a single subtelescope.

2   Coherent optical communications

Figure 1 shows the basic building block of a phased telescope array for coherent optical reception. It consists of two subtelescopes coupling the incident optical wave into two polarization-maintaining single-mode fibers. The relative phase $\phi_1 - \phi_2$ between the optical subfields propagating into the polarization-maintaining directional coupler is set by a piston actuator. The directional coupler superimposes both subfields which are assumed to carry identical optical power (P). At one output port, an optical power sensor detects the power P_B, which is proportional to $1 - \cos(\phi_1 - \phi_2)$. The desired phase difference is $\phi_1 - \phi_2 = 0$, implying $P_B = 0$ and $P_A = 2P$ at the second output. Periodically dithering around the operating point causes the
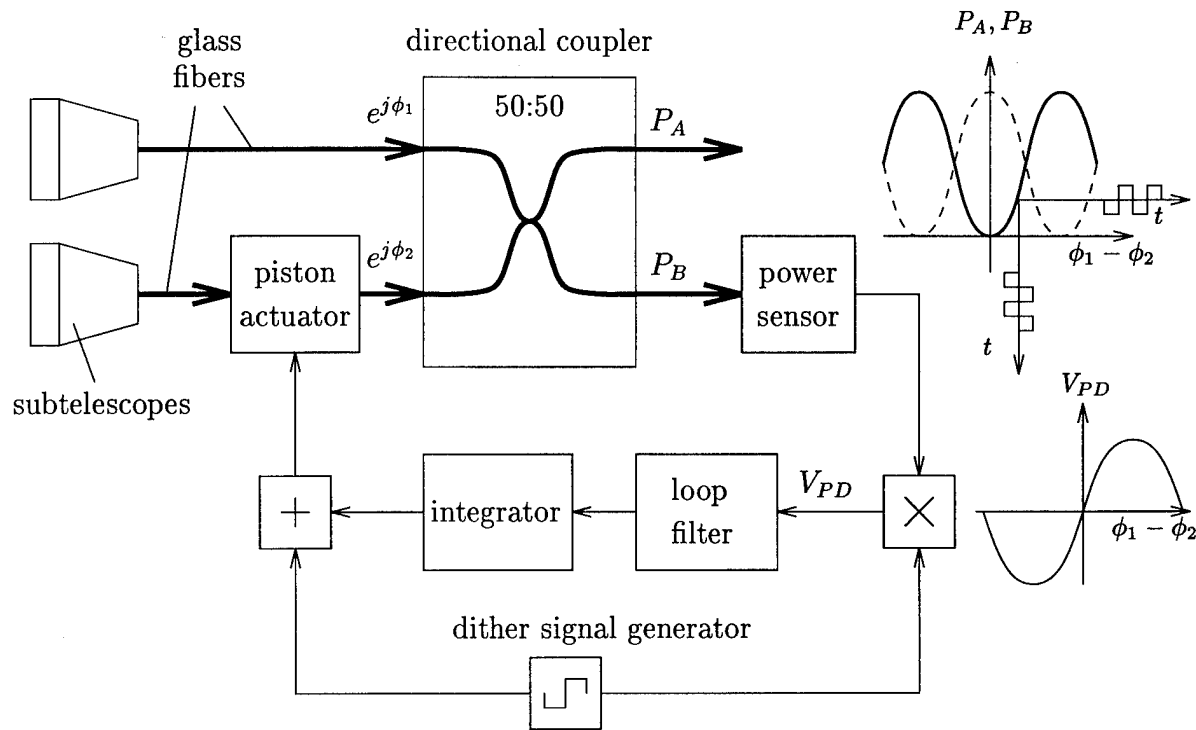
Figure 1: Basic building block of a phased telescope array operating in receive mode

power sensor to detect a signal at the dither frequency f_d. The power sensor output is synchronously demodulated into the baseband, resulting in a phase detector voltage V_{PD} proportional to $\sin(\phi_1 - \phi_2)$. In combination with a loop filter and an integrator V_{PD} is used to close an optical phase-locked loop (OPLL). The dither frequency f_d must be higher than the bandwidth of the phase-locked loop, and the dither amplitude must be very small compared to 2π. The OPLL locks at $\phi_1 - \phi_2 = 0$ and directs the total optical input power to output port A.

If more than two subtelescope signals have to be combined, the simple structure shown in Figure 1 can be cascaded. To demonstrate the feasibility and the capabilities of such a receive telescope array, we implemented a proof-of-principle laboratory experiment [1]. The optical input wave ($\lambda = 1064nm$) is collected by four subtelescopes and coherently combined into a single output fiber. Within the field of view of a single subtelescope, the RTA adapts itself to the direction of the incident wave, maxmizing the optical output power. For a step-like change of the input wavefront, we measured a response time of $0.8ms$.

3   Imaging

The telescope array concept developed for coherent optical reception may also be used to obtain images from astronomical objects. In this case the optical phase-locked loops are used to

compensate wavefront variations caused by atmospheric turbulence. Within the subtelescopes' field of view, the adaptive RTA automatically locks at an operating point where the RTA output power is maximum. The dither signals necessary for the optical phase-locked loops can be chosen so that the RTA's total field of view is periodically scanned. Recording the RTA output power and relating it to the current scan angle finally results in the desired image. To achieve a sufficiently high signal-to-noise ratio, the average of many scans can be formed.

To successfully apply the present RTA concept to imaging applications, an additional requirement must be met, i.e. the lengths of the subtelescope paths must be exactly equal. For laser communication signals with bandwidths of a few GHz, sufficient subtelescope phasing can be achieved if the path length differences are multiples of the wavelength. Since the bandwidth of the astronomical sources to be observed is much higher, the path length differences must be exactly zero. This requirement can be fulfilled, as has been experimentally demonstrated [5].

4   Conclusion

It has been shown that the concept of an adaptive receive telescope array developed for coherent optical communications can also be used to implement an imaging telescope array to observe astronomical objects. Due to the simple structure and the possible use of fiber technology and integrated optics technology, very large arrays can be implemented with relatively little effort.

References

[1] K. H. Kudielka et al. Adaptive optical multi-aperture receive antenna for coherent inter-satellite communications. In *Proc. SPIE*, volume 2210, pages 61–70, 1994.

[2] J. E. Pearson. Atmospheric turbulence compensation using coherent optical adaptive techniques. *Applied Optics*, 15(3):622–631, 1976.

[3] S. Shaklan. Fiber optic beam combiner for multiple-telescope interferometry. *Optical Engineering*, 29(6):684–689, 1990.

[4] C. R. De Hainaut et al. Wide field performance of a phased array telescope. *Optical Engineering*, 34(3):876–880, 1995.

[5] F. Reynaud et al. Interferometric control of fiber lengths for a coherent telescope array. *Applied Optics*, 31(19):3736–3743, 1992.

High Speed Micro-Machine Device for Adaptive Correction of Aero-Optic Effects

Mr. Rod Clark, Mr. John Karpinsky, Mr. Gregg Borek, Mr. Eric Johnson
SY Technology, Inc.
4900 University Square, Suite 8, Huntsville, AL 35816
Phone: (205) 722-9095, Fax: (205) 722-9097, E-Mail: rclark@sy.com

Dr. Natalie Clark
Phillips Laboratory
Advanced Imaging Technologies Interferometric Group
PL/LMI 3550 Aberdeen SE, Kirtland AFB, NM 87117
Phone: (505) 846-4410, Fax: (505) 846-2045, E-Mail: nclark@plk.af.mil

Introduction

Current adaptive optical l systems which provide wavefront correction operate at or below 100 Hz, a frequency response suitable for correcting atmospheric effects for such applications as ground-based astronomy[1]. These systems are limited to such low frequency operating bandwidths by the speed of the processing and drive electronics, and the large, slow, deformable mirror devices utilized by these system designs. SY Technology, Inc. has developed a micro-machine based, high frequency, adaptive device which, when inserted into the proposed interferometric design, will have the potential to correct wavefronts at frequencies of hundreds of kilohertz[2]. This tremendous bandwidth is achieved by a device fabricated using photolithographic techniques, with its drive electronics controlled through light-addressed circuitry (see Figure 1). In this paper, a closed-loop adaptive, interferometric micro-machine device to correct for aero-optic effects is described and demonstrated[3].
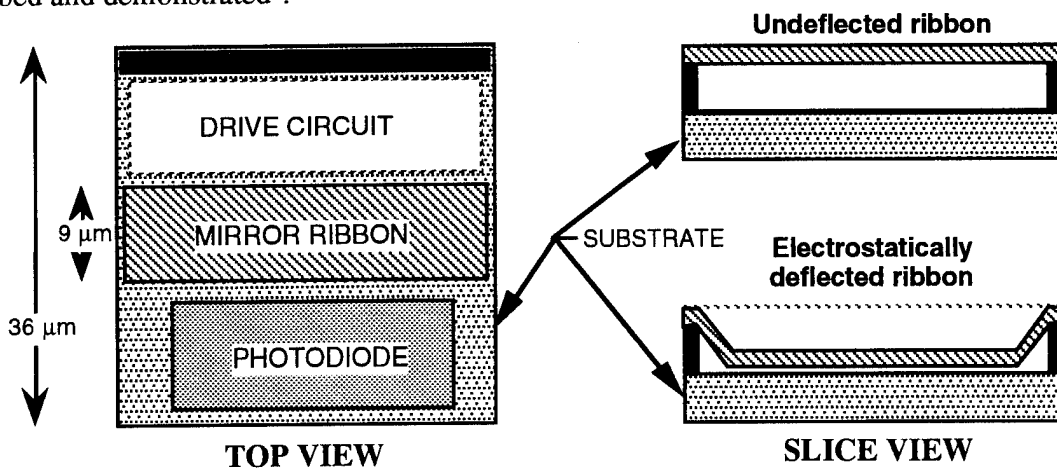
Figure 1. Pixel Layout for High Bandwidth Adaptive Wavefront Correction Spatial Light Modulator (SLM).

[1] S.R. Restaino, E.L. Gates, R.A. Carreras, R. Dymale, G.C. Loos, "On the use of electro-optical devices for O.P.L. compensation", SPIE Vol.2200, 494

[2] E.M. Motamedi, "Micro-Opto-Electro-Mechanical Systems", Optical Engineering, November 1994, Vol33, No. 11.3505

[3] A. Fisher and C. Warde, "Simple closed-loop system for real-time optical phase measurement", Optical Letters, Vol. 4, No. 5, May 1979

Detailed Description of Corrector Operation

Figure 2 shows a diagram of the high bandwidth, closed-loop, interferometric aero-optic correction system. The system shown in Figure 2 is a classical Michelson interferometer. A source beam of monochromatic, coherent radiation is expanded and collimated by beam collimation optics (Element 1 in the figure). The partially reflective, partially transmissive beam splitter (Element 2 in the figure) forms the two legs of the interferometer. The first leg reflects off the beam splitter at an angle of 90°, and continues to the broadband flat mirror (Element 4 in the figure), passing through the turbulent flow (Element 3 in the figure). The beam reflects off the flat mirror (Element 4) and makes a second pass through the turbulence. This beam then returns through the beam splitter and reflects off the diachronic beam splitter (Element 5 in the figure), continuing on to strike the Spatial Light Modulator (SLM) (Element 6 in the figure) at an incidence angle of θ_2°. The second leg of the interferometer passes through the beam splitter to strike the SLM at normal incidence. In striking the SLM at normal incidence, this beam is reflected from the mirror ribbon element of the SLM pixels and returns back to the beam splitter where it is reflected at a 90° angle and continues on to the diachronic beam splitter (Element 5). From the turning mirror, this leg is directed by reflection onto the SLM also at an incidence angle of θ_2°. The two legs, the first making a double pass through the turbulence and the second reflecting from the mirror ribbon elements of the SLM, are allowed to interfere on the SLM at the photodiode site.
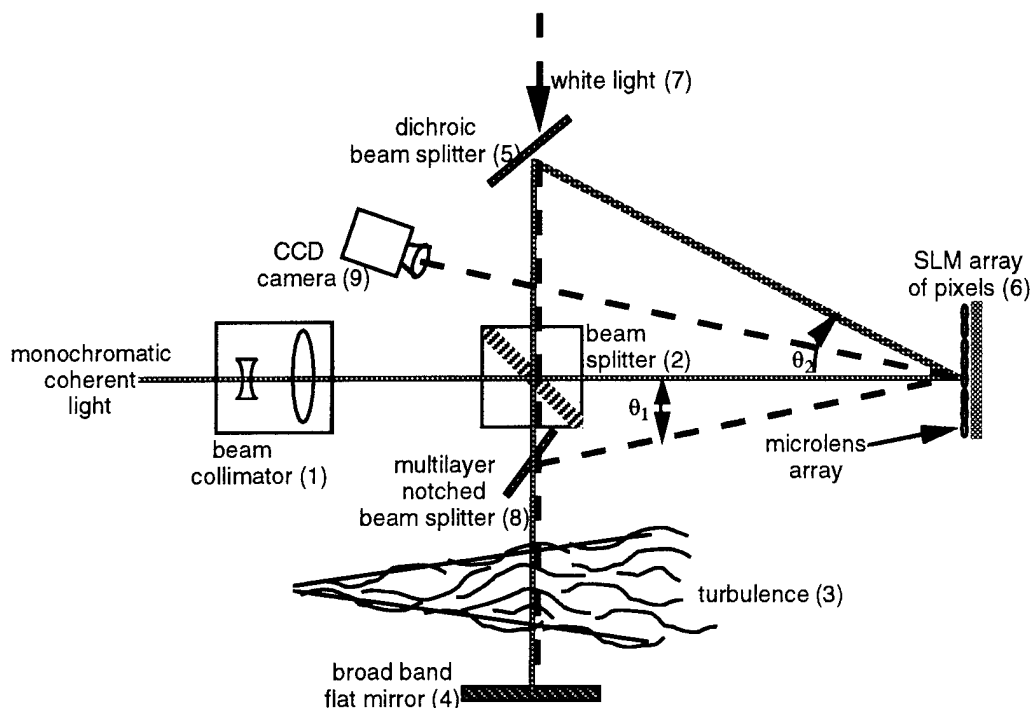
Figure 2. Optical Layout of Closed-Loop Interferometric Wavefront Correction Device.

Figure 3 shows a diagram of the two beams incident on a single pixel of the SLM device, one at normal incidence and one with an incidence angle $\theta_2°$. Each SLM pixel is covered by a microlens and consists of a photodetector site, a drive circuit, and a mirror ribbon. The microlens is used to focus all near normal incident light onto the small ribbon mirror of the pixel. This device is designed such that light at near normal incidence is reflected from the micro-machined deformable mirror ribbon. The phase of near normal incident light is modulated by the distance the light must travel before reflection from the deflected mirror ribbon.
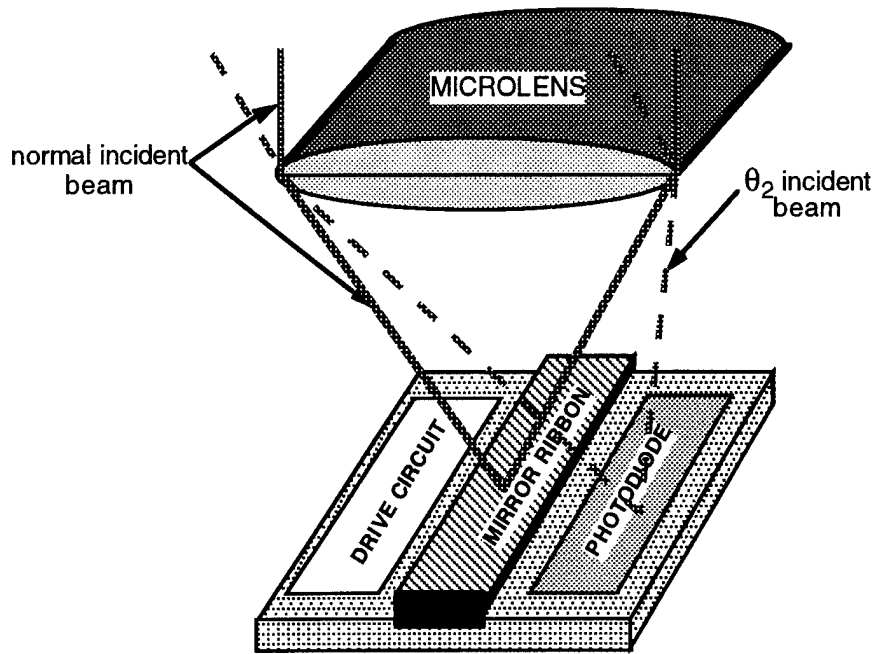
Figure 3. Diagram of the Beams Incident on a Single Pixel of the SLM Device in the Interferometric Aero-Optic Corrector.

The reflected light is again collimated by returning through the microlens. The SLM also has the interesting property that light at an incidence angle of $\theta_2°$ misses the mirror ribbon and impinges on the photodetector element of the SLM. The photodetector output is amplified and connected to a drive circuit which controls the deflection of the mirror ribbon, moving the mirror in response to incident light. With no light incident on the photodetector, the mirror ribbon remains in the off position.

SY Technology, Inc. has fabricated a test 8 x 8 array of these devices, and is in the process of testing the array[4].

---

[4]Clark R.L, Karpinsky J., Borek G., and Johnson E., "High Speed Interferometric Device for Real-Time Correction of Aero-Optic Effects", AIAA paper 95-1984, June 1995, AIAA 26th Plasmadynamics and Lasers Conf., San Diego, CA.

Site Characterizations and Novel Concepts

ThC 2:00 pm-3:00 pm
Auditorium

Don Walters, *Presider*
U.S. Naval Postgraduate School

Site Atmospheric Characterization

Marc Sarazin

The past decade has seen the development of new devices to reliably monitor atmospheric seeing and several observatories are now routinely proposing to the observers new services including online visualization of the site seeing as in addition to standard meteorological parameters.

As adaptive optics techniques come out of the prototype phase and turn into integrated systems, designers are urging for independent routine monitoring of additional atmospheric parameters characterizing the spatiotemporal behavior of the optical turbulence above large ground-based telescopes. The ambitious goal is to obtain in real-time the velocity, direction and altitude of the fluctuations of the index of refraction and their spatial coherence as well.

The aim of this paper is to review the quantities involved and to describe some of the experimental setups currently available to the community. For that purpose, the classical Taylor hypothesis of a 'frozen atmosphere' moving at the average velocity of the flow is restricted to individual layers inside which the spatial fluctuations of the potential temperature follow the inertial law of the Kolmogorov turbulence spectrum. The thickness of such a layer is characterized by its outer scale of turbulence L_0 inside which the strength of the turbulence is given by a single structure coefficient. It is important to note that, in a stably stratified nocturnal atmosphere, the spatial scale of thermal turbulence can be much smaller than the scale of the largest dynamic vortices.

Each thermally turbulent layer, characterized by its altitude, velocity, direction, outer scale and index of refraction structure coefficient, will affect the wavefront, creating phase and amplitude corrugations. The former to be later corrected by the adaptive optical element of the telescope or instrument.

For Classical imaging, the effects of successive turbulent layers are purely additive in terms of index of refraction structure coefficient and give birth to the well known *seeing*, characterized at the telescope by the Fried parameter r_0 of the wavefront in the entrance pupil plane or the FWHM (Full Width at Half Maximum of a stellar image) in the focal plane.

The altitude of a given layer changes its apparent angular scale, as viewed from the telescope, and thus determines its contribution to the *isoplanatic angle,*

defined as the maximum angular separation of two stellar objects producing identical wavefronts at the telescope entrance pupil. The isoplanatic angle is a major restriction to the selection of bright reference stars in the surrounding of a faint object observed with adaptive optics. The higher the turbulence occurs above the telescope, the smaller is the available portion of sky. A selection of a reference star outside the isoplanatic field decreases the correction efficiency by adding noise in the higher orders.

An Adaptive Optics system is mainly sensitive to the speed at which the phase of the wavefront moves over the pupil. The fact that not all layers move in the same direction creates a distinction between the boiling part of the short exposure wavefront corrugations and the frozen part. In other words, one defines for the set of turbulent layers a dispersion velocity and a mean characteristic velocity , the latter associated to a mean direction of motion determines the *optimum response time* of the correction system.

Finally, the *outer scale of the wavefront,* a combination of the geophysical outer scales of the set of layers will determine in particular the shape of the tilt power density spectrum after averaging by the pupil of the telescope, and decide whether tilt correction is necessary on large telescope systems.

Those tuning parameters vary in time by a large magnitude because the vertical distribution of thermal turbulence is rarely immutable: a thin turbulent layer of a large horizontal extent is forced to move vertically following changes in the pressure field and may as well vanish after a few hours as split apart into several smaller ones reaching different altitudes. It is easy to understand that the higher number of layers involved, the smaller the temporal stability of the tuning parameters. It may be possible to conceive Adaptive Optics Systems which would periodically (eg.: ca. 5 min) optimize their operating parameters. If this is the case, it is necessary to design reliable instruments, attached to the observatory rather than to individual telescopes, capable of accurately depicting the current observing environment.

Two Decades of Atmospheric Site Characterization

D. L. Walters

US Naval Postgraduate School

Monterey, California 93943

Tele: 408-656-2267: Fax 408-656-2834: Email walters@physics.nps.navy.mil

Since the mid 1970's, a number of US Department of Defense programs have needed atmospheric-optical site characterization data that included the following: atmospheric-optical coherence length r_o, isoplanatic angle θ_o, thermal probe C_T^2 and acoustic echo-sounder data. In order to make these measurements, a suite of instruments were developed and have evolved to become reference standards. A partial listing of sites where data has been collected includes:

Site:	Date	Measurements
White Sands Missile Range, NM	1977+ 1983+	r_o, tower C_T^2, acoustic sounder θ_o
China, Lake Ca	1978-79	r_o, tower C_T^2, acoustic sounder
Capistrano, Ca	1981-83	r_o, tower C_T^2, acoustic sounder
Haliakala, Hi	1985-92	r_0, θ_o balloon C_T^2,
Starfire Optical Range , NM	1985+	r_o, θ_o
Mt Wilson, Ca	1986-90	r_0, θ_o
Anderson Peak, Ca	1986-90	r_o, θ_o, acoustic sounder
Mt. Hamilton (Lick), Ca	1986-87	r_o, θ_o
McDonald, Observatory, Tx	1985-86	r_o, θ_o

Rock Springs, Pa	1986	r_o, θ_o, balloon C_T^2
Kihei, Hi	1988-90	r_o, θ_o, balloon C_T^2
Melborne, Fl	1989-90	r_o, θ_o
Vieques, Pr	1989	r_o, θ_o
Mt. Laguna, Ca	1990	r_o, θ_o
Anderson Mesa (Flagstaff, Az)	1990-92	r_o, θ_o

In many cases, the same equipment and personnel were involved in each of these site evaluations. Consequently, it has been possible to compare common features and characteristics in the data in an attempt to understanding the underlying atmospheric dynamics producing the turbulence . The influence of the polar jet stream and cold fronts on the coherence length, and the isoplanatic angle are clearly evident as well as the effects of elevated surface boundary layer and the local, topographic, surface-shear-layer, and in a few cases, the internal dome and telescope turbulence. This presentation will discuss the data collection methods as well as similarities and differences in the site data sets, with an emphasis towards describing predictable phenomena.

Adaptive optics requirements for a ground-to-space laser communications system

Robert K. Tyson

W. J. Schafer Associates
321 Billerica Road
Chelmsford, Masachusetts 01824-4191
Telephone: (508) 256-2070
Fax: (508) 256-2139

Advances in adaptive optics have made it possible to consider their use to enhance ground-to-space laser communications systems. Adaptive optics are used to counteract the effects of atmospheric turbulence and deliver a beam undistorted through the atmosphere. This paper examines the system level requirements of an adaptive optical system in terms of communication parameters. An optical communications link must deliver a modulated beam to a receiving sensor with minimal distortion of the modulated signal. Distortion which stretches pulses, distorts pulse shapes, or otherwise randomizes the pulse intensity or location contributes to a higher bit error rate. The ability of adaptive optics to compensate for atmospheric scintillation is studied with respect to its effect on signal fade and surge.

Atmospheric turbulence phase distortions result in intensity variations (scintillation) which corrupt communication signal information. The fade (reduction below the mean signal strength) and surge (enhancement of the signal above the mean) is related to the log-amplitude variance of the scintillated beam. Temporal statistics are an important consideration as well, since the frequency of fades and surges correlates to the modulation bandwidth of the communication system. The variance of the intensity is related to the log-amplitude variance

$$\sigma^2_{Int} = \exp\left[4\sigma^2_\chi\right] - 1 \quad .$$

The fade of a signal (in dB) is defined as 10 times the logarithm of the ratio between the instantaneous intensity and its mean. Surge is similarly defined with a change of sign. The fraction of time that a signal fades (or surges) is a function of the fade (or

surge) level and the log-amplitude variance. Since the intensity is varying with time, the temporal spectral characteristics of the intensity variance are also important. This paper discusses the relationship between the temporal spectrum, the log-amplitude variance, and the frequency of the fades and surges. Scintillation can be passively reduced through aperture averaging or actively reduced with adaptive optics.

For the space-to-ground communications downlink, the beam is distorted in phase as it enters down through the atmosphere. By the time it propagates to the ground, scintillation arises. The entrance aperture of the ground receiver witnesses both phase distortion (much of it from lower altitude turbulence) and intensity distortion (from the phase disturbance located far from the aperture). A finite aperture will average some of the spatial intensity distortion. A phase-only adaptive optics system cannot reverse the scintillation effects, but it can conjugate the phase from the aperture to the detector to remove some or all of the phase variation that would have lengthened individual pulses or information carriers in the modulated beam.

For the ground-to-space communications uplink, without adaptive optics, the beam would get most of its phase error near the transmitter and be significantly scintillated when it reached the space-borne receiver. The spread of the beam during the long propagation from the top of the atmosphere results in the irradiance correlation length at the receiver being much larger than the receiving aperture. Thus, very little aperture averaging takes place. With adaptive optics, however, the beam is pre-corrected for the atmosphere before it leaves the transmitter. Ideally, the phase conjugate of the atmospheric turbulence layers are put on the phase of the beam so that very little scintillation occurs and the beam leaves the top of the atmosphere as a plane wave (or actually a spherical wave focussing at a distant receiver).

The amount of spatial compensation is limited by the number of channels, or subapertures, in the adaptive optics system, and also limited by the finite temporal bandwidth of tilt and adaptive optics control loops. Laser communications systems may use a source on the space platform as the wavefront beacon or a laser guide star. Without anisoplanatism compensation, the communication system will experience losses from point-ahead effects. Calculations indicate that the reduction in intensity variance follow

the form $\sigma^2_{Int,compensated} \propto \dfrac{\sigma^2_{Int,uncompensated}}{N}$ where N is the number of fully-compensated

Zernike modes. This agrees with experimental observation.

The amount of correction is limited by anisoplantic effects and finite bandwidth effects of the adaptive optics system configuration. Many variations of aperture diameters, wavelengths, zenith angles, and site conditions can be traded to examine the effects of adaptive optics improvements in terms of realistic anisoplanatic difficulties and servo bandwidths. Examples are given to guide the systems designer through the process without greatly restricting the range of parameters that can be considered.

Results of system trade studies show the utility of adaptive optics for laser communications. Two scenarios with a laser wavelength of 1.0 μm, ground and space apertures of 0.5 meters, a tilt bandwidth of 200 Hz, and an adaptive optics bandwidth of 100 Hz are studied. A downlink from a satellite at 400 km circular orbit shows that aperture averaging is sufficient for removing the effects of scintillation. Adaptive optics with over 30 channels are required for even a minimal improvement. On the other hand, an uplink study to a geosynchronous (40 Mm) satellite shows that significant improvement (reduction in signal fade by a factor of three) can be obtained with an adaptive optics system with 50 channels or more with the natural point-ahead angle of 23 μrad slightly more than the isoplanatic angle. With the anisoplanatism removed by an artificial beacon, the laser communication system shows improvement with as few as 9 channels and signal fade reduced by a factor of 4 with 30 channels.

Mesospheric Metals for Guide Star Generation

GEORGE C. PAPEN

Department of Electrical and Computer Engineering, University of Illinois
1406 W. Green St., Urbana, Illinois 61801 USA
Ph. (217) 244-4115 Fax (217) 333-4303 e-mail: g-papen@uiuc.edu

Introduction

Elemental Na has been the tracer of choice for the generation of high altitude (mesospheric) guide stars because of its relatively large natural abundance and large absorption cross section. Dye based systems using Na are currently under development for several large aperture telescopes. However, robust solid state laser technology to generate high power narrow linewidth light at 589 nm has progressed slowly. Here we consider both the tracer and the transmitter technology and show that using either the K D_1 line at 769 nm or the 372 nm line of Fe ($a\ ^5D$-$z\ ^5F°$) for the tracer may provide robust solutions until solid state Na transmitter technology can be more fully developed. The comparable performance is primarily due to the fact that both lines can be generated with existing solid state materials (Alexandrite, Ti:Sapphire).

Cross Sections and Natural Abundance

The origin of all mesospheric metals is believed to be meteor ablation. Assuming a linear response, the return signal from these mesospheric metals is proportional to the product of the laser power at the layer, the absorption cross section and the total column abundance.

The Doppler broadened cross sections of the three tracers at 200 K are shown in Figure 1 where the Fe cross section has been magnified 10×. A useful approximation is that the cross sections of Na D_2 line and K D_1 are comparable and that the cross section 372 nm line of Fe is a factor of 10 less. We note that even though Na and K are both group 1a elements and thus have similar spectroscopy, the location of the hyperfine lines for K is such that it closely resembles the single Doppler broadened line of Fe and not the double humped Na D_2 feature. The shape of the cross section is important when saturation is considered and will discussed in the next section.

The abundance for all three tracers has significant latitude and seasonable dependence (1, 2, 3). This dependence is caused by the overall latitude and seasonal dependence of the mesospheric temperature structure and effects the reaction rates of the various sink mechanisms for the tracers (4). Measurements of the mid-latitude column abundances for all three metals are shown in Table 1. We note that there are

significantly fewer measurements for Fe and K relative to Na and very few at low latitude sites (5). Thus, the seasonal dependence of these tracers at low latitudes is not well known and the comparison was done only for mid-latitude values.

Using the product of the linear cross section from Figure 1 and the minimum (worst case) column abundance from Table 1, Na has an overall linear backscatter efficiency ratio roughly 5× better that Fe and 15× better than K. Thus assuming equal cost and complexity in the transmitter per unit power and a linear response, Na is clearly superior. However, in practice the backscatter efficiency is not proportional to the linear cross section due to saturation effects and the cost and complexity per collected photoelectron in a subaperture is vastly different for the three tracers because of the difference in the transmitter technology. We consider these effects in the following sections.
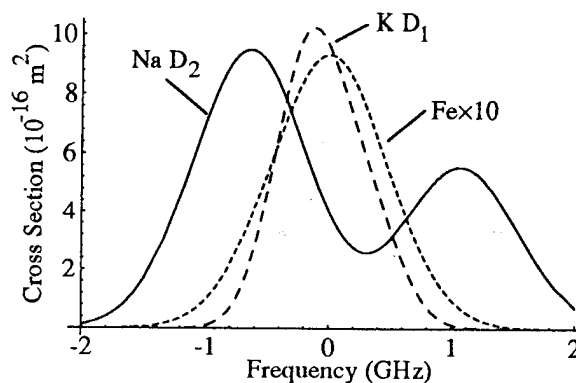

Figure 1. Absorption cross sections of the D_2 line for Na, the D_1 line for K and the 372 nm line for Fe at 200 K. Note that for Fe, the cross section is scaled by a factor of 10.

	Na	**Fe**	**K**
Maximum Abundance	7±1.5	15±2.5	0.4±0.12
Minimum Abundance	2.5±1.5	5±2.5	0.15±0.045

Table 1. The minimum and maximum column abundances (atoms/cm^2) for the three tracers at mid latitudes(3, 6).

Saturation

Saturation occurs when the probability of an individual metal atom being in the excited state increases to the point where stimulated emission in the forward direction (away from the receiver) begins to *decrease* the overall backscattering efficiency. For long pulsed systems where atomic (Rabi) oscillations are negligible, this effect is approximately inversely proportional to the cross section so that metals with higher cross sections will saturate at lower intensities. Several theoretical results indicate that the most efficient excitation of the metal tracer occurs when the laser spectrum is matched to the cross section (7, 8). For K and Fe, this spectral matching is more straightforward that for Na because of the single lobed feature of the cross sections (See Figure 1). To spectrally match the Na D_2 line, modulation techniques must be used with a narrowband (or CW) transmitter.

The effect of saturation is a primary design consideration because the outgoing beam must be expanded and focused to generate a guide star of small angular extent. As an example, to generate a 0.25 *arcsec* spot at 100 *km* requires a 6 *cm* radius beam at the mesospheric metal layer with a total area of roughly 100 cm^2. For a 10 *mJ* 100 *ns* pulse, the peak intensities at the layer can exceed 100 kW/m^2. If the pulse is spectrally matched to the absorption cross section, this power is distributed over the entire velocity distribution minimizing the effect of an individual velocity component saturating (9).

To accurately model saturation for a spatially and temporally spot over the Doppler broadened velocity distribution requires solving a complete set of rate equations (10). Figure 2 shows a sample saturation calculation for Na as a function of the outgoing beam divergence. In the limit of CW excitation, it is inversely proportional to the cross section. Thus for any given system, Na and K will have similar saturation characteristics while saturation of the Fe transition will not occur until the pulse energies are roughly an order of magnitude higher. For comparison purposes, without reference to a specific system, we will use a saturation figure of 50% for both Na and K implying that the backscatter efficiency is half what it would be without saturation relative to a system using Fe.

Transmitter Technology

We will assume that whatever technology is chosen to generate light at 769 *nm* (Alexandrite Ti:Sapphire etc.) can also generate light at 372 *nm* using frequency doubling techniques with 50% conversion efficiency and minimal added complexity. Both these lines are roughly Gaussian with RMS widths of ~350 MHz at 200 *K*. Generating pulses with

that spectral linewidth at either 769 *nm* or 372 *nm* is well within commercial systems. Thus we have a relative comparison transmitter technology of Fe with respect to K and the same system could be used for either tracer. Relating these systems to Na transmitter technology is somewhat more difficult. For a back of the envelope comparison, we will use a factor of 5 to account for the difference in the cost and complexity of a Na system at 589 *nm* relative to a K system at 769 *nm*. This implies for the same cost and complexity, one can obtain 5 times more power at 769 *nm* than at 589 *nm*. This factor accounts for the fact that both K and Fe can be generated using solid state technology.
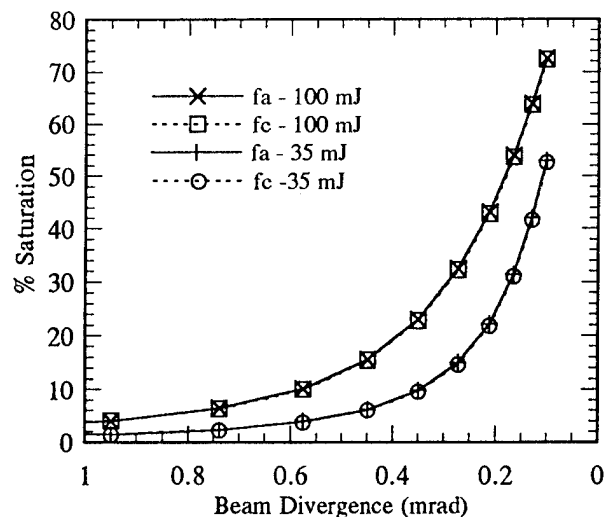

Figure 2. Plot of the saturation (% deviation from a linear response) of Na D_2 line as a function of divergence (RMS of the intensity) at the peak of the D_{2a} line (f_a) and a point halfway between the D_{2a} and D_{2b} peaks (f_c). The pulse width is 7 *ns* (RMS) and is assumed to be transform limited.

System Comparison

Using the estimates of the previous sections, Table 2 provides an order of magnitude comparison of the three tracers for guide star generation. The system efficiency factors (1.2 for K 0.5 for Fe) account for the quantum efficiency of a Si CCD array and for the fact that the atmosphere and the optics are not as transmisive at 372 *nm* as they are at 589 or 769 *nm*. due to increased Rayleigh scattering and loss. All the quantities are relative and scaled to Na. The table indicates that the three tracers are roughly comparable under the assumptions that Na and K are derated by 50% due to saturation and that 5x more power can be

generated at 769 *nm* relative to 589 *nm* for the same cost and complexity. However, we caution that until a system and transmitter technology is specified, these are very rough estimates and the results are only illustrative of the fact that the Na may not be the tracer of choice for all systems and locations.

	Na	K	Fe
Relative Power	1	5	2.5
Relative Cross Section	1	1	0.1
Relative Abundance	1	0.067	2
Saturation Factor	1	1	2
System Efficiency	1	1.20	0.5
Overall Efficiency	**1**	**0.4**	**0.5**

Table 2. Estimates of factors effecting overall guide star performance scaled to Na guide star generation.

Conclusion

In the long term, if transmitter technology comparable to near-IR solid state systems can be developed for Na, then it will still be the tracer of choice for guide star generation. However, in the interim, the combination of the tracer and the transmitter technology may make K and Fe viable candidates for tracers. Given the long lead time to develop mesospheric guide star systems, the overall cost involved, and the latitude and seasonal dependence of the tracers, we believe a prudent course of action would be to conduct a set of year long measurements at each potential site using modest power lidars. The factors considered in this paper can then be readily quantified and an informed decision on the optimal tracer can be determined with confidence.

References

1. C. S. Gardner, D. G. Voelz, *J. Geophys. Res.* **92**, 4673-4694 (1987).
2. B. R. Clemesha, D. M. Simonich, P. P. Batista, *Geophys. Res. Lett.* **19**, 457-460 (1992).
3. T. J. Kane, C. S. Gardner, *J. Geophys. Res.* **98**, 16,875-16886 (1993).
4. J. M. C. Plane, *Int. Rev. Phys. Chem.* **10**, 55-106 (1991).
5. M. Alpers, J. Hoffner, U. von Zahn, *J. Geophys. Res.* **99**, 14,971-14,985 (1994).
6. G. Megie, F. Bos, J. E. Blamont, M. L. Chanin, *Planet. Space Sci.* **26**, 27-35 (1978).
7. P. W. Milonni, L. E. Throde, *Appl. Opt.* **31**, 785-799 (1992).
8. J. R. Morris, *JOSA A* **11**, 832-845 (1994).
9. C. S. Gardner, B. M. Welsh, L. A. Thompson, *Proc. IEEE* **78**, 1721-1743 (1990).
10. G. C. Papen, W. M. Pfenninger, D. M. Simonich, *Appl. Opt.* **34**, 480-498 (1995).

Adaptive Optics
Experimental Results

FA 8:30 am-10:15 am
Auditorium

Marc Séchaud, *Presider*
Office National d'Etudes et de Recherches Aérospatiales, France

Laser and Natural Guide Star Measured Turbulent Wavefront Correlation

Ruy Deron, Sylvain Laurent, Marc Séchaud and Gérard Rousset

Office National d'Etudes et de Recherches Aérospatiales (ONERA)
High Resolution Optical Imaging Division
29 Avenue de la Division Leclerc, BP 72, F 92322 Châtillon cedex, France
Phone: 33 1 46 73 47 81, Fax: 33 1 46 73 41 48

The laser guide star concept was proposed for the application of adaptive optics in astronomy in order to overcome the problem of natural star requisite brightness which significantly limits the sky coverage [1, 2]. Recently, the adaptive optics compensation of turbulent wavefront using laser guide star has been demonstrated [3, 4].

A Rayleigh-Mie scattering laser guide star experiment called ATLAS (Analyse des Turbulences par LASer) has been developed, implemented [5, 6] and operated by ONERA on the 1.5m telescope of the Lunar Laser Ranging Station at CERGA Observatory. The experiment is set-up at the Nasmyth focus. The main components are two intercalibrated Hartmann-Shack wavefront sensors equipped with gated intensified CCD. The wavefront sensors have a square array of 16x16 subapertures of 10cm diameter. A time delay unit allows the selection of the backscattering layer altitude and depth. The two wavefront sensor CCD signals are simultaneously digitized. The tilt between the two wavefronts and the mean curvature of the laser wavefront are displayed in quasi real-time and controlled. Modal wavefront reconstruction is used. Wavefront expansion is made on the set of Zernike polynomials.

A 900mJ/10Hz Nd:YAG laser is propagated through the coudé path. The transmitted and received beams are optically separated. The telescope is used both as transmitter, but only on a 25cm diameter area of the primary mirror, and as receiver over the remainder of the 1.5m aperture.

Prior to the field tests, the wavefront sensors have been tested and intercalibrated in laboratory using a turbulence simulation cell. The wavefront intercorrelations between the two sensors are very good (better than 95%) after noise bias correction.

The primary results of the experiment are the simultaneous measurements of laser guide star and nearby natural star wavefronts and their correlation. Subsidiary results are the determinations of the isoplanatic angle and the turbulence strength of the high altitude layers.

Wavefront measurements have been done from a laser guide star located between 8 and 17km. For a low altitude guide star, the correlation is degraded by cone effect, whereas for high altitude the detection noise limits the measurement accuracy. The results are analysed using

numerical simulation of the modal angular and focal decorrelations. The following figure shows an example of the measured degree of correlation between the natural and laser guide star wavefronts. The correlation is given versus the radial degree of the Zernike polynomials. The correlation coefficient is averaged over the polynomials of a same radial degree, up to the degree 10 (65 Zernike polynomials). In this example, the laser is focused at an altitude of 15 km and the depth of the backscattering layer is 1.5 km. The measured value of r_0 is 5 cm. The mean position of the laser guide star is in the direction of the natural star and the fluctuation of this position due to turbulence is found to be ± 2 arcsec peak to peak. The relatively low decorrelation in function of the radial degree can be interpreted by an important turbulence at the telescope level and near the ground (site altitude 1100m). Other results will be presented with different seeing conditions.
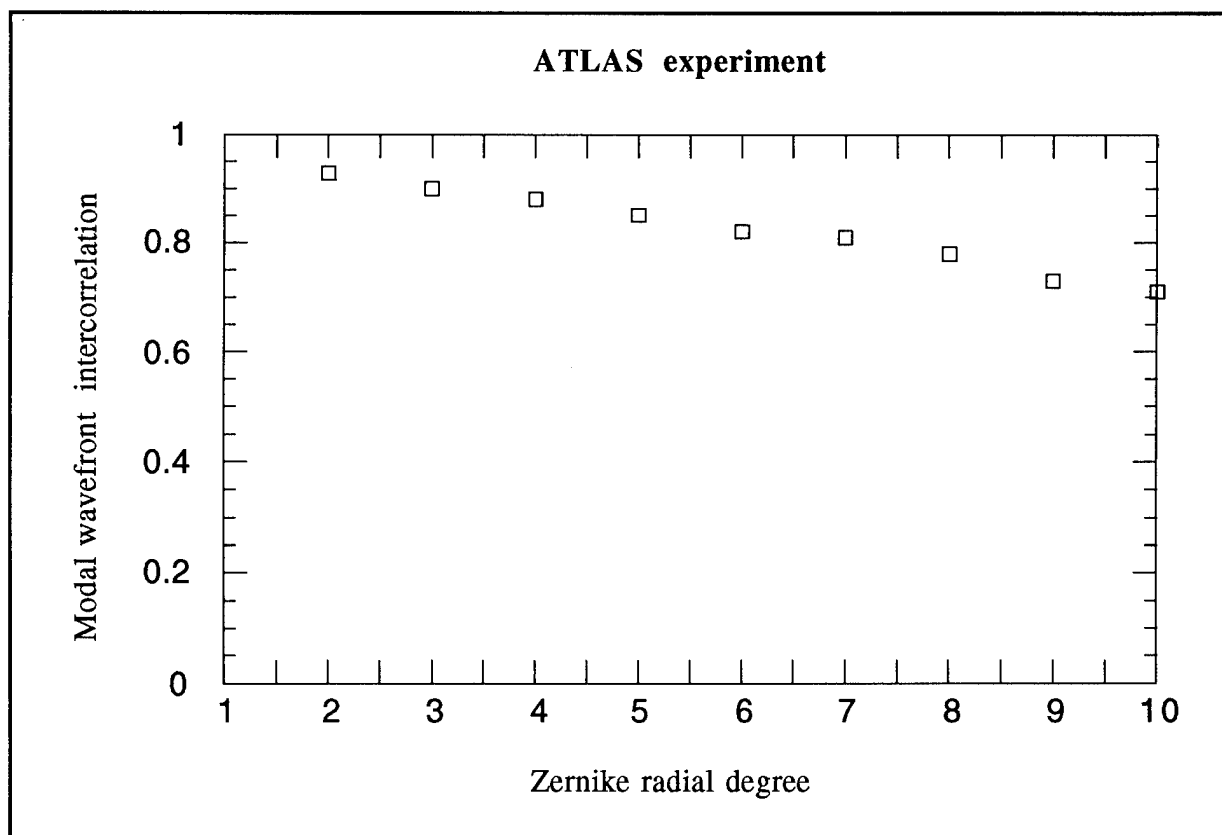
References:

[1] S.L. McCall and A. Passner, in Adaptive Optics and Short Wavelength Sources (S.F. Jacobs, M. Sargent and M.O. Scully Eds.), Physics of Quantum Electronics 6, 149 (Addison-Wesley 1978)

[2] R. Foy and A. Labeyrie, Astron. Astrophys. 152, L29-L31 (1985)

[3] R.Q. Fugate, D.L. Fried, G.A. Ameer et al., Nature 353, 144 (1991)

[4] C.A. Primmerman, D.V. Murphy, D.A. Page et al., Nature 353, 141 (1991)

[5] M. Séchaud, N. Hubin, L. Brixon et al., ESO Proceedings No. 30, 705 (1988)

[6] R. Foy, M. Tallon, M. Séchaud and N. Hubin, Proc. SPIE 1114, 174 (1989)

Short-Exposure Measurements of Anisoplanatism using Binary Stars

Brent L. Ellerbroek, Julian C. Christou, James F. Riker, and J. Timothy Roark

U.S. Air Force Phillips Laboratory
3550 Aberdeen Blvd. SE, Kirtland Air Force Base, NM 87117

The compensated field-of-view of a ground-based adaptive-optics system is limited because the phase distortions introduced by atmospheric turbulence vary with the direction of the source. This effect is referred to as anisoplanatism. More specifically, *tilt anisoplanatism* denotes the differential image motion of two separated point sources observed through a common aperture, while *higher-order anisoplanatism* refers to variations between the shapes of the two point spread functions. Previous long-exposure observations of a multiple star system [1] have measured the combined effect of these two degradations upon the imaging performance of an adaptive-optics system, but the individual values of these two separate error sources have never been independantly determined. Such measurements would provide a sharper test for theoretical models of anisoplanatic effects, and enable sky coverage calculations for laser guide star adaptive-optics systems to be based upon measured data.

In this paper we describe recent short-exposure measurements of tilt- and higher-order anisoplanatic effects for natural and laser guide star adaptive optics. These results were derived from I band observations of the binary star Mizar (HR 5054/5055) recorded from March to May 1995 using the 1.5-meter telescope at the U.S. Air Force Phillips Laboratory Starfire Optical Range [2]. The focal plane used for these measurements was a high speed, 64 by 64 pixel MIT/Lincoln Laboratory CCD array with high quantum efficiency and relatively low readout noise. With visual magnitudes of 2.2 and 3.9, both components of Mizar were sufficiently bright to enable short exposure imaging with Nyquist-rate sampling, with a signal-to-noise ratio high enough to accurately determine the shape and position of each point spread function. Analysis of this data is in progress at the time of this writing. Preliminary results are illustrated in Fig.'s 1 through 3 and discussed further below.

Fig. 1 is a individual 0.010 second exposure of Mizar A and B obtained using Mizar B as the reference for natural guide star adaptive optics. Please note that the separation between the two stars is not to scale. Fig. 2 illustrates shift-and-add (SAA) average images computed from 256 0.010 second exposures. The SAA image of Mizar A (center) has a somewhat stronger halo than the image of Mizar B (left), but the full-wide, half-maximum (FWHM) of the two images is nearly equal. The stronger halo is due to higher-order anisoplanatism, because Mizar A is offset from the direction of the guide star used for adaptive optics. The final image is a second SAA image of Mizar A computed using Mizar B to determine the tilt adjustments to be applied to each short exposure. The increased FWHM of this image is due to tilt anisoplanatism. Fig. 3 plots the tilt anisoplanatism values computed for each of the 256 0.010 second exposures. The RMS magnitude and orientation of the tilt anisoplanatism between the two stars is in good agreement with theoretical predictions for this first sample data set, but the effect of higher-order anisoplanatism upon the Mizar A
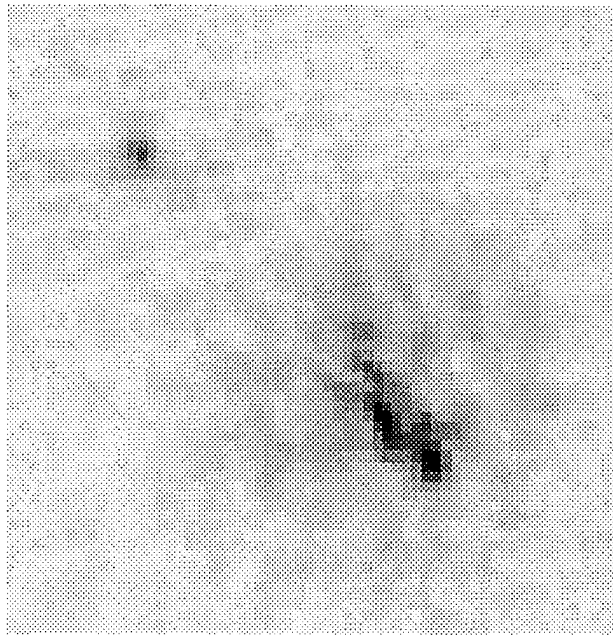
Figure 1: Short exposure image of the binary star Mizar obtained using adaptive optics with Mizar B as the guide star

image in the center of Fig. 2 is significantly less than expected.

REFERENCES

1. J.C. Christou, B.L. Ellerbroek, R.Q. Fugate, D. Bonaccini, and R. Stanga, "Rayleigh Beacon Adaptive Optics Imaging of ADS 9731: Measurements of the Isoplanatic Field of View," to appear in Astrophys. J., Sept. 1995.

2. R.Q. Fugate, B.L. Ellerbroek, C.H. Higgins, M.P. Jelonek, W.J. Lange, A.C. Slavin, W.J. Wild, D.M. Winker, J.M. Wynia, J.M. Spinhirne, B.R. Boeke, R.E. Ruane, J.F. Moroney, M.D. Oliker, D.W. Swindle, and R.A Cleis, "Two generations of laser-guide-star adaptive-optics experiments at the Starfire Optical Range," J. Opt. Soc. Am. A **11**,310-324 (1994).
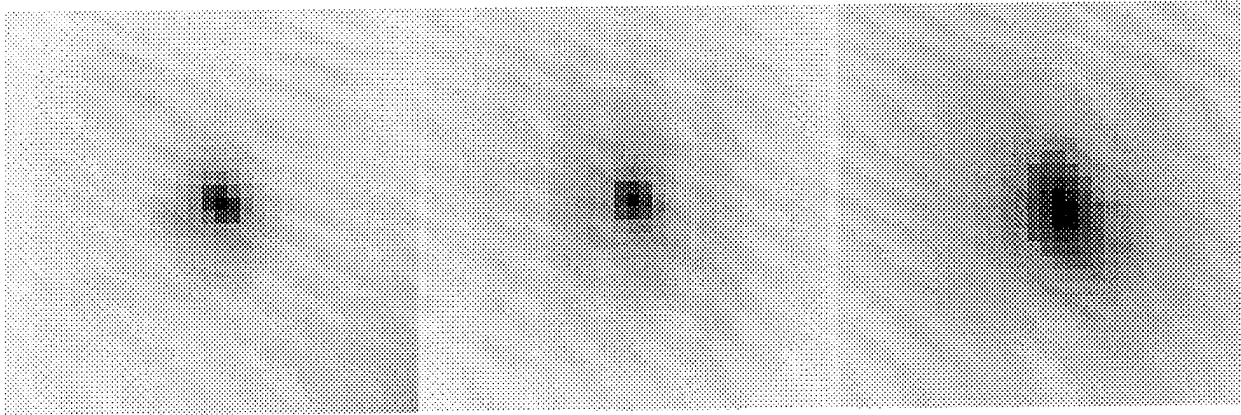
Figure 2: Shift-and-add (SAA) averages of 256 short exposure images of Mizar A and B

Left: Mizar B, the adaptive optics guide star. Center: Mizar A. Right: Mizar A, with Mizar B used to determine the tilt adjustment applied to each short exposure.
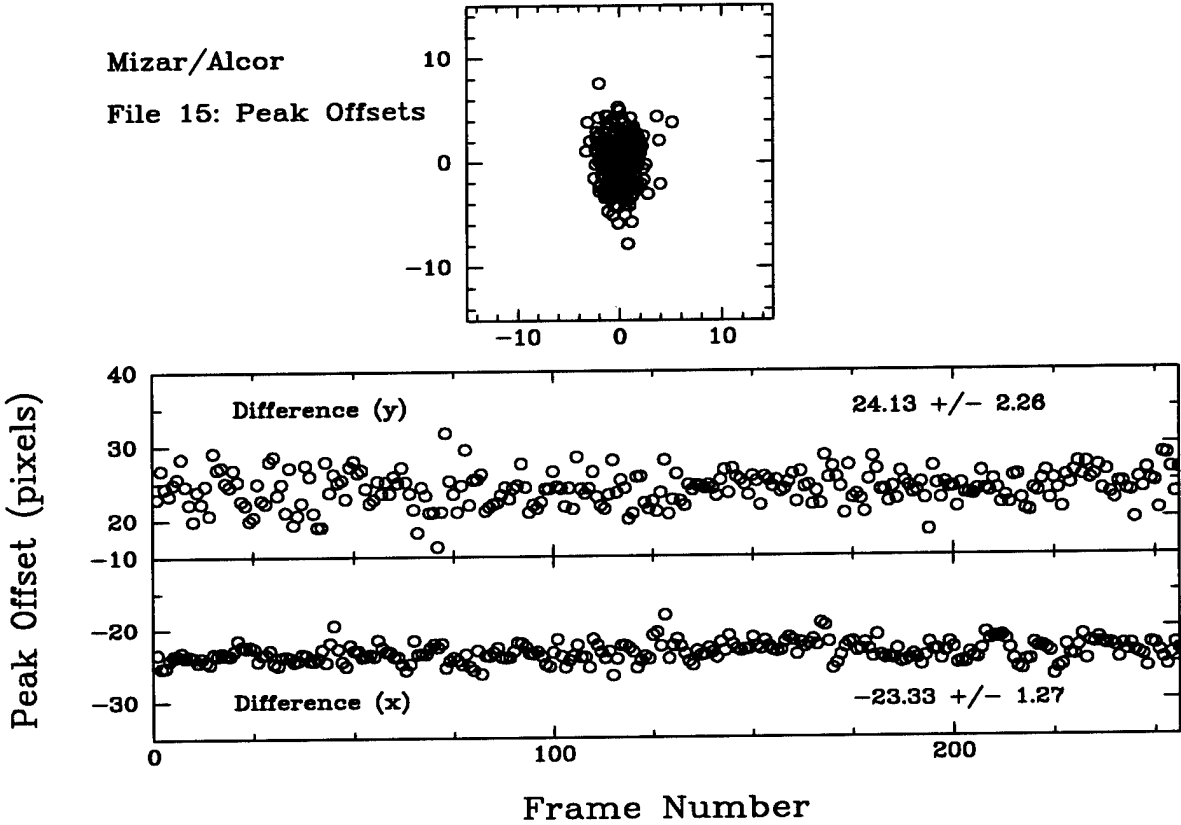
Figure 3: Tilt anisoplanatism values for 256 short exposure images of Mizar

Top: scatter plot of the frame-to-frame variations in the measured separation vector between Mizar A and B due to tilt anisoplanatism. Bottom: Time history of the variations.

Analysis and Calibration of Natural Guide Star Adaptive Optics Data

Eric Tessier

Royal Greenwich Observatory, Madingley Road,
Cambridge, U.K. CB3 0EZ
E-mail: tessier@mail.ast.cam.ac.uk, fax: 44 223 374700, tel: 44 223 374742

1. ON-AXIS POINT SPREAD FUNCTION SHAPE

Full Width Half Maximum and Strehl ratio Diagram

The point spread function (PSF) calibrator data from the Come-On Plus instrument (COP, see Beuzit et al. 1994) were obtained on the 1st January 1994 at 8:54, 8:59 and 9:03 UT respectively for the KHJ bands as continous series of one-second exposure frames respectively 120 in the K band and 60 in the H band and of three 20-second exposure frame in the J band. Left part of Fig. 1 shows the distribution of the full width half maximum (FWHM) versus Strehl ratio (SR) for each individual exposures of the calibrator in JHK. The FWHM is rescaled by a factor λ/D (which corresponds to the diffraction limit at the wavelength λ for a telescope of diameter D), points clearly gather along a single curve. This curve could be interpreted as the Adaptive Optics (AO) response to differents seeing conditions since r_0 and t_0 vary with the wavelength as $\lambda^{\frac{6}{5}}$ and have changed during the observations. Indeed, long exposure (approximately 1 minute) from a set of data obtained during different nights of observation and so in different turbulence conditions have been overplotted. Again points fit pretty well the same curve. However, at the same FWHM, the SR seems to be a bit higher for shorter wavelength. This may be explained as follows: the decrease in the SR value comes from the widening of the PSF core and the power in the residual seeing halo; at shorter wavelength, the contribution of the seeing halo compare to the widening would be relatively higher due to a shorter t_0 at equivalent D/r_0. Anyway, this curve is the PSF response of the Come-On Plus experiment. Other AO systems may give different responses (especially, some curvature sensor system may produce a sharp PSF even for low Strehl ratios). However, five 500ms CCD frames of PSF calibrator from the Starfire Optical range (SOR, see Fugate et al. 1994) Gen II instrument which were obtained on 15 December 1994 from 5:34 UT to 5:36 UT in the I band are overplotted on Fig. 1 and roughly fit the curve.

As shown by this curve, the Strehl ratio describes very well the PSF with a SR above 10% but poorly for lower values. In the latter case, the FWHM will provide additional information on the PSF. Anyway, these plots could be used to define the best strategy during AO observation. As a rule, the turbulence effects get worst as one goes to shorter wavelengths; consequently, the correction and the SR are poorer. However, in some cases, by going to shorter wavelengths one can get higher resolution in spite of a lower SR; this is because the FWHM becomes sharper thanks to the narrower diffraction core (following a λ/D law). For example, in terms of FWHM, the best individual images are in the H-band rather than in the K-band (see Fig. 1).

2. POINT SPREAD FUNCTION TEMPORAL STABILITY

Strehl ratio

SR is an excellent tracer of the PSF stability in time. As seen on the right plot of Fig. 1, the SR is highly variable in time. These variations could be induced by either seeing variations or by the wavefront sensor noise plus the uncorrected high Zernike orders at constant seeing. The answer is probably both, but seeing variations is certainly predominant. Some breaks or slopes superimposed to the short time scale variations are likely related to the seeing which is known to vary in a comparable way. We shall see in the next section how that affects the calibration and the deconvolution process.

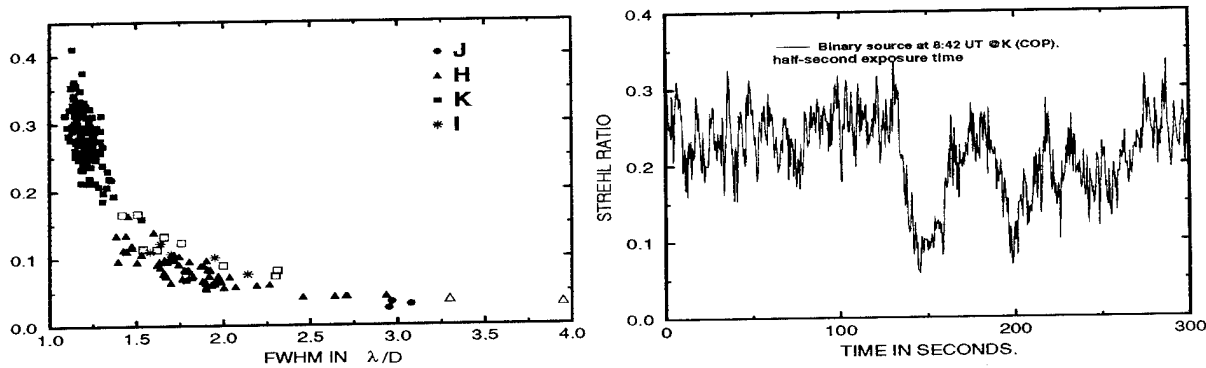Few conclusions can be derived first.

Figure 1: Left. Position of the PSF in a SR-FWHM diagram. PSFs are one-second exposure and 20 seconds image obtained within 10 minutes time with the Adaptive Optics system COP in HK and J respectively and 500 ms exposure image taken with the SOR Gen II AO system in the I band within 2 minutes. FWHM is rescaled by λ/D which is respectively 121, 72, 95, 126 milliarcseconds in IJHK respectively. Long exposure (one minute) PSFs obtained with the adaptive optics system COP in HK during various nights are overplotted in open symbols. Right. Strehl ratio in function of time. SR variations from half-second exposure continuous frames. See text.

i) In the partial correction regime, the PSF is very sensitive to the seeing.

ii) When calibrating the PSF, it is necessary to integrate long enough to sample seeing variations.

iii) As in infrared speckle interferometry, seeing variations will likely limit the accuracy of the PSF calibration.

3. RESIDUALS FROM DECONVOLUTION AND PERFORMANCES

The typical COP observation of a close binary (0″13) has been used to present the results in this section (see Tessier et al. 1994). These results are given as an example and do not be interpreted as the ultimate performances of this system since they depend on the seing stability, the quality of the calibration, and the observational procedure during the observations; the two last points can be improved.

Seeing variations as the main source of the deconvolution residuals

We have seen that the PSF is not stable. Sources are bright enough to make the other sources of noise negligible in front of the PSF noise in the deconvolution process of the data. Do we gain by integrating as the square root of the time? If the variations of the PSF were only induced by high Zernike uncorrected terms and the wavefront sensor noise, we expect a such signal to noise behavior. On the contrary, seeing variations make the PSF as a non-stationary process which does not follow this law.

From the cube of continous PSF frames, we have derived a statistic standard deviation of the PSF during the observation. The PSF standard deviation increases as the Strehl ratio drops. We compare the profile of the standard deviation of the PSF (divided by the square root of the number of frames minus one) to the profile of the residuals after deconvolution of the binary with the PSF. Residuals level is above the PSF standard deviation. The PSF mismatch due to different seeing conditions history for the calibrator and the source is responsible for the level of residuals. In J, the calibrator was pointed too much time after the binary source (45 minutes) and deconvolved image reveals a strong residual halo. At K, the calibrator was observed 12 minutes after the source, the residuals are lower but still up to five times larger than the PSF standard deviation. The quality of the calibration directly affects the residuals level. Incidently, the first airy ring is a sensitive area, it may happen to get artifact in the deconvolution process up to 10% of the peak level in the worst case.

Procedure to get a good quality PSF calibration

Observers cannot control the seeing variations but they can adjust the observation procedure so as to minimize its effets. Here are the few rules to follow.

i) Choose a PSF calibrator close to the astronomical target
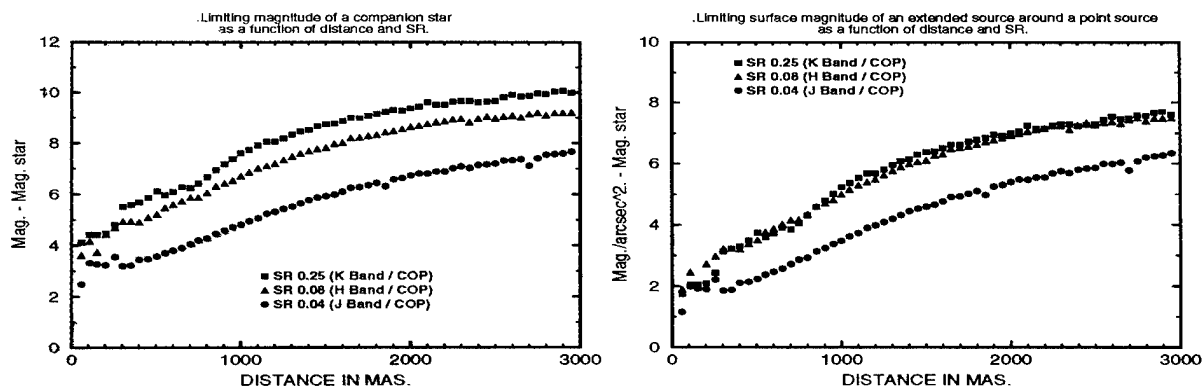
Figure 2: Left. COP sensisitivy curve for the detection of a companion in magnitude difference to the main component as a function of the separation for different Strehl ratios. Same but for the detection of an extended structure around a point source in magnitude per arc-second^2 relative to the central source as a function of the radial distance. A pixel width of 50 mas is assumed. See text.

ii) Match its flux to the astronomical target (use density filters e.g.).
iii) Observe the PSF calibrator longer enough to smooth the short timescale seeing variations (one or two minutes).
iv) Observe the PSF calibrator as shortly as possible before or after the source observations to avoid long-time scale seeing variations or the seeing variation with the elevation.
v) If possible, repeat several times this alternate observation procedure.

Sensitivity curves

Detection of a companion star We use the residuals to compute the typical level of detection for a companion. This curve could be compared to two results from COP. First, the observation of the R 136 cluster has revealed stars in the field as faint as a magnitude difference of 9 relatively to the brightest star in the field (See Brandl et al. Messenger). Secondly, a faint companion in K with a flux ratio of 10^4 at 4″ have been detected around the object HR4796 (See Léna 1994).

Detection of an extended source around a point source We define an extended source as a source much larger than the 50% energy radius of the PSF. Sensitivity curve are shown on Fig. 2 with a pixel of 50 mas. Binning data will gain in sensitivity as the binning factor. The detection of the disk around β Pictoris (A.-M. Lagrange, private communication) at 2″ is consistent with this curve.

4. ACKNOWLEDGMENTS

5. REFERENCES

1. Beuzit J.-L., Hubin N., Gendron E., Demailly L., Gigan P., Lacombe F., Chazallet F., Rabaud D., Rousset G., 1994, Proc. SPIE 2201, p955
2. Brandl B., Sams B. and Eckart A., The messenger, March 1995.
3. Fugate R., Ellerbroek B., Higgind c., Jelonek, Lange W., Slavin A., Wild W., Winker J., Spinhirne J., Boeke B., Ruane R., Moroney J., Oliker D., Swindle D., Cleis R., 1994, JOSA, Vol. 11, 1, p310
4. Léna P., 1994, Proc. SPIE 2201, p1099
5. Tessier E., Bouvier J., Beuzit J.-L. and Brandner W., The messenger. Dec 1994.

Post-detection Correction of Compensated Imagery using Phase-Diverse Speckle

John H. Seldin and Richard G. Paxman

Electro-Optics Laboratory
Environmental Research Institute of Michigan
P.O. Box 134001, Ann Arbor, Michigan 48113-4001
(313) 994-1200 ext. 2361; email: seldin@erim.org

Brent L. Ellerbroek

Starfire Optical Range
U.S. Air Force Phillips Laboratory
Kirtland Air Force Base
New Mexico 87117-5776
(505) 846-4712 ext. 364; email: ellerbrb@plk.af.mil

1. BACKGROUND

Developments in adaptive-optics technology have allowed astronomers using ground-based telescopes to overcome much of the loss of resolution due to aberrations introduced by the intervening atmosphere. Although adaptive-optics systems work quite well, they have their limitations and regimes of operation, and residual aberrations are often a problem. While research into expanding the capabilities of pre-detection correction continues, post-detection restoration of ground-based astronomical data is still desired and often required. Over the years, researchers have developed a variety of clever post-detection techniques for recovering image resolution, including stellar speckle imaging and deconvolution from wave-front sensing. We have been applying a novel data-collection and processing approach to correct for the effects of atmospheric seeing called *phase-diverse speckle imaging.* Phase-diverse speckle imaging has been used recently to restore images of solar granulation [1], and we present here the first application of this technique to nighttime astronomy data.

As its name suggests, phase-diverse speckle imaging [2] is a blend of two powerful concepts: *phase diversity* and *speckle imaging.* The method of phase diversity [3,4], first proposed by Gonsalves in 1979, requires the simultaneous collection of two images. The first is the conventional focal-plane image that is degraded by the atmosphere. A simple beam splitter and a second detector array, translated along the optical axis, affords the collection of the second image, which is further degraded due to a known defocus. An alternative to translating the second detector array to obtain defocus would be to insert a glass plate of known thickness in front of the CCD. This was the method used for these experiments. The goal then is to identify an object that is consistent with both collected images, given the known defocus or "phase diversity".

The second concept is speckle imaging. Over 20 years ago, Labeyrie recognized that a short-exposure astronomical image, or specklegram, for which the exposure time is short relative to the evolution of the atmosphere, contains fine-resolution information. Speckle imaging requires the collection of many (between 10^2 and 10^5) short-exposure images of the same object. A rather involved data-processing sequence is required to reduce all of these
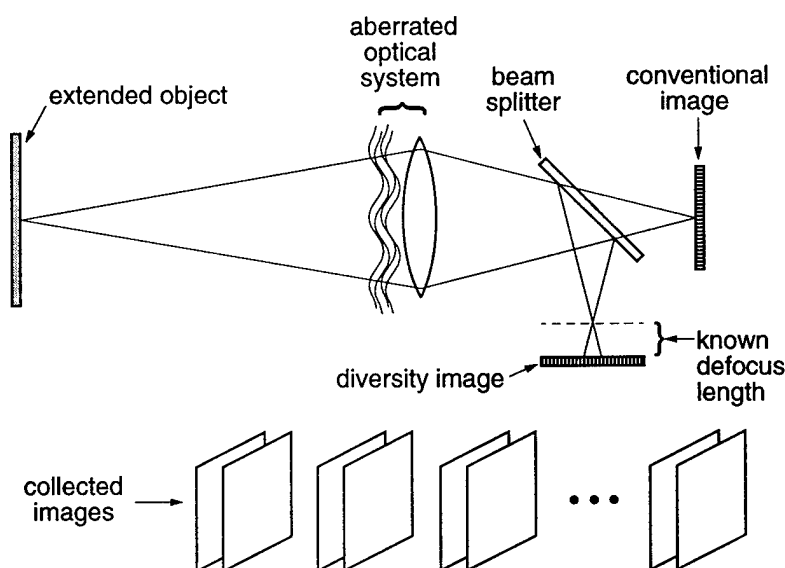
Figure 1: Optical layout for phase-diverse speckle imaging.

images into a single fine-resolution image. The important point is that the collection of many short-exposure images contains more information than a single long-exposure image.

In phase-diverse speckle imaging we collect one conventional specklegram and a second defocused specklegram for each of multiple atmospheric realizations, as shown in Figure 1. This makes for a relatively simple data-collection scheme. Fortunately, the strengths of the two constituent methods persist. We have developed computationally-demanding, but tractable, algorithms that find the maximum-likelihood estimate of the object and the aberrations, given all of the collected images. It is important to note that in the context of post-detection processing of compensated imagery, this algorithm estimates the residual, uncompensated phase errors along with the object being imaged. Thus, phase-diverse speckle imaging has the added benefit of being a wavefront sensor diagnostic tool in addition to an image-restoration technique.

2. DATA COLLECTION

Images of binary stars were collected with the 1.5 m telescope at the U.S. Air Force Phillips Laboratory Starfire Optical Range with the purpose of demonstrating the use of phase-diverse speckle for nighttime astronomical imaging. The image data were collected at a center wavelength of 0.8 μm with a full-width at half-maximum optical bandwidth of about 0.1 μm using a single, 12-bit CCD array built by M.I.T Lincoln Laboratory. The separation of the two stars in each binary was small enough to accommodate the use of a single camera, so *both* the conventional and the diversity channels were imaged onto separate sides of the 64 × 64 array. The light was divided into two channels with a polarizing beamsplitter, and combinations of glass plates of various thicknesses were inserted into the diversity channel to obtain a range of defocus values, from 0.2 to 1.3 waves (peak-to-valley) of quadratic phase error. Because the maximum-likelihood phase-diverse speckle imaging algorithm is based in

large part on a statistical model of the received images, sequences of dark frames and twilight sky flats at various exposures were collected. These calibration data were used to convert the measured images into units of photo-detection events. An additional set of calibration data was collected using a point source to help determine the fixed aberrations in the two imaging channels. These fixed aberrations are accounted for during restorations so that the estimated phase errors are truly estimates of the uncompensated atmospheric aberrations.

Three binary stars spanning a range of visual magnitudes from 2 to 5 were imaged using both natural and artificial guide star compensation. Variations of the adaptive-optics loop bandwidth yielded a range of degrees of compensation. With exposure times varying between 1 and 10 *msec*, the collected data exhibit signal levels ranging from several thousands to hundreds of thousands of total photo-detections. This enables us to explore the performance over a wide range of signal-to-noise ratios. Restoration quality is judged primarily with two criteria: the error in the estimated ratio of the intensities of the two stars and their separation. Also, the full-width at half-maximum of each star is reported and compared to the diffraction-limited ideal. In simulations modelling these collected data we found that high-quality restorations are obtained for a wide range of signal levels, and that even the most closely-spaced binary star with 0.2 *arcsec* separation was resolved. The natural guide star compensation yielded smaller residual phase aberrations to correct, and restorations were in general better in this case than for cases of imaging with artificial guide star compensation. We anticipate similar results when processing the real data.

3. CONCLUSIONS

We present here the first demonstration of phase-diverse speckle imaging both with a compensated imaging system and with nighttime astronomy data. By correctly pre-processing the data to match the statistical model employed by the algorithm and including systematic errors found in the imaging system, we demonstrate that this technique can successfully be used in low signal regimes with many fewer frames than is typically required when restoring uncompensated imagery. Phase-diverse speckle imaging is an attractive modality for imaging through turbulence for several reasons, including (1) the optical hardware is simple, (2) speckle calibration measurements are not required, (3) the method is robust to systematic errors, and (4) the method can be used with partially compensated imagery.

REFERENCES

1. J.H. Seldin and R.G. Paxman, "Phase-diverse speckle reconstruction of solar data," in *Image Reconstruction and Restoration*, T.J. Schulz and D.L. Snyder, eds., Proc. SPIE **2302**, 268-280 (1994).

2. R.G. Paxman, T.J. Schulz, and J.R. Fienup, "Phase-diverse speckle interferometry," in *Topical Meeting on Signal Recovery and Synthesis IV*, Technical Digest Series **11**, (Optical Society of America, Washington DC, 1992), New Orleans, LA, April 1992.

3. R.A. Gonsalves and R. Childlaw, "Wavefront sensing by phase retrieval," in *Applications of Digital Image Processing III*, A.G. Tescher, ed., Proc. SPIE **207**, 32-39 (1979).

4. R.G. Paxman, T.J. Schulz, and J.R. Fienup, "Joint estimation of object and aberrations using phase diversity," J. Opt. Soc. Am. A **9**, 1072-1085 (1992).

Experimental Results of a Low-Order
Adaptive Optics Experiment on the Starfire 3.5m Telescope

John D. Gonglewski
USAF Phillips Laboratory
Albuquerque, New Mexico, USA 87109
Phone: 01-505-846-4405
Fax: 01-505-846-2045

David Dayton, Steven Sandven, Darren Laughlin
Applied Technology Associates
1900 Randolf SE
Albuquerque, New Mexico, USA 87106
Phone: 505-845-6110
Fax: 505-768-1391

Sam Rogers, Scot McDermott
Logicon R & D Associates
2600 Yale SE
Albuquerque, NM 87106
Phone 505-842-8911
Fax 505-242-2249

Stephen Browne
the Optical Sciences Company
P.O. Box 25309
Anaheim, California, USA 92825-5309
Phone: 01-714-772-7668
FAX: 01-714-772-9870

Robert Babnick, Joe Rae, Joe Gallegos
Rockwell Power Systems
P.O. Box 5670
Kirtland AFB, New Mexico   87185
Phone 505-846-4405
Fax 505-846-6621

Ron Highland
Kaman Sciences Corporation
6400 Uptown Blvd
Abluquerque, NM   87112
Phone: 01-505-889-7027
FAX: 01-505-889-7040

An experiment with a nasmyth adaptive optics system mounted on the SOR 3.5m telescope is described. The 183 actuator mirror allows only partial compensation in the near IR, and the imagery is enhanced by postprocessing methods. We describe the system design, and evaluate the performance based on long-to-short exposure SNR ratio metrics.

Near-Infrared Imaging at the Starfire Optical Range

Paul M. Harvey, Chris D. Koresko
University of Texas at Austin

Julian C. Christou, Robert Q. Fugate
USAF Phillips Laboratory

We present preliminary results from one-half night of NSF-supported observing on the 1.5-m SOR telescope via a NICMOS-3 camera at 1.6 μm.

Optimization of Closed-Loop Adaptive Optics Wavefront Reconstruction Algorithms Using Experimentally Measured Performance Data: Experimental Results

Troy A. Rhoadarmer
Starfire Optical Range, PL/LIG
3550 Aberdeen Avenue. SE
Kirtland Air Force Base, NM 87117-5776
phone: (505) 846-4712 ext 339
fax: (505) 846-2213

Brent L. Ellerbroek
Starfire Optical Range, PL/LIG
3550 Aberdeen Avenue. SE
Kirtland Air Force Base, NM 87117-5776
phone: (505) 846-4712 ext 364
fax: (505) 846-2213

Experiments have shown the reward adaptive optics provides in improving the resolution of ground-based astronomical telescopes.[1-2] A critical contributor to adaptive optics system performance is the reconstruction algorithm that converts wavefront sensor (WFS) measurements into the deformable mirror (DM) actuator commands.[3-4] Minimum variance reconstruction algorithms have been developed extensively to optimize the performance of adaptive optics systems given specific atmospheric conditions.[5-7] These algorithms depend on atmospheric parameters which are seldom known exactly and are constantly fluctuating. This is especially true for systems incorporating multiple WFS beacons that require knowledge of the wind speed profile, the vertical distribution of atmospheric turbulence, and the intensity of the wavefront sensing beacons to calculate the optimal reconstructor.[7] This uncertainty and continual changing of atmospheric conditions implies that an optimal degree of turbulence compensation cannot be achieved or maintained over long time intervals with static reconstructor coefficients. A need exists for a method of updating these coefficients in real time based on actual closed-loop performance.

This paper presents a technique using experimentally measured performance data from a closed-loop adaptive optics system that can be used for real time optimization of the reconstruction algorithm. This method is applicable to single-guidestar-single-deformable-mirror adaptive optics systems as well as more complex systems incorporating multiple guidestars and multiple DM's.[8] Figure 1 shows the adaptive-optics control system block diagram for the work presented here. The top half of the diagram describes how the closed-loop WFS slopes s_c are employed to determine the DM actuator commands and the bottom half describes the system performance metric σ^2 used to calculate an adjustment E' to the initial reconstructor E_0. The performance data is supplied by an auxiliary scoring sensor providing the high resolution, low
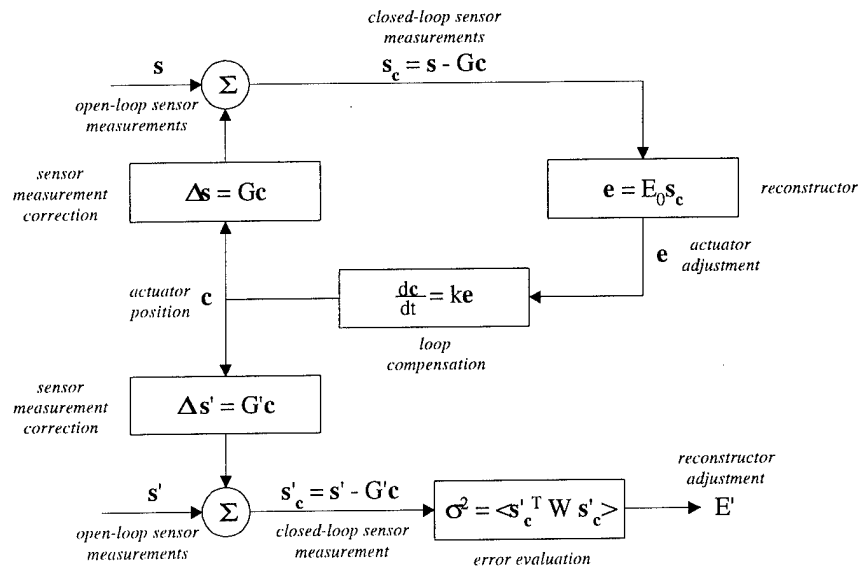
Figure 1. Adaptive optics system control loop diagram.

noise closed-loop slope measurements s_c' and the metric σ^2 is defined as the residual wavefront error for the reconstructed scoring sensor phase profile. Empirical correlations between the scoring sensor data s_c' and the WFS measurements s_c are used to calculate the reconstructor correction factor which minimizes σ^2. This approach is similar to that used to calculate reconstructors from theoretical statistics except that closed-loop slope data is used and the reconstructor adjustment is required to satisfy certain linear constraints in order to maintain system stability.[7] Lagrange multiplier methods are used to minimize σ^2 while maintaining these stability constraints.

For the work presented here the scoring sensor required a bright natural guidestar and the reconstructor is upgraded once. The method could be used to optimize the reconstructor before an extended observation of an actual target field. The much more difficult problem of iterative reconstruction optimization is not addressed directly.

Experimental results obtained with the hybrid adaptive-optics system of the 1.5 m telescope facility at the Starfire Optical Range are presented. The system consisted of a laser guidestar (LGS), a natural guidestar (NGS), a Hartmann WFS for each guidestar, and a single DM. During the experiments the initial reconstructor algorithm used only the LGS slopes and the reconstructor adjustment was used to incorporate the NGS slopes into the algorithm in an effort to reduce focus anisoplanatism.[9-10] The slope vectors s_c and s_c' were simulated from the two WFS's and reduced resolutions for the NGS WFS were simulated to study the improvement in performance gained when dim natural stars are used as beacons. Strehl ratios and average optical transfer functions are calculated for images collected before and after the reconstruction algorithm was adjusted.

REFERENCES

1. R.Q. Fugate, B.L. Ellerbroek, C.H. Higgins, M.P. Jelonek, W.J. Lange, A.C. Slavin, W.J. Wild, D.M. Winkler, J.M. Wynia, J.M. Spinhirne, B.R. Boeke, R.E. Ruane, J.F. Moroney,

M.D. Oliker, and D.W. Swindle, "Two generations of laser-guide-star adaptive optics experiments at the Starfire Optical Range," *JOSA-A*, vol. 11, pp. 310-324, 1994.

2. C.A. Primmerman, D.V. Murphy, D.A. Page, B.G. Zollars, and H.T. Barclay, "Compensation of atmospheric optical distortion using a synthetic beacon," *Nature*, vol. 353, pp. 141-143, 1991.

3. D.L. Fried, "Least-squares fitting a wave-front distortion estimate to an array of phase difference measurements," *JOSA*, vol. 67, pp. 370-375, 1977.

4. R.H. Hudgin, "Wave-front reconstruction for compensated imaging," *JOSA*, vol. 67, pp. 375-378, 1977.

5. E.P. Wallner, "Optimal wave-front compensation using slope measurements," *JOSA*, vol. 73, pp. 1771-1776, 1983.

6. B.M. Welsh and C.S. Gardner, "Performance analysis of adaptive-optics systems using laser-guidestars and slope sensors," *JOSA-A*, vol. 6, pp. 1913-1923, 1989.

7. B.L. Ellerbroek, "First-order performance evaluation of adaptive-optics systems for atmospheric-turbulence compensation in extended-field-of-view astronomical telescopes," *JOSA-A*, vol. 11, pp. 783-805.

8. D.C. Johnston and B.M. Welsh, "Analysis of multiconjugate adaptive optics," *JOSA-A*, vol. 11, pp. 394-408, 1994.

9. B.M. Welsh and C.S. Gardner, "Effects of turbulence induced anisoplanatism on the imaging performance of adaptive-astronomical telescopes using laser guidestars," *JOSA-A*, vol. 8, pp. 69-80, 1991.

10. D.L. Fried, "Anisoplanatism in adaptive optics," *JOSA*, vol. 72, pp. 52-61, 1982.

THE ALTERNATIVE LARGE TELESCOPE CONSTRUCTION

Victor V. Sychev, Valery B. Kaspersky

123424 Russia, Moscow, Volokolamskoye shosse, 112.
State Research Center of Russia
"Scientific and Production Association ASTROPHYSICA"

ABSTRACT

They propose a new conception of the large astronomical telescope with a primary segmented mirror 10 m. Constructively the telescope is supposed to make using an alt-azimuthal scheme as an upper moving part having a sphere-like shape.

1. INTRODUCTION

During last years an intensive development of the optical astronomical devices of new generation is observed in the world, and the main efforts are concentrated on development of the optical telescopes with large diameter up to 10 meters and more, using adaptive optical devices for realization of ultimate quality characteristics.

At present in Russia the works has began on designing 10 meters adaptive segmented telescope "AST-10". Key scientific institutes and observatories of Russian Academy of Sciences and industrial enterprises take part in this project. The key organization is State Research Center of Russia "Scientific and Production Association ASTROPHYSICA" in Moscow [1].

2. GENERAL

From the analysis of the main project such as VLT (four separate 8.2 meter telescopes with interferometry), "Columbus" (two 8.4 meter telescopes on one mounting), "Magellan" (one 8 meter mirror), "Geminy" (two 8 meter mirrors in the North and in the South semispheres), JNLT - "Subaru" (one 8.3 meter mirror) etc. one can make a conclusion that all these projects are oriented to the use of the continuous thin mirrors of approximately 8 meter in diameter.

The development and operation of such mirrors meet with some technological and design difficulties. The necessity to make a continuous mirror more light in weight leads to the inevitable losses in its rigidity, the technology of the optical surface treatment and of its maintenance becomes more complex. Besides, a unique large and expensive equipment is needed - the furnaces to make workpieces (smelting and sintering), the machines for grinding and polishing, vacuum equipment to make optical coatings, the equipment for checking of the optical surface

parameters etc. The further increase of the continuous mirror diameter is practically impossible. That's why we assume this way to have no perspective in the development of the large-scale telescopes.

The other way to create a telescope with high diameter aperture is the employment of the segmented primary mirrors (SPM) and of the sets of telescopes on one mounting (multimirror telescopes).

The tipical examples of the multimirror concept are the projects MMT and "Columbus". The MMT telescope was installed in 1990 and it was substantionally based on the simultaneous use of the six separate low diameter subtelescopes arranged on one mounting with the following bringing all focuses together. It has not revealed to be justified because it couldnot meet the requirements of the high precision automatic co-adjustment of subtelescopes.

Built in 1992 in the USA the telescope "Keck" having the primary mirror of 10 meter in diameter composed of 36 elements 1.8 meter each one, and the German project "ZAS" with segmented primary mirror with 20 meter diameter are the most close to the "AST" concept.

In these projects the most promising way to lighten the weight is applied - the use of the segmented primary mirror consisting of the rigid optical elements (segments) fitted with the automatic system for their positioning and control, that provides the following advantages:

1. Stiffness of a separate element is high that facilitates the realization of the necessary accuracy of its surface processing.

2. The lowering of a mirrir mass in its frame with the lowering of demands to the frame stiffness at the same time.

3. The technology of optics manufacture for SPM is simplified and made cheaper because there are no large dimension elements.

4. The telescope exploitation is simplified and, consequently, its reliability is raised.

5. The convenience of adaptive distortion correction of an image with a help of SPM elements.

6. Step-by-step putting the telescope into operation is possible as the SPM elements are produced.

The AST telescope concept (segmented adaptive telescope) is being developed taking into acount the four main conceptual features [2, 3].

1. System approach to the telescope error budget validation is

employed considering application of adaptive means in the telescope.

2. The original optical scheme is applied with a segmented spherical primary mirror especially meant for the low frequency instrumental errors compensation.

3. The original technical solution of the telescope mounting is applied, one spherical assembly integrating a dome and a telescope functions;

4. The most modern and advanced solutions in the scheme, design and technology of a large-scale telescope (rigid truss structures, multimotor drive without reductors etc.) are applied;

Formation of the telescope error budget assumes consideration of influence of different factors distorting the image [4] and existing level of technology and element base development.

Error budget analysis of large sizes telescopes led to the following interesting results. If to use all achievements of modern optical technology, distribution of responsibility for the image quality of non-adaptive telescope can be shown in the form of a gistogram (Fig. 2a).

Main conclusion is that the image size ($\delta_{\Sigma}=0,68$)" is defined on the whole by atmosphere condition and doesn't depend on the telescope optics much. That is why forces on the telescope improvement from the point of wiew of the image quality will be ineffective.

Distribution of distorting factors influence on the image quality essentially changes for the telescope provided with adaptive means compensating atmosphere influence (Fig. 2b). In this case besides direct improvement of the image quality ($\delta_{\Sigma}=0,39$)" reserve for further decrease of scattering disk appears as it will mainly depend on the telescope optics.

The main task of the adaptive means is that compensation of factors influence distorting the image is provided with coordinated solution of three tasks.

Firstly, it is necessary to minimize quantity and degree of influence of different factors distorting the image, providing simultaneously high quality of initial optical elements of the telescope and its adjustment.

Secondly, it is necessary to provide safety of this state during operation - regime of automatic stabilisation of a given pozition of optical elements during adjustment.

Thirdly, actually task of adaptive correction of wave front

is solved according to results of distortion measurement in real time or program adaptation.

The problem of making large sizes segmented mirror is solved more simple and effectively if it has a spherical form. Developments of the last years showed the possibility of such a decision in centered four-mirror system [5, 6].

Constructively the telescope is supposed to make using an alt-azimuthal scheme as an upper moving part having a sphere-like shape with a hole rotating around horizontal angle of elevation axis, and lower part as an opposite spherical bed rotating togethere with upper part around vertical azimuthal axis. Upper part of telescope is at the same time the "tube" of telescope with optical system components mounted inside of it, "upper mount" allowing to change smoothly the orientation of telescope axis in space, and a "dome" as well, that provides for a protection of optics and telescope apparatus from interaction with environment (Fig. 1).

As required, for example, for protection from wind gust, conception allows modernisation including the use of a light dome on isolated foundation.

The results of preliminary estimates by a finite element analyses of power spherical truss steel frame:

- weight   not more than 140 t;
- maximum deformation   not more than 1.6 mm;
- primary frequency of natural ascillations 8.5 Hz.

SPM element is a rectilinear hexagon with a diameter of inscribed circle 105 cm. According to our evaluations this size is an optimal trade off taking into account the quality of an image and also complexity, reliability and price of AST.

The most possible places for location of astronomical complexes with large telescopes are defined by criterium of an average atmospheric image quality, number of clear night time hours in a year and by an average atmosphere transparency. The of a future large telescope - Hawaii or the Canary Islands in the Northern hemisphere and Chile in the Southern hemisphere. This can be seen from the comparative astroclimate characteristics of the main observatories of the world.

Main specifications of a telescope AST-10.

- primary mirror diameter .... 10 m
- field of view (with corrector) .... 20 arc.min.
- number of controlled SPM elements 84
- diameter of inscribed circle of a one
  hexagonal element .... 1.05 m
- diameter of a secondary mirror .... 2 m

- dimensions .... 23 x 28 m
- weight of a movable part (max) .... 250 t
- image size (rms) .... 0.3...0.5 arcsec

Telescope AST-10 will be the main instrument of a multitelescope astronomical complex having also a number of telescopes with a smaller diameter and designed for solving those tasks of observation cosmology, galaxy physics and star astronomy that reflect a real existing subjects of research with a help of large telescopes (with diameter more than 4 meters), and evidently, those tasks will be the main ones in the area of fundamental researches for the nearest decade.

3. CONCLUSIONS

The telescope AST-10 in comparison with the analogous foreign developed telescopes (Keck Telescope (USA), ZAS (Germany), et.al.) has the following main advantages:

- lower dimensions, weight, compactness, simplicity and technological guality of the construction (production, assembly, alignment are provided by the exsisting level of technology and manufacture), reliability of operation;

- simplisity of telescope development and exploitation because it is not necessary to develop new specialized enterprises and complex technological processes;

- moderate terms of development because of the moderate dimensions of the construction;

- moderate price of the project.

Simaltancously writh it three tasks will be solved.

1. The possibility of project realization of developing a large telescope is opened on an alternative basis.

2. The development of such a telescope of world class will allow to consolidate scientific community of various countries, to wake up creative potential and to step to new boundaries of productional and technological culture.

3. The presence of such a perfect optical instrument will give to researchers the possibility of making fundamental works in a new way and to take a considerable step in the matter of knouring the mystrics of World and Universe.

Interested scientific and industrial organizations and specialists are invited to take part in this project on mutually advantageous conditions. Beside this the interested sides are suggested to discuss the problem of location the telescope AST-10 in the areas with the best astroclimate (Chile, Canary Islands, Hawaii, etc.).

4. REFERENCES

1. Belkin N.D., Kaspersky V.B., Sychev V.V. Large optical astronomical telescope constructing in Russia (Development program). Rep. Int. Symp. "Applied Optics-94," November 15-17 1994, S.-Petersburg.

2. A.A. Boyarchuk, N.V. Steshenko, N.D. Belkin, V.B. Kaspersky, V.V. Sychev. Design project of large astronomical telescope AST-10. SPIE Press, 1994, v.2199, Advanced Technology Optical Telescopes V, p.76-79.

3. Belkin N.D., Kaspersky V.B., Sychev V.V. Large astronomical telescope of Russia. Conceptual design. // Optical Journal, 1994, v 3, p. 5-11.

4. N.V. Steshenko, V.V. Sychev. Optical radiation spatial distribution control. In series "Science and technology results". M., 1990, v.1 - p.107-167.

5. D.T. Puryayev. Afocal two-mirror system. // Optical Engineering, 1993, v.32, N 6, - p.1325-1327.

6. R.N. Wilson, B. Delabre, F. Franza. A new 4-mirror optical concept for very large telescopes with spherical primary and secondary mirrors, giving excellent field and abstruction characteristics. SPIE Press, 1994, v.2199, Advanced Technology Optical Telescopes V, p.1052-1062.

7. Kaspersky V.B., Sychev V.V. Reduced weight mirror and method of its fabrication. RF Patent Nr.1811620. Bulletin of inventions Nr.15, 1993.
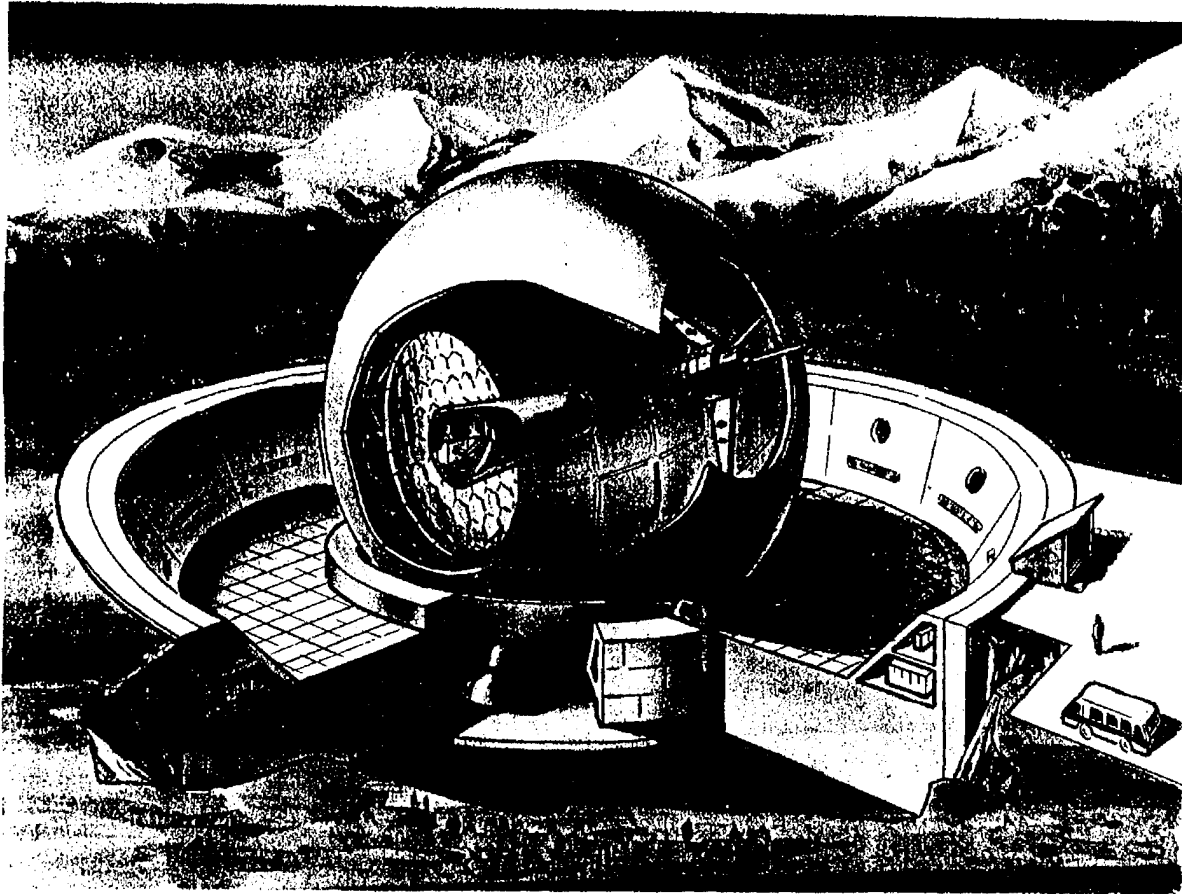
Fig. 1. General view of telescope "AST-10"

(a) non-adaptive telescope

$\tilde{\delta}_{\Sigma} = 0,68''$

65% 27% 8%

Atmosphere Optics Construc-
tion and
drive

(b) adaptive telescope

$\tilde{\delta}_{\Sigma} = 0,39''$

67% 19% 7% 7%

Atmosphere Optics Construc- Adaptive
tion and means
drive
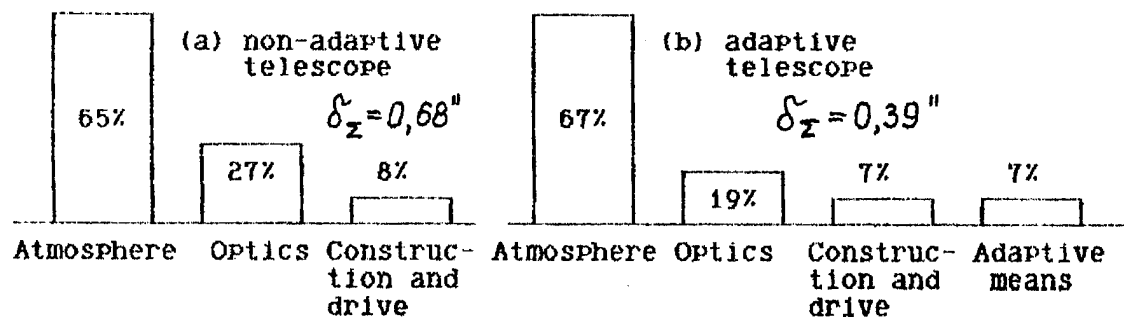
Fig. 2. Distribution of distorting factors influence
on the image quality

Abreu, Rene — TuA2
Africano, J. — WA3
Aguirre, Eduardo — ThA6
Aiello, Roberto — TuA29
Aitken, George J. M. — TuA5
Albetski, J. — WA3
An, Jong — MC4
Anderson, D. S. — ThA4
Andrews, N. — MC2, MC3
Angel, J. R. P. — MB4, TuA4, TuA35, TuA49, WA5, WA6
Ash, D. L. — TuA11
Avicola, Kenneth — MC4
Avizonis, Petras V. — TuA50

Babnick, Robert — FA5
Barnes, T. H. — ThB4
Barrett, Todd K. — MB4, TuA34, TuA35
Berger, Paul J. — TuA2
Beuzit, J. L. — MC1
Biasi, Roberto — TuA29, TuA30, TuA35
Bigelow, B. C. — TuA12
Biliotti, Valdemaro — TuA29
Bingham, Richard G. — TuA43
Bissinger, Horst D. — MC4
Black, J. — WA5
Bohn, Willy L. — ThB
Bold, G. T. — ThB4
Bonaccini, D. — MA4, MC1, TuA8, TuA53
Bonshtedt, B. E. — WC4
Borek, Gregg — ThB6
Bourimborde, Lea V. — ThA6
Brase, James M. — MC4
Browne, Stephen — TuA13, TuA37, FA5
Bruno, Terry — MA3
Bruns, Donald G. — MB4, TuA35, TuA49
Brusa, Guido — TuA29, TuA35, TuA49
Bryant, J. J. — MA5, TuA54
Burns, Mike — TuA40
Buscher, D. F. — MC2, MC3
Butenko, Lev N. — TuA18

Cagigal, M. P. — TuA51
Carreras, Richard A. — TuA47, ThB2
Chazallet, F. — MC1
Chen, Li — TuA21
Cheselka, M. — TuA49
Christou, Julian C. — WA2, FA2, FA6
Clark, Natalie — ThB6
Clark, Rod — ThB6
Close, L. M. — TuA49
Cochetti, F. — TuA15
Conan, Jean-Marc — WB3
Consortini, A. — TuA15
Cook, G. — ThB3
Cova, S. — TuA53
Cram, L. E. — MA5, TuA54
Cullum, Martin — MA
Currie, Douglas G. — TuA50

Dainty, J. C. — TuA9
Dayton, David — TuA37, TuA39, WB1, FA5

Del Vecchio, C. — TuA33
Demailly, L. — MC1
Deron, Ruy — FA1
Dillon, Nick — TuA40
Doel, P. — MC3
Dowling, Daniel M. — TuA50
Drummond, Jack D. — WA2
Dunlop, C. — MC2, MC3

Ealey, Mark A. — TuA2, TuA44
Eisenhauer, F. — MC1
Ellerbroek, Brent L. — TuA2, WB4, ThA2, FA2, FA4, FA7
Engvold, OddBjorn — ThA3
Erbert, Gaylen V. — TuA28
Esposito, S. — TuA32
Etsin, I. Sh. — WC4

Fedina, L. G. — WC4
Fekete, P. W. — MA5, TuA54
Fender, Janet S. — TuA2
Fini, L. — TuA32
Firsov, N. T. — WC4
Fortes, Boris V. — TuA23, TuA24
Franchini, M. — WA3
Fridman, Peter A. — TuA18
Fried, David L. — WB5
Friedman, Herbert W. — MC4, TuA28
Fugate, Robert Q. — TuA1, TuA48, TuA50, WA5, FA6

Gallegos, Joe — FA5
Gallieni, Daniele — TuA8, TuA29, TuA30, TuA35
Gallieni, W. — TuA33
Garavaglia, Mario — ThA6
Gavel, Donald T. — MC4, TuA28
Ge, J. — WA5
Gendron, E. — MC1
Gheser, R. — TuA53
Ghioni, M. — TuA53
Giampieretti, R. — TuA8
Gigan, P. — MC1
Gilmore, Gerry — MA2
Gleckler, Anthony D. — MB1
Gonglewski, John D. — TuA13, TuA37, TuA39, WB1, FA5
Gourlay, J. — ThB1
Graves, J. E. — WA4
Gray, P. M. — MB4, TuA33, TuA49
Groesbeck, T. D. — TuA49
Gureyev, T. E. — TuA19

Haniff, C. A. — MC2
Harvey, Paul M. — FA6
Haskell, T. G. — ThB4
Hayano, Yutaka — MB3
Hemmer, P. R. — TuA45
Herriot, Glenn — TuA3
Highland, Ron — TuA37, FA5
Hofmann, R. — MC1
Hogan, G. P. — TuA36
Holohan, M. L. — TuA14
Hubin, N. — MA1, MC1
Hughes, J. M. — TuA49